Distribution Agreement

In presenting this thesis or dissertation as a partial fulfillment of the requirements for an advanced degree from Emory University, I hereby grant to Emory University and its agents the non-exclusive license to archive, make accessible, and display my thesis or dissertation in whole or in part in all forms of media, now or hereafter known, including display on the world wide web. I understand that I may select some access restrictions as part of the online submission of this thesis or dissertation. I retain all ownership rights to the copyright of the thesis or dissertation. I also retain the right to use in future works (such as articles or books) all or part of this thesis or dissertation.

Signature:

_____ _____

Ryan A. Allen Date

Natural Product Inspired Complementary Approaches to Counter Antimicrobial Resistance:

Synthetic and Biological Investigations of Antibacterial Small Molecules

By

Ryan A. Allen
Doctor of Philosophy

Chemistry

William M. Wuest, Ph.D.
Advisor

Christine Dunham, Ph.D.
Committee Member

Monika Raj, Ph.D.
Committee Member

Accepted:

Kimberly Jacob Arriola
Dean of the James T. Laney School of Graduate Studies

_____
Date

Natural Product Inspired Complementary Approaches to Counter Antimicrobial Resistance: Synthetic and Biological Investigations of Antibacterial Small Molecules

By

Ryan A. Allen

B.S., Villanova University, 2018

Advisor: William M. Wuest, Ph.D.

An abstract of

A dissertation submitted to the Faculty of the

James T. Laney School of Graduate Studies of Emory University

In partial fulfillment of the requirements for the degree of

Doctor of Philosophy in Chemistry

2023

Abstract

NATURAL PRODUCT INSPIRED COMPLEMENTARY APPROACHES TO COUNTER ANTIMICROBIAL RESISTANCE: SYNTHETIC AND BIOLOGICAL INVESTIGATIONS OF ANTIBACTERIAL SMALL MOLECULES

By Ryan A. Allen

Natural products are small molecules produced by living organisms for a specific purpose in an ecological niche. These small molecules oftentimes have complex structures and activities that lend themselves to development into novel therapies for diseases. Development of these novel therapies is increasingly important with the rise of antibiotic resistant bacteria that threaten modern day medicine. To this end, the total synthesis and modification of natural products and natural product-like scaffolds to identify novel mechanisms of action and activities has been undertaken. To identify novel mechanisms of action for the development of antibiotics, the total synthesis of the mindapyrroles and investigation into their photoactivity for use in affinity-based protein profiling experiments was explored. To combat prevalent disinfectant resistance, our collaborators in the Minbiole Lab at Villanova University synthesized novel quaternary ammonium compounds (QACs) to test against common pathogenic bacteria. Inspired by this work, we undertook the total synthesis of the ianthelliformisamines, a class of polyamine natural products, for the development of novel QAC scaffolds.

Natural Product Inspired Complementary Approaches to Counter Antimicrobial Resistance: Synthetic and Biological Investigations of Antibacterial Small Molecules

By

Ryan A. Allen

B.S., Villanova University, 2018

Advisor: William M. Wuest, Ph.D.

A dissertation submitted to the Faculty of the

James T. Laney School of Graduate Studies of Emory University

In partial fulfillment of the requirements for the degree of

Doctor of Philosophy in Chemistry

2023

Acknowledgements

"Don't be discouraged. It's often the last key in the bunch that opens the lock."
- Anonymous

First, I would like to thank my advisor Prof. Bill Wuest for the continual guidance along my pathway to the PhD. He has taught me how to sell my research and myself through the art of telling a compelling story. Furthermore, he has encouraged me to expand my ideas of what is possible through chemistry and reimagine what a "right" answer could be. I would also like to thank my committee members, Prof. Christine Dunham and Prof. Monika Raj, for their excellent advice not just in research, but in my career as well. I would also like to thank the Emory chemistry community, especially Steve Krebs, Kira Walsh, and the entire staff that makes the building a comfortable and welcoming environment.

In addition to the Emory chemistry faculty, I would be remiss if I did not also thank my undergraduate chemistry department at Villanova University, specifically Prof. Kevin Minbiole and Prof. Jennifer Palenchar. Thank you to both of you for mentoring me through my first research experiences and helping me discover my passion for scientific discovery (and steering me away from med school!).

I would like to thank the Wuest Lab, past and current members, for being a grounding and supportive group to go through the fire and flames of grad school with. I would like to thank Dr. Kelly Morrison for being my first graduate student mentor in the lab and pushing me to do my best work. I cannot express how grateful I am to have gone through grad school with Prof. Dr. Cassie Zaremba and Dr. Andrew Mahoney; you both made my dark days bright and were such a joy to work with. I count myself lucky to be amongst your lifelong friends! Thank you to Adrian Demeritte for being a sounding board for my chemical queries and listening to my complaints about pyrrole and *n*-BuLi. I would be remiss if I didn't also mention my quick witted and fabulous office mate Martina Golden; thank you for discussing chemistry problems and Taylor Swift theories! Shoutout to Ben Deprez for being a friend and chemical confidant as well! Additionally, I would like to thank my two undergraduate mentees; Caroline McCormack and Tamecka Marecheau-Miller for being willing to learn and willing to develop your skillsets in the lab, even

when chemistry was not cooperating. You are both excellent scientists and I am so incredibly proud of you both!

Last and certainly not least, I would like to thank my friends and family who have supported me over the years and helped me grow into my authentic self. To Jackie and Maddie, thank you for being close friends over the years, and for helping me escape the lab every now and again. To Jake, Rachel K., Zach, Brit, and Rachel A., thank you for giving me a relaxed place to land whenever I come home to Pittsburgh. I would like to thank my boyfriend Jay Howen for giving me space to feel the weight of my endeavor, supporting me through it, and helping me smile again. To my cats Mona and Copper, for their emotional support over the years and always making me smile. To my siblings David, Michael, and Michelle, thank you for growing with me and accepting new sprouts as prosperous evolvement and not pernicious weeds. Thank you to my father Bill Allen for teaching me the values of hard work, perseverance, and excellence in the small things. Lastly, to my mother Roberta Allen; to put it simply, thank you for always being there for me and being the touchstone of my values. I can say without a shadow of a doubt that I would be the person I am today without you.

Table of Contents

Table of Schemes

Table of Figures

Table of Tables

Chapter 1: Introduction to Natural Product Antimicrobials and the Rise of Antibiotic Resistance

This chapter is a select summation on the field of antibiotic development and the rise of resistance.

Natural products are, in the simplest context, small molecules that are produced by living organisms and not involved in primary metabolism.[1,2] Going beyond that definition, chemists, biologists, and biochemists seek to understand the chemical properties, biological activities, and biosynthesis of these molecules so as to exploit them for a desired purpose. Chemists often use a natural product scaffold as inspiration to develop novel reactions that expand the chemical toolbox with which synthetic chemists work. Biologists draw from the wellspring of natural products for a variety of purposes such as treatments for human disease, probe molecules to understand biological systems and pathways, and agricultural manipulation. Biochemists often look to the producing organism, where researching the biosynthetic pathways and manipulations of such pathways can be used to generate novel green catalysts as well as a source of bioinformatic data to be utilized by other scientists. These lines are often blurred, as researchers and companies find their niches and expand beyond these distinct areas into interdisciplinary research, where collaboration leads to incredible discoveries. One such results of this cross pollination of ideas and intellect is the chemical biologist, a scientist who utilizes synthetic chemistry to produce small molecules, often inspired by but not limited to natural products, to study and manipulate biological systems. Such is the focus of this work, where synthetic organic chemistry inspired by natural products is leveraged for the development of novel therapies to treat and prevent multidrug resistant bacterial infections.

1.1 The History of Natural Product Antimicrobials

1.1.1 Uses in Traditional Medicine

The planet Earth has been producing life for about 3.7 billion years, during which time evolution has allowed for the expansion of single and multicellular organisms to find their biological niche, utilize its resources, and defend it from predators.[3] Oftentimes, this takes the form of the secretion of natural products to weaken invading organisms and form mutually beneficial relationships with symbionts, thereby increasing their fitness.[4–6] Humans, being relatively new to life, have taken note of this natural evolution and leveraged it for early treatments to typically life-threatening infections (**Figure 1.1**). Malaria in Ethiopia was often treated with the bark of *Terminalia brownii*, colloquially known are sebaea. The bark would be pounded then homogenized with water to give a medicine that would be drunk on an empty stomach every morning for four days.[7] The activity of this extract has been corroborated in recent years as the extract was found to have good *in vivo* activity against *Plasmodium berghei* in mouse models.[7]

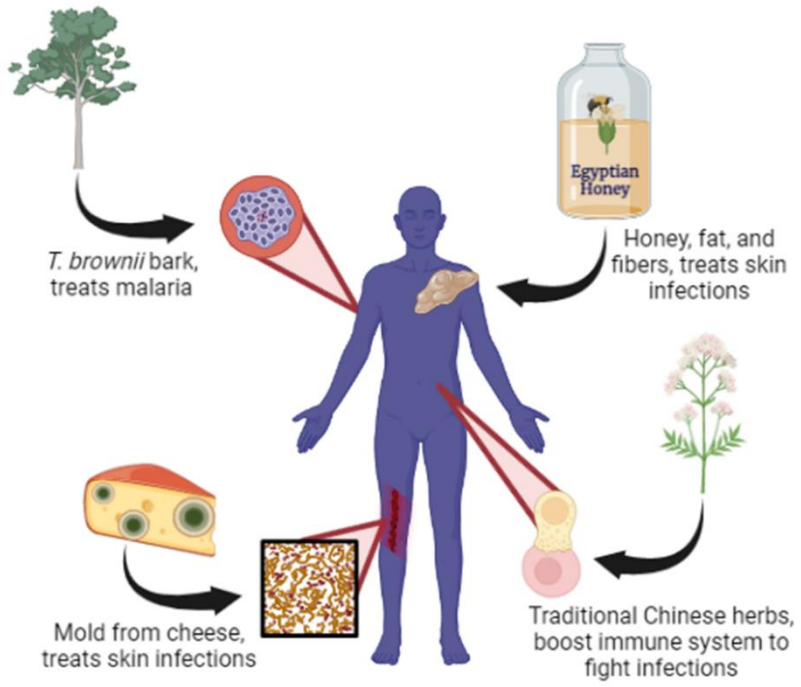

Figure 1.1 Uses of natural product-containing herbs, honey, and mold in traditional medicine to treat infections.

Wounds in ancient Egypt were typically covered with a salve made from honey, fat, and fibers, with the active ingredient being honey.[8] The antibacterial activity of honey has largely been attributed to its low pH, concentration of hydrogen peroxide, and phenolic compounds such as methyl

syringate.[9] Traditional Chinese medicines have been prescribed to treat skin and soft tissue infections for centuries through today, and they have been proven to have synergy with common antibiotics against extensively drug resistant enterobacteria.[10] Three herbs, namely jin yin hua, huang qi, and dang gui, are extensively used in traditional Chinese medicine and have been shown to have such benefits as boosting the immune system and renal health, antiviral activity, and decreasing inflammation, thereby owing their synergy to helping the body clear the infection naturally.[11–14]

Exploring more than just plant material, humans have also used molds and fungi for millennia to treat and prevent bacterial infections (**Figure 1.1**). Ancient Aborigines would take the mold from the sheltered side of a eucalyptus tree and apply it to a wound to treat an infection.[15] Similarly, a Greek king had a peasant woman treat his injured soldiers with mold scraped from cheese.[15] The folklore of Devon County, England mentions hanging a Good Friday bun from the rafters in the kitchen, allowing for mold to grow, and then mixing moldy bits of the bread with water to cure a variety of ailments in both humans and cows.[16] This treatment is similar to those written about in the Jewish Talmud, where a mix of moldy corn soaked in date wine, called kutach bayli, is prescribed to treat infections.[15] Additionally, the ancient Chinese prescribed the mold of soya beans for skin infections.[17] The active ingredients of these mixtures were not the fungi themselves, but rather the natural product antibiotic compounds they produced. This is corroborated by tetracycline being found on a first century skeleton in Sudan, demonstrating the persistent power of natural product antibiotics.[18] In hindsight, it is no surprise that Alexander Fleming discovered penicillin from a fungus growing on a petri dish.

1.1.2 The Golden Age of Antibiotic Discovery

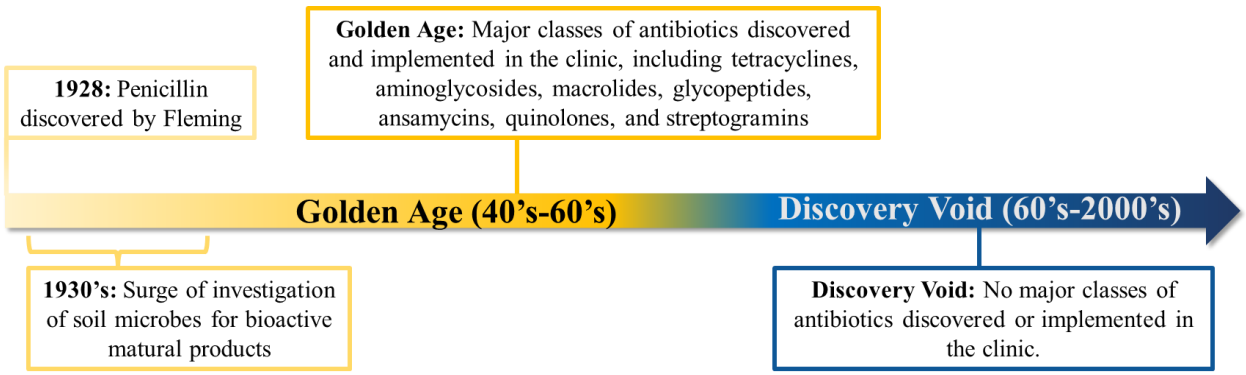

Figure 1.2 Timeline of antibiotic discovery, highlighting the Golden Age and Discovery Void eras.

Following Alexander Fleming's discovery of penicillin in 1928, a surge of research went into antibiotic discovery and development (**Figure 1.2**). Selman Waksman was instrumental to this research, as he led a systematic screen of soil microorganisms for antibiotic compounds during the 1930's.[19–21] This led to what is now known as the golden age of antibiotic discovery, a period starting in the late 1940's through the 1960's. During this time, roughly half of the currently clinically used antibiotics were discovered and implemented in the clinic, many of which were natural products or natural product inspired.[22] Following the golden age, there was a discovery void of novel antibiotics, wherein no major classes of antibiotics were introduced in the clinic between 1962 and 2000.[23] Partially to blame for this lack of discovery is that many antibiotics that had already been discovered were being rediscovered in screens of novel strains of microbes.[24] Microorganisms collected were also only from a few phyla of bacteria, with actinoycetota being the most heavily mined, leaving the roughly 99.999% of undiscovered bacteria unexploited.[24,25] Additionally, cryptic and otherwise silenced gene clusters were not known or activated under culture conditions, thereby giving rise to a lack of novel structures and targets.[26–28] After the golden age, there was also a false sense of accomplishment insofar as pharmaceutical companies thought antibiotics had solved bacterial infections once and for all; therefore, many pharmaceutical companies shut down their antibiotic discovery labs.[29] These conditions have given rise to the antibiotic crisis we face today.

1.2 The Rise of Antibiotic Resistance

Antibiotic resistance is the leading threat currently facing modern medicine, as antibiotic resistant bacteria threaten the safety and efficacy of many standard medical procedures.[30] Antibiotics are routinely prescribed to patients going through chemotherapy as well as patients who have undergone surgery to prevent life threatening infections before they start. However, these treatment options become less effective in the presence of drug-, multidrug- and extensively drug-resistant bacteria (DRB, MDRB and XDRB, respectively), which is currently being seen in the clinic. In 2019, the Center for Disease Control (CDC) reported that antibiotic resistant pathogens were responsible for 2,868,700 infections and 35,900 deaths in the United States alone.[31] Additionally, the financial burden for these types of infections is estimated to be over $55 billion annually.[32] Although these figures are staggering, they are projected to increase to about 10 million deaths per year and cost $16.7 trillion by 2050 unless interventions are made now.[33]

1.2.1 Mechanisms of Antibiotic Resistance

The antibiotic resistance crisis predates the discovery of penicillin, as clinical resistance to the first clinically used antibiotic Salvarsan was detected in 1924.[34] Prehistorically speaking, the first beta-lactamases, a common type of resistance mechanism to penicillins, are reported to have

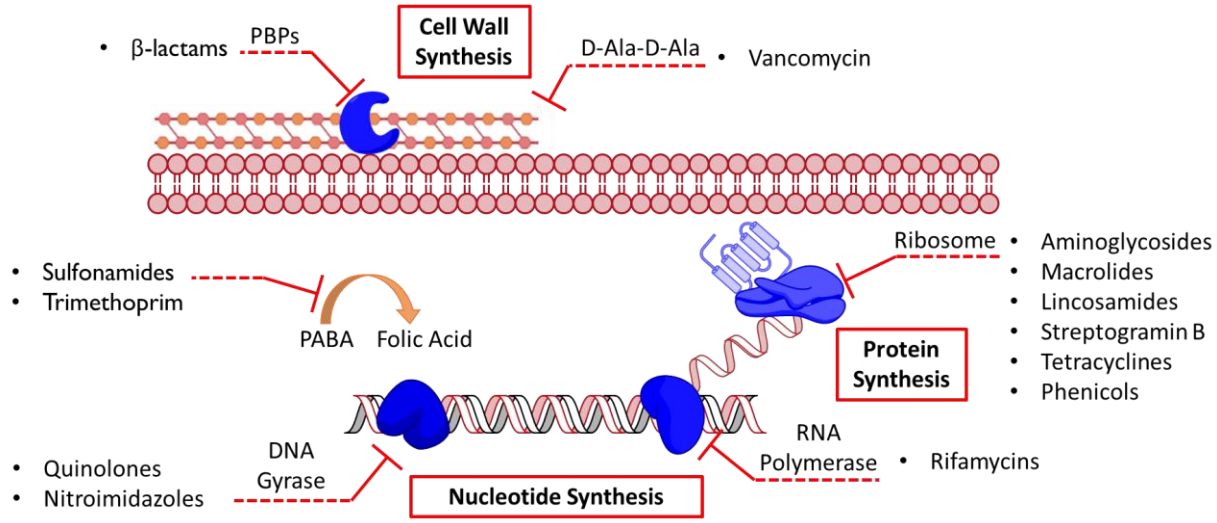

Figure 1.3 Essential life processes inhibited by antibiotics.

first evolved around 2-3 billion years ago; however, they were first identified before penicillin was introduced into the clinic.[35,36] Since then, bacteria have been developing and sharing clever ways to resist antibiotics. This is concerning as many antibiotics used in the clinic target one of three essential life processes: cell wall synthesis, nucleotide synthesis, and protein synthesis (**Figure 1.3**).[37] This is particularly troublesome as resistance to one antibiotic can confer resistance to another antibiotic, thereby limiting the efficacy of entire classes of antibiotics. For example, when bacteria modify ribosomal adenine 2058 via a double methylation, cross-resistance to macrolides, lincosamides, and streptogramins B's observed.[38]

Acquisition of resistance to antibiotics can occur either through natural evolution or horizontal gene transfer (**Figure 1.4**). When bacteria are exposed to subminimal inhibitory concentrations of antibiotics for an extended period of time, they can evolve mechanism with which to evade cell death. This has led to a variety of mutations that can evade antibiotic activity, such as *E. coli* mutating to acquire resistance to trimethoprim. Bacteria grown in increasing concentrations of trimethoprim over 12 days were able to acquire a number of mutations to increase the MIC and survive at higher concentrations.[39] FolA, the protein targeted by trimethoprim, was most often mutated in these strains as mutations typically decreased the binding affinity of the drug and lessened its effect in the bacterium.[39]

Additionally, a method all bacteria exploit *ad nauseam* is that of efflux pumps (**Figure 1.4**). These transporters can eject a variety of antibiotics from the interior of the cell, thereby raising the minimum inhibitory concentration (MIC) by stopping the antibiotics from ever reaching their target.[40] For gram positive bacteria, some of the most troublesome efflux pumps are chromosomally encoded multidrug efflux pumps, such as MdeA. Upregulation of this multidrug efflux pump can cause resistance to fluoroquinolones, novobiocin, and quaternary ammonium

compounds.[41,42] Strains of *S. aureus* have been found to have mutated promoter regions of this efflux pump, which causes consistent upregulation and consistent resistance to the previously mentioned antibacterial compounds.[41] These pathogens also harbor efflux pumps are encoded on plasmids and give resistance to a specific antibiotic, such as tetracycline resistance efflux pump TetK.[43]

Gram negative pathogens also harbor a plethora of chromosomally encoded efflux pumps, some of the most infamous being the resistance-nodulation-division (RND) superfamily efflux

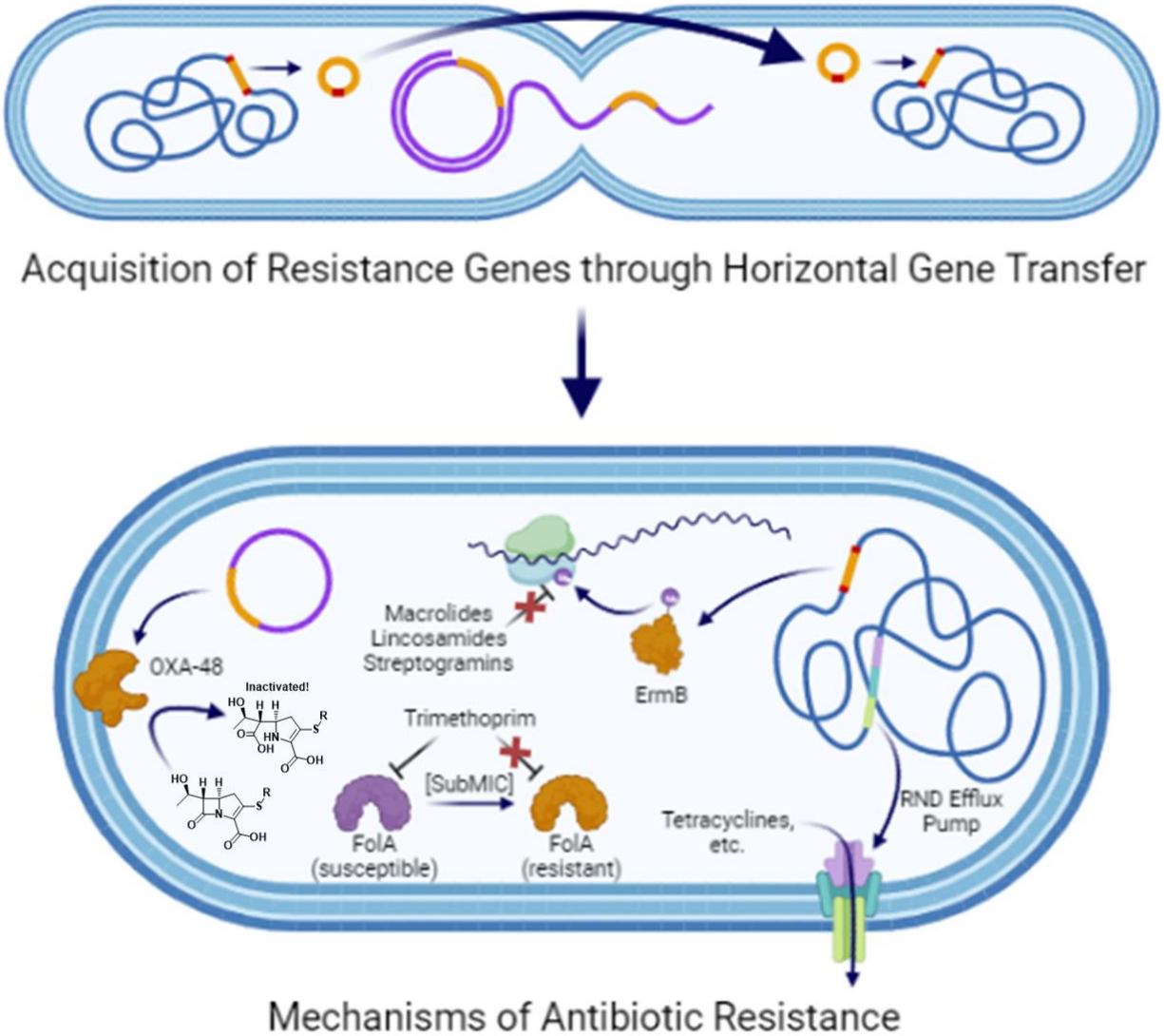

Figure 1.4 Diagrams of horizontal gene transfer, evolution of resistance, and mechanisms of resistance employed by bacteria to counter antibiotics. Purple circle: plasmid with gold resistance gene. Gold band: conjugative transposon with resistance gene, red bands are integrase sites.

pump AcrAB-TolC of *E. coli* and MexXY-OprM of *P. aeruginosa* (**Figure 1.4**). The AcrAB-TolC system is known to efflux a variety of structurally unrelated compounds from the cytoplasm and periplasm, and it can be upregulated to resist tetracycline treatment.[44–46] Similarly, the MexXY-OprM system can be upregulated in the presence of colistin and is partially responsible for colistin resistance in this bacterium.[47,48] Gram negative pathogens can also acquire plasmids that encode for efflux pumps, such as the RND efflux pump TMexCD1-TOprJ. Originally isolated from pan-resistant *K. pneumoniae* animal isolates, this efflux pump increased MICs of tetracyclines, quinolones, cephalosporins, and aminoglycosides in *K. pneumoniae, E. coli* and *Salmonella*.[49] Additionally, this efflux pump has been found on plasmids that carry carbapenemase genes.[50,51]

The sharing of different antibiotic resistant strategies can occur through horizontal gene transfer between one another, either through plasmids or conjugative transposons (**Figure 1.4**). A conjugative transposon carrying rRNA methyltransferase *ermB* has been discovered in *Bacteroides* species, and a plasmid containing aminoglycoside resistance gene *armA* and β-lactamase gene $bla_{\text{KPC-2}}$ has been discovered that can transfer from multidrug resistant *K. pneumoniae* to *E. coli*.[52,53] Clinical resistance and cross-resistance genes that are transferred amongst bacteria are in part responsible for the rise of all levels of drug resistant bacteria and the threat to modern medicine. It has been shown that resistance of glycopeptide antibiotics such as vancomycin did often arises in *S. aureus* via horizontal gene transfer from vancomycin-resistance *Enterococci*.[54] Therefore, novel therapies and preventions are needed to combat these deadly and financially draining pathogens.

1.3 Current Methods to Combat Antibiotic Resistance

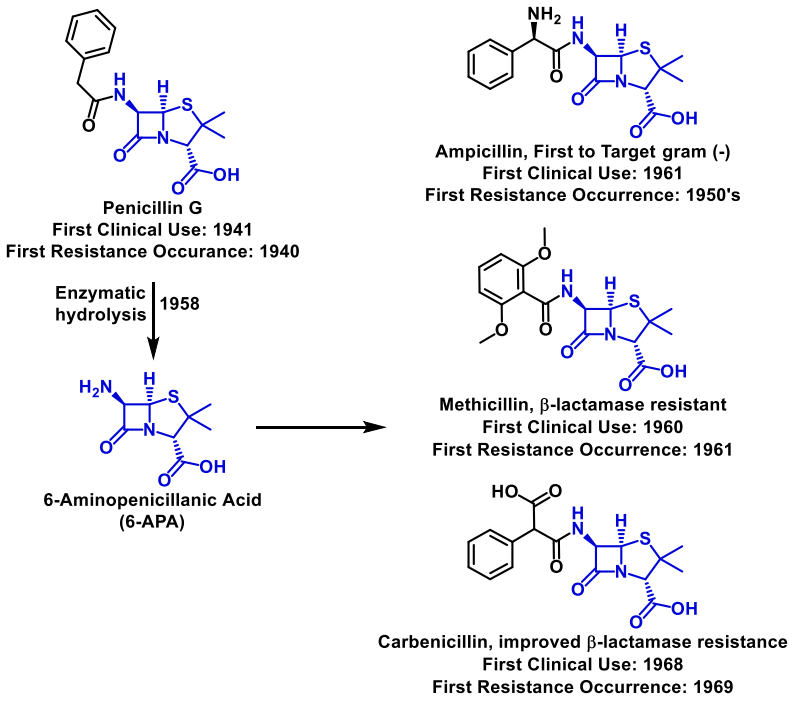

Figure 1.5 Derivatives of penicillin, their introduction to the clinic, and when resistance was first observed.

Given the current state of widespread resistance to antibiotics, much research has been conducted in order to discover innovative and synergistic solutions to stave off the rapid rise of antibiotic resistant bacteria.

1.3.1 Repurposing Previously Active Scaffolds

From a pharmaceutical company perspective, it is much easier to repurpose an antibiotic that has a known mechanism than to discover a new drug that has a new mechanism and unknown pharmacokinetic properties. Therefore, many pharmaceutical companies have repurposed previously active scaffolds that have gained resistance. Perhaps the most famous example is the slew of β-lactam antibiotics derived from penicillin (**Figure 1.5**). Once chemists were able to mass produce 6-aminopenicillanic acid (6-APA) via enzymatic hydrolysis of the acyl sidechain, they were able to append a variety of sidechains onto the core scaffold to investigate novel bioactivity.[55] This led to the discovery of methicillin, the first β-lactam antibiotic that could resist the β-lactamase that killed penicillin's activity.[56] From there, scientists were able to fashion a β-lactam that could target gram negative bacteria, namely ampicillin.[57] Shortly thereafter, carbenicillin was developed as a more β-lactamase stable derivative.[58] However, none of these compounds lasted in the clinic long before

resistance to them was reported, thereby limiting the efficacy of this counterattack on antibiotic resistance.[59]

1.3.2 Combination Therapies and Polypharmacology

A variety of combination therapies have been developed to address the rising concern of antibiotic resistance to a particular antibiotic (**Figure 1.6**). In keeping with the β-lactam theme, an adjuvant therapy that has been incredibly successful is that of using a β-lactamase inhibitor with a β-lactam. β-lactamase inhibitor clavulanic acid, isolated from *Streptomyces clavuligerus*, has been used with amoxicillin to extend its clinical efficacy.[60] Similarly, adjuvants of β-lactam ceftazidime with β-lactamase inhibitor avibactam extend the efficacy of this carbapenem by inhibiting extended spectrum β-lactamases and plasmid-borne carbapenemase isolated from *K. pneumoniae*.[61,62] However, these adjuvant therapies are not without their downfalls. Shortly after

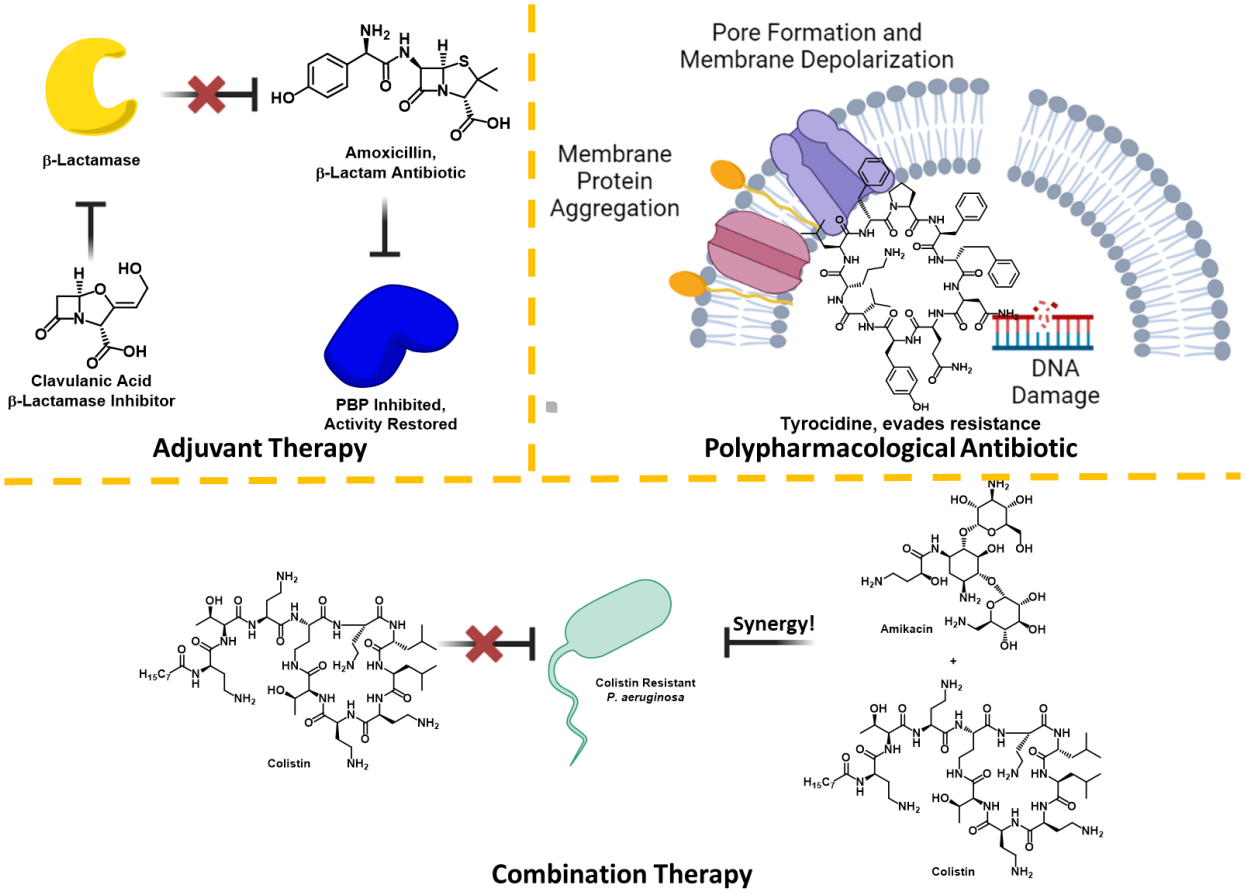

Figure 1.6 Combination therapy and polypharmacological strategies that evade resistance.

the introduction of clavulanic acid as an adjuvant in the clinic, isolates of *E. coli* and *K. pneumoniae* that were resistant to the amoxicillin-clavulanic acid treatment.[63,64] This was a result of either acquisition of a β-lactamase not susceptible to clavulanic acid from another species (horizontal gene transfer) or hyperexpression of the β-lactamase itself. Although novel β-lactamase inhibitors seem promising, bacteria may still acquire penicillin binding proteins that evade current β-lactam antibiotics and render these adjuvant treatments useless altogether. Additionally, these adjuvant therapies are useless against gram negative pathogen with defective or under expressed porins, such as a strain of OmpF-defective *E. coli*, that does not allow for periplasmic β-lactam penetration.[65]

In addition to adjuvant therapies, synergistic therapies of two or more antibiotics offer an avenue of circumventing antibiotic resistance (**Figure 1.6**). *In vitro* experiments have shown that synergy can overcome polymyxin B resistance in *P. aeruginosa* when treated with amikacin. Metabolomic profiling revealed that the cause of this synergistic pairing was possibly due to early inhibition of the pentose phosphate pathway.[66] Similarly, colistin-resistant isolates of *K. pneumoniae*, *A. baumannii*, and *E. coli* were made sensitive to typically non-gram negative active antibiotics such as fusidic acid and clindamycin when used with colistin.[67,68] The authors attributed this synergism to colistin still permeabilizing the outer membrane to allow these antibiotics to cross the typically impenetrable outer membrane.[67] Although these synergistic combination therapies are promising, resistance may still occur to both antibiotics used, thereby rendering the combination inefficacious.

Similar to combination therapy, polypharmacology gives an antibiotic multiple mechanisms of action (**Figure 1.6**). This is favorable as bacteria would have to acquire more than one resistance mechanism in order to become fully resistant, and resistance that does occur may

not invoke cross-resistance to other classes of antibiotics, depending on the mechanism.[24,69] Additionally, the multiple mechanisms of resistance may cause the bacterium to have a reduced fitness, thereby making it unviable in an infection model.[70] The polypeptide antibiotic tyrocidine enacts its multifaceted mechanism of action by forming ion-conducting pores, decreasing membrane fluidity, causing lipid phase separation, damaging DNA, and interacting with DNA associated proteins in gram positive bacteria.[71] Despite tyrocidine being used as a topical antibiotic for decades, no clinical resistance has been detected, and only marginal levels of resistance have been induced in a laboratory setting.[72–74] However, these antibiotics typically suffer from poor selectivity for bacterial cells over mammalian cells, thereby limiting their clinical use.[75] Despite this, polypharmacological antibiotics could present a promising avenue for future antibiotic development.

1.3.3 Discovery of Novel Mechanisms of Action

Novel mechanisms of action provide a way forward with antibiotic development that allows for a complete avoidance of cross resistance. By targeting a new protein or pathway, DRB, MDRB, XDRB, and pan-resistant bacteria can be effectively killed when no other options are available, provided they can surpass the membrane(s) and cell wall and accumulate at significant concentrations inside the cell. One recent report is a natural product inspired macrocyclic polypeptide antibiotic that inhibits BamA, a protein necessary for folding beta-barrel proteins on the outer membrane surface.[76] This antibiotic had activity against all tested gram negative pathogens, including MDR gram negative ESKAPE pathogens, defined by the World Health Organization as particularly concerning threats to modern medicine, many of which align with the CDC's concerns.[77] One drawback of developing antibiotics with novel mechanisms of action is the need for an appropriate assay to detect compounds that inhibit the desired pathway or process.

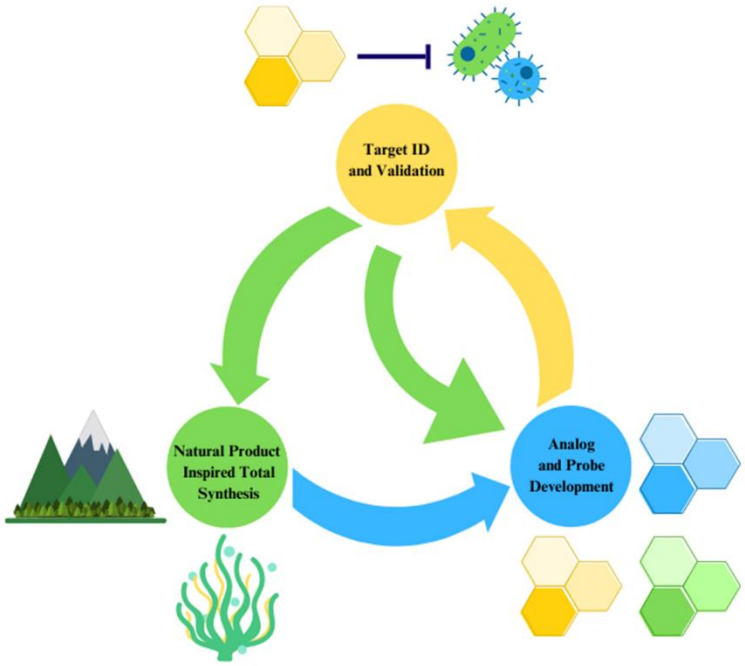

Figure 1.7 Cycle of natural product inspired total synthesis, which leads to analog design and target identification and validation. The information garnered from target identification can be used to iteratively design better analogs.

Additionally, these pathways and proteins need to be validated as potential antibiotic targets before the assay can even be developed. Despite these drawbacks, novel mechanisms of action still offer a viable route forward for antibiotic development that can counter antibiotic resistance.

1.3.4 The Wuest Lab Approach

Seeing the development of antibiotics with novel mechanisms of action as the most promising way to create therapies that are active against all levels of drug resistant bacteria, the Wuest Lab investigates natural products and synthetic molecules that have been identified as active against these problematic pathogens (**Figure 1.7**). We then conduct a total synthesis of the desired molecules if one has not been previously developed, followed by synthesis of a slew of analogs to probe structure activity relationships (SAR). Once activity has been validated *in vitro* and SAR has determined amenable portions of the molecule, probe molecules can be designed for mechanism of action studies. Once a target has been validated, a cycle of analog design and activity validation can ensue, using the mechanistic information obtained to design better analogs. This can give rise to potent antibacterial compounds that potentially have novel or polypharmacological mechanisms of action that can serve as a starting point for development of therapeutics that can target and eliminate drug resistant pathogens.

1.4 Conclusions

Utilizing the Wuest Lab approach, I undertook the total synthesis of pyoluteorin and the similarly structured mindapyrroles to allow for future investigations of their mechanism of action, detailed in Chapter 2. Due to their structural similarity to molecules previously investigated, I have reason to believe they are polypharmacological. As previously discussed, this is favorable for antibiotic development as it hinders the development of resistance. This work expands upon the known chemical reactivity of resorcinol and γ-resorcylic acid dimers, as well as 2-acylpyrroles. Specifically, the deacylation of 4,5-dichloro-2-trichloroacetylpyrrole under basic conditions for the regioselective acylation of methylene-linked resorcinol dimer was discovered. In addition to their total synthesis, the antibacterial activity of the mindapyrroles was explored against a variety of clinically relevant bacteria, and *S. aureus* was shown to not develop resistance to pyoluteorin over a 24-day period in a serial passage resistance selection assay.

Additionally, the activity of amphiphilic disinfectants and antibiotics appended with a quaternary ammonium were explored through a variety of collaborations, wherein I acted as the microbiologist performing minimum inhibitory concentration assays, hemolysis assays, and aiding with resistance selection assays. This work is detailed in Chapter 3. With the Pires lab, the activity of novel polymyxin B analogs with appended quaternary ammoniums was explored, demonstrating the ability to switch this molecule's native activity to being broad spectrum instead of narrow spectrum for gram negative pathogens. Collaborating the with Minbiole lab, we tested a library of amphiphilic disinfectants with novel structures, demonstrating the activity of novel trivalent sulfonium compounds (TSCs), ferrocene containing quaternary ammonium compounds (QACs), and expanding the rigidity-activity relationships of QACs. Additionally, we tested the best-in-class disinfectants synthesized by the Minbiole lab against multidrug- and pan-resistant

clinical isolates of *A. baumannii* and *P. aeruginosa*, demonstrating the relative inactivity of commercial QAC disinfectants and the efficacy of a novel quaternary phosphonium compound (QPC) against all *A. baumannii* strains tested. Additionally, we synthesized ianthelliformisamine C and QAC analogs and investigated their activity and mechanism of action against a panel of clinically relevant bacteria.

1.5 Chapter 1 References

(1) Dias, D. A.; Urban, S.; Roessner, U. A Historical Overview of Natural Products in Drug Discovery. *Metabolites* **2012**, *2* (2), 303–336. https://doi.org/10.3390/metabo2020303.

(2) Pham, J. V.; Yilma, M. A.; Feliz, A.; Majid, M. T.; Maffetone, N.; Walker, J. R.; Kim, E.; Cho, H. J.; Reynolds, J. M.; Song, M. C.; Park, S. R.; Yoon, Y. J. A Review of the Microbial Production of Bioactive Natural Products and Biologics. *Front. Microbiol.* **2019**, *10*.

(3) *History of Life on Earth | Smithsonian National Museum of Natural History*. http://naturalhistory.si.edu/education/teaching-resources/life-science/early-life-earth-animal-origins (accessed 2023-04-03).

(4) Williams, D. H.; Stone, M. J.; Hauck, P. R.; Rahman, S. K. Why Are Secondary Metabolites (Natural Products) Biosynthesized? *J. Nat. Prod.* **1989**, *52* (6), 1189–1208. https://doi.org/10.1021/np50066a001.

(5) Koh, E. G. L.; Sweatman, H. Chemical Warfare among Scleractinians: Bioactive Natural Products from Tubastraea Faulkneri Wells Kill Larvae of Potential Competitors. *J. Exp. Mar. Biol. Ecol.* **2000**, *251* (2), 141–160. https://doi.org/10.1016/S0022-0981(00)00222-7.

(6) Schmidt, E. W. Trading Molecules and Tracking Targets in Symbiotic Interactions. *Nat. Chem. Biol.* **2008**, *4* (8), 466–473. https://doi.org/10.1038/nchembio.101.

(7) Nigussie, G.; Wale, M. Medicinal Plants Used in Traditional Treatment of Malaria in Ethiopia: A Review of Ethnomedicine, Anti-Malarial and Toxicity Studies. *Malar. J.* **2022**, *21* (1), 1–16. https://doi.org/10.1186/s12936-022-04264-w.

(8) Sipos, P.; Gyõry, H.; Hagymási, K.; Ondrejka, P.; Blázovics, A. Special Wound Healing Methods Used in Ancient Egypt and the Mythological Background. *World J. Surg.* **2004**, *28* (2), 211–216. https://doi.org/10.1007/s00268-003-7073-x.

(9) Mandal, M. D.; Mandal, S. Honey: Its Medicinal Property and Antibacterial Activity. *Asian Pac. J. Trop. Biomed.* **2011**, *1* (2), 154–160. https://doi.org/10.1016/S2221-1691(11)60016-6.

(10) Li, J.; Feng, S.; Liu, X.; Jia, X.; Qiao, F.; Guo, J.; Deng, S. Effects of Traditional Chinese Medicine and Its Active Ingredients on Drug-Resistant Bacteria. *Front. Pharmacol.* **2022**, *13*. https://doi.org/10.3389/fphar.2022.837907.

(11) Li, H.; Lu, C. Lonicera Japonica Thunb 金银花 (Jinyinhua, Honey Suckle). *Diet. Chin. Herbs* **2015**, 693–702. https://doi.org/10.1007/978-3-211-99448-1_78.

(12) Chen, Z.; Liu, L.; Gao, C.; Chen, W.; Vong, C. T.; Yao, P.; Yang, Y.; Li, X.; Tang, X.; Wang, S.; Wang, Y. Astragali Radix (Huangqi): A Promising Edible Immunomodulatory Herbal Medicine. *J. Ethnopharmacol.* **2020**, *258*, 112895. https://doi.org/10.1016/j.jep.2020.112895.

(13) Wu, Y.-C.; Hsieh, C.-L. Pharmacological Effects of Radix Angelica Sinensis (Danggui) on Cerebral Infarction. *Chin. Med.* **2011**, *6*, 32. https://doi.org/10.1186/1749-8546-6-32.

(14) Ma, D.; Wang, S.; Shi, Y.; Ni, S.; Tang, M.; Xu, A. The Development of Traditional Chinese Medicine. *J. Tradit. Chin. Med. Sci.* **2021**, *8*, S1–S9. https://doi.org/10.1016/j.jtcms.2021.11.002.

(15) Moulds in Folk Medicine: Folklore: Vol 100, No 2. *Folklore*.

(16) Thompson, S. E. *Holiday Symbols*, 2nd ed.; Omnigraphics, 1998.

(17) Foster, S.; Duke, J. A. *A Field Guide to Medicinal Plants and Herbs of Eastern and Central North America*; Houghton Mifflin Harcourt, 2000.

(18) Bassett, E. J.; Keith, M. S.; Armelagos, G. J.; Martin, D. L.; Villanueva, A. R. Tetracycline-Labeled Human Bone from Ancient Sudanese Nubia (A.D. 350). *Science* **1980**, *209* (4464), 1532–1534. https://doi.org/10.1126/science.7001623.
(19) Waksman, S. A.; Woodruff, H. B. The Soil as a Source of Microorganisms Antagonistic to Disease-Producing Bacteria. *J. Bacteriol.* **1940**, *40* (4), 581–600. https://doi.org/10.1128/jb.40.4.581-600.1940.
(20) Waksman, S. A.; Woodruff, H. B. Actinomyces Antibioticus, a New Soil Organism Antagonistic to Pathogenic and Non-Pathogenic Bacteria 1. *J. Bacteriol.* **1941**, *42* (2), 231–249.
(21) Kresge, N.; Simoni, R. D.; Hill, R. L. Selman Waksman: The Father of Antibiotics. *J. Biol. Chem.* **2004**, *279* (48), e7–e8. https://doi.org/10.1016/S0021-9258(20)67861-9.
(22) Aminov, R. I. A Brief History of the Antibiotic Era: Lessons Learned and Challenges for the Future. *Front. Microbiol.* **2010**, *1*, 134. https://doi.org/10.3389/fmicb.2010.00134.
(23) Silver, L. L. Challenges of Antibacterial Discovery. *Clin. Microbiol. Rev.* **2011**, *24* (1), 71–109. https://doi.org/10.1128/CMR.00030-10.
(24) Miethke, M.; Pieroni, M.; Weber, T.; Brönstrup, M.; Hammann, P.; Halby, L.; Arimondo, P. B.; Glaser, P.; Aigle, B.; Bode, H. B.; Moreira, R.; Li, Y.; Luzhetskyy, A.; Medema, M. H.; Pernodet, J.-L.; Stadler, M.; Tormo, J. R.; Genilloud, O.; Truman, A. W.; Weissman, K. J.; Takano, E.; Sabatini, S.; Stegmann, E.; Brötz-Oesterhelt, H.; Wohlleben, W.; Seemann, M.; Empting, M.; Hirsch, A. K. H.; Loretz, B.; Lehr, C.-M.; Titz, A.; Herrmann, J.; Jaeger, T.; Alt, S.; Hesterkamp, T.; Winterhalter, M.; Schiefer, A.; Pfarr, K.; Hoerauf, A.; Graz, H.; Graz, M.; Lindvall, M.; Ramurthy, S.; Karlén, A.; van Dongen, M.; Petkovic, H.; Keller, A.; Peyrane, F.; Donadio, S.; Fraisse, L.; Piddock, L. J. V.; Gilbert, I. H.; Moser, H. E.; Müller, R. Towards the Sustainable Discovery and Development of New Antibiotics. *Nat. Rev. Chem.* **2021**, *5* (10), 726–749. https://doi.org/10.1038/s41570-021-00313-1.
(25) Thompson, L. R.; Sanders, J. G.; McDonald, D.; Amir, A.; Ladau, J.; Locey, K. J.; Prill, R. J.; Tripathi, A.; Gibbons, S. M.; Ackermann, G.; Navas-Molina, J. A.; Janssen, S.; Kopylova, E.; Vázquez-Baeza, Y.; González, A.; Morton, J. T.; Mirarab, S.; Zech Xu, Z.; Jiang, L.; Haroon, M. F.; Kanbar, J.; Zhu, Q.; Jin Song, S.; Kosciolek, T.; Bokulich, N. A.; Lefler, J.; Brislawn, C. J.; Humphrey, G.; Owens, S. M.; Hampton-Marcell, J.; Berg-Lyons, D.; McKenzie, V.; Fierer, N.; Fuhrman, J. A.; Clauset, A.; Stevens, R. L.; Shade, A.; Pollard, K. S.; Goodwin, K. D.; Jansson, J. K.; Gilbert, J. A.; Knight, R. A Communal Catalogue Reveals Earth's Multiscale Microbial Diversity. *Nature* **2017**, *551* (7681), 457–463. https://doi.org/10.1038/nature24621.
(26) Lim, F. Y.; Sanchez, J. F.; Wang, C. C. C.; Keller, N. P. Chapter Fifteen - Toward Awakening Cryptic Secondary Metabolite Gene Clusters in Filamentous Fungi. In *Methods in Enzymology*; Hopwood, D. A., Ed.; Natural Product Biosynthesis by Microorganisms and Plants, Part C; Academic Press, 2012; Vol. 517, pp 303–324. https://doi.org/10.1016/B978-0-12-404634-4.00015-2.
(27) Nguyen, C. T.; Dhakal, D.; Pham, V. T. T.; Nguyen, H. T.; Sohng, J.-K. Recent Advances in Strategies for Activation and Discovery/Characterization of Cryptic Biosynthetic Gene Clusters in Streptomyces. *Microorganisms* **2020**, *8* (4), 616. https://doi.org/10.3390/microorganisms8040616.
(28) Hoskisson, P. A.; Seipke, R. F. Cryptic or Silent? The Known Unknowns, Unknown Knowns, and Unknown Unknowns of Secondary Metabolism. *mBio* **2020**, *11* (5), e02642-20. https://doi.org/10.1128/mBio.02642-20.
(29) Lewis, K. Recover the Lost Art of Drug Discovery. *Nature* **2012**, *485* (7399), 439–440. https://doi.org/10.1038/485439a.
(30) Antibiotic-Resistant Infections Threaten Modern Medicine. *Mod. Med.*
(31) Centers for Disease Control and Prevention (U.S.). *Antibiotic Resistance Threats in the United States, 2019*; Centers for Disease Control and Prevention (U.S.), 2019. https://doi.org/10.15620/cdc:82532.
(32) Ventola, C. L. The Antibiotic Resistance Crisis. *Pharm. Ther.* **2015**, *40* (4), 277–283.
(33) Dadgostar, P. Antimicrobial Resistance: Implications and Costs. *Infect. Drug Resist.* **2019**, *12*, 3903–3910. https://doi.org/10.2147/IDR.S234610.
(34) Stekel, D. First Report of Antimicrobial Resistance Pre-Dates Penicillin. *Nature* **2018**, *562* (7726), 192–192. https://doi.org/10.1038/d41586-018-06983-0.
(35) Risso, V. A.; Gavira, J. A.; Mejia-Carmona, D. F.; Gaucher, E. A.; Sanchez-Ruiz, J. M. Hyperstability and Substrate Promiscuity in Laboratory Resurrections of Precambrian β-Lactamases. *J. Am. Chem. Soc.* **2013**, *135* (8), 2899–2902. https://doi.org/10.1021/ja311630a.
(36) Abraham, E. P.; Chain, E. An Enzyme from Bacteria Able to Destroy Penicillin. *Nature* **1940**, *146* (3713), 837–837. https://doi.org/10.1038/146837a0.
(37) Kohanski, M. A.; Dwyer, D. J.; Collins, J. J. How Antibiotics Kill Bacteria: From Targets to Networks. *Nat. Rev. Microbiol.* **2010**, *8* (6), 423–435. https://doi.org/10.1038/nrmicro2333.

(38) Leclercq, R.; Courvalin, P. Bacterial Resistance to Macrolide, Lincosamide, and Streptogramin Antibiotics by Target Modification. *Antimicrob. Agents Chemother.* **1991**, *35* (7), 1267–1272.
(39) Baym, M.; Lieberman, T. D.; Kelsic, E. D.; Chait, R.; Gross, R.; Yelin, I.; Kishony, R. Spatiotemporal Microbial Evolution on Antibiotic Landscapes. *Science* **2016**, *353* (6304), 1147–1151. https://doi.org/10.1126/science.aag0822.
(40) Ebbensgaard, A. E.; Løbner-Olesen, A.; Frimodt-Møller, J. The Role of Efflux Pumps in the Transition from Low-Level to Clinical Antibiotic Resistance. *Antibiotics* **2020**, *9* (12), 855. https://doi.org/10.3390/antibiotics9120855.
(41) Huang, J.; O'Toole, P. W.; Shen, W.; Amrine-Madsen, H.; Jiang, X.; Lobo, N.; Palmer, L. M.; Voelker, L.; Fan, F.; Gwynn, M. N.; McDevitt, D. Novel Chromosomally Encoded Multidrug Efflux Transporter MdeA in Staphylococcus Aureus. *Antimicrob. Agents Chemother.* **2004**, *48* (3), 909–917. https://doi.org/10.1128/AAC.48.3.909-917.2004.
(42) Piddock, L. J. V. Clinically Relevant Chromosomally Encoded Multidrug Resistance Efflux Pumps in Bacteria. *Clin. Microbiol. Rev.* **2006**, *19* (2), 382–402. https://doi.org/10.1128/CMR.19.2.382-402.2006.
(43) Lee, J.-H.; Heo, S.; Jeong, M.; Jeong, D.-W. Transfer of a Mobile Staphylococcus Saprophyticus Plasmid Isolated from Fermented Seafood That Confers Tetracycline Resistance. *PLOS ONE* **2019**, *14* (2), e0213289. https://doi.org/10.1371/journal.pone.0213289.
(44) Du, D.; Wang, Z.; James, N. R.; Voss, J. E.; Klimont, E.; Ohene-Agyei, T.; Venter, H.; Chiu, W.; Luisi, B. F. Structure of the AcrAB–TolC Multidrug Efflux Pump. *Nature* **2014**, *509* (7501), 512–515. https://doi.org/10.1038/nature13205.
(45) Hobbs, E. C.; Yin, X.; Paul, B. J.; Astarita, J. L.; Storz, G. Conserved Small Protein Associates with the Multidrug Efflux Pump AcrB and Differentially Affects Antibiotic Resistance. *Proc. Natl. Acad. Sci.* **2012**, *109* (41), 16696–16701. https://doi.org/10.1073/pnas.1210093109.
(46) Langevin, A. M.; El Meouche, I.; Dunlop, M. J. Mapping the Role of AcrAB-TolC Efflux Pumps in the Evolution of Antibiotic Resistance Reveals Near-MIC Treatments Facilitate Resistance Acquisition. *mSphere* **2020**, *5* (6), e01056-20. https://doi.org/10.1128/mSphere.01056-20.
(47) Puja, H.; Bolard, A.; Noguès, A.; Plésiat, P.; Jeannot, K. The Efflux Pump MexXY/OprM Contributes to the Tolerance and Acquired Resistance of Pseudomonas Aeruginosa to Colistin. *Antimicrob. Agents Chemother.* **2020**, *64* (4), e02033-19. https://doi.org/10.1128/AAC.02033-19.
(48) Poole, K.; Lau, C. H.-F.; Gilmour, C.; Hao, Y.; Lam, J. S. Polymyxin Susceptibility in Pseudomonas Aeruginosa Linked to the MexXY-OprM Multidrug Efflux System. *Antimicrob. Agents Chemother.* **2015**, *59* (12), 7276–7289. https://doi.org/10.1128/AAC.01785-15.
(49) Lv, L.; Wan, M.; Wang, C.; Gao, X.; Yang, Q.; Partridge, S. R.; Wang, Y.; Zong, Z.; Doi, Y.; Shen, J.; Jia, P.; Song, Q.; Zhang, Q.; Yang, J.; Huang, X.; Wang, M.; Liu, J.-H. Emergence of a Plasmid-Encoded Resistance-Nodulation-Division Efflux Pump Conferring Resistance to Multiple Drugs, Including Tigecycline, in Klebsiella Pneumoniae. *mBio* **2020**, *11* (2), e02930-19. https://doi.org/10.1128/mBio.02930-19.
(50) Dong, N.; Zeng, Y.; Wang, Y.; Liu, C.; Lu, J.; Cai, C.; Liu, X.; Chen, Y.; Wu, Y.; Fang, Y.; Fu, Y.; Hu, Y.; Zhou, H.; Cai, J.; Hu, F.; Wang, S.; Wang, Y.; Wu, Y.; Chen, G.; Shen, Z.; Chen, S.; Zhang, R. Distribution and Spread of the Mobilised RND Efflux Pump Gene Cluster TmexCD-ToprJ in Clinical Gram-Negative Bacteria: A Molecular Epidemiological Study. *Lancet Microbe* **2022**, *3* (11), e846–e856. https://doi.org/10.1016/S2666-5247(22)00221-X.
(51) Xiao, T.; Peng, K.; Chen, Q.; Hou, X.; Huang, W.; Lv, H.; Yang, X.; Lei, G.; Li, R. Coexistence of TmexCD-ToprJ, BlaNDM-1, and BlaIMP-4 in One Plasmid Carried by Clinical Klebsiella Spp. *Microbiol. Spectr. 10* (3), e00549-22. https://doi.org/10.1128/spectrum.00549-22.
(52) Gupta, A.; Vlamakis, H.; Shoemaker, N.; Salyers, A. A. A New Bacteroides Conjugative Transposon That Carries an ErmB Gene. *Appl. Environ. Microbiol.* **2003**, *69* (11), 6455–6463. https://doi.org/10.1128/AEM.69.11.6455-6463.2003.
(53) Zhou, Y.; Ai, W.; Guo, Y.; Wu, X.; Wang, B.; Xu, Y.; Rao, L.; Zhao, H.; Wang, X.; Yu, F. Co-Occurrence of Rare ArmA-, RmtB-, and KPC-2–Encoding Multidrug-Resistant Plasmids and Hypervirulence Iuc Operon in ST11-KL47 Klebsiella Pneumoniae. *Microbiol. Spectr.* **2022**, *10* (2). https://doi.org/10.1128/spectrum.02371-21.
(54) McGuinness, W. A.; Malachowa, N.; DeLeo, F. R. Vancomycin Resistance in Staphylococcus Aureus. *Yale J. Biol. Med.* **2017**, *90* (2), 269–281.
(55) Rolinson, G. N.; Batchelor, F. R.; Butterworth, D.; Cameron-Wood, J.; Cole, M.; Eustace, G. C.; Hart, M. V.; Richards, M.; Chain, E. B. Formation of 6-Aminopenicillanic Acid from Penicillin by Enzymatic Hydrolysis. *Nature* **1960**, *187* (4733), 236–237. https://doi.org/10.1038/187236a0.

(56) Knox, R. A Survey of New Penicillins. *Nature* **1961**, *192* (4802), 492–496. https://doi.org/10.1038/192492a0.
(57) Acred, P.; Brown, D. M.; Turner, D. H.; Wilson, M. J. Pharmacology and Chemotherapy of Ampicillin—a New Broad-Spectrum Penicillin. *Br. J. Pharmacol. Chemother.* **1962**, *18* (2), 356–369.
(58) Smith, C. B.; Finland, M. Carbenicillin: Activity In Vitro and Absorption and Excretion in Normal Young Men. *Appl. Microbiol.* **1968**, *16* (11), 1753–1760.
(59) Bush, K. Past and Present Perspectives on β-Lactamases. *Antimicrob. Agents Chemother.* **2018**, *62* (10), e01076-18. https://doi.org/10.1128/AAC.01076-18.
(60) Matsuura, M.; Nakazawa, H.; Hashimoto, T.; Mitsuhashi, S. Combined Antibacterial Activity of Amoxicillin with Clavulanic Acid against Ampicillin-Resistant Strains. *Antimicrob. Agents Chemother.* **1980**, *17* (6), 908–911.
(61) Zasowski, E. J.; Rybak, J. M.; Rybak, M. J. The β-Lactams Strike Back: Ceftazidime-Avibactam. *Pharmacotherapy* **2015**, *35* (8), 755–770. https://doi.org/10.1002/phar.1622.
(62) Mosley, J. F.; Smith, L. L.; Parke, C. K.; Brown, J. A.; Wilson, A. L.; Gibbs, L. V. Ceftazidime-Avibactam (Avycaz). *Pharm. Ther.* **2016**, *41* (8), 479–483.
(63) Stapleton, P.; Wu, P. J.; King, A.; Shannon, K.; French, G.; Phillips, I. Incidence and Mechanisms of Resistance to the Combination of Amoxicillin and Clavulanic Acid in Escherichia Coli. *Antimicrob. Agents Chemother.* **1995**, *39* (11), 2478–2483. https://doi.org/10.1128/AAC.39.11.2478.
(64) Yan, J.-J.; Ko, W.-C.; Jung, Y.-C.; Chuang, C.-L.; Wu, J.-J. Emergence of Klebsiella Pneumoniae Isolates Producing Inducible DHA-1 β-Lactamase in a University Hospital in Taiwan. *J. Clin. Microbiol.* **2002**, *40* (9), 3121–3126. https://doi.org/10.1128/JCM.40.9.3121-3126.2002.
(65) Choi, U.; Lee, C.-R. Distinct Roles of Outer Membrane Porins in Antibiotic Resistance and Membrane Integrity in Escherichia Coli. *Front. Microbiol.* **2019**, *10*, 953. https://doi.org/10.3389/fmicb.2019.00953.
(66) Hussein, M.; Han, M.-L.; Zhu, Y.; Zhou, Q.; Lin, Y.-W.; Hancock, R. E. W.; Hoyer, D.; Creek, D. J.; Li, J.; Velkov, T. Metabolomics Study of the Synergistic Killing of Polymyxin B in Combination with Amikacin against Polymyxin-Susceptible and -Resistant Pseudomonas Aeruginosa. *Antimicrob. Agents Chemother.* **2019**, *64* (1), e01587-19. https://doi.org/10.1128/AAC.01587-19.
(67) Brennan-Krohn, T.; Pironti, A.; Kirby, J. E. Synergistic Activity of Colistin-Containing Combinations against Colistin-Resistant Enterobacteriaceae. *Antimicrob. Agents Chemother.* **2018**, *62* (10), e00873-18. https://doi.org/10.1128/AAC.00873-18.
(68) Phee, L. M.; Betts, J. W.; Bharathan, B.; Wareham, D. W. Colistin and Fusidic Acid, a Novel Potent Synergistic Combination for Treatment of Multidrug-Resistant Acinetobacter Baumannii Infections. *Antimicrob. Agents Chemother.* **2015**, *59* (8), 4544–4550. https://doi.org/10.1128/AAC.00753-15.
(69) Tyers, M.; Wright, G. D. Drug Combinations: A Strategy to Extend the Life of Antibiotics in the 21st Century. *Nat. Rev. Microbiol.* **2019**, *17* (3), 141–155. https://doi.org/10.1038/s41579-018-0141-x.
(70) Melnyk, A. H.; Wong, A.; Kassen, R. The Fitness Costs of Antibiotic Resistance Mutations. *Evol. Appl.* **2015**, *8* (3), 273–283. https://doi.org/10.1111/eva.12196.
(71) Wenzel, M.; Rautenbach, M.; Vosloo, J. A.; Siersma, T.; Aisenbrey, C. H. M.; Zaitseva, E.; Laubscher, W. E.; van Rensburg, W.; Behrends, J. C.; Bechinger, B.; Hamoen, L. W. The Multifaceted Antibacterial Mechanisms of the Pioneering Peptide Antibiotics Tyrocidine and Gramicidin S. *mBio* **2018**, *9* (5), e00802-18. https://doi.org/10.1128/mBio.00802-18.
(72) Marques, M. A.; Citron, D. M.; Wang, C. C. Development of Tyrocidine A Analogues with Improved Antibacterial Activity. *Bioorg. Med. Chem.* **2007**, *15* (21), 6667–6677. https://doi.org/10.1016/j.bmc.2007.08.007.
(73) Hancock, R. E. W.; Chapple, D. S. Peptide Antibiotics. *Antimicrob. Agents Chemother.* **1999**, *43* (6), 1317–1323. https://doi.org/10.1128/AAC.43.6.1317.
(74) Zasloff, M. Antimicrobial Peptides of Multicellular Organisms. *Nature* **2002**, *415* (6870), 389–395. https://doi.org/10.1038/415389a.
(75) Robinson, H. J.; Molitor, H. Some Toxicological and Pharmacological Properties of Gramicidin, Tyrocidine and Tyrothricin. *J. Pharmacol. Exp. Ther.* **1942**, *74* (1), 75–82.
(76) McLaughlin, M. I.; van der Donk, W. A. The Fellowship of the Rings: Macrocyclic Antibiotic Peptides Reveal an Anti-Gram-Negative Target. *Biochemistry* **2020**, *59* (4), 343–345. https://doi.org/10.1021/acs.biochem.9b01086.
(77) *WHO publishes list of bacteria for which new antibiotics are urgently needed*. https://www.who.int/news/item/27-02-2017-who-publishes-list-of-bacteria-for-which-new-antibiotics-are-urgently-needed (accessed 2023-04-03).

Chapter 2: The Mindapyrroles

This work was completed in its entirety by Ryan A. Allen. A manuscript is in preparation to be submitted to Tetrahedron Letters titled "Total Synthesis of Mindapyrroles A and B and Initial Investigations of their Antibacterial Activity". Authors: Ryan A. Allen and William M. Wuest.

As previously discussed, one way to combat antibiotic resistance is to develop antibacterials that possess novel, clinically underutilized, or polypharmacological mechanisms of action. To this end, the recently isolated mindapyrroles, two dimers and one trimer of previously identified and studied antibacterial pyoluteorin, were selected as targets for studying potentially novel mechanisms of action.

2.1 Isolation and Background of Pyoluteorin and the Mindapyrroles

2.1.1 History of Pyoluteorin

Pyoluteorin (**2.1**) was first isolated from a strain of *Pseudomonas aeruginosa*, and since has been found in various other species of soil and ocean dwelling Pseudomonads, including *P. fluorescens* and *P. protegens* (**Figure 2.1**).[1–3] More recently, it has been found that certain strains of the fungus *Aspergillus niger* can also produce pyoluteorin.[4] The broad spectrum of species that can produce this metabolite has garnered the interests of many research groups, and the biosynthesis of pyoluteorin has thus been extensively studied (**Figure 2.2**). A non-ribosomal peptide synthase (NRPS) pathway starts the biosynthesis by loading a unit of L-proline onto carrier protein PltL.[5,6] The pyrrolidine ring is then oxidized to pyrrole via PltE, followed by chlorination of the 4 and 5 positions of the pyrrole ring by PltA.[7,8] An adenylation reaction then transfers the acylpyrrole moiety to PltB, a three-module type I

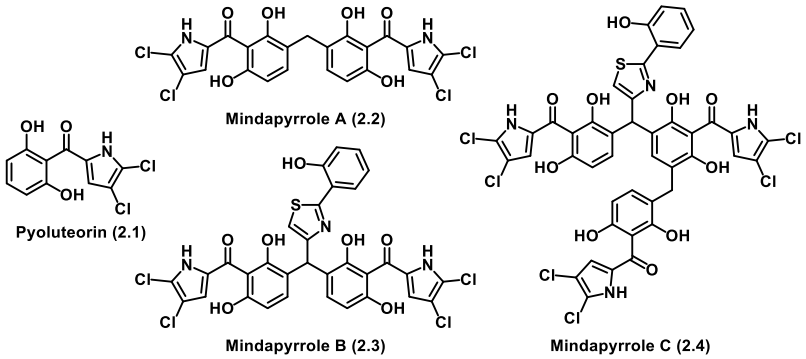

Figure 2.1 Structures of pyoluteorin and the mindapyrroles.

polyketide synthase, which facilitates the initial elongation of the acyl chain. The next module of PltB adds another acetyl group via another adenylation reaction, which is then transferred to PltC, where an additional adenylation reaction and reduction gives the acyclic molecule.[3,9] The cyclization catalyzes the cleavage of the molecule from the enzyme, and spontaneous aromatization gives the final product **2.1**.

Although much effort has been extended towards its biosynthesis, much less research has been conducted on pyoluteorin's mechanism of action. Its initial activity was confirmed against various strains of gram-positive and -negative bacteria; however, pyoluteorin has more recently been found to have even broader spectrum activity that extends to fungi and human cancer cells.[10–12] This indicates that its mechanism of action is multifaceted as it targets both prokaryotic and eukaryotic organisms. The mechanism of action study that has been published was limited to cancer cells, where the authors found that this particular drug causes the depolarization of mitochondrial membranes, leading to the upregulation of reactive oxygen species (ROS) and apoptosis-related proteins.[12] This could be due to pyoluteorin acting as a protonophore, which is typical for pyrrolomycin-like compounds.[13] Similarly structured armeniaspirol A was shown to

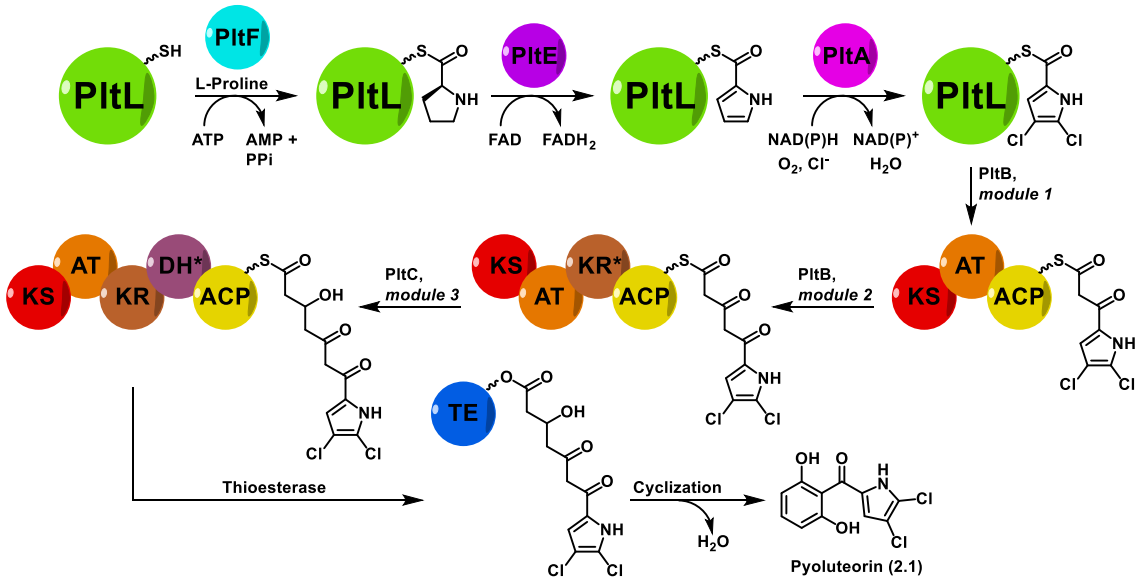

Figure 2.2 Biosynthesis of pyoluteorin.

cause bacterial cell death in gram positive bacteria via destruction of the membrane potential in addition to inhibition of the proteasome complex ClpXP.[14,15] The membrane perturbation mechanism was recapitulated in human mitochondria, where the mitochondrial membrane was shown to be depolarized via destruction of the proton gradient. Additionally, pyoluteorin has been shown to depolarize the membrane of *M. luteus*; however, it is likely that this is an incomplete explanation of its full mechanism of action.[14]

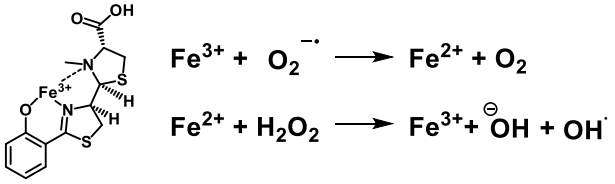

Figure 2.3 Haber-Weiss reaction catalyzed by pyochelin.

An additional explanation for pyoluteorins broad spectrum of activity could be that it binds to metals. One way antibacterials can cause cell death via metal binding is through the Haber-Weiss reaction. Specifically, the *Pseudomonas* siderophore metabolite pyochelin is known to catalyze the Haber-Weiss reaction *in vitro* and *in vivo* in *E. faecalis* (**Figure 2.3**). This occurs via reduction of iron (III) to iron (II), catalyzed by pyochelin, which in turn causes the formation of the hydroxyl radical and oxidative damage to living systems.[16] Pyochelin is also known to bind zinc (II) and copper (II), albeit in lower affinities than iron (III).[17] Pyrrole-containing compounds are known to bind metal ions, as demonstrated by the porphyrin ring of heme (**Figure 2.4**). Here, four connected pyrrole rings form a macrocycle capable of transporting iron, perhaps most famously used in oxygen and carbon dioxide transport in human hemoglobin. Other pyrrole-containing compounds, both synthetic and biometabolites, have been implicated in binding various

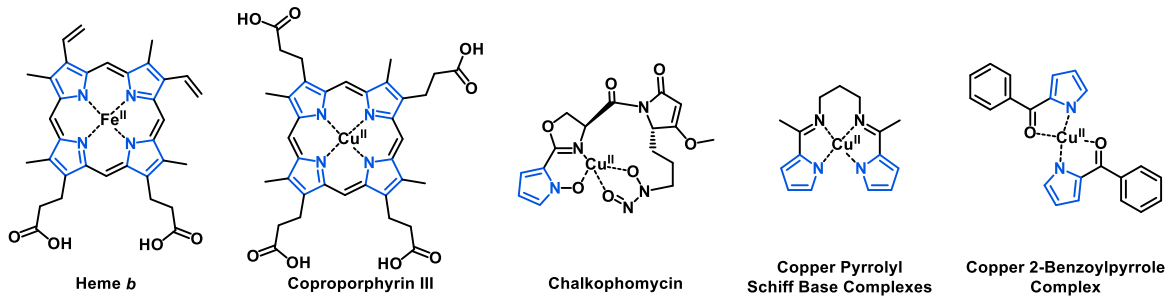

Figure 2.4 Select metal binding pyrrole-containing compounds.

other metals, such as copper and zinc. Copper has been implicated in upregulation of ROS, and it is often used as an antimicrobial in clothing.[18,19] Copper chelating biomolecules, known as chalkophores, are produced by certain species of bacteria for the tight regulation of this toxic yet necessary metal.[20] Similarly structured to heme is coproporphyrin III, a chalkophore created by such species of bacteria as *Paracoccus denitrificans* and *Rubrivivax gelatinosus* under copper starved, anaerobic conditions (**Figure 2.4**). Although these bacteria produce this molecule in copper starved conditions, the molecule can also bind zinc.[21,22] Another chalkophore, namely chalkophomycin, contains an N-hydroxypyrrole that is necessary for binding of copper (II) (**Figure 2.4**).[23] Additionally, several synthetic pyrrole-containing molecules have been assessed for their metal binding capabilities, showing the breadth of structures that can bind a breadth of metals (**Figure 2.4**). One such molecule, a pyrrolyl Schiff base complex, was shown to be able to bind copper (II), zinc (II), cobalt (II), iron (II), and nickel (II). These metal complexes were tested against *Streptococcus pyogenes* and *Klebsiella pneumonia*, with the copper (II) bound complex having MICs against both bacteria.[24] Most relatable to this work is the copper (II) complex of 2-benzoylpyrrole, which forms air and water stable crystals, suggesting that the core 2-benzoylpyrrole moiety of pyoluteorin could be binding copper.[25] Therefore, in addition to being a protonophore, pyoluteorin may also enact its mechanism of action through metal binding, catalysis of ROS generation, or general disruption of metal homeostasis.

2.1.2 Isolation of the Mindapyrroles

The mindapyrroles, along with their monomer pyoluteorin, were isolated from a species of *Pseudomonas aeruginosa* that was obtained from the gill of a shipworm (**Figure 2.1**). The authors initially found these compounds via screening in the Antibiotic Mode of Action Profiling (BioMAP) platform, which allows for hypotheses of mechanism of action by clustering with

known antibiotic activities. Pyoluteorin and the mindapyrroles clustered with other antibiotics such as monensin, a known ionophore.[26] In addition to the pyoluteorin moiety as a potential metal binder, mindapyrrole B and C have an aeruginaldehyde fragment that has been previously implicated in binding iron (III). Therefore, these aeruginaldehyde containing derivatives could be exerting their inhibitory activity through binding of iron (III) through the aeruginaldehyde moiety and binding of other metals through the 2-benzoylpyrrole moiety, as Kaplan et. al. demonstrated the specificity of aeruginaldehyde for iron (III).[27] Aside from this initial hypothesis, the mechanism of antibacterial action of the mindapyrroles remains unknown and unstudied.

2.1.3 Methods for Determining Mechanism of Action

Determination of the mechanism(s) of action (MoA) of an antibacterial compound are paramount for determining potential side effects as well as potential for resistance development. Additionally, knowing how a pharmacophore enacts its effect on living systems can be exploited to design novel drugs that could have fewer off target affects and higher affinity for the desired

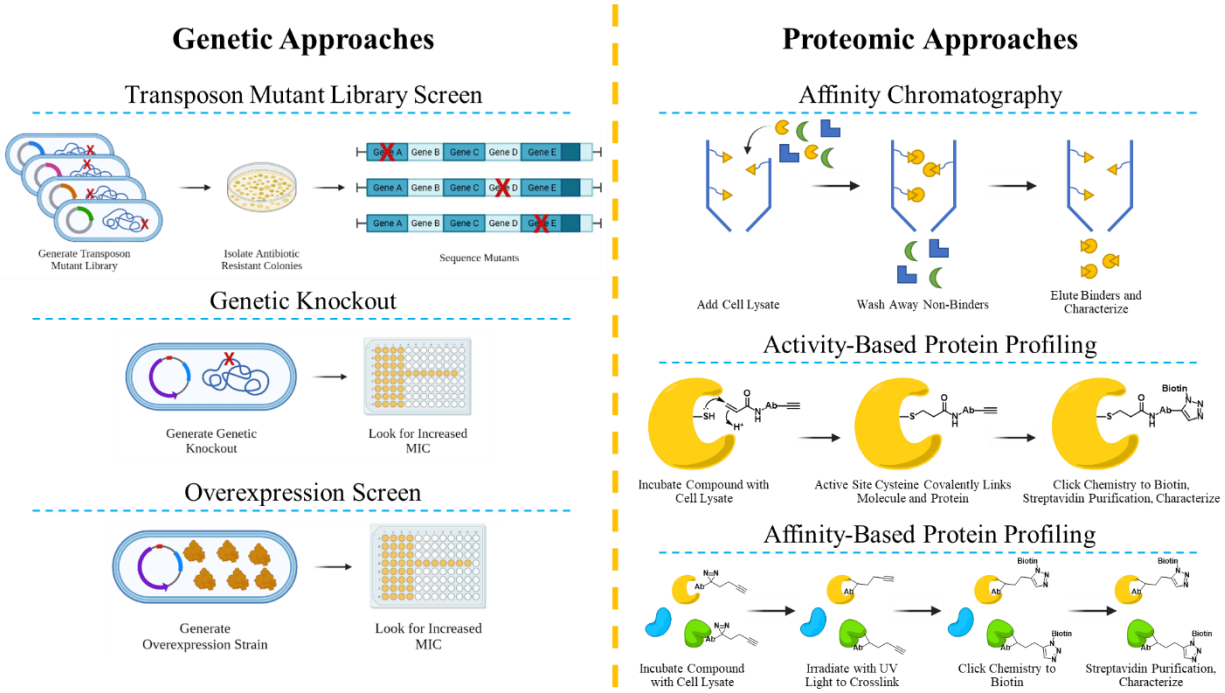

Figure 2.5 Overview of approaches to determine mechanism of action.

target. The field of MoA studies is therefore extensive and offers a variety of complimentary methods for determining how a molecule interacts with a living system. These methods can be broken down into genetic and proteomic approaches (**Figure 2.5**).

Genetic methods for determining the protein target for a molecule include such strategies as transposon mutagenesis and genetic knockouts. These types of assays can directly correlate the activity of a molecule with a certain protein or pathway. Genetic knockouts are most useful when a molecule is hypothesized to target a particular protein or pathway, as specific proteins can be genetically deleted.[28] If the molecule does target this protein or pathway, the MIC will be increased relative to the wildtype (**Figure 2.5**). A transposon mutant library shines brightest when there is no hypothesis for what protein or pathway the molecule targets, as a library of mutants can be screened to determine how the molecule enacts its mode of action by using growth inhibition as an output.[29] Transposon mutagenesis itself involves using transposons to generate this library where each mutant has a single gene knocked out, allowing for correlation of a molecule's activity with a specific gene. Similar to a genetic knockout, if a mutant does not have the protein target or pathway of the molecule, the MIC will be increased relative to the wildtype (**Figure 2.5**). However, these methods have some major drawbacks, including transposon mutants or genetic knockouts may not be viable. They may also only give information on one protein partner, making these approaches difficult for polypharmacological compounds. One way to combat the viability issues of certain genetic knockouts is to create an overexpression strain of the potential protein target; however, this requires that the strain is viable, and that the protein target is known (**Figure 2.5**).[30,31] These approaches also require a large amount of work upfront to create and validate a library of genetic knockouts, transposon mutants, or overexpression strains.

Proteomic methods typically offer a broader sweep of potential protein partners that genetic approaches typically lack (**Figure 2.5**). One of the most well utilized proteomic methods for determining the protein target of a drug is affinity chromatography. This has the advantage of purifying proteins that bind to the target molecule directly, but it suffers from a lack of sensitivity for weak binders and requires a handle to append the target molecule to a bead (**Figure 2.5**).[32–34] A more sensitive proteomic approach is activity-based protein profiling (AcBPP), where a covalent inhibitor of a protein is appended with a purification handle and is pulled from the lysate with its protein partner once covalently linked (**Figure 2.5**). This method is much more sensitive for weak binders than affinity chromatography, but it requires that the molecule covalently inhibits the protein it targets.[35,36] Although this method also requires a purification tag, it can typically be a minimally invasive alkyne, which can be appended at a variety of positions so as not to perturb protein binding. An offshoot of AcBPP is affinity-based protein profiling (AfBPP), which expands the arsenal of AcBPP to any molecule that has an affinity to binding to a protein (**Figure 2.5**). The novelty of this approach lies in appending a photoprobe with a purification tag to the molecule. The photoprobe can be activated by a typically near UV wave of light, upon which irradiation it can covalently link the molecule to its protein target.[37] Once linked, the workflow is similar for AcBPP, and multiple binding partners can be determined. This method is ideal for determining the MoA of a molecule that is potentially polypharmacological and is unknown to covalently inhibit a protein.

2.1.4 Affinity-Based Protein Profiling Overview

Affinity-based protein profiling (AfBPP) is a commonly used method for determining the MoA of a drug, especially since it can be used to identify multiple potential protein targets in a single experiment, making it ideal for compounds that may be polypharmacological. One

drawback this type of assay suffers from is that it typically requires a photoprobe and an affinity tag appended to the molecule (**Figure 2.6**).[38] This typically requires that structure activity relationships (SAR) of the molecule be determined, which can involve months of additional work to find an optimized appendage point. Additionally, the appended photoprobe may change the binding of the molecule to its protein target by masking a hydrogen bond donor/acceptor or adding additional steric bulk, which may give false negatives in the experiment.[39] Some initial photoprobes included such photoactive molecules as benzophenone. Although such a moiety can be appended to a molecule via high yielding Suzuki cross coupling chemistry, it is quite bulky and likely changes the binding mode of the molecule in the binding pocket.[40] These drawbacks have been minimized by recent advances in photoprobes, including the suite of Yao minimalist probes and the iridium photocatalysts developed by MacMillan.[41–43] However, these photoprobes still suffer from needing an appendage point, which may change the binding mode.

In more recent years, the molecule itself has been used as the photoprobe. This was in part pioneered by the Sieber group at Technical University of Munich, where they used the inherent benzophenone moiety as a photoprobe for AfBPP experiments (**Figure 2.6**). By simply appending a minimally invasive alkyne, they were able to use click chemistry to purify bound protein targets and determine that elegaphenone inhibits AlgP among other proteins in *P. aeruginosa*.[44] This

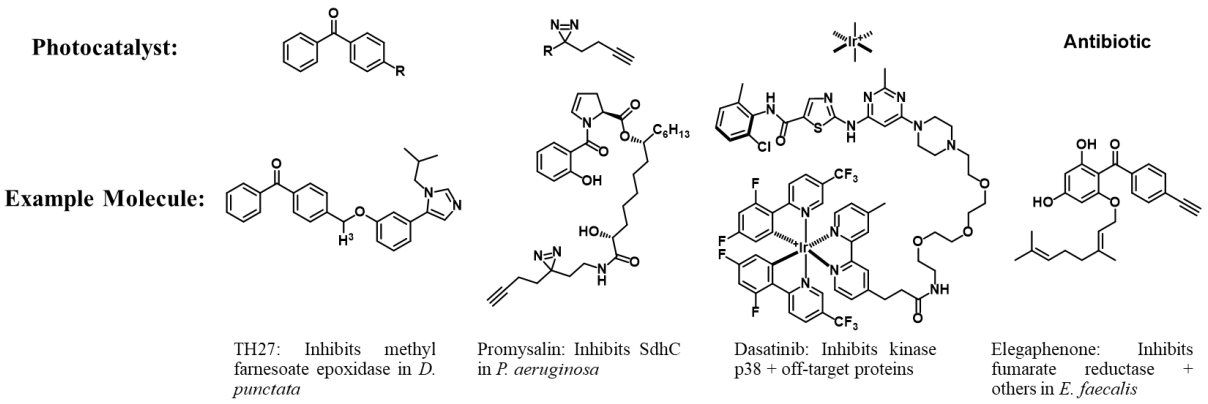

Figure 2.6 Photoprobes previously used in affinity-based protein profiling.

approach is optimal, as an alkyne affinity tag is as minimally invasive as possible for a probe-based assay. Additionally, thanks to the work of Sonogashira, alkyne cross coupling chemistry can be used to append an alkyne in minimally invasive positions that do not mask hydrogen bond donors/acceptors. This work seeks to use this type of technology in order to determine any protein binding partners of pyoluteorin and the mindapyrroles, which would implicate them as polypharmacological and give further insight into their MoA.

2.2 The 2-Benzoylpyrrole Moiety

2.2.1 2-Benzoylpyrrole in Antibacterials

The 2-benzoylpyrrole moiety is ubiquitous in both sea and soil natural product extracts, and therefore has extensive bioactivities depending on the substitution patterns of the rings (**Figure 2.7**).[45,46] Similar to both pyoluteorin and the mindapyrroles, many of them contain phenols and some degree of halogenation. The differentiation of these features is what gives each of them their specific bioactivity, although most of them share being protonophores. In addition to being protonophores, some have unique bioactivities, such as binding to actin, inhibiting virulence through inhibition of sortase A in *S. aureus*, and inhibiting proteolysis through inhibition of the ClpXP proteosome.[15,47,48] Therefore, it is plausible that the similarly structured pyoluteorin and the mindapyrroles may have a protein or enzyme target in addition to being ionophores.

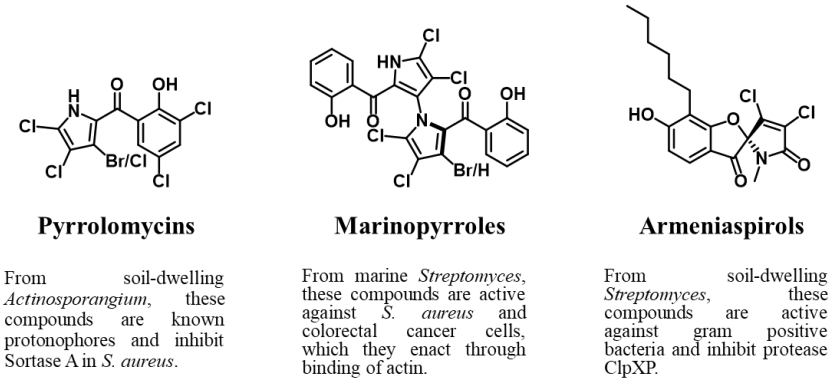

Figure 2.7 Structures and activities of previously studied 2-benzoylpyrroles.

2.2.2 Photoactivity of 2-Benzoylpyrrole

In addition to 2-benzoylpyrrole being bioactive, it is known to be photoactive as well.[49] This core scaffold behaves similarly to benzophenone insofar as both have two aromatic rings joined by a ketone bridgehead. This is where their similarities end, as they undergo two separate excitation patterns when irradiated with light (**Figure 2.8**). When irradiated with near UV light (365 nm), benzophenone is initially excited to a singlet (π-π^*) state, which then relaxes down through an internal conversion to a singlet (n-π^*) state. This state is almost isoenergetic with the triplet (π-π^*) state, which the excited molecule can access through an intersystem crossing. Once in the triplet (π-π^*) state, the molecule can relax through a second internal conversion to reach the reactive triplet (n-π^*) state.[50,51] This species can either relax back down to the ground state or react with a nearby molecule to cause hydrogen atom extraction, Patterno-Büchi oxetane formation, or triplet sensitized dimerization (**Scheme 2.1**).[51–54] Although the triplet (n- π^*) state is most reactive, recent evidence supports reaction from the triplet (π-π^*) state as well, especially in polar solvents such as water.[51,55,56]

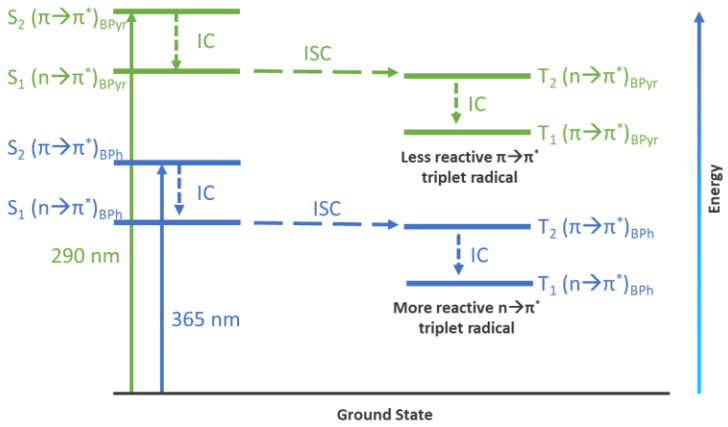

Figure 2.8 Jablonski diagrams of benzophenone (BPh, blue) and benzoylpyrrole (BPyr, green) in a polar solvent such as water.

Substituents on the benzophenone ring can have variable effects on the excitation patterns of the system. Electron donating substituents cause the energy of the n orbital to decrease and the energy of the π^* orbital to increase in polar solvents, which decreases the excitation

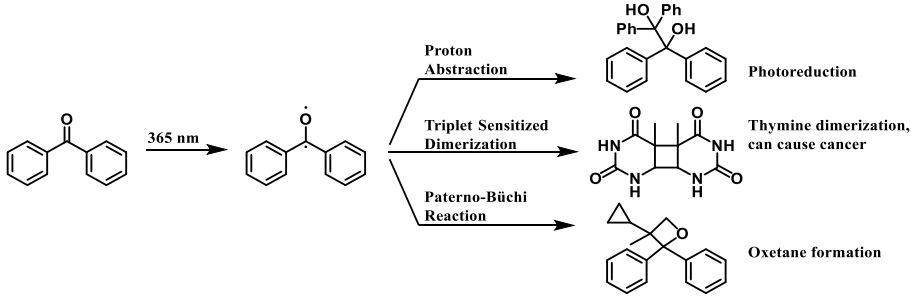

Scheme 2.1 Reactions of benzophenone triplet intermediate.

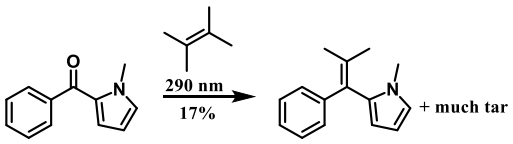

Scheme 2.2 Photocyclization of *N*-methyl-2-benzoylpyrrole with 2,3-dimethylbutene.

wavelength and conversely increases the energy required to excite the molecule to the initial singlet (*n*-π^*) state. Additionally, the triplet (*n*-π^*) diradical is electrophilic, and the addition of electron donating substituents decreases the electrophilicity and therefore reactivity of the species. Electron withdrawing substituents have the inverse effect, causing the electrophilic diradical to be more reactive.[57,58] In terms of the position of the substituents on the rings, *ortho* substituents are generally avoided as they can lead to intramolecular reactivity, thereby killing intermolecular reactivity.[51,57] However, the *ortho* and electron donating impacts on reactivity can be mitigated when the molecule is bound in an enzyme binding pocket, as was shown by the Sieber group in their work with elegaphenone.[44]

2-benzoylpyrrole varies from benzophenone in its excited state levels. The pyrrole ring, being markedly more electron rich than an aryl ring, can donate electron density into the ketone, thereby decreasing the *n* orbital energy and increasing the π^* orbital energy (**Figure 2.8**). This decreases the wavelength necessary to activate the molecule for photochemical reactions, which was reported by Cantrell.[49] Also in this report, Cantrell found that *N*-methyl-2-benzoylpyrrole reacts violently in the presence of 2,3-dimethylbutene under UV irradiation with light >290 nm. This reaction leads to "much tar" and well as a 17% yield of [2+2] cycloaddition product (**Scheme 2.2**).[49] This product is indicative of reaction through the *singlet* (*n*-π^*) state, as is the case for phenyl-β-naphthyl ketones.[59] Given this evidence, it is possible for 2-benzoylpyrroles to become excited to the somewhat reactive singlet (*n*-π^*) or triplet (π-π^*) state and react with nearby molecules. In a protein binding pocket, nearby amino acids should be the nearest reactive moieties,

which would allow for hydrogen atom abstraction followed by crosslinking, permitting the downstream steps in AfBPP.

2.3 Total synthesis of Mindapyrroles A and B

2.3.1 Retrosynthetic Design

With the ultimate goal of determining the mechanism of action of pyoluteorin and the mindapyrroles through metal fluorescence quenching titration and AfBPP, several retrosyntheses were designed to access these molecules using the simplest analog, mindapyrrole A (**2.2**), as a test scaffold (**Scheme 2.3**). Given that the total synthesis of pyoluteorin had already been completed by several different research groups,[60,61] the first route I designed focused on the dimerization of pyoluteorin (Route A). Although dimerization conditions are known for acyl phenols,[62–68] the dimerization of a 2-benzoylpyrrole containing phenols had not been previously accomplished. However, given the electronic similarity of the phenolic ring to previously dimerized phloroglucinols and the proposed biosynthesis, I hypothesized that conditions could be optimized to obtain the desired dimerized product. When biomimetic dimerization of the 2-benzoylpyrrole scaffold proved fruitless, I designed routes B and C (**Scheme 2.3**). Route B exploits the literature reported optimized conditions for acylphenol dimerizations to allow for easy access to the dimeric phenol core. The route then proceeds via the optimized synthesis of pyoluteorin, which favorably utilizes already known chemistry. Route C was inspired by the Friedel-Crafts acylation reaction and various deviations thereof, whereby resorcinol or protected derivatives can be dimerized and then reacted with acylpyrrole derivatives with or without protecting groups. The advantage of this

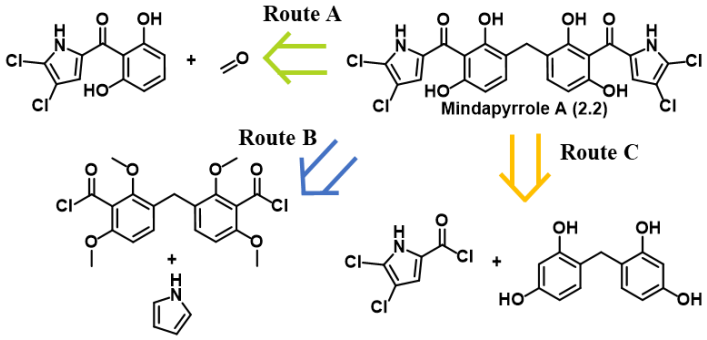

Scheme 2.3 Designed retrosynthetic routes to access the mindapyrroles using mindapyrrole A (**2.2**) as a test scaffold.

approach lies in its convergent nature, allowing for higher synthetic efficiency and a lower step count. The total synthesis of the mindapyrroles was first undertaken via route A. After this approach failed, routes B and C were attempted concurrently. After a recent total synthesis of mindapyrrole A was published, route A was revisited and used to complete the total synthesis of mindapyrroles A and B.

2.3.2 Total synthesis of Pyoluteorin and Biomimetic Dimerization Attempts

The biosynthesis of the mindapyrroles is hypothesized to take place via a dimerization of **2.1** in the cytosol onto either formaldehyde or aeruginaldehyde (**2.5**), yielding **2.2** and **2.3** (**Scheme 2.4**). Another equivalent of **2.1** and either **2.2** or **2.3** can react with the corresponding linker molecule to access **2.4**. This biosynthesis was hypothesized based on the racemic nature of **2.4**, as the highlighted bridging carbon in **Scheme 2.4** would theoretically have stereochemistry if it were synthesized by an enzyme.[26] Therefore, the biomimetic synthesis of the mindapyrroles by leveraging a stronger version of the ionic nature of the cytosol was undertaken.

Pyoluteorin was synthesized concisely following the literature precedent of Cue et al., albeit with several modifications to optimize for synthetic ease and safety (**Scheme 2.5**).[61] The

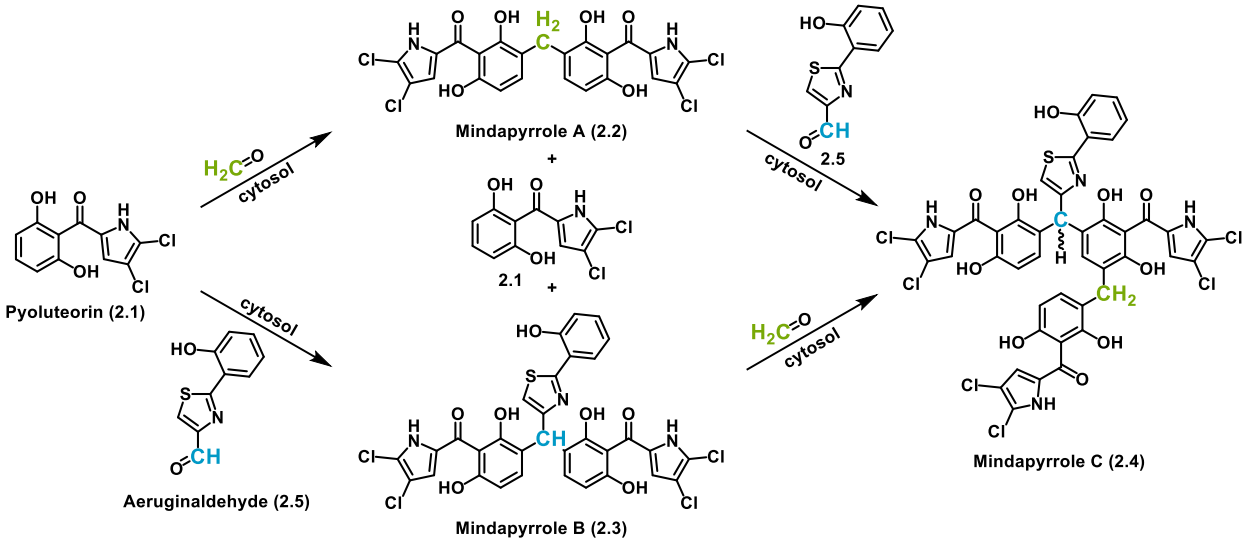

Scheme 2.4 Proposed biosynthesis of the mindapyrroles.

first reaction, a Friedel-Crafts acylation of pyrrole with tin (IV) chloride, was completed without the use of the tin catalyst as it was found to coordinate to the final product, even after aqueous workup and normal phase column purification. This was the first piece of evidence that suggested that the core 2-(2',6'-dihydroxy)benzoylpyrrole moiety of pyoluteorin could efficiently bind metals. Without the use of the tin catalyst, I was able to obtain a yield consistent with the report by Cue without the need for the toxic and strongly coordinating Lewis Acid catalyst. It is worth noting that several other literature precedents, including activating the acid with 2,2'-dithiobipyridine followed by nucleophilic addition of pyrrole deprotonated with methyl magnesium chloride first reported by K.C. Nicolaou,[69] were attempted for this reaction; however, in my hands, they did not produce product and typically returned starting materials or activated intermediates. This could be due to the nature of these reactions, typically requiring use of a Grignard reagent for the deprotonation of pyrrole, which can be easily quenched by even miniscule amounts of water. It also could be due to the electron rich nature of this particular carboxylic acid, as two ortho methoxy groups add significant electron density to the vacant π^* orbital. The next step, a methoxy deprotection, I was able to complete with boron tribromide instead of aluminum (III) bromide while increasing the yield by 9%. Aluminum (III) bromide typically comes as a fuming solid that must be weighed out, which creates corrosive hydrobromic acid gas. On the other hand, boron tribromide comes as a solution in dichloromethane that is safely transferred via syringe. The literature precedent set by Cue et al. was followed for the remaining

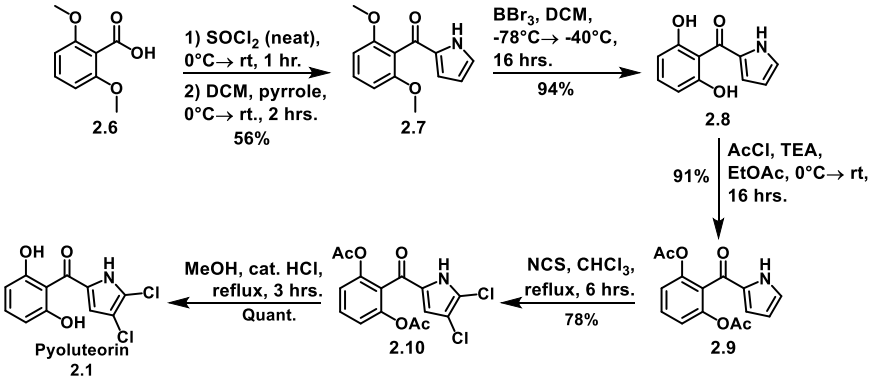

Scheme 2.5 Total synthesis of pyoluteorin (**2.1**).

three steps, albeit in slightly higher yields, to give pure pyoluteorin in 5 steps with a 37% overall yield.

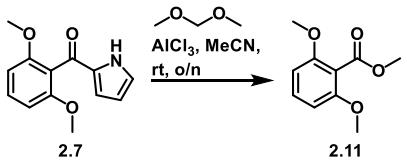

Scheme 2.6 Attempted dimerization with aluminum (III) chloride and dimethoxymethane.

With the successful synthesis of pyoluteorin, the biomimetic dimerization was attempted. Optimization proceeded mainly with different commercially available versions of formaldehyde using Brønsted-Lowry acids and bases following literature precedent to access mindapyrrole A in a biomimetic manner (**Table 2.1**).[62,65] In the case of acids, both hydrochloric acid (HCl) and phosphoric acid were tried with paraformaldehyde, both of which led to recovery of starting materials. In the case of the bases, both triethylamine and potassium hydroxide were tried with aqueous formaldehyde. Triethylamine led to recovery of starting materials, while potassium hydroxide led to degradation of pyoluteorin. This potentially could be due to nucleophilic substitution of a chlorine atom with a hydroxide on the pyrrole ring, as was seen with the substitution of a thiol for a bromine in the biosynthesis of pentabromopseudilin.[70] The dimerization was also attempted in a less biomimetic way using Lewis acids titanium (IV) chloride (**Table 2.1**) and aluminum (III) chloride (**Scheme 2.6**). When the titanium catalyst was used, some product was observed in the NMR but degraded overnight. This is potentially due to the product coordinating to the strong Lewis acid and catalyzing its own degradation. When the aluminum catalyst was used with dimethoxymethane and **2.7**, the pyrrole ring was replaced with methanol to give methoxy ester **2.11** (**Scheme 2.6**). Given these initial failures, this route was abandoned in favor of more promising routes B and C.

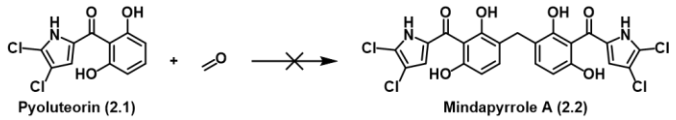

Reagent(s)	Solvent	Temperature	Activator	Result
p-formaldehyde	DCM	rt	HCl (g)	No reaction
p-formaldehyde	9:1 H_2O:DMF	85˚C	H_3PO_4	No reaction
Formaldehyde	MeOH	rt	KOH	Degradation of SM
Formaldehyde	MeOH	45˚C	TEA	No reaction
DMM	DCM	0˚C	$TiCl_4$	Product formed, then degraded

Table 2.1 Conditions attempted to dimerize **2.1** onto formaldehyde derivatives.

2.3.3 The Benzoyl Chloride Dimer Route

After the pyoluteorin dimerization route was proven to be fruitless under the tested conditions, the total synthesis of the mindapyrroles was moved forward with the benzoyl chloride dimer route (**Scheme 2.7**). This route begins with the previously troublesome dimerization that was unable to be formed with pyoluteorin. After some brief optimization, the dimerization of the benzyl ester gave **2.12** in 76% yield. The benzyl ester was selected over a typical methyl ester as the methyl ester proved to be incredibly stable to acidic or basic hydrolytic conditions. After dimerization, boiling in 4 M HCl in 1,4-dioxane, boiling in 1:1 methanol:water with sodium hydroxide, or boiling in 3:1:1 cyclopentyl methyl ether:methanol:water with lithium hydroxide failed to hydrolyze the methyl ester. Additionally, after deprotonating pyrrole with methylmagnesium bromide, addition of the pyrrole into the methyl ester did not afford any product **2.14**, as had been previously reported.[71] The free acid dimer **2.13** could also be made via direct dimerization without a carboxylic acid protecting group, albeit in a lower 45% yield and with more difficult purifications.

After the dimerization of the benzyl ester, the route proceeds by deprotection of the benzyl ester with palladium on carbon while hydrogen gas is bubbled through the solution in methanol. Ethyl acetate was found to be an unsuitable solvent for this reaction, as no product was observed when it was used, even at 50˚C. The hydrogen gas also had to be bubbled through the solution as

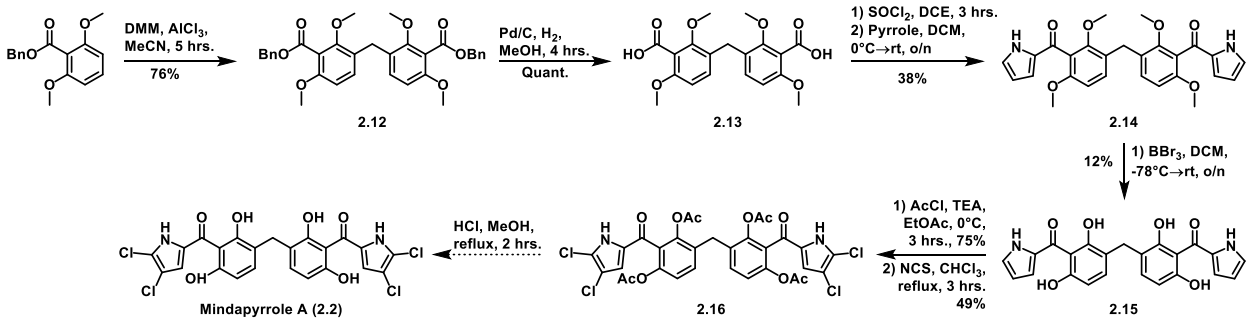

Scheme 2.7 Benzoyl chloride dimer route.

only small amounts of product **2.13** and monodeprotected product formed when the hydrogen gas was added via balloon with no bubbling. After the carboxylic acid was deprotected, thionyl chloride was used to generate the diacyl chloride for the Friedel-Crafts on pyrrole, much in the same manner as the pyoluteorin total synthesis. This Friedel-Crafts acylation did have lower yields than the pyoluteorin Friedel-Crafts due to hydrolysis of one acyl chloride to give mono-benzoylpyrrole, as well as a mixture of acylation of the 2 and 3 positions on the pyrrole.

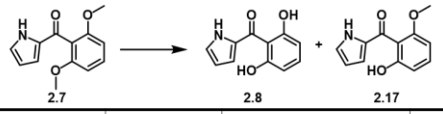

Reagent(s)	Solvent	Temperature	Time	Result
NaH, EtSH	DMF	0˚C to reflux	6 hours	**2.7** and **2.17** detected
Mg, I_2	THF	0˚C to rt	4 days	No reaction
$AlBr_3$	THF	rt	o/n	No reaction
$AlBr_3$	Toluene	rt	o/n	No reaction
$AlBr_3$	Benzene	rt	5 hours	37% of **2.8**

Table 2.2 Other methyl deprotection conditions attempted during pyoluteorin synthesis.

After the pyrrole was successfully added to the dimer, the methyl deprotection conditions optimized from the total synthesis of pyoluteorin were tried on the dimer benzoylpyrrole **2.14**. Unfortunately, this reaction stalled at the di- and tri-deprotected scaffolds and gave the fully deprotected scaffold **2.15** in poor yields. Attempts to optimize this reaction by increasing temperature or equivalents of boron tribromide led to degradation of the material. Further attempts to optimize this reaction via varying reagents was not attempted as various literature reported deprotection conditions were tried on the pyoluteorin scaffold **2.7**, none of which were higher yielding than boron tribromide (**Table 2.2**).[61,72,73] After deprotection, the acetyl protection of the phenols and chlorination of the pyrrole ring proceeded smoothly, albeit the tetrachlorination proceeded in modest yield. Finally, the acetyl hydrolysis of the protected mindapyrrole A scaffold

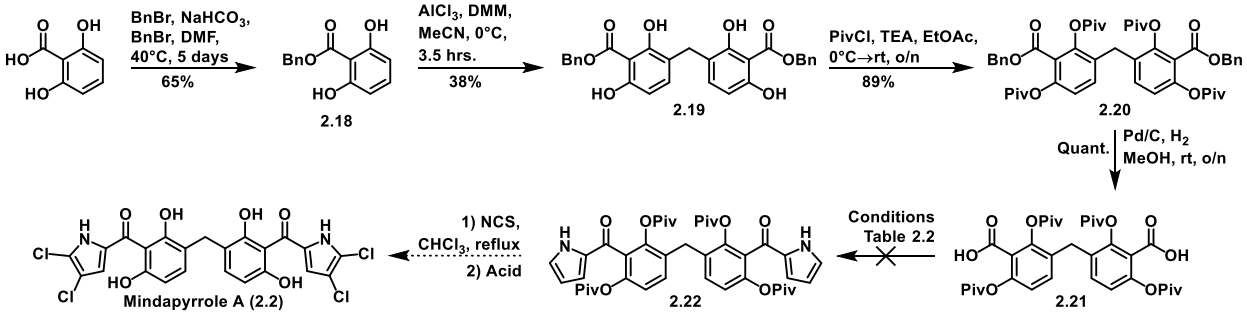

Scheme 2.8 Reinvention of the benzoyl chloride dimerization route.

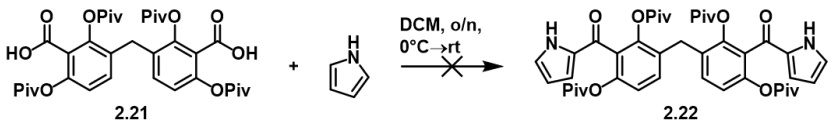

2.21 2.22

Thionyl Chloride	Temp 1	Time 1	TEA	Result
5 eq.	0˚C to rt	3 hrs.	8.7 eq.	Degradation of SM
6.1 eq.	0˚C to rt	2.5 hrs.	N/A	SM plus degradation
8.1 eq.	0˚C to 45˚C	2.5 hrs.	21 eq.	Small amounts of possible product with degraded SM

Table 2.3 Friedel-Crafts on pyrrole with dibenzoyl chloride. Temperature and time 1 refer to the temperature and time used for the formation of the acyl chloride with thionyl chloride.

was attempted with catalytic hydrochloric acid in methanol at reflux. This reaction, which typically proceeds in high yields for the monomer pyoluteorin scaffold **2.10**, gave a mixture of products that confounded the crude proton NMR. A column was attempted on the material, but as the reaction was run on only a 3.4 mg scale, the products of the reaction were lost on the column.

In an attempt to skip the low yielding methyl deprotection step, a reimagination of this route was undertaken (**Scheme 2.8**). This route features the use of the acyl protecting group from the start, thereby circumventing the need for the methyl deprotection and acyl reprotection steps. It starts with the benzyl protection of 2,6-dihydroxybenzoic acid, followed by dimerization of **2.18** onto dimethoxymethane with aluminum (III) catalysis. The phenols of **2.19** were then acyl protected with pivaloyl chloride, followed by quantitative benzyl deprotection of **2.20**. With molecule **2.21** primed for the Friedel-Crafts acylation of pyrrole, it was attempted using several different conditions (**Table 2.3**). From crude NMRs and collected fractions from columns, it seems that the acyl chloride may have formed, but the HCl side product from this formation caused the degradation of the intermediate via hydrolysis of the pivaloyl protecting groups on the phenols. Once deprotected, the phenols could add into the acyl chloride, leading to polymerization of the intermediates and their lack of reactivity to pyrrole.

2.3.4 The Friedel-Crafts Inspired Route

As deprotection and acylation strategies frustrated the benzoyl chloride dimer route, progress was made on the Friedel-Crafts inspired route. This route offered what the previous two

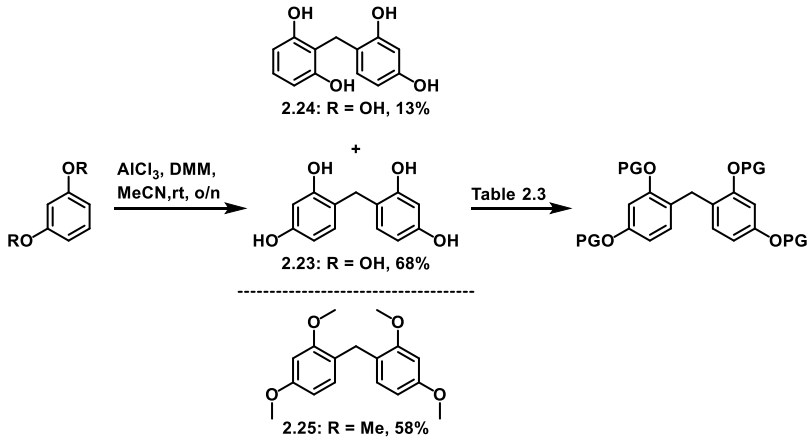

Scheme 2.9 Route to resorcinol dimer and protected derivatives thereof.

routes did not; a convergent synthesis that would allow for modularity in protecting groups and a lower longest linear step count. The chemistry for this route was also more known, as the Friedel-Crafts reaction was first discovered in 1877.[74] Since then, the Friedel-Crafts acylation has been expanded from the first reports to using a wide variety of reagents and substrates, although the best substrates are typically electron rich aryl rings.[75] This plays perfectly with the electron rich resorcinol ring that would be utilized for these reactions. Another positive factor for this route is the dimerization of resorcinol derivatives, as it is likewise well precedented.[76–78] These resorcinol dimers, trimers, and oligomers have a plethora of uses, such as wood-to-epoxy bond durability, alkali cation sequestration, and organic aerogels and xerogels.[79–81] Additionally, Labana et al reported using 1-H-pyrrole-2-carbonyl chloride as an acylating agent of a 1,3-dimethoxybenzene scaffold in their total synthesis of the armeniaspirols.[15] This route could also be amended to a derivative of the Friedel-Crafts acylation, namely the Fries rearrangement. Therefore, I sought to utilize this breadth of chemistry in the total synthesis of the mindapyrroles.

The route begins with a Friedel-Crafts dimerization of resorcinol onto dimethoxymethane (**Scheme 2.9**). This reaction proceeds cleanly to **2.23** in 68% when a large excess of resorcinol

Entry	Reagents	Temp	Time	Protecting Group	Yield
2.26	AllylBr, K_2CO_3, Acetone	rt to reflux	4 hrs.	Allyl ether	23%
2.27	BnBr, NaH, DMF	rt to 60˚C	o/n	Benzyl ether	69%
2.28	SEM-Cl, NaH, DMF	0˚C to rt	o/n	2-(trimethylsilyl) ethoxymethyl ether	14%
2.29	TBS-Cl, DBU, DCM	rt	o/n	*t*-butyldimethylsilyl ether	87%

Table 2.4 Synthesis of protected resorcinol dimers.

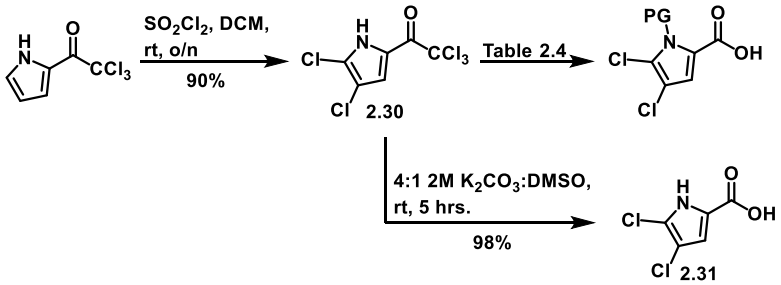

Scheme 2.10 Synthesis of un/protected pyrrolyl carboxylic acids.

is used (8 eq. of resorcinol to 1 eq. of dimethoxymethane). The large excess prevents the excessive trimerization and oligomerization products that are seen when only a small excess is used. This reaction also suffers from formation of a small amount of the undesired regioisomer, namely the ortho-ortho ortho-para isomer **2.24** (**Scheme 2.9**). This isomer is usually formed in yields between 10-15% and has been seen previously in these types of reactions.[77] The methoxy protected dimer **2.23** could also be formed using the same conditions in 58% yield. From dimer **2.23**, multiple types of protecting groups can be appended onto the molecule if deemed necessary (**Table 2.4**). Because the yields for these reactions varied greatly and typical protecting groups that can withstand the harsh conditions (O-methyl) would be difficult to remove, as previously seen, the unprotected phenol was prioritized in the Friedel-Crafts reaction.

The resorcinol dimer portion of the route then converges with the pyrrolyl acyl chloride route (**Scheme 2.10**). This synthesis begins with the dichlorination of commercially available 2-(trichloroacetyl)pyrrole, which proceeds smoothly with sulfuryl chloride in 90% yield. Some of the monochlorinated species was observed, but the trichlorinated species was not. Formation of the pyrrolyl carboxylic acid species proceeds through hydrolysis of the trichloroacetyl group in 2 M potassium carbonate, leading to a 98% yield of the carboxylic acid. The nitrogen of the pyrrole can also be protected prior to the hydrolysis (**Scheme 2.10**).

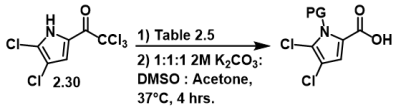

Entry	Reagents	Temp	Time	Protecting Group	Yield
2.33	AllylBr, NaH, DMF	0˚C to rt	o/n	Allyl	74%
2.34	BnBr, KO*t*Bu, 18-crown-6,	0˚C to rt	24 hrs.	Benzyl	56%
2.35	SEM-Cl, NaH, DMF	0˚C to rt	o/n	2-(trimethylsilyl) ethoxymethyl	86%
2.36	MeI, NaH, DMF	0˚C to rt	o/n	Methyl	85%

Table 2.5 Synthesis of protected pyrrolyl carboxylic acids.

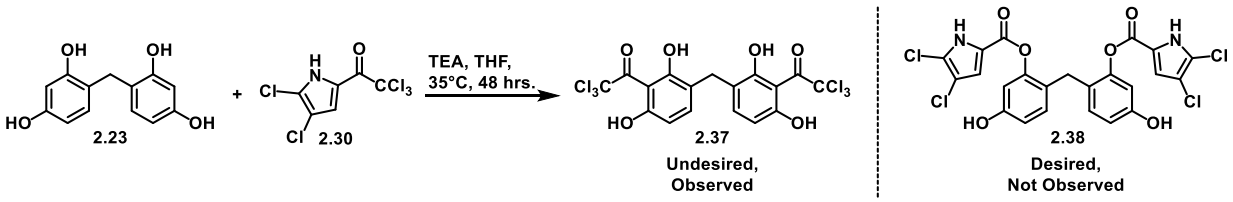

Scheme 2.11 Acylation of dimer **2.22** with trichloromethyl ketone.

This proceeds via a one-pot reaction wherein the nitrogen is protected with sodium hydride and appropriate protecting group halogen, followed by hydrolysis in 2 M potassium carbonate. This stepwise one-pot reaction yields protected pyrroles in moderate to good yields (**Table 2.5**). It is worth noting that conditions were tried to protect **2.30** with a tosyl protecting group; however, this proved fruitless despite a variety of literature reported conditions, even with freshly made tosyl chloride. The protected derivatives **2.32**, along with the unprotected **2.31**, were then ready to be coupled to the resorcinol dimers.

Given the synthetic ease of accessing **2.30**, and the wealth of literature on acyl substitutions of trichloroacetyl groups, I first attempted to acylate the phenols of the resorcinol dimer **2.23** with pyrrole derivative **2.30** using triethylamine in THF at 35˚C (**Scheme 2.11**).[82–84] Surprisingly, this reaction led only to formation of the Friedel-Crafts product **2.37**. An acyl substitution where pyrrole acts as a leaving group has been previously reported by two groups in 1983 and 1984, where they sought to use acetyl and formyl groups as protecting groups for pyrrole to prevent undesired reactivity.[85,86] These reactions typically required heating in acetic acid or refluxing benzene with *p*-toluenesulfonic acid and ethylene glycol, neopentyl glycol, or ethanedithiol to catalyze the deacylation. The subsequent Friedel-Crafts of the acyl group is, to our knowledge, novel. The regioselectivity of this reaction is also remarkable, as electrophilic aromatic substitutions at the 2 position of resorcinol are known to be challenging due to steric hinderance.[77,87] When this same reaction was catalyzed under Lewis acidic conditions, only starting materials were isolated. Similarly, when the same reaction was attempted with *N*-methyl

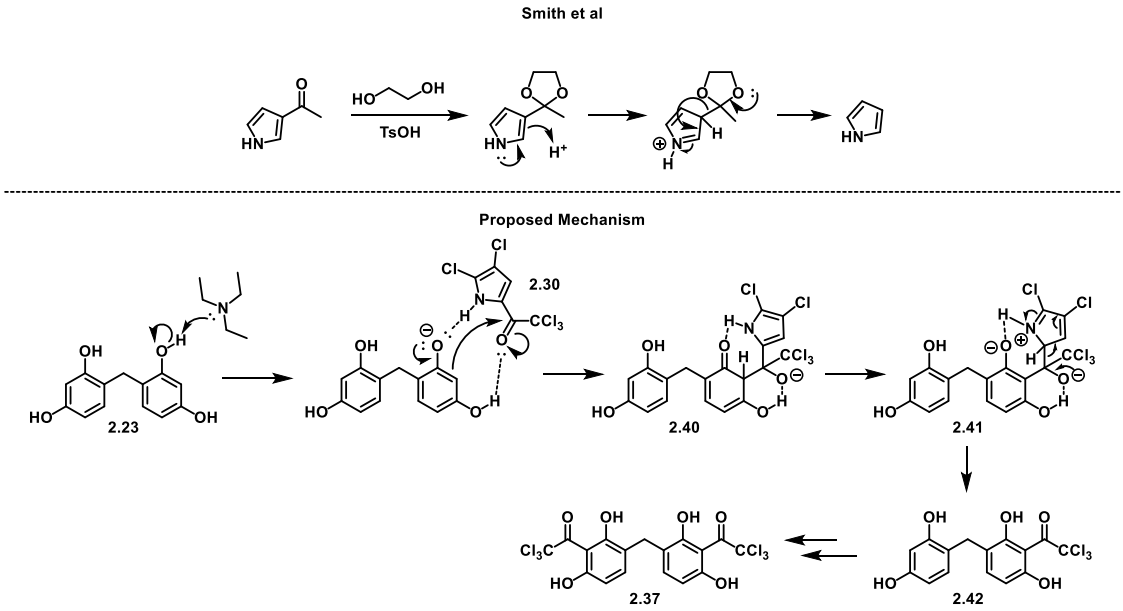

Scheme 2.12 Mechanism proposed by Smith et al for the deacylation of pyrrole with ethylene glycol an the proposed mechanism for the deacylation and Friedel-Crafts acylation of dimer **2.23** and pyrrolyl ketone **2.30**.

pyrrole derivative **2.33**, no reaction occurred and starting materials were isolated. A potential mechanism to explain this reactivity under the triethylamine buffered conditions is proposed and is based on the mechanism reported by Smith et al (**Scheme 2.12**).[85] Prior to nucleophilic attack, a hydrogen bonding network likely forms between the acyl pyrrole and dimer phenols, which likely guides the regioselectivity of this reaction to C-3. The deprotonated dimer **2.37** allows for nucleophilic addition of the phenyl ring into the carbonyl of **2.30**, which then allows for proton transfer to reform the phenyl ring aromaticity and protonate the pyrrole ring at C-2'. The positively charged pyrrole nitrogen **2.41** is likely stabilized by hydrogen bonding with the deprotonated phenol or triethylamine, and the negatively charged oxygen could be stabilized by the other phenol or triethylammonium. After the electrons from the oxygen reform the ketone and eliminate the pyrrole, the ring can rearomatize to give 2,3-dichloropyrrole. After elimination and quench, the

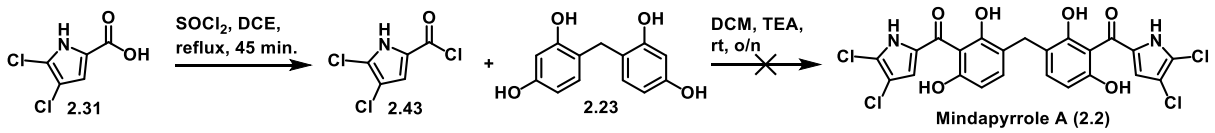

Scheme 2.13 Acylation of dimer **2.23** with pyrrolyl acyl chloride **2.43**.

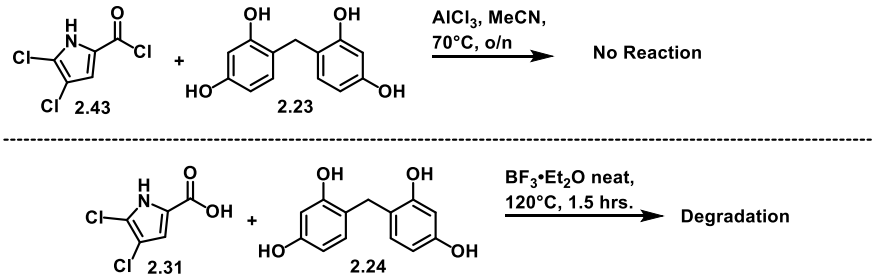

Scheme 2.14 Attempts to catalyze either a Friedel-Crafts or one-pot O-acylation then Fries rearrangement.

2,3-dichloropyrrole likely quickly degrades, as is typical for unprotected halogenated pyrroles.[88] This reaction is likely enhanced by the electron withdrawing nature of the trichloro group, as it inductively makes the carbonyl more electrophilic.

Given this initial result that proved that the resorcinol ring could be regioselectively acylated, efforts were then made to catalyze the Friedel-Crafts without need for protecting groups on the phenol. The initial triethylamine reaction was attempted with the pyrrolyl acyl chloride **2.43**, but the products were either ambiguous or degradation (**Scheme 2.13**). Given that the triethylamine catalyzed reaction seemed specific to the trichloroacetyl pyrrole **2.30**, this route was abandoned in favor of more typical Friedel-Crafts conditions, namely those that used Lewis acids.

Using the resorcinol dimer **2.23**, a variety of Lewis acids were screened to attempt to catalyze the Friedel-Crafts acylation of the unprotected system (**Scheme 2.14**). Given the demonstrated ability of the phenols to form the ester, these reactions were heated to high temperatures to attempt to catalyze the Fries rearrangement in a one-pot reaction. Starting with typical Lewis acids like aluminum (III) chloride and boron trifluoride diethyl etherate, these test reactions gave monoacylation of the unprotected phenols or

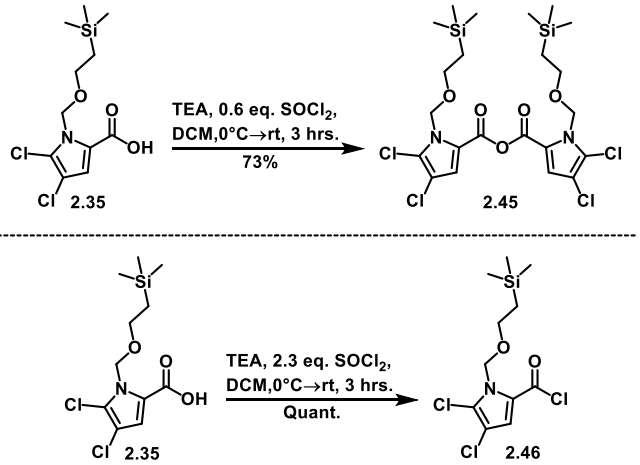

Scheme 2.15 Syntheses of *N*-SEM pyrrolyl anhydride and acyl chloride.

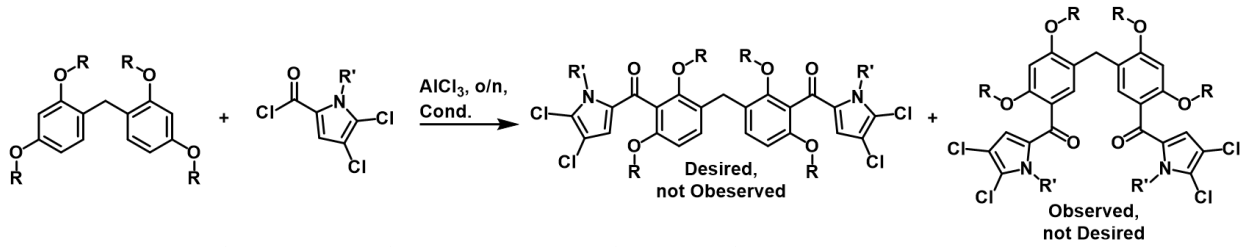

R	R'	Solvent	Temp	Result
Bn	H	DCM	-78˚C	No reaction
Bn	H	Acetonitrile	-30˚C	No reaction
Bn	SEM	DCM	-78˚C	No reaction
Bn	SEM	Acetonitrile	-30˚C	No reaction
SEM	H	DCM	-78˚C	SM + possible undesired regioisomer
SEM	H	Acetonitrile	-30˚C	SM + possible undesired regioisomer
SEM	SEM	DCM	-78˚C	SM + possible undesired regioisomer
SEM	SEM	Acetonitrile	-30˚C	SM + possible undesired regioisomer
TBS	H	DCM	-78˚C	SM + possible undesired regioisomer
TBS	H	Acetonitrile	-30˚C	SM + possible undesired regioisomer
TBS	SEM	DCM	-78˚C	SM + possible undesired regioisomer
TBS	SEM	Acetonitrile	-30˚C	SM + possible undesired regioisomer
Bn	H	Toluene	85˚C	Degradation of dimer
Bn	H	Toluene	rt	Degradation of dimer
Bn	SEM	Toluene	85˚C	Degradation of dimer
Bn	SEM	Toluene	rt	Degradation of dimer

Table 2.6 Conditions screened for the O-protected Fredel-Crafts.

no reaction in the case of aluminum (III) chloride and degradation in the case of boron trifluoride etherate.

Moving forward, various protecting groups were used on both the phenols and the nitrogen of the pyrrole to prevent potential side reactions, such as O-acylation of the dimer or N-acylation of the pyrrole. Additionally, the anhydride **2.41** was selected for screening for its ease of formation an isolation (**Scheme 2.15**). While making the SEM-protected anhydride, a byproduct was observed that had a chemical shift further downfield than the anhydride. Despite an aqueous quench and a silica gel column, the acyl chloride **2.42** was isolated from this reaction, demonstrating the unique stability of *N*-protected pyrrolyl acyl chlorides. A quick optimization of this reaction led to reproducible high yields, leading to the protected acyl chloride being screened in place of the anhydride as its higher reactivity should give better results.

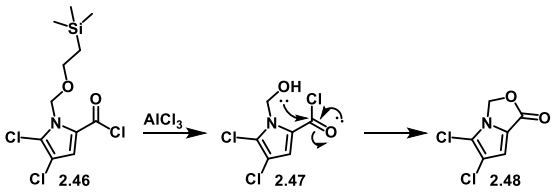

Scheme 2.16 Formation of lactone side product during the Friedel-Crafts acylation.

For the phenols, a screen of different O-protecting groups were tried (**Table 2.6**), giving a variety of deprotection condition options should they succeed. For the pyrrole, SEM was initially selected for its ease of incorporation onto the pyrrole nitrogen as well as stability over typical nitrogen protecting groups such as *tert*-butyl carbamate (Boc). These efforts proved fruitless, as any acylation that was observed was the undesired regioisomer. This reaction also demonstrated a temperature dependence, as reactions that were run above 0˚C lead to degradation of the starting materials, at least in the case of O-benzyl protected **2.27**. In the instances of no acylation observed, this was either due to no reaction taking place or the starting materials degraded. A pernicious side product that kept forming and preventing reactivity was partial cleavage of the SEM group on pyrrole to give a free alcohol, which could then add into the pyrrolyl acyl chloride, giving stable lactone **2.48** that was unreactive (**Scheme 2.16**).

Seeing as the protected phenols were giving the undesired regioselectivity, a lithium-halogen exchange was implemented to force the regioselectivity to the desired position (**Scheme 2.17**). This route starts with the dimerization of commercially available 2-bromo-1,3-dimethoxybenzene onto *para*-formaldehyde (*p*-formaldehyde). This reagent was used instead of the typical dimethoxymethane because the freed methanol byproduct typically did a nucleophilic aromatic substitution for the bromine, giving 1,2,3-trimethoxybenzene. Regardless of the methylene source, this reaction always resulted in a low yield of product due to a small amount of

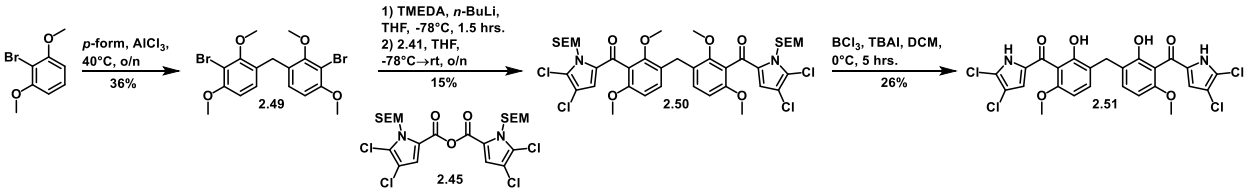

Scheme 2.17 Lithium halogen exchange route to access partially deprotected mindapyrrole A.

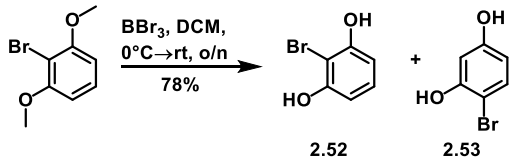

Scheme 2.18 Bromine swapping seen in methyl deprotection of 2-bromo-1,3-dimethoxybenzene.

bromine swapping between the monomers and dimers. This has been previously reported with phenol, where bromine was used as a protecting group for a nucleophilic aromatic position.[89] This reactivity is exemplified by a methyl deprotection of the monomer in the presence of boron tribromide, as bromine swapping is unavoidable (**Scheme 2.18**). Dimer **2.49** then underwent a lithium halogen exchange with *n*-butyllithium in the presence of tetramethylethylenediamine, followed by nucleophilic addition into pyrrolyl anhydride **2.45**. This reaction similarly always gave a low yield, possibly due to the steric hinderance of the ortho-ortho position of the lithiated species and the bulky anhydride. Attempts were made to optimize this reaction by using the acyl chloride **2.46** as well as the Weinreb amide; however, neither of these species gave any product using similar conditions. The methyl deprotection of the phenols was tried with boron trichloride and tetrabutylammonium iodide instead of boron tribromide as these conditions are milder and would prevent degradation of the starting material. Unfortunately, this reaction only yielded di-demethylated mindapyrrole A **2.47** in 26% yield. This reaction also serendipitously SEM deprotected the pyrrole; however, there was some degradation and the methyl deprotection did not go to completion in the given timeframe.

Given that the lithium halogen exchange route suffered from continuous low yields and the Friedel-Crafts was forming the undesired regioisomer, a protecting strategy based on previously

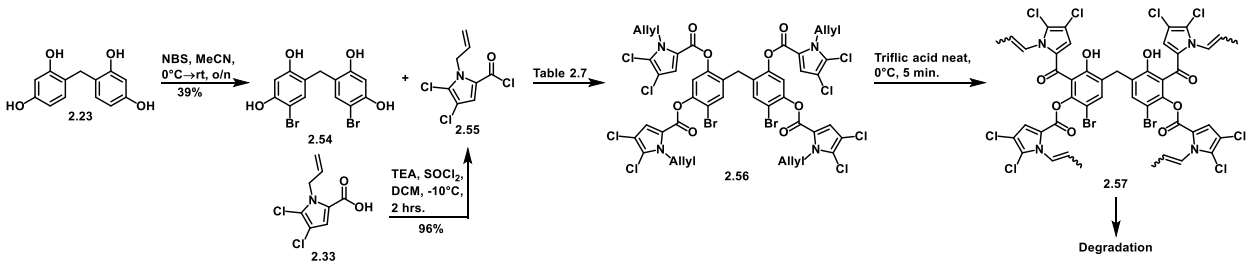

Scheme 2.19 Synthesis of the O-peracylated dimer made during the one-pot O-acylation Fries rearrangement sequence, followed by Fries rearrangement with triflic acid.

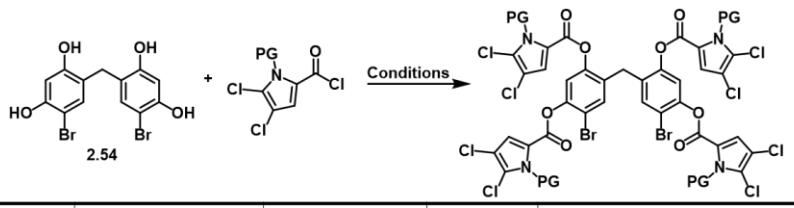

Pyrrole PG	Catalyst	Solvent	Temperature	Time	Result
Allyl	$AlCl_3$	MeCN	0˚C to reflux	2 days	Inseparable mixture of unidentifiable products
Methyl	$AlCl_3$	MeCN	0˚C to reflux	2 days	Inseparable mixture of unidentifiable products
Allyl	HFIP	HFIP	rt to 50˚C	3 days	No reaction
Methyl	HFIP	HFIP	rt to 50˚C	3 days	No reaction
Allyl	$AlCl_3$	CS_2, Nitrobenzene	50˚C	3.5 hrs.	No reaction
None	$SnCl_4$	2: DCE:MeCN	rt	o/n	Possible acylation + monomer
Allyl	$SnCl_4$	5:1 DCE:MeCN	0˚C to rt	o/n	Possible O- and C-acylation + degradation
Allyl	$AlCl_3$	20:1 DCE:MeCN	50˚C to 80˚C	5 days	42% of **2.52** + varying degrees of O-acylation
Allyl	$CsCO_3$	MeCN	rt	o/n	77% of **2.52**

Table 2.7 Conditions tried for acylation of brominated dimer **2.54**. HFIP = hexafluoroisopropanol.

seen bromine scrambling was employed to protect the problematic carbon (**Scheme 2.19**). By first dimerizing then brominating, dimer **2.50** gave rise to a variety of options for forming the desired acyl bond, including protecting group manipulations on the phenols. A plethora of conditions were then tested on the unprotected scaffold to determine the reactivity profile of this C-bromo dimer in the hopes that a one-pot O-acylation followed by a Fries rearrangement could occur without the need for additional protecting groups (**Table 2.7**). When aluminum (III) chloride was used with either the allyl or methyl protected pyrrole in acetonitrile, the reaction gave a complex mixture of varying degrees of acylation that could not be separated from one another, thereby confounding the results. Hexafluoroisopropanol (HFIP) and aluminum (III) chloride in carbon disulfide and nitrobenzene both returned unreacted starting materials. When the pyrrolyl acyl chloride was either unprotected or allyl protected, the use of tin (IV) chloride catalyzed some degree of acylation while also causing the dimer to split into its monomers. The most promising result was when aluminum (III) chloride was used in the presence of *N*-allyl pyrrolyl acyl chloride in a DCM and acetonitrile cosolvent system to give the O-peracylated dimer **2.52** in 42% yield. Some C-acylation may have occurred as well; however, the proton NMR's of the isolated products were confounded by purification difficulties and inability to differentiate between pyrrole protons and aryl protons. The

cosolvent system likely worked better than the single solvent system because aluminum (III) chloride is known to form complexes with acetonitrile. This complexation likely tamed the reactivity of the aluminum catalyst, thereby decreasing the efficiency of acylation. This reaction could also be performed with cesium carbonate to give **2.52** in 77% yield. The Fries rearrangement was then attempted on this scaffold (**Scheme 2.19**). When typical Fries rearrangement catalyst aluminum (III) chloride was used, no reaction occurred and starting materials was isolated. This result explains why aluminum (III) chloride could not catalyze the one-pot O-acylation Fries rearrangement previously attempted, as it is not a strong enough Lewis acid to do so. When trifluoromethanesulfonic acid (triflic acid) was used, the desired Fries rearrangement occurred. However, this reaction also led to the isomerization of the allyl protecting groups, which caused the products to degrade over a few hours.

The direct Friedel-Crafts acylation of brominated dimer **2.50** was also attempted by first protecting the dimer with either allyl or methyl groups (**Scheme 2.20**). A variety of temperatures were screened for this reaction; however, each temperature led to a variety of degradation products including bromine swapping and dimer splitting as seen in **Scheme 2.19**. Both aluminum (III) chloride and tin (IV) chloride catalysts led to the results shown in **Scheme 2.19**, where bromine swapping and dimer breaking into monomers was prevalent.

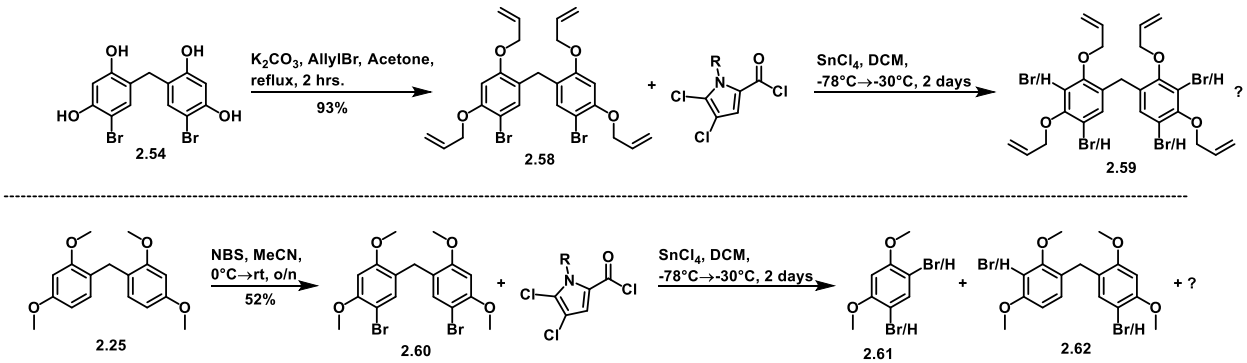

Scheme 2.20 Best attempts of the acylation of the protected brominated dimer.

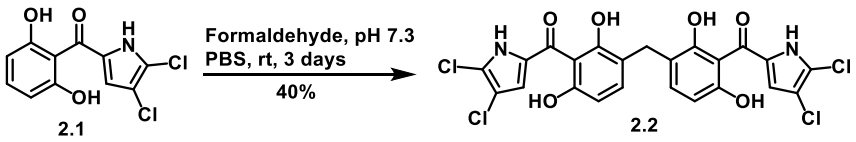

Scheme 2.21 Conditions used by Liu et al to dimerize pyoluteorin.

Although this route was initially promising as the electronics of the system seemed matched, these results demonstrate that the pyrrolyl acyl chloride and derivatives thereof are not sufficiently electron withdrawn to allow for the Friedel-Crafts reaction to occur without an abundance of side products or with desired regioselectivity. Additionally, the 2-position on resorcinol is too sterically hindered to allow for the desired reactivity in most cases.

2.3.5 Total Synthesis of Mindapyrroles A and B

As routes B and C frustratingly ground to a halt, a report from 2022 surfaced that gave credence to repursue route A. Zhi Liu and coworkers reported a biomimetic total synthesis of mindapyrrole A, where they used a phosphate buffered saline (PBS) solution to dimerize pyoluteorin onto formaldehyde (**Scheme 2.21**).[90] These exact conditions were tried in the Wuest lab, but to no avail; in my hands, the reaction returned only unreacted starting materials. Taking inspiration from this route and recognizing that the methylene source likely needs to be further activated, a rescreen of harsher conditions were tried for the total synthesis of mindapyrrole A and B using Lewis acids (**Table 2.8**). Titanium (IV) chloride was tried first as it did give some promising preliminary results; however, despite keeping the reaction as cold as possible for both the synthesis of **2.2** and **2.3**, the reagent only led to degradation of the starting materials and products. Reflecting on how well aluminum (III) chloride catalyzed the dimerization for resorcinol, it was tried in the reaction with refluxing acetonitrile. Gratifyingly, this led to formation of mindapyrrole A (**2.2**) in 81% yield. Concurrently, the dimerization was tried with

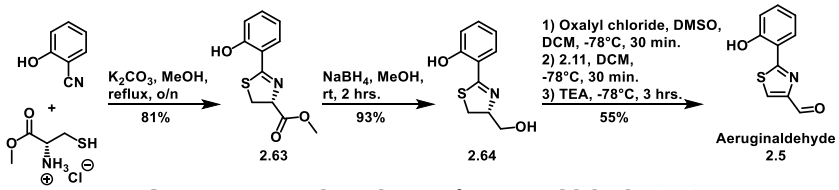

Scheme 2.22 Total synthesis of aeruginaldehyde (**2.5**).

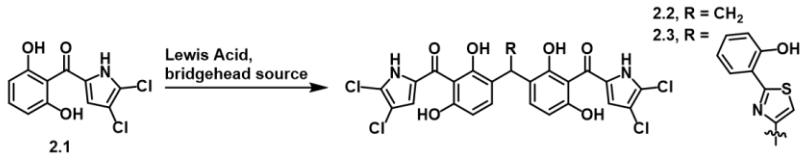

Reagent(s)	Solvent	Temperature	Activator	Result
DMM	DCM	0˚C to rt	$TiCl_4$	Product formed, then degraded
p-formaldehyde	MeCN, DCM	-42˚C to rt	$TiCl_4$	Product formed, then degraded
DMM	DCM	-78˚C	$TiCl_4$	Reaction occurred, but no product formed
DMM	MeCN	Reflux	$AlCl_3$	**2.2** in yield
Aeruginaldehyde	DCM	-12˚C	$TiCl_4$	4.1% yield, degraded later
Aeruginaldehyde	MeCN, DCM	-42˚C to rt	$TiCl_4$	Product formed, could not be purified
Aeruginaldehyde	MeCN	0˚C to rt	$AlCl_3$	Single addition of Plt
Aeruginaldehyde	MeCN	0˚C to rt	$AlCl_3$	**2.3** in 33% yield

Table 2.8 Conditions screened to access mindapyrrole A (**2.2**) and B (**2.3**).

aeruginaldehyde (**2.5**), which was synthesized following a literature reported procedure (**Scheme 2.21**).[27,91] Briefly, O-methyl cysteine is condensed onto 2-hydroxybenzonitrile to form the thiazoline ring. After reduction of the ester to the alcohol, the thiazoline ring is oxidized to the thiazole and the alcohol is oxidized to the aldehyde in a double Swern oxidation. With aeruginaldehyde (**2.5**) in hand, it was first screened with titanium (IV) chloride. Similar to the reactions with formaldehyde derivatives, this led to formation of some product that later degraded. When the reaction was tried with aluminum (III) chloride at cold temperatures, no reaction occurred. When **2.1** and **2.61** were refluxed in acetonitrile with aluminum (III) chloride, a 33% yield of mindapyrrole B (**2.3**) was obtained. This is the first reported total synthesis of mindapyrrole B and the second reported total synthesis of mindapyrrole A. It is likely that mindapyrrole C (**2.4**) could also be synthesized using these conditions, but the biological questions asked in this work could be answered with scaffolds **2.1**, **2.2**, and **2.3**.

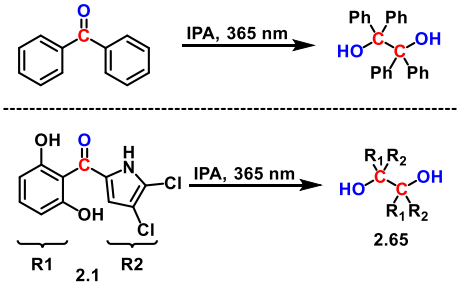

Scheme 2.22 Reported photoreduction of benzophenone in isopropanol and the analogous photoreduction with pyoluteorin (**2.1**).

2.4 Initial Photochemical Investigations of Pyoluteorin

In order to determine the ability of pyoluteorin to undergo the photochemical transformations necessary for

affinity-based protein profiling, a preliminary photoreaction was conducted. The known photoreduction of benzophenone to benzopinacol in the presence of isopropanol is a reaction that requires the intermediate goes through the reactive triplet ($n \rightarrow \pi^*$) state (**Scheme 2.22**).[92,93] This reaction was attempted on **2.1** by dissolving it in isopropanol and irradiating it with 365 nm light for 2 days. The results shown on the TLC plate in **Figure 2.9** indicate that some type of reaction occurred, as two spots other than starting material appeared on the plate. The spot on the baseline was UV active and the spot slightly above that one stained in vanillin. It is reasonable to propose that pinacol **2.62** formed, as it would likely stick to the baseline in the TLC conditions as it is extremely polar and an excellent hydrogen bond donor and acceptor with six alcohols. A proton NMR was run on the crude mixture; however, this small scale reaction did not go to completion and only miniscule amounts of the products formed, making it impossible to determine the identities of the products. This reaction is likely inefficient as **2.1** has 2 ortho groups on the phenyl ring, which can easily react with the triplet ($n \rightarrow \pi^*$) radical that is formed (**Scheme 2.23**). These ortho phenols with likely be involved in hydrogen bonding in the protein binding pocket, so these ortho reactivities will be mitigated. Additionally, only a small amount of reactivity is needed to covalently link the molecule to its protein binding partner, giving more credence to the photoactivity of **2.1**.

Figure 2.9 TLC analysis of the photoreduction of **2.1** in IPA. Left lane is starting material, middle lane is a co-spot, and right lane is the reaction mixture. TLC as run in 50% ethyl acetate in hexanes.

2.5 Biological Investigations of Pyoluteorin and the Mindapyrroles

Pyoluteorin and mindapyrroles A and B were tested against a panel of clinically relevant pathogens in a minimum inhibitory assay (**Table 2.9**). These values matched those previously reported, except for the *P. aeruginosa* strains. The original isolation paper of the mindapyrroles reported that pyoluteorin and the mindapyrroles inhibited this bacterium; however, I did not observe any inhibition of either PAO1 or PA14. As *P. aeruginosa* is the producing strain and much work has been done on the biosynthesis of pyoluteorin, it is known that this bacterium has an efflux pump encoded in the pyoluteorin operon that causes resistance to pyoluteorin in both *P. aeruginosa* and in *E. coli* when it was genetically manipulated into this strain via plasmid.[94] Additionally, this work broadened the scope of gram negative species the mindapyrroles were tested against, demonstrating their moderate to poor inhibitory activity against *E. coli* and *A. baumannii*. The MICs against the hospital-acquired (HA) and community-acquired (CA) methicillin-resistant *S. aureus* (MRSA) strains were also interesting as the HA strain was more resistant than its CA counterpart. The HA strain has been reported to be multidrug resistant, thereby giving credence to this result.[95] In a preliminary attempt to determine the mechanism of action of pyoluteorin, *S. aureus* was plated on agar plates containing either 0.25X, 0.5X, 1X, 2X, or 4X the MIC. However, no cells grew above 0.5X the MIC, even after growing for seven days. A serial passage resistance selection was then attempted, wherein MSSA cells were grown in 0.25 X, 0.5X, 1X, 2X, and 4X the MIC of pyoluteorin for 24 hours. The cells that grew in the highest MIC were then transferred over the

MIC (μM)				
	2.1	**2.2**	**2.3**	**Oxacillin**
MSSA	16	32	8	1
HA-MRSA	125	>250	250	250
CA-MRSA	16	32	16	32
E. faecalis	63	>250	>250	>250
E. coli	125	>250	>250	250
PAO1	>250	>250	>250	>250
PA14	>250	>250	>250	>250
A. baumannii	63	125	125	250

Table 2.9 MIC values of pyoluteorin and the mindapyrroles against a panel of clinically relevant bacteria.

next day to fresh wells containing concentrations adjusted for the new MIC, if there was one. Despite this assay running for 24 days, no resistance was observed against pyoluteorin.

2.6 Conclusions and Future Work

Herein I report the second total synthesis of mindapyrrole A and the first total synthesis of mindapyrrole B via dimerization of pyoluteorin onto dimethoxymethane and aeruginaldehyde. The photoactivity of pyoluteorin was assessed via a photoreduction in isopropanol, which demonstrated pyoluteorin's weak photoactivity. Pyoluteorin and the mindapyrroles were also tested against a panel of clinically relevant bacteria, and these values were in agreement with the literature or the results were supported by prior research evidence.[26,94,95] Two resistance selection assays were attempted on pyoluteorin; however, neither the solid support nor the liquid broth assay demonstrated any generation of resistance to pyoluteorin over the indicated time periods. Future work will include assessment of the photoactivity of mindapyrrole A and B as well as their antibacterial activity. Metal binding fluorescence titration assays will also be conducted to determine the metal binding portfolios of these compounds. All three compounds mentioned will then be subjected to AfBPP to determine their mechanism(s) of action.

2.7 Chapter 2 References

(1) Takeda, R. STRUCTURE OF A NEW ANTIBIOTIC, PYOLUTEORIN. *J. Am. Chem. Soc.* **1958**, *80* (17), 4749–4750. https://doi.org/10.1021/ja01550a093.

(2) Pellicciaro, M.; Padoan, E.; Lione, G.; Celi, L.; Gonthier, P. Pyoluteorin Produced by the Biocontrol Agent Pseudomonas Protegens Is Involved in the Inhibition of Heterobasidion Species Present in Europe. *Pathogens* **2022**, *11* (4), 391. https://doi.org/10.3390/pathogens11040391.

(3) Nowak-Thompson, B.; Chaney, N.; Wing, J. S.; Gould, S. J.; Loper, J. E. Characterization of the Pyoluteorin Biosynthetic Gene Cluster of Pseudomonas Fluorescens Pf-5. *J Bacteriol* **1999**, *181* (7), 2166–2174.

(4) Yu, R.; Liu, J.; Wang, Y.; Wang, H.; Zhang, H. Aspergillus Niger as a Secondary Metabolite Factory. *Front Chem* **2021**, *9*, 701022. https://doi.org/10.3389/fchem.2021.701022.

(5) Thomas, M. G.; Burkart, M. D.; Walsh, C. T. Conversion of L-Proline to Pyrrolyl-2-Carboxyl-S-PCP during Undecylprodigiosin and Pyoluteorin Biosynthesis. *Chemistry & Biology* **2002**, *9* (2), 171–184. https://doi.org/10.1016/S1074-5521(02)00100-X.

(6) Jaremko, M. J.; Lee, D. J.; Opella, S. J.; Burkart, M. D. Structure and Substrate Sequestration in the Pyoluteorin Type II Peptidyl Carrier Protein PltL. *J. Am. Chem. Soc.* **2015**, *137* (36), 11546–11549. https://doi.org/10.1021/jacs.5b04525.

(7) Thapa, H. R.; Robbins, J. M.; Moore, B. S.; Agarwal, V. Insights into Thiotemplated Pyrrole Biosynthesis Gained from the Crystal Structure of Flavin-Dependent Oxidase in Complex with Carrier Protein. *Biochemistry* **2019**, *58* (7), 918–929. https://doi.org/10.1021/acs.biochem.8b01177.
(8) Dorrestein, P. C.; Yeh, E.; Garneau-Tsodikova, S.; Kelleher, N. L.; Walsh, C. T. Dichlorination of a Pyrrolyl-S-Carrier Protein by FADH2-Dependent Halogenase PltA during Pyoluteorin Biosynthesis. *Proc Natl Acad Sci U S A* **2005**, *102* (39), 13843–13848. https://doi.org/10.1073/pnas.0506964102.
(9) Nowak-Thompson, B.; Gould, S. J.; Loper, J. E. Identification and Sequence Analysis of the Genes Encoding a Polyketide Synthase Required for Pyoluteorin Biosynthesis in Pseudomonas Fluorescens Pf-5. *Gene* **1997**, *204* (1), 17–24. https://doi.org/10.1016/S0378-1119(97)00501-5.
(10) Kraus, J.; Loper, J. E. Lack of Evidence for a Role of Antifungal Metabolite Production by Pseudomonas Fluorescens Pf-5 in Biological Control of Pythium Damping-Off of Cucumber. *Mol. Plant Pathol.* **1992**, *8* (3).
(11) Fan, D.; Yu, S.; Yang, Y.; Qu, S. Pyoluteorin Induces Apoptosis and Autophagy in NSCLC Cells. *Biological and Pharmaceutical Bulletin* **2021**, *44* (7), 976–983. https://doi.org/10.1248/bpb.b21-00120.
(12) Ding, T.; Yang, L.-J.; Zhang, W.-D.; Shen, Y.-H. Pyoluteorin Induces Cell Cycle Arrest and Apoptosis in Human Triple-Negative Breast Cancer Cells MDA-MB-231. *Journal of Pharmacy and Pharmacology* **2020**, *72* (7), 969–978. https://doi.org/10.1111/jphp.13262.
(13) Valderrama, K.; Pradel, E.; Firsov, A. M.; Drobecq, H.; Bauderlique-le Roy, H.; Villemagne, B.; Antonenko, Y. N.; Hartkoorn, R. C. Pyrrolomycins Are Potent Natural Protonophores. *Antimicrob Agents Chemother* **2019**, *63* (10), e01450-19. https://doi.org/10.1128/AAC.01450-19.
(14) Arisetti, N.; Fuchs, H. L. S.; Coetzee, J.; Orozco, M.; Ruppelt, D.; Bauer, A.; Heimann, D.; Kuhnert, E.; Bhamidimarri, S. P.; Bafna, J. A.; Hinkelmann, B.; Eckel, K.; Sieber, S. A.; Müller, P. P.; Herrmann, J.; Müller, R.; Winterhalter, M.; Steinem, C.; Brönstrup, M. Total Synthesis and Mechanism of Action of the Antibiotic Armeniaspirol A. *Chem. Sci.* **2021**, *12* (48), 16023–16034. https://doi.org/10.1039/D1SC04290D.
(15) Labana, P.; Dornan, M. H.; Lafrenière, M.; Czarny, T. L.; Brown, E. D.; Pezacki, J. P.; Boddy, C. N. Armeniaspirols Inhibit the AAA+ Proteases ClpXP and ClpYQ Leading to Cell Division Arrest in Gram-Positive Bacteria. *Cell Chemical Biology* **2021**, *28* (12), 1703-1715.e11. https://doi.org/10.1016/j.chembiol.2021.07.001.
(16) Ong, K. S.; Cheow, Y. L.; Lee, S. M. The Role of Reactive Oxygen Species in the Antimicrobial Activity of Pyochelin. *Journal of Advanced Research* **2017**, *8* (4), 393–398. https://doi.org/10.1016/j.jare.2017.05.007.
(17) Sass, G.; Miller Conrad, L. C.; Nguyen, T.-T. H.; Stevens, D. A. The Pseudomonas Aeruginosa Product Pyochelin Interferes with Trypanosoma Cruzi Infection and Multiplication in Vitro. *Trans R Soc Trop Med Hyg* **2020**, *114* (7), 492–498. https://doi.org/10.1093/trstmh/trz136.
(18) Cervantes-Cervantes, M. P.; Calderón-Salinas, J. V.; Albores, A.; Muñoz-Sánchez, J. L. Copper Increases the Damage to DNA and Proteins Caused by Reactive Oxygen Species. *Biol Trace Elem Res* **2005**, *103* (3), 229–248. https://doi.org/10.1385/BTER:103:3:229.
(19) Grass, G.; Rensing, C.; Solioz, M. Metallic Copper as an Antimicrobial Surface. *Appl Environ Microbiol* **2011**, *77* (5), 1541–1547. https://doi.org/10.1128/AEM.02766-10.
(20) Kenney, G. E.; Rosenzweig, A. C. Chalkophores. *Annu Rev Biochem* **2018**, *87*, 645–676. https://doi.org/10.1146/annurev-biochem-062917-012300.
(21) Anttila, J.; Heinonen, P.; Nenonen, T.; Pino, A.; Iwaï, H.; Kauppi, E.; Soliymani, R.; Baumann, M.; Saksi, J.; Suni, N.; Haltia, T. Is Coproporphyrin III a Copper-Acquisition Compound in Paracoccus Denitrificans? *Biochim Biophys Acta* **2011**, *1807* (3), 311–318. https://doi.org/10.1016/j.bbabio.2010.12.014.
(22) Azzouzi, A.; Steunou, A.-S.; Durand, A.; Khalfaoui-Hassani, B.; Bourbon, M.; Astier, C.; Bollivar, D. W.; Ouchane, S. Coproporphyrin III Excretion Identifies the Anaerobic Coproporphyrinogen III Oxidase HemN as a Copper Target in the Cu+-ATPase Mutant CopA− of Rubrivivax Gelatinosus. *Molecular Microbiology* **2013**, *88* (2), 339–351. https://doi.org/10.1111/mmi.12188.
(23) Gong, B.; Bai, E.; Feng, X.; Yi, L.; Wang, Y.; Chen, X.; Zhu, X.; Duan, Y.; Huang, Y. Characterization of Chalkophomycin, a Copper(II) Metallophore with an Unprecedented Molecular Architecture. *J. Am. Chem. Soc.* **2021**, *143* (49), 20579–20584. https://doi.org/10.1021/jacs.1c09311.
(24) Bandyopadhyay, D.; Layek, M.; Fleck, M.; Saha, R.; Rizzoli, C. Synthesis, Crystal Structure and Antibacterial Activity of Azido Complexes of Cobalt(III) Containing Heteroaromatic Schiff Bases. *Inorganica Chimica Acta* **2017**, *461*, 174–182. https://doi.org/10.1016/j.ica.2017.02.018.
(25) Rubino, S.; Petruso, S.; Pierattelli, R.; Bruno, G.; Stocco, G. C.; Steardo, L.; Motta, M.; Passerotto, M.; Giudice, E. D.; Gulì, G. Synthesis, Characterization, and Cytotoxic Activity of Copper(II) and Platinum(II) Complexes of 2-Benzoylpyrrole and X-Ray Structure of Bis[2-Benzoylpyrrolato(N,O)]Copper(II). *Journal of Inorganic Biochemistry* **2004**, *98* (12), 2071–2079. https://doi.org/10.1016/j.jinorgbio.2004.09.012.

(26) Lacerna, N. M. I.; Miller, B. W.; Lim, A. L.; Tun, J. O.; Robes, J. M. D.; Cleofas, M. J. B.; Lin, Z.; Salvador-Reyes, L. A.; Haygood, M. G.; Schmidt, E. W.; Concepcion, G. P. Mindapyrroles A–C, Pyoluteorin Analogues from a Shipworm-Associated Bacterium. *J. Nat. Prod.* **2019**, *82* (4), 1024–1028. https://doi.org/10.1021/acs.jnatprod.8b00979.
(27) Kaplan, A. R.; Musaev, D. G.; Wuest, W. M. Pyochelin Biosynthetic Metabolites Bind Iron and Promote Growth in Pseudomonads Demonstrating Siderophore-like Activity. *ACS Infect Dis* **2021**, *7* (3), 544–551. https://doi.org/10.1021/acsinfecdis.0c00897.
(28) Paul, A.; Anand, R.; Karmakar, S. P.; Rawat, S.; Bairagi, N.; Chatterjee, S. Exploring Gene Knockout Strategies to Identify Potential Drug Targets Using Genome-Scale Metabolic Models. *Sci Rep* **2021**, *11*, 213. https://doi.org/10.1038/s41598-020-80561-1.
(29) Freed, N. E. Creation of a Dense Transposon Insertion Library Using Bacterial Conjugation in Enterobacterial Strains Such As Escherichia Coli or Shigella Flexneri. *J Vis Exp* **2017**, No. 127, 56216. https://doi.org/10.3791/56216.
(30) Prelich, G. Gene Overexpression: Uses, Mechanisms, and Interpretation. *Genetics* **2012**, *190* (3), 841–854. https://doi.org/10.1534/genetics.111.136911.
(31) Palmer, A. C.; Kishony, R. Opposing Effects of Target Overexpression Reveal Drug Mechanisms. *Nat Commun* **2014**, *5*, 4296. https://doi.org/10.1038/ncomms5296.
(32) Rodriguez, E. L.; Poddar, S.; Iftekhar, S.; Suh, K.; Woolfork, A. G.; Ovbude, S.; Pekarek, A.; Walters, M.; Lott, S.; Hage, D. S. Affinity Chromatography: A Review of Trends and Developments over the Past 50 Years. *J Chromatogr B Analyt Technol Biomed Life Sci* **2020**, *1157*, 122332. https://doi.org/10.1016/j.jchromb.2020.122332.
(33) Hage, D. S. Affinity Chromatography: A Review of Clinical Applications. *Clin Chem* **1999**, *45* (5), 593–615.
(34) Raut, N.; Mhasade, S.; Khade, P.; Veer, V.; Bhosale, D. A. Review on Affinity Chromatography. **2021**, *6* (3).
(35) Wang, S.; Tian, Y.; Wang, M.; Wang, M.; Sun, G.; Sun, X. Advanced Activity-Based Protein Profiling Application Strategies for Drug Development. *Frontiers in Pharmacology* **2018**, *9*.
(36) Zweerink, S.; Kallnik, V.; Ninck, S.; Nickel, S.; Verheyen, J.; Blum, M.; Wagner, A.; Feldmann, I.; Sickmann, A.; Albers, S.-V.; Bräsen, C.; Kaschani, F.; Siebers, B.; Kaiser, M. Activity-Based Protein Profiling as a Robust Method for Enzyme Identification and Screening in Extremophilic Archaea. *Nat Commun* **2017**, *8* (1), 15352. https://doi.org/10.1038/ncomms15352.
(37) Murale, D. P.; Hong, S. C.; Haque, M. M.; Lee, J.-S. Photo-Affinity Labeling (PAL) in Chemical Proteomics: A Handy Tool to Investigate Protein-Protein Interactions (PPIs). *Proteome Sci* **2016**, *15* (1), 1–34. https://doi.org/10.1186/s12953-017-0123-3.
(38) Pasquer, Q. T. L.; Tsakoumagkos, I. A.; Hoogendoorn, S. From Phenotypic Hit to Chemical Probe: Chemical Biology Approaches to Elucidate Small Molecule Action in Complex Biological Systems. *Molecules* **2020**, *25* (23), 5702. https://doi.org/10.3390/molecules25235702.
(39) Medvedev, A.; Kopylov, A.; Buneeva, O.; Zgoda, V.; Archakov, A. Affinity-Based Proteomic Profiling: Problems and Achievements. *Proteomics* **2012**, *12* (4–5), 621–637. https://doi.org/10.1002/pmic.201100373.
(40) H. Wright, M.; A. Sieber, S. Chemical Proteomics Approaches for Identifying the Cellular Targets of Natural Products. *Natural Product Reports* **2016**, *33* (5), 681–708. https://doi.org/10.1039/C6NP00001K.
(41) Li, Z.; Hao, P.; Li, L.; Tan, C. Y. J.; Cheng, X.; Chen, G. Y. J.; Sze, S. K.; Shen, H.-M.; Yao, S. Q. Design and Synthesis of Minimalist Terminal Alkyne-Containing Diazirine Photo-Crosslinkers and Their Incorporation into Kinase Inhibitors for Cell- and Tissue-Based Proteome Profiling. *Angewandte Chemie International Edition* **2013**, *52* (33), 8551–8556. https://doi.org/10.1002/anie.201300683.
(42) Li, Z.; Wang, D.; Li, L.; Pan, S.; Na, Z.; Tan, C. Y. J.; Yao, S. Q. "Minimalist" Cyclopropene-Containing Photo-Cross-Linkers Suitable for Live-Cell Imaging and Affinity-Based Protein Labeling. *J. Am. Chem. Soc.* **2014**, *136* (28), 9990–9998. https://doi.org/10.1021/ja502780z.
(43) Trowbridge, A. D.; Seath, C. P.; Rodriguez-Rivera, F. P.; Li, B. X.; Dul, B. E.; Schwaid, A. G.; Buksh, B. F.; Geri, J. B.; Oakley, J. V.; Fadeyi, O. O.; Oslund, R. C.; Ryu, K. A.; White, C.; Reyes-Robles, T.; Tawa, P.; Parker, D. L.; MacMillan, D. W. C. Small Molecule Photocatalysis Enables Drug Target Identification via Energy Transfer. *Proceedings of the National Academy of Sciences* **2022**, *119* (34), e2208077119. https://doi.org/10.1073/pnas.2208077119.
(44) Zhao, W.; Cross, A. R.; Crowe-McAuliffe, C.; Weigert-Munoz, A.; Csatary, E. E.; Solinski, A. E.; Krysiak, J.; Goldberg, J. B.; Wilson, D. N.; Medina, E.; Wuest, W. M.; Sieber, S. A. The Natural Product Elegaphenone Potentiates Antibiotic Effects against Pseudomonas Aeruginosa. *Angew Chem Int Ed Engl* **2019**, *58* (25), 8581–8584. https://doi.org/10.1002/anie.201903472.

(45) Ezaki, N.; Koyama, M.; Shomura, T.; Tsuruoka, T.; Inouye, S. PYRROLOMYCINS C, D AND E, NEW MEMBERS OF PYRROLOMYCINS. *J. Antibiot.* **1983**, *36* (10), 1263–1267. https://doi.org/10.7164/antibiotics.36.1263.
(46) Hughes, C. C.; Prieto-Davo, A.; Jensen, P. R.; Fenical, W. The Marinopyrroles, Antibiotics of an Unprecedented Structure Class from a Marine Streptomyces Sp. *Org. Lett.* **2008**, *10* (4), 629–631. https://doi.org/10.1021/ol702952n.
(47) Raimondi, M. V.; Listro, R.; Cusimano, M. G.; La Franca, M.; Faddetta, T.; Gallo, G.; Schillaci, D.; Collina, S.; Leonchiks, A.; Barone, G. Pyrrolomycins as Antimicrobial Agents. Microwave-Assisted Organic Synthesis and Insights into Their Antimicrobial Mechanism of Action. *Bioorganic & Medicinal Chemistry* **2019**, *27* (5), 721–728. https://doi.org/10.1016/j.bmc.2019.01.010.
(48) Hughes, C. C.; Yang, Y.-L.; Liu, W.-T.; Dorrestein, P. C.; La Clair, J. J.; Fenical, W. Marinopyrrole A Target Elucidation by Acyl Dye Transfer. *J Am Chem Soc* **2009**, *131* (34), 12094–12096. https://doi.org/10.1021/ja903149u.
(49) Cantrell, T. S. Photochemical Reactions of 2-Acylthiophenes, -Furans, and -Pyrroles with Alkenes. *J. Org. Chem.* **1974**, *39* (15), 2242–2246. https://doi.org/10.1021/jo00929a024.
(50) Marazzi, M.; Mai, S.; Roca-Sanjuán, D.; Delcey, M. G.; Lindh, R.; González, L.; Monari, A. Benzophenone Ultrafast Triplet Population: Revisiting the Kinetic Model by Surface-Hopping Dynamics. *J. Phys. Chem. Lett.* **2016**, *7* (4), 622–626. https://doi.org/10.1021/acs.jpclett.5b02792.
(51) Dormán, G.; Nakamura, H.; Pulsipher, A.; Prestwich, G. D. The Life of Pi Star: Exploring the Exciting and Forbidden Worlds of the Benzophenone Photophore. *Chem. Rev.* **2016**, *116* (24), 15284–15398. https://doi.org/10.1021/acs.chemrev.6b00342.
(52) Murai, H.; Jinguji, M.; Obi, K. Activation Energy of Hydrogen Atom Abstraction by Triplet Benzophenone at Low Temperature. *J. Phys. Chem.* **1978**, *82* (1), 38–40. https://doi.org/10.1021/j100490a010.
(53) Gut, I. G.; Wood, P. D.; Redmond, R. W. Interaction of Triplet Photosensitizers with Nucleotides and DNA in Aqueous Solution at Room Temperature. *J. Am. Chem. Soc.* **1996**, *118* (10), 2366–2373. https://doi.org/10.1021/ja9519344.
(54) D'Auria, M.; Racioppi, R. Oxetane Synthesis through the Paternò-Büchi Reaction. *Molecules* **2013**, *18* (9), 11384–11428. https://doi.org/10.3390/molecules180911384.
(55) Liu, Q.; Locklin, J. L. Photocross-Linking Kinetics Study of Benzophenone Containing Zwitterionic Copolymers. *ACS Omega* **2020**, *5* (16), 9204–9211. https://doi.org/10.1021/acsomega.9b04493.
(56) Darmanyan, A. P.; Foote, C. S. Solvent Effects on Singlet Oxygen Yield from n,.Pi.* and .Pi.,.Pi.* Triplet Carbonyl Compounds. *J. Phys. Chem.* **1993**, *97* (19), 5032–5035. https://doi.org/10.1021/j100121a029.
(57) Boscá, F.; Miranda, M. A. Photosensitizing Drugs Containing the Benzophenone Chromophore. *J Photochem Photobiol B* **1998**, *43* (1), 1–26. https://doi.org/10.1016/s1011-1344(98)00062-1.
(58) Demeter, A.; Horváth, K.; Böőr, K.; Molnár, L.; Soós, T.; Lendvay, G. Substituent Effect on the Photoreduction Kinetics of Benzophenone. *J. Phys. Chem. A* **2013**, *117* (40), 10196–10210. https://doi.org/10.1021/jp406269e.
(59) Yang, N. C.; Kimura, Masaru.; Eisenhardt, William. Paterno-Buechi Reactions of Aromatic Aldehydes with 2-Butenes and Their Implication on the Rate of Intersystem Crossing of Aromatic Aldehydes. *J. Am. Chem. Soc.* **1973**, *95* (15), 5058–5060. https://doi.org/10.1021/ja00796a054.
(60) Davies, D. G.; Hodge, P. A Synthetic Route to Pyoluteorin. *Tetrahedron Letters* **1970**, *11* (19), 1673–1675. https://doi.org/10.1016/S0040-4039(01)98051-7.
(61) Cue Jr., B. W.; Dirlam, J. P.; Czuba, L. J.; Windisch, W. W. A Practical Synthesis of Pyoluteorin. *Journal of Heterocyclic Chemistry* **1981**, *18* (1), 191–192. https://doi.org/10.1002/jhet.5570180136.
(62) Chauthe, S. K.; Bharate, S. B.; Periyasamy, G.; Khanna, A.; Bhutani, K. K.; Mishra, P. D.; Singh, I. P. One Pot Synthesis and Anticancer Activity of Dimeric Phloroglucinols. *Bioorganic & Medicinal Chemistry Letters* **2012**, *22* (6), 2251–2256. https://doi.org/10.1016/j.bmcl.2012.01.089.
(63) Ohba, Y.; Irie, K.; Zhang, F. S.; Sone, T. Synthesis and Inclusion Properties of Carbonyl-Bridged Analogs of Acyclic p-t-Butylphenol–Formaldehyde Oligomers. *BCSJ* **1993**, *66* (3), 828–835. https://doi.org/10.1246/bcsj.66.828.
(64) Ingenfeld, B.; Straub, S.; Frömbgen, C.; Lützen, A. Synthesis of Monofunctionalized Calix[5]Arenes. *Synthesis* **2018**, *50* (3), 676–684. https://doi.org/10.1055/s-0036-1589127.
(65) Kusumaningsih, T.; E. Prasetyo, W.; R. Wibowo, F.; Firdaus, M. Toward an Efficient and Eco-Friendly Route for the Synthesis of Dimeric 2,4-Diacetyl Phloroglucinol and Its Potential as a SARS-CoV-2 Main Protease Antagonist: Insight from in Silico Studies. *New Journal of Chemistry* **2021**, *45* (17), 7830–7843. https://doi.org/10.1039/D0NJ06114J.

(66) Duarte, M. O.; Lunardelli, S.; Kiekow, C. J.; Stein, A. C.; Müller, L.; Stolz, E.; Rates, S. M. K.; Gosmann, G. Phloroglucinol Derivatives Present an Antidepressant-like Effect in the Mice Tail Suspension Test (TST). *Natural Product Communications* **2014**, *9* (5), 1934578X1400900522. https://doi.org/10.1177/1934578X1400900522.
(67) Chauthe, S. K.; Bharate, S. B.; Sabde, S.; Mitra, D.; Bhutani, K. K.; Singh, I. P. Biomimetic Synthesis and Anti-HIV Activity of Dimeric Phloroglucinols. *Bioorganic & Medicinal Chemistry* **2010**, *18* (5), 2029–2036. https://doi.org/10.1016/j.bmc.2010.01.023.
(68) Bharate, S. B.; Mudududdla, R.; Bharate, J. B.; Battini, N.; Battula, S.; Yadav, R. R.; Singh, B.; Vishwakarma, R. A. Tandem One-Pot Synthesis of Flavans by Recyclable Silica–HClO4 Catalyzed Knoevenagel Condensation and [4 + 2]-Diels–Alder Cycloaddition. *Org. Biomol. Chem.* **2012**, *10* (26), 5143–5150. https://doi.org/10.1039/C2OB25376C.
(69) Nicolaou, K. C.; Claremon, D. A.; Papahatjis, D. P. A Mild Method for the Synthesis of 2-Ketopyrroles from Carboxylic Acids. *Tetrahedron Letters* **1981**, *22* (46), 4647–4650. https://doi.org/10.1016/S0040-4039(01)83003-3.
(70) El Gamal, A.; Agarwal, V.; Rahman, I.; Moore, B. S. Enzymatic Reductive Dehalogenation Controls the Biosynthesis of Marine Bacterial Pyrroles. *J Am Chem Soc* **2016**, *138* (40), 13167–13170. https://doi.org/10.1021/jacs.6b08512.
(71) Wang, N.-C.; Anderson, H. J. Pyrrole Chemistry. XVI. Acylation of the Pyrrolyl Ambident Anion. *Can. J. Chem.* **1977**, *55* (23), 4103–4111. https://doi.org/10.1139/v77-582.
(72) Bao, K.; Fan, A.; Dai, Y.; Zhang, L.; Zhang, W.; Cheng, M.; Yao, X. Selective Demethylation and Debenzylation of Aryl Ethers by Magnesium Iodide under Solvent-Free Conditions and Its Application to the Total Synthesis of Natural Products. *Org. Biomol. Chem.* **2009**, *7* (24), 5084. https://doi.org/10.1039/b916969e.
(73) Dodge, J. A.; Stocksdale, M. G.; Fahey, K. J.; Jones, C. D. Regioselectivity in the Alkaline Thiolate Deprotection of Aryl Methyl Ethers. *J. Org. Chem.* **1995**, *60* (3), 739–741. https://doi.org/10.1021/jo00108a046.
(74) Friedel, C.; Crafts, J. M. The Alkylation or Acylation of Aromatic Compounds Catalyzed by Aluminum Chloride or Other Lewis Acids. *Compt. Rend.* **1877**, *84* (1392), 1450.
(75) M. Heravi, M.; Zadsirjan, V.; Saedi, P.; Momeni, T. Applications of Friedel–Crafts Reactions in Total Synthesis of Natural Products. *RSC Advances* **2018**, *8* (70), 40061–40163. https://doi.org/10.1039/C8RA07325B.
(76) Bouthenet, E.; Oh, K.-B.; Park, S.; Nagi, N. K.; Lee, H.-S.; Matthews, S. E. Synthesis and Antimicrobial Activity of Brominated Resorcinol Dimers. *Bioorganic & Medicinal Chemistry Letters* **2011**, *21* (23), 7142–7145. https://doi.org/10.1016/j.bmcl.2011.09.072.
(77) Li, T.; Cao, M.; Liang, J.; Xie, X.; Du, G. Mechanism of Base-Catalyzed Resorcinol-Formaldehyde and Phenol-Resorcinol-Formaldehyde Condensation Reactions: A Theoretical Study. *Polymers (Basel)* **2017**, *9* (9), 426. https://doi.org/10.3390/polym9090426.
(78) Lewicki, J. P.; Fox, C. A.; Worsley, M. A. On the Synthesis and Structure of Resorcinol-Formaldehyde Polymeric Networks – Precursors to 3D-Carbon Macroassemblies. *Polymer* **2015**, *69*, 45–51. https://doi.org/10.1016/j.polymer.2015.05.016.
(79) Sorokin, V. P.; Bobylev, V. A.; Eselev, A. D. Epoxy Resins Based on Resorcinol and Its Derivatives. *Polym. Sci. Ser. C* **2007**, *49* (3), 272–275. https://doi.org/10.1134/S1811238207030149.
(80) Vicens, J.; Böhmer, V. *Calixarenes: A Versatile Class of Macrocyclic Compounds*; Springer Science & Business Media, 2012.
(81) Tamon, H.; Ishizaka, H.; Mikami, M.; Okazaki, M. Porous Structure of Organic and Carbon Aerogels Synthesized by Sol-Gel Polycondensation of Resorcinol with Formaldehyde. *Carbon* **1997**, *35* (6), 791–796. https://doi.org/10.1016/S0008-6223(97)00024-9.
(82) Barker, P.; Gendler, P.; Rapoport, H. 2-(Trichloroacetyl)Pyrroles as Intermediates in the Preparation of 2,4-Disubstituted Pyrroles. *J. Org. Chem.* **1978**, *43* (25), 4849–4853. https://doi.org/10.1021/jo00419a029.
(83) Tietze, L. F.; Wichmann, J. Synthesis of Functionalized 1,2,3,4-Tetrahydro-β-Carbolines from Enamino Ketones. *Liebigs Annalen der Chemie* **1992**, *1992* (10), 1063–1067. https://doi.org/10.1002/jlac.1992199201175.
(84) Boche, G.; Heidenhain, F.; Thiel, W.; Eiben, R. [논문]ChemInform Abstract: AROMATICITY AS A FUNCTION OF ION-PAIR CHARACTER: ACCEPTOR-SUBSTITUTED CYCLONONATETRAENYL ANIONS, ENOLATE ANIONS WITH VARIABLE CHARGE DISTRIBUTIONS AND UNUSUAL

CONFORMATIONAL PROPERTIES. *Chemischer Informationsdienst* **1982**, *13* (48). https://doi.org/10.1002/chin.198248053.
(85) Smith, K. M.; Miura, M.; Tabba, H. D. Deacylation and Deformylation of Pyrroles. *J. Org. Chem.* **1983**, *48* (24), 4779–4781. https://doi.org/10.1021/jo00172a067.
(86) Moon, M. W.; Wade, R. A. Deacylation of Pyrrole and Other Aromatic Ketones. *J. Org. Chem.* **1984**, *49* (15), 2663–2669. https://doi.org/10.1021/jo00189a002.
(87) Durairaj, R. B. *Resorcinol: Chemistry, Technology and Applications*; Springer Science & Business Media, 2005.
(88) Cordell, G. A. 2-Halopyrroles. Synthesis and Chemistry. *J. Org. Chem.* **1975**, *40* (22), 3161–3169. https://doi.org/10.1021/jo00910a001.
(89) Effenberger, F. How Attractive Is Bromine as a Protecting Group in Aromatic Chemistry? *Angewandte Chemie International Edition* **2002**, *41* (10), 1699–1700. https://doi.org/10.1002/1521-3773(20020517)41:10<1699::AID-ANIE1699>3.0.CO;2-N.
(90) Liu, Z.; Yin, S.; Zhang, R.; Zhu, W.; Fu, P. High-Efficiency Synthesis of Carbon-Bridged Dimers via Bioinspired Green Dimerization Involving Aldehydes. *ACS Sustainable Chem. Eng.* **2022**, *10* (1), 655–661. https://doi.org/10.1021/acssuschemeng.1c07635.
(91) Zamri, A.; Abdallah, M. An Improved Stereocontrolled Synthesis of Pyochelin, Siderophore of Pseudomonas Aeruginosa and Burkholderia Cepacia - ScienceDirect. *Tetrahedron* **2000**, *56* (2), 249–256.
(92) Filipescu, N.; Minn, F. L. Photoreduction of Benzophenone in Isopropyl Alcohol. *J. Am. Chem. Soc.* **1968**, *90* (6), 1544–1547. https://doi.org/10.1021/ja01008a025.
(93) Churio, M. S.; Grela, M. A. Photochemistry of Benzophenone in 2-Propanol: An Easy Experiment for Undergraduate Physical Chemistry Courses. *J. Chem. Educ.* **1997**, *74* (4), 436. https://doi.org/10.1021/ed074p436.
(94) Huang, X.; Yan, A.; Zhang, X.; Xu, Y. Identification and Characterization of a Putative ABC Transporter PltHIJKN Required for Pyoluteorin Production in Pseudomonas Sp. M18. *Gene* **2006**, *376* (1), 68–78. https://doi.org/10.1016/j.gene.2006.02.009.
(95) Tsouklidis, N.; Kumar, R.; Heindl, S. E.; Soni, R.; Khan, S. Understanding the Fight Against Resistance: Hospital-Acquired Methicillin-Resistant Staphylococcus Aureus vs. Community-Acquired Methicillin-Resistant Staphylococcus Aureus. *Cureus 12* (6), e8867. https://doi.org/10.7759/cureus.8867.

Chapter 3: Quaternary Ammonium Compounds

This worked was completed in collaboration with the Pires lab, Minbiole lab, and fellow members of the Wuest lab. Publications and dissemination of workload indicated before each subchapter.

3.1 Introduction to Quaternary Ammonium Compounds: Past to Present

Quaternary ammonium compounds (QACs) are amphipathic molecules that consist of a positively charged nitrogen with four carbon-nitrogen bonds (head group), wherein at least one of the carbon-containing groups has a long alkyl chain (tail) (**Figure 3.1**).[1] They are ubiquitously used as surface disinfectants, antibiofouling agents, and general surfactants in a wide variety of commercial products, including toothpaste and fabric softeners.[2–6] Because of their amphipathic nature, they are excellent membrane disruptors, as membranes also typically consist of a charged head group and long alkyl tails. The mechanism of QAC membrane disruption is such that the charged nitrogen head group is electrostatically attracted to the charged cell membrane, displaces stabilizing divalent cations, followed by the long alkyl tails intercalating into the phospholipid bilayer (**Figure 3.1**).[7] Once situated in the membrane, concentration greatly affects the mechanism of these compounds, making them either bacteriostatic or bactericidal. At low concentrations, QACs permeabilize the membrane by forming a monolayer on the cell surface, causing the leakage of potassium ions and protons and an inability for the cell to regulate its turgor pressure.[7–9] At intermediate concentrations, accumulation on the inner surface of the cell membrane occurs, causing pores to form in the cell membrane and the leakage of larger cell contents such as ATP

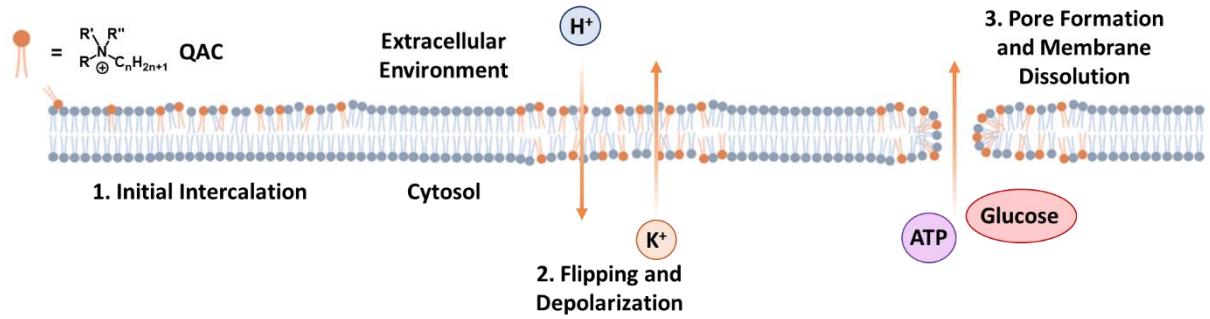

Figure 3.1 General structure of a QAC and their mechanism of action.

and metabolic pool material. At higher concentrations, QACs enact their bactericidal action by causing the complete solubilization of the membrane and coagulation of the cytosol, thereby leading to cell death.[7,10,11] Because of their positive charge, QACs tend to have selectivity for the mostly negatively charged cell membrane of bacteria, but they can also lyse more neutrally charged mammalian cells.[12] Additionally, they have been proven active against fungi and viruses, making them ideal surface disinfectants.[13]

3.1.1 Initial Discovery and Widespread Use through Covid-19

Quaternary ammonium compounds were first commercially released around 1933, although they were first discovered in 1916.[14,15] Since their release, they have been used extensively to disinfect hospital and home surfaces. Indeed, many manufacturers of hospital disinfectant sprays and home cleaning products contain QACs for their ability to kill bacteria at high concentrations. However, many of these formulations only use four types of QACs (**Figure 3.2**), and little innovation has occurred in these commercial formulations since their first sale. More specifically, these common commercial disinfectants are monoQACs, or QACs with only one positive charge.[1] Recent research has shown the improved efficacy and impedance of resistance of multicationic QACs, or QACs bearing multiple positive charges.[16,17] This lack of commercial innovation has led to the rise of disinfectant resistance amongst many strains of pathogenic bacteria, especially in light of the Covid-19 pandemic.

The pandemic caused by SARS-CoV-2 led to a massive increase in surface disinfectant usage throughout the globe. The CDC led the charge with this increase, as they recommended a list of disinfectants, almost half of them QACs, to effectively clean surfaces and kill SARS-CoV-2.[18] Indeed, studies have found increased levels

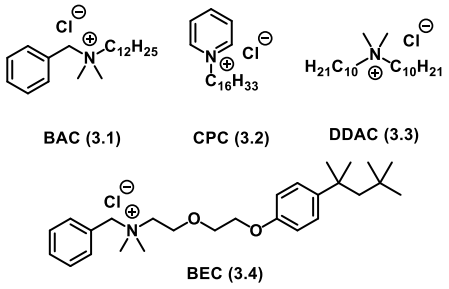

Figure 3.2 The four most common commercial QACs.

of QACs in dust samples in homes and human blood samples because of these increased cleaning protocols.[19,20] It is particularly concerning as QACs can have varied half-lives in the environment, depending on where they settle. Photolysis studies suggest they degrade within 12 to 94 days when exposed to light in water, but soil samples taken from Jamaica Bay sediments indicated that QACs did not significantly degrade over a 2 year period.[21,22] These extended half-lives, coupled with their increased use, has led to and exacerbated the problem of disinfectant resistance.

3.1.2 Development of QAC Resistance

Although the heightened use of QACs during the Covid-19 pandemic have exacerbated the QAC resistance crisis, it is certainly not novel that bacteria have acquired resistance to quaternary ammonium disinfectants. The first reported case of this type of resistance was in 1951, where a strain of *P. pyocyanea* was found to be able to live on solid cetrimide (trimethyltetradecylammonium bromide).[23] Since then, several outbreaks of this QAC resistant bacterium and others have been reported as a result of contaminated hospital disinfectant solutions.[24–26] Aside from these reports, the mechanisms of QAC resistance in gram negative pathogens is relatively understudied and underreported, although a 2004 study showed that a few bacteria known to live in drains can develop low levels of QAC resistance (2-4-fold MIC increase).[27] A 2018 report by Knauf and coworkers delved deeper into the mechanism of action of BAC (**1**) by measuring protein aggregation at sub-MIC levels. They noticed, in addition to membrane permeabilization, that **3.1** did cause a higher level of protein aggregation than the nontreated control, and therefore confirmed coagulation of the

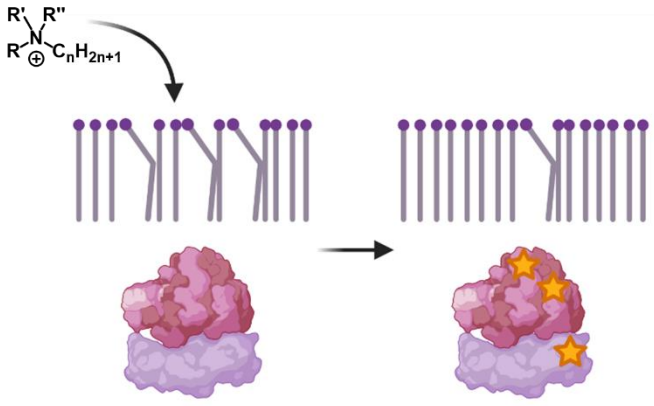

Figure 3.3 Gram negative resistance to QACs, namely through membrane rigidification and ribosomal mutations.

cytosol, albeit at lower concentrations than originally hypothesized. They then generated *A. baumannii* strains that were resistant to **3.1** via single pass treatment on an agar plate with twice the MIC (**Figure 3.3**). Interestingly, the mutations found in the genomes of the isolates were mostly in the ribosome encoding DNA, suggesting that mutations in the ribosome were somehow stabilizing the proteome.[28] Adding to this, a study from 2014 in *P. putida* demonstrated that the fatty acid content varies greatly after addition of tetradecyltrimethlyammonium bromide (**Figure 3.3**). They discovered that this bacterium decreases the unsaturated fatty acid content while upregulating its saturated fatty acid content, decreasing the fluidity of the membrane to resist QAC intercalation. Moreover, the levels of cardiolipin were found to be decreased in the presence of this QAC, thereby providing further evidence that the membrane is being rigidified to protect the bacterium.[29] In addition to these mechanisms, gram negative pathogens also upregulate efflux pumps like the small molecule resistance (SMR) efflux pumps AbeS in *A. baumannii* and EmrE in *E. coli* and *P. aeruginosa* that are known to efflux cationic disinfectants.[30–33] Much like QAC resistance in gram-negative pathogens, gram-positive resistance is likewise multifaceted and warrants further investigation.

One method gram positive bacteria are known to acquire resistance to QACs is via upregulation of efflux pumps, with one of the most notorious bacteria to do so being *S. aureus* (**Figure 3.4**). Strains of this bacterium, including MRSA strains, are known

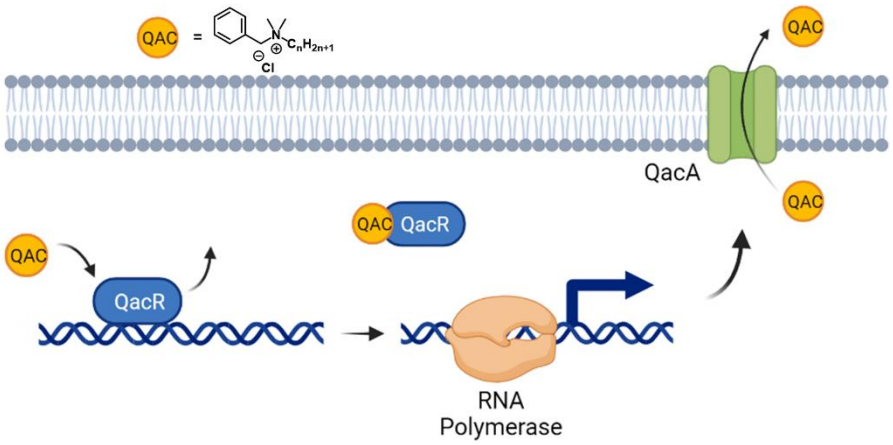

Figure 3.4 Efflux pump mechanism of resistance in gram positive bacteria such as *S. aureus*.

to harbor plasmid pSK1, which contains *qacA/R*, an efflux pump notorious for effluxing cationic small molecules.[34–36] This plasmid can also carry aminoglycoside and trimethoprim resistance, one example of the correlation between QAC resistance and antibiotic resistance.[34,37] *qacR* encodes the transcriptional regulator for *qacA*, and QacR is known to have preferential binding affinity for aryl QACs.[36,38] Once a QAC has bound to QacR, it releases the promoter region and allows for transcription and eventual translation of efflux pump QacA, which is known to efflux mono- and bis-cationic QACs.[36] However, this efflux pump system is not alone responsible for QAC resistance in community-acquired methicillin resistant *S. aureus* (CA-MRSA), a strain known to harbor multiple drug resistance genes.[38] It is likely that this strain may be rigidifying its membrane or otherwise decreasing its susceptibility to QACs by decreasing their ability to cross the membrane.

Alternatively to CA-MRSA, a recent report on QAC usage in produce processing facilities demonstrated that gram positive *L. monocytogenes* was able to achieve QAC resistance via upregulation and mutation of efflux pumps. When facility isolates were treated with sub-MIC levels of a commercial QAC disinfectant mixture, they were able to gain several mutations in fluoroquinolone efflux pump *fepR*, which corresponded with the observed increase in MIC. What is more concerning is that these mutations also caused cross resistance to 7 out of 17 tested antibiotics, such as chloramphenicol, ciprofloxacin, and kanamycin.[39] This troublesome result points to the need to develop novel QAC scaffolds that have improved activity against gram-positive and negative pathogens.

3.1.3 Novel QAC Scaffolds

A review was written on this topic was written by Kelly R. Morrison and Ryan A. Allen.
Citation: Morrison, K. R., **Allen, R. A.**, Minbiole, K. P. C., Wuest, W. M. More QACs, More Questions: Recent advances in structure activity relationships and hurdles in understanding resistance mechanisms. *Tetrahedorn Lett.* **2019** *60* (37) 150935.

To combat QAC resistance, several research groups have undertaken the development of novel QAC scaffolds.

3.1.3.1 Polymeric QAC Scaffolds

Polymeric QAC (polyQAC) scaffolds offer the opportunity for these cationic surfactants to be grafted onto coatings, thereby yielding antimicrobial surfaces.[40] Additionally, polyQACs offer a high density of positive charge to the disinfectant, which is known to positively correlate with antibacterial activity.[17] The Haldar group has provided a plethora of research on this topic, and they have thus generated a variety of polyQAC scaffolds (**Figure 3.5**). The non-surface polyQAC was based on polymaleimide (**Figure 3.5A**). These QACs were found to be selective for a variety of gram-positive and -negative pathogens, and they lysed red blood cells only at high concentrations (as measured by $Lysis_{50}$). Moreover, these QACs were able to sequester lipopolysaccharides (LPS) released by gram negative pathogens that are known to cause inflammation during infection.[41] The Haldar group was also able to design and synthesize a

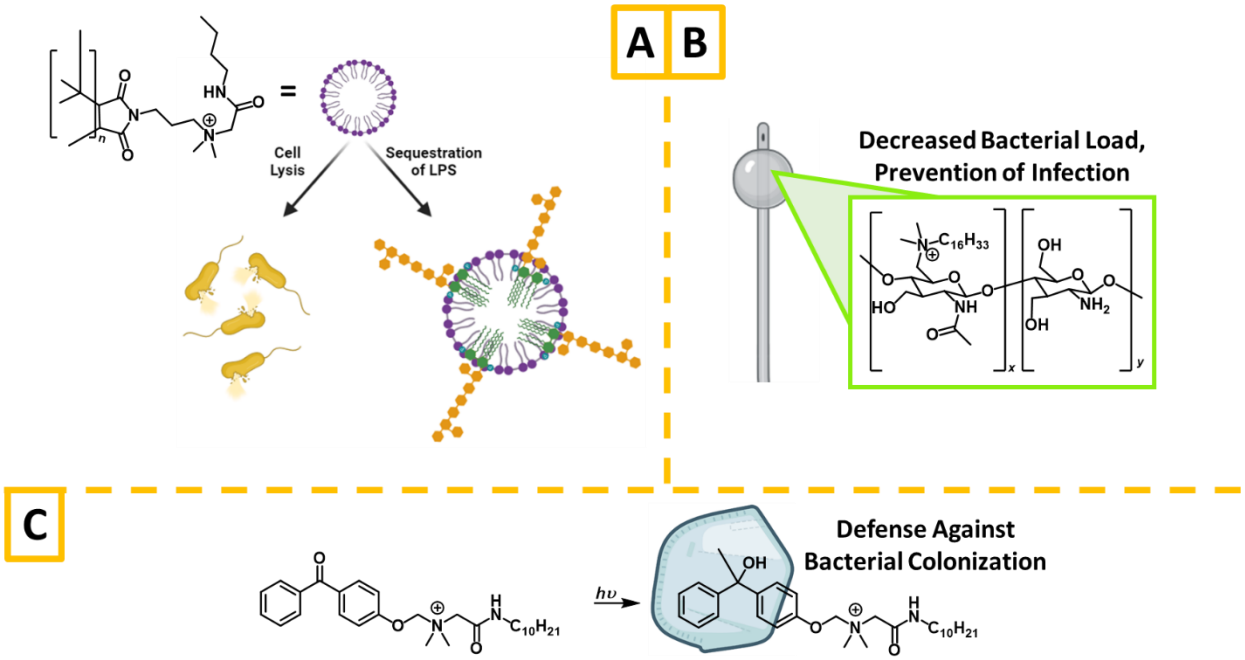

Figure 3.5 Polymeric QACs developed by the Haldar Lab.

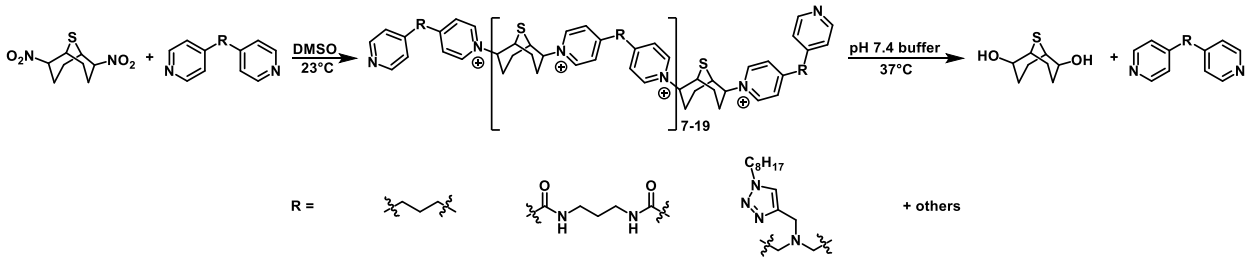

Scheme 3.1 Degradable PolyQACs synthesized by the Finn Group.

polyQAC and monoQAC that could be used as coatings. They initially developed a chitin based polyQAC that was organic soluble and aqueous insoluble that they used to coat catheters (**Figure 3.5B**). These coatings were found to significantly decrease the bacterial load and prevent the formation of biofilms on a catheter in a mouse model.[42] They were also able to append a QAC to benzophenone, which they then used to crosslink via photoexcitation to a variety of porous and nonporous surfaces (**Figure 3.5C**). Regardless of the surface, the QAC coating was able to prevent bacterial growth, thereby lending its utility to a variety of uses in the biomedical field.[43]

In addition to the Haldar group, the Finn group has developed a polyQAC that can degrade in the environment (**Scheme 3.1**).[44,45] Based on pyridinium QACs, this polymer was made with a variety of linkers between the 4-position on the pyridines and quaternized at the nitrogen using thiabicyclo[3.3.1]nonane (BCN) dinitrate. These polyQACs had an average length of 12 units, although some were as long as 20 units. The tested polyQACs had good to great activity against two gram positive and two gram negative pathogens, and they were found to degrade in aqueous media to give the BCN diol and pyridine monomers.[45] This degradation would stop them from persisting in the environment at sub-MIC levels, thereby preventing one mechanism of resistance acquisition.

3.1.3.2 QAC Appended Antibiotics

In addition to disinfecting surfaces, QACs have been appended to antibiotics to restore their efficacy against by adding another mechanism of action. As previously mentioned, this is a

viable strategy for antibiotic development, as polypharmacological compounds are more likely to resist resistance

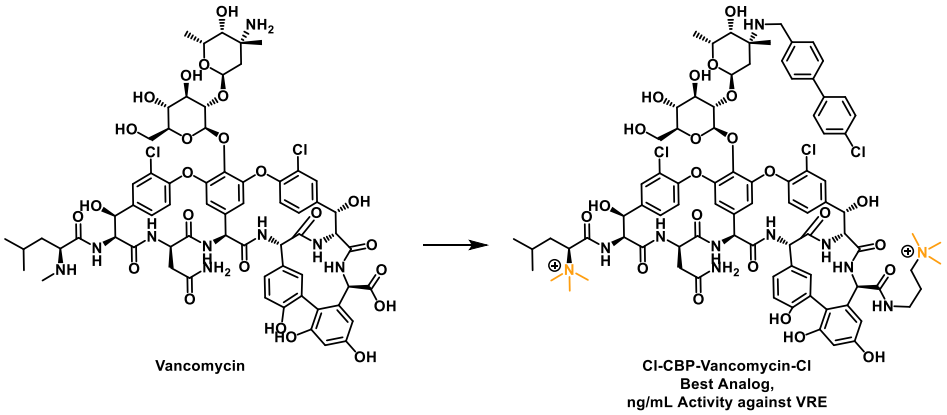

Figure 3.6 Development of vancomycin QAC analogs that can evade vancomycin resistance. QACs highlighted in gold.

development. The Boger lab achieved this by quaternizing the N-terminus of vancomycin and appending a trimethyl QAC to the C-terminus via an amide linker, among other analogs (**Figure 3.6**). Through this study, they were able to restore vancomycin's efficacy against VanA and VanB vancomycin-resistant *E. faecalis* and *E. faecium*. Additionally, they were able to show that the membrane was being depolarized as a result of the QAC additions.[46]

3.1.3.3 Small Molecule QACs

One of the most prolific groups in terms of small molecule QAC development is the Minbiole group at Villanova University. Since their first series of biscephalic QACs,[47] they have generated a library of over 800 compounds, exploring a range of cationic amphiphiles with multiple cations, varying chain lengths, and varying core architectures. One of the core innovations

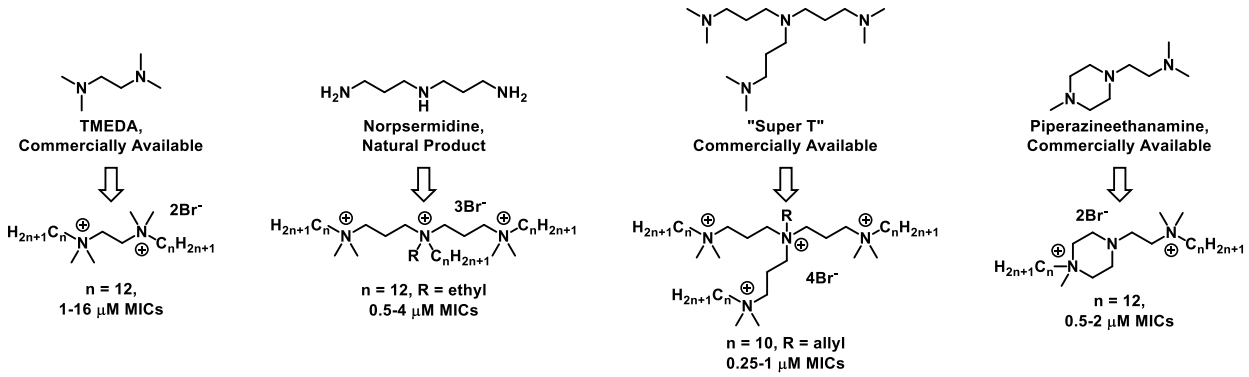

Figure 3.7 Especially efficacious multiQACs based on natural product and natural product-like polyamine scaffolds.

they have added to the field is the exploration of quaternized natural product polyamines that resemble commercial QAC DDAC (**3.3**) (**Figure 3.7**). Starting from industrially made tetramethylethylenediamine (TMEDA), they quickly spread into quaternizing amines based on natural products such as norspermidine.[48] These bis-, tris-, and tetraQACs had increased efficacy against CA-MRSA, as well as gram negative pathogens such as *P. aeruginosa* and *E. coli*, when compared to commercial monoQACs.[17,48–50] Additionally, they were found to not induce resistance over 24 days in methicillin-susceptible *S. aureus* (MSSA). On the contrary, commercial monoQACs quickly induced resistance over 10-17 days.[51] These results show promise for the development of commercially affordable and extremely effective QACs that are likely to slow resistance development in the environment.

Also noting the efficacy of pyridinium- and benzyl-based QACs like commercial BAC (**3.1**) and CPC (**3.2**), the Minbiole lab also undertook the development of novel multiQACs based on these structures (**Figure 3.8**). Starting with pyridiniums, some of the most efficacious QACs developed were among the first. Their bispyridinium "paraquats" consisted of a range of 4,4'-bisQACs with chain lengths varying from 8-20 carbons in length. The side chains were also varied on either side, thereby giving rise to unsymmetrical bisQACs. Regardless, the most active QAC was symmetrical with 12 carbon chains on either side.[52] Expanding beyond directly linked aryl

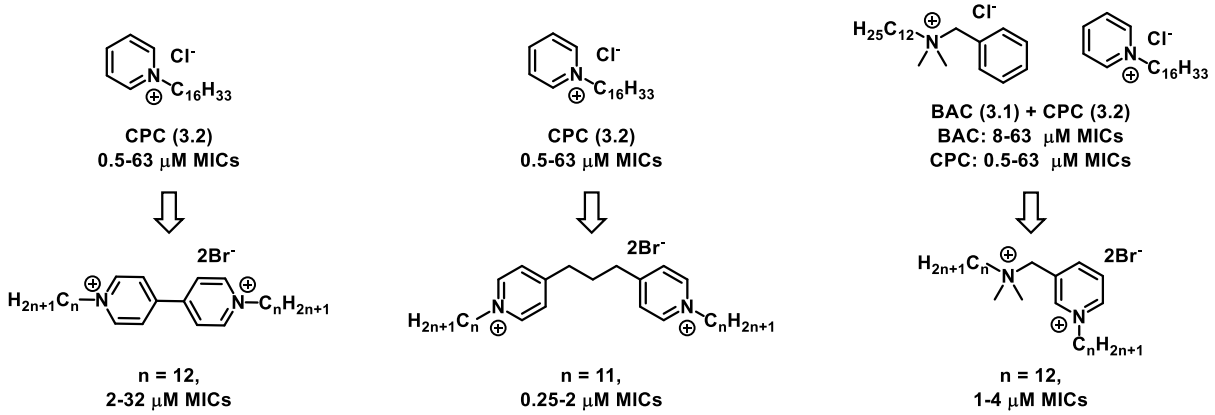

Figure 3.8 Pyridinium bisQACs based on commercial CPC (**3.2**).

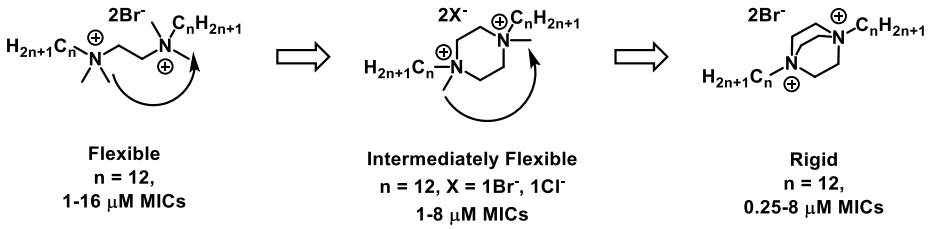

Figure 3.9 Rigidity-activity studies on bisQACs, ranging from flexible/unconstrained to rigid/constrained.

systems, they also developed a range of linked bis- and tris-pyridinium QACs, the most active being the 3-carbon linked bisQACs with two 11 carbon chains.[53] Again noting the structures of commercial QACs, they combined **3.1** and **3.2** to give bisQACs that had increased efficacy over their commercial monoQAC counterparts.[54]

After confirming the increased efficacy of flexible multiQACs over monoQACs, the Minbiole Lab prepared a series of linked bisQACs, ranging from unconstrained TMEDA to cyclic dimethyl piperazine to constrained bicyclic 1,4-diazabicyclo[2.2.2]octane (DABCO) to determine the effect of rigidity on activity (**Figure 3.9**). Synthesizing a range of QACs from 8 to 18 carbons in long alkyl chain length with some having amides in the long chain, they found that as the structures became more rigid, the activity increased. The most active DABCO compound had a 12-carbon chain, which is typical for QACs, as previously discovered. This trend was true for the other tested QACs as well. The increased activity for these constrained compounds was attributed to the alkyl chains being 180˚ from one another, although the study warranted further investigation.[55]

More recently, the Minbiole Lab has delved into developing novel amphiphilic compounds that have a different heteroatom than a nitrogen as the cationic core. The most efficacious of these classes is the quaternary phosphonium compounds

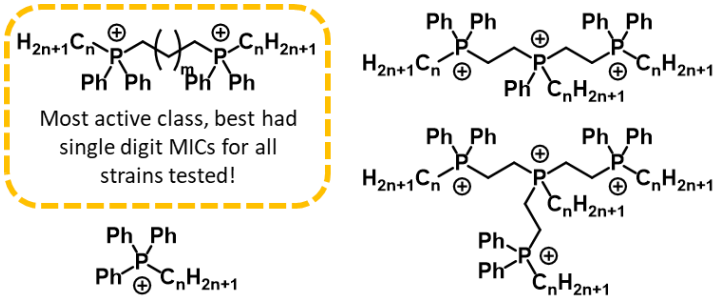

Figure 3.10 Novel QPCs, with the bisQPCs being most active.

(QPCs) (**Figure 3.10**). Much like QACs, the QPCs developed had better activity when they contained more than one cationic warhead. Interestingly, the best activity was seen when bisQPCs were used, as tris- and tetraQPCs led to decreased activity. This is contrary to QACs, who display equally or more potent activity when appended with tris- and tetracationic charges. Additionally, the best compounds were equally effective against MSSA, HA-MRSA, and CA-MRSA, indicating that they may evade traditional QAC resistance mechanism in gram positive bacteria. They were found to induce cell lysis against both *P. aeruginosa* and *E, faecalis*, as well as depolarize their membranes.[56] These compounds represent a potent new development in disinfectant research.

3.2 Appending Quaternary Ammoniums to Polymyxin B to Broaden Activity

The synthesis of these compounds was completed by members of the Pires lab at the University of Virginia. MIC and hemolysis assays were completed by Ryan A. Allen and Kelly. R. Morrison with equal contribution. Citation: Ongwae, G. M., Morrison, K. R., **Allen, R. A.**, Seonghoon, K., Im, W., Wuest, W. M., Pires, M. M. Broadening Activity of Polymyxin by Quaternary Ammonium Grafting *ACS Infect. Dis.* **2020** *6* (6) 1427-35.

As discussed, appending a quaternary ammonium salt to an antibiotic can increase its efficacy, especially against resistant pathogens, in addition to giving it another mechanism of action. Therefore, the Pires lab at University of Virginia undertook the synthesis of polymyxin B (**3.5**) analogs with appended QACs (**Figure 3.11**).[57] Polymyxin B (PMB) was chosen for this study as its mechanism of action is binding to LPS on the outer membrane of gram negative bacteria. By appending a QAC to this scaffold, the LPS targeting abilities would be able to deliver a QAC directly to the membrane of the bacterium, thereby giving it a dual mechanism of action. As previously discussed, polypharmacology is preferential for antibiotic development as bacteria are less likely to develop resistance to them.

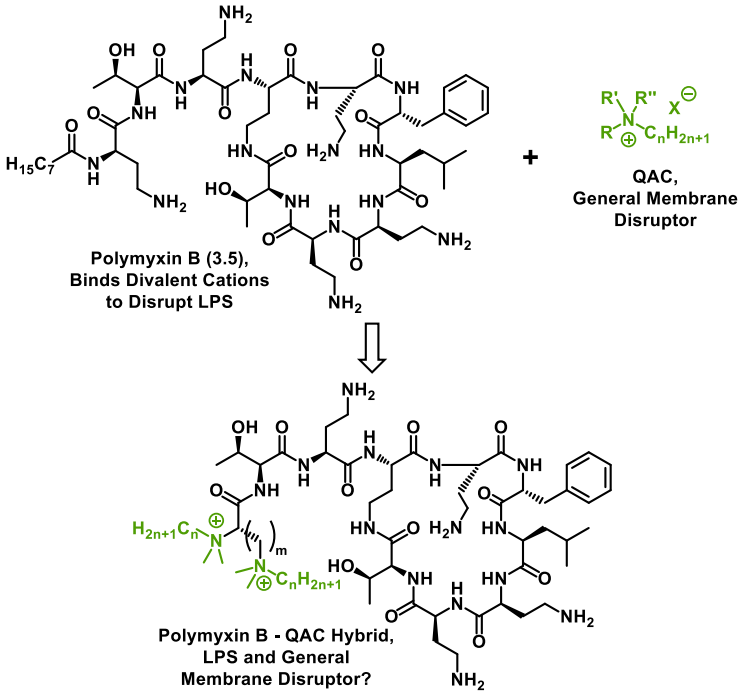

Figure 3.11 General strategy for grafting QACs onto polymyxin B.

Utilizing solid phase synthesis, they were able to first generate the linear precursor using Oxyma/DIC, followed by quaternization of the desired amine, cleavage from the resin, macrocyclization, and finally global deprotection (**Scheme 3.2**). They focused on the quaternization of the *N*-terminal diaminobutyric acid (DAB) residue by directly quaternizing the side chain amine, exchanging the *N*-terminal long acyl chain for a glycine followed by quaternization of that nitrogen to mimic polymyxin B's scaffold, exchanging the DAB for lysine and quaternizing the amine, or replacing the *N*-terminal DAB with glycine and quaternizing the amine (**Table 3.1**).

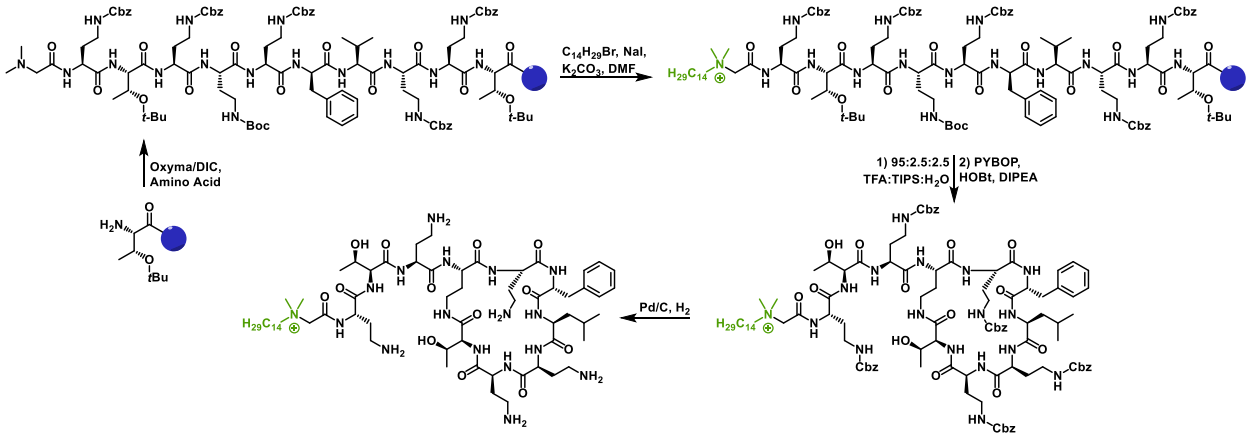

Scheme 3.2 General synthetic procedure for polymyxin B–QAC hybrids. Appended QAC highlighted in green.

After successful completion of these syntheses, they library of 13 compounds plus polymyxin B were shipped to the Wuest lab for biological testing. Here, an MIC assay was conducted in parallel with hemolysis assay (**Table 3.2**). Hemolysis is used as a proxy for mammalian toxicity. The trends were less clear than for typical QAC libraries, as chain length usually coincides with activity for all bacteria tested. Regardless of chain length or type of QAC appended, no analogs had an MIC against a colistin resistant strain of *A. baumannii*. The best analogs typically had an MIC within a dilution of polymyxin B, although there was no analog that was the best at killing all bacteria than the other analogs. Typically, shorter chain QACs between 7 and 8 carbons that were appended to the *N*-terminal DAB residue or replaced glycine residue were the most active against *E. coli* and *P. aeruginosa*. When the DAB residue was retained and not replaced with glycine, they also had activity against *A. baumannii*. When the side chain amine

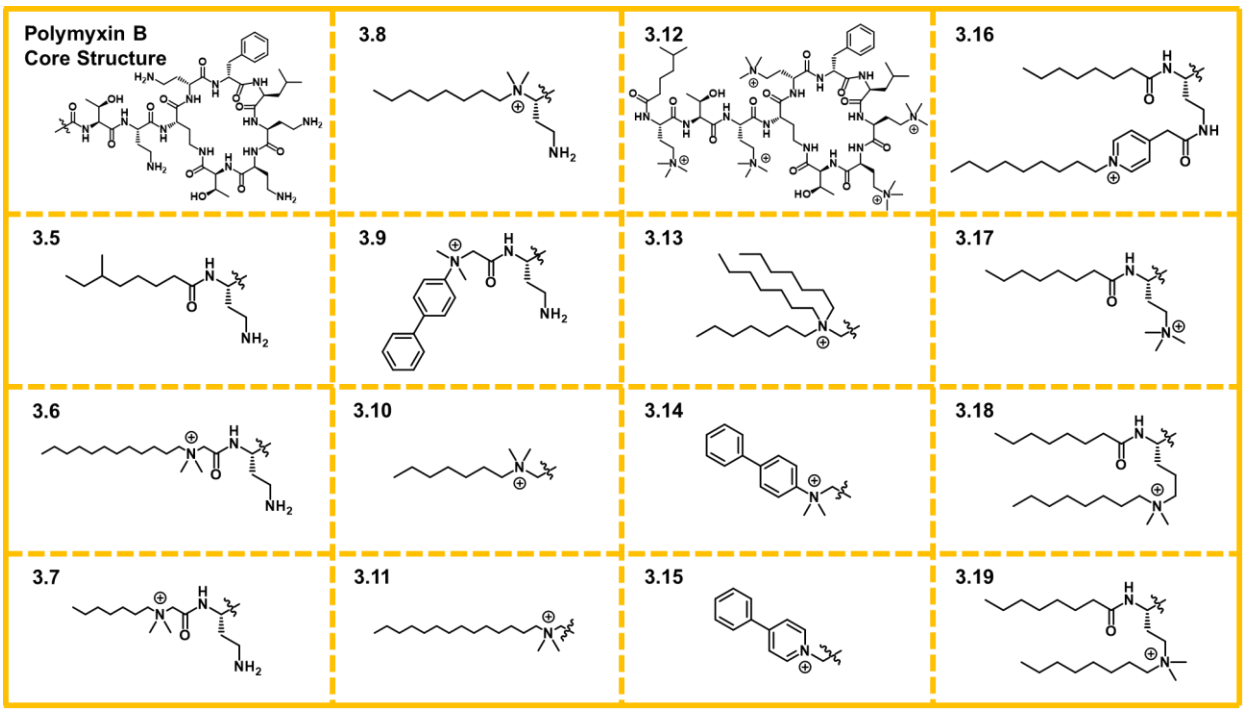

Table 3.1 Structures of the polymyxin B-QAC hybrids.

Minimum Inhibitory Concentration (μg/mL)							
Compound	***A. Baumannii* ATCC 19606**	***A. Baumannii* MRSN 17493**	***P. aeruginosa* PAO1**	***P. aeruginosa* PA14**	***E. coli* ATCC 22922**	***S. aureus* MRSA USA300**	**$Lysis_{20}$**
PMB (**3.5**)	2	>63	1	0.5	1	63	32
3.6	8	>63	4	8	16	8	32
3.7	16	>63	2	2	4	>63	32
3.8	8	>63	2	1	2	>63	32
3.9	>63	>63	>63	>63	25	>63	32
3.10	>63	>63	8	8	1	>63	32
3.11	>63	>63	4	4	8	4	32
3.12	>63	>63	>63	>63	32	>63	>63
3.13	>63	>63	16	8	32	16	32
3.14	>63	>63	>63	63	32	>63	>63
3.15	>63	>63	>63	>63	32	>63	32
3.16	>63	>63	>63	>63	32	>63	>63
3.17	16	>63	4	2	4	>63	32
3.18	>63	>63	32	63	16	>63	32
3.19	>63	>63	>63	>63	8	16	32

Table 3.2 MIC and $hemolysis_{20}$ data for the PMB-QAC hybrids against clinically relevant bacteria and sheep's blood. PMB = polymyxin B.

of the *N*-terminal DAB was quaternized via trimethylation, it also had activity against *A. baumannii*, *E. coli*, and *P. aeruginosa*. Given these data it seems that the *N*-terminal DAB residue is necessary for activity in *A. baumannii* and preferential for activity in *E. coli* and *P. aeruginosa*.

Although polymyxin B is typically only active against gram negative bacteria, these QAC analogs were tested for the gram positive activity as well.[58] By quaternizing the amine of the *N*-terminal DAB side chain with two methyl groups and a seven carbon alkyl chain, the activity of polymyxin B can switch from strictly gram negative to gram positive, giving it a good MIC of 16 μg/mL against CA-MRSA. Activity could be achieved against this strain by either appending a quaternized glycine with a 14-carbon chain to the *N*-terminus, replacing the *N*-terminal DAB residue with the aforementioned glycine, or by replacing the *N*-terminal DAB residue with a glycine quaternized with three 7-carbon chains. The hemolysis for all compounds was about the same (32 to >63 μg/mL). By appending QACs to the core scaffold of polymyxin B, activity was more or less retained for some analogs against gram negative bacteria while adding an additional mechanism of action, while some analogs were able to flip their activity from strictly gram negative activity to also include the gram positive pathogen CA-MRSA.

3.3 Investigations of Activity-Rigidity Relationships in Bispyridinium QACs

The synthesis of these compounds was completed by members of the Minbiole lab. MIC and hemolysis assays were completed by Ryan A. Allen and Kelly R. Morrison in equal contribution. Citation: Leitgeb, A. J., Feliciano, J. A., Sanchez, H. A., **Allen, R. A.**, Morrison, K. R., Sommers, K. J., Carden, R. G., Wuest, W. M., Minbiole, K. P. C. Further Investigations into Rigidity-Activity Relationships in BisQAC Amphiphilic Antiseptics. *ChemMedChem* **2020** *15* (8) 667-70.

In order to further probe the activity-rigidity relationships of QACs, the Minbiole lab synthesized a library of bispyridinium QACs connected with an ethyl chain at the 4 position (**Figure 3.12**).[59] The ethyl chain was varied in desaturation, ranging from flexible to rigid with alkyl to alkenyl to alkynyl. These QACs were facilely synthesized by refluxing bispyridines with long alkyl bromides in acetonitrile (alkane) or DMF (alkene) (**Scheme 3.3**). Tragically, the alkynyl bispyridine refused to react under these conditions, even when alkyl iodides or tosylates were used. To circumvent this lack of reactivity, and acknowledging the previous successes with α-amido bromides, the Minbiole lab was able to achieve the synthesis of these alkynyl linked bispyridinium QACs by refluxing the alkynyl bispyridine in acetonitrile with α-amido bromides. Inspired by this triumph, they also synthesized the long chain amide analogs of the alkane and alkene linked bisQACs.

Having synthesized a library of 36 compounds, the Minbiole lab shipped series to the Wuest lab for biological testing. We then tested the compounds against the typical panel of clinically relevant bacteria in minimum inhibitory concentration (MIC) and hemolysis$_{20}$ assays (**Table 3.3**). Herein, we found a similar trend for alkyl chain lengths as previously seen; the best activity was seen with chain lengths between 10 and 14 carbons. Moreover, bromide

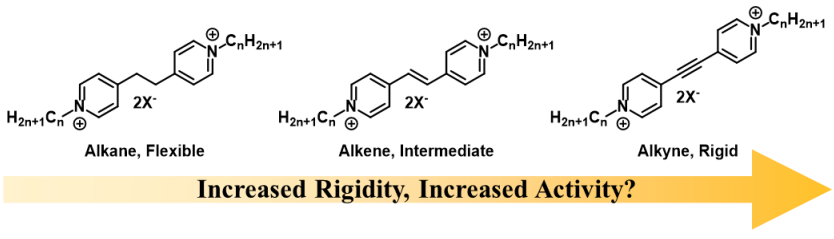

Figure 3.12 Strategy for assessing rigidity-activity relationships in linked bispyridinium QACs.

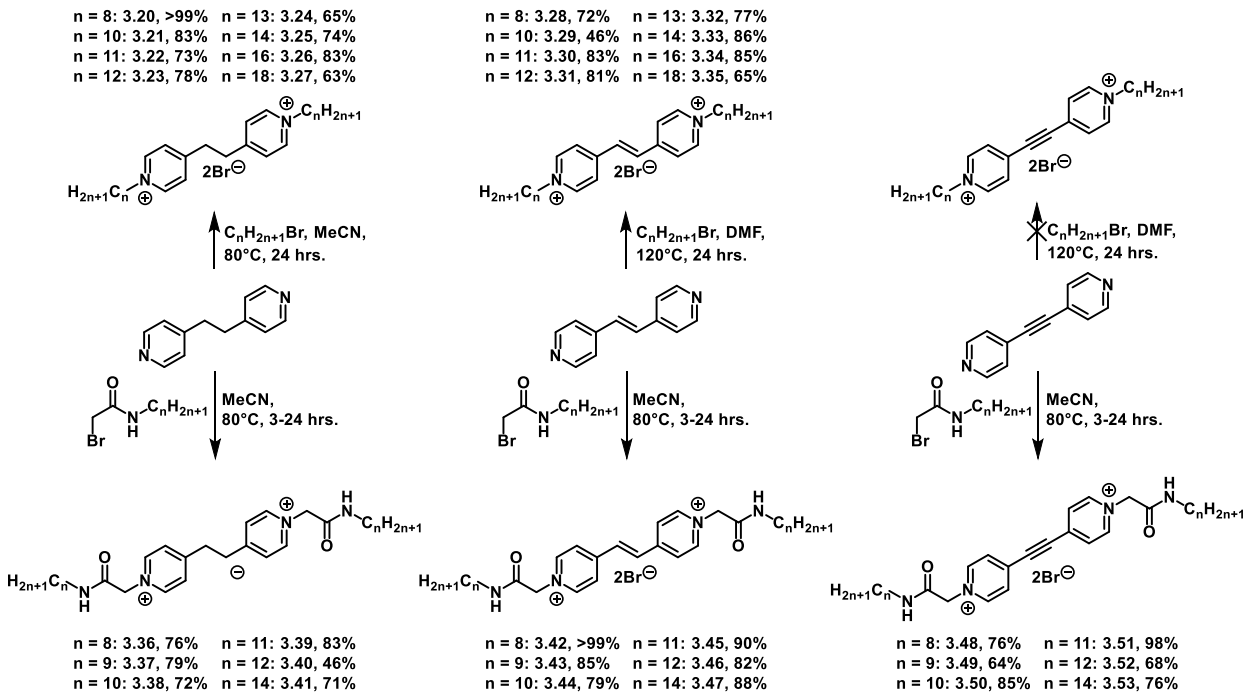

Scheme 3.3 Synthetic route for synthesizing rigidity-activity series of bispyridinium QACs **3.20**-**3.53**.

counterions were typically slightly more efficacious and less hemolytic than a tosylate counterion. We also discovered that these QACs were generally less hemolytic than typical QACs, thereby giving a better therapeutic index. When compared to the commercial QACs benzalkonium chloride (BAC) and cetylpyridinium chloride (CPC), our best QACs were typically 4-fold more active. In addition to these findings, we observed a moderate negative correlation with rigidity, meaning the alkane bisQACs were generally more active than the alkene bisQACs, and both series were more active than the alkynyl bisQACs counterparts. This is contrary to the previous rigidity series; however, when comparing the proximity of the positive charges together in both series, the trend holds. For the TMEDA, piperazine, and DABCO rigidity series, the positive charges in the DABCO analogs were closer together, possibly lending themselves to cooperative binding with the negatively charged cell membrane.[55] Similarly, the alkane analogs are free to move their quaternary nitrogens closer to each other to allow for the same cooperative binding, whereas the alkene and alkyne analogs are trapped in their conformation. Additionally, the previously

Minimum Inhibitory Concentration (μM)							
Compound	**MSSA**	**HA-MRSA**	**CA-MRSA**	***P. aeruginosa***	***E. coli***	***E. faecalis***	**$Lysis_{20}$**
BAC (**3.1**)	N.T.	16	32	63	32	8	63
CPC (**3.2**)	1	2	1	125	16	63	8
3.20	32	63	32	>250	125	>250	125
3.21	1	2	2	63	2	32	63
3.22	1	1	1	4	1	4	63
3.23	2	1	1	4	1	4	125
3.24	8	8	4	16	4	16	125
3.25	4	4	8	>250	16	>250	125
3.26	32	16	8	>250	>250	>250	32
3.27	63	63	63	>250	>250	>250	125
3.28	16	32	16	125	4	250	125
3.29	1	2	2	8	1	8	63
3.30	1	0.5	2	2	1	2	63
3.31	8	4	4	32	8	16	125
3.32	16	8	8	>250	16	>250	125
3.33	125	63	63	>250	250	>250	125
3.34	>250	>250	>250	>250	>250	>250	125
3.35	>250	>250	>250	>250	>250	>250	125
3.36	8	8	4	>250	16	125	125
3.37	2	2	1	16	4	8	32
3.38	2	4	2	8	4	8	16
3.39	4	4	4	32	8	32	32
3.40	16	16	16	>250	32	>250	125
3.41	63	63	32	>250	125	>250	63
3.42	4	4	2	32	8	32	32
3.43	4	4	4	32	16	32	8
3.44	16	32	32	250	63	250	63
3.45	8	16	16	>250	32	>250	63
3.46	63	63	32	>250	125	>250	63
3.47	63	250	32	>250	>250	>250	63
3.48	16	32	16	63	32	63	32
3.49	32	32	32	125	32	63	125
3.50	32	32	63	>250	63	>250	125
3.51	63	125	125	>250	125	>250	125
3.52	125	32	125	>250	>250	>250	63
3.53	250	63	125	>250	>250	>250	63

Table 3.3 MIC and $hemolysis_{20}$ values for rigidity-activity series of bispyridinium QACs **3.20**-**3.53** against clinically relevant bacteria and sheep's blood. MSSA = methicillin-susceptible *S. aureus*, MRSA = methicillin-resistant *S. aureus*, HA = hospital acquired, CA = community-acquired.

synthesized paraquat PQ-12,12 had improved activity over the similar alkyne analog, also possibly due to the closeness of the charges.[52] This series broadens the scope of rigidity-activity relationships of QACs, wherein the closeness of the charges lending themselves to improved activity was reconfirmed.

3.4 Explorations of Ferrocene-Containing QACs

The synthesis of these compounds was completed by members of the Minbiole lab. MIC and hemolysis assays were completed by Ryan A. Allen and Savannah J. Post in equal contribution. Citation: Sommers, K. J., Bentley, B. S., Carden, R. G., Post, S. J., **Allen, R. A.**, Kontos, R. C., Black, J. W., Wuest, W. M., Minbiole, K. P. C. Metallocene QACs: The Incorporation of Ferrocene Moieties into monoQAC and bisQACs Structures. *ChemMedChem* **2021** *16* (4) 467-71.

Iron is an essential nutrient that all organisms need for life processes such as cellular respiration, gas transport, and DNA repair. Bacteria, being organisms pining for life, have multiple ways to acquire iron from the environment (**Figure 3.13**). These avenues include importing heme from the environment, secreting siderophores to gather ferric iron from the environment, and transporters such as the Feo system for the transport of ferrous iron.[60–65] Although the Feo system is most widely distributed amongst bacterial species and most specific for ferrous iron, there are

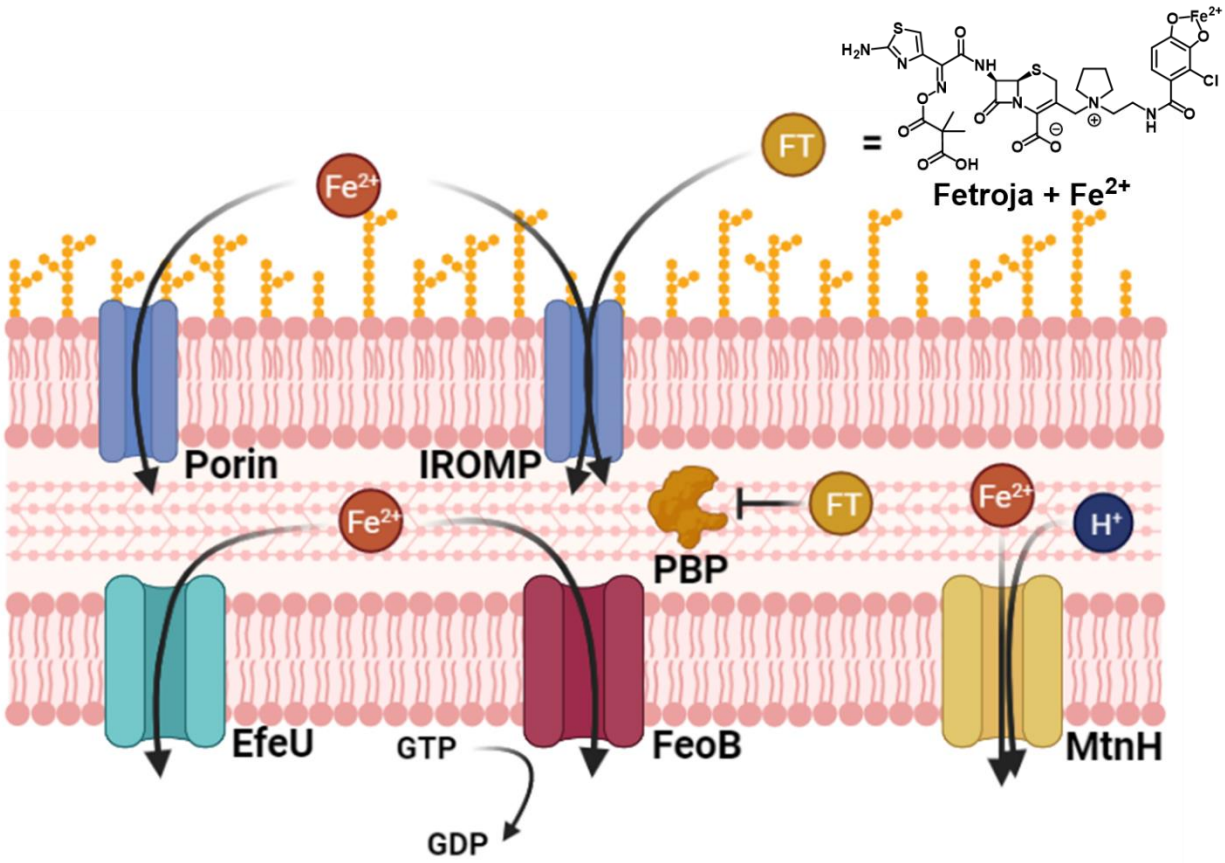

Figure 3.13 Mechanisms of iron acquisition in gram negative pathogens, highlighint how Fetroja exploits these systems to inhibit penicillin binding proteins (PBPs) in the periplasm. Similar systems also transport ferrous iron in gram positive pathogens, namely EfeU and FeoB. IROMP = iron-regulated outer membrane protein.

several other transporters that can sequester ferrous iron from the environment, such as divalent metal ion/proton symporter MntH and permease EfeU.[66–69] Additionally, iron regulated outer membrane proteins (IROMPs) are known to uptake ferrous iron from the environment in gram negative species.[70–72] These iron transport systems have been exploited for antibacterial development previously in a strategy termed "trojan horse", where the bacteria is tricked into allowing in an antibacterial compound in the guise of a necessary nutrient. One of the most successful trojan horse strategies is Fetroja (**Figure 3.13**). Fetroja is an FDA approved antibiotic that uses a catechol siderophore moiety to be actively imported into the periplasm by gram negative bacteria, then a cephalosporin to inhibit penicillin binding proteins (PBP) to enact cell death.[73,74]

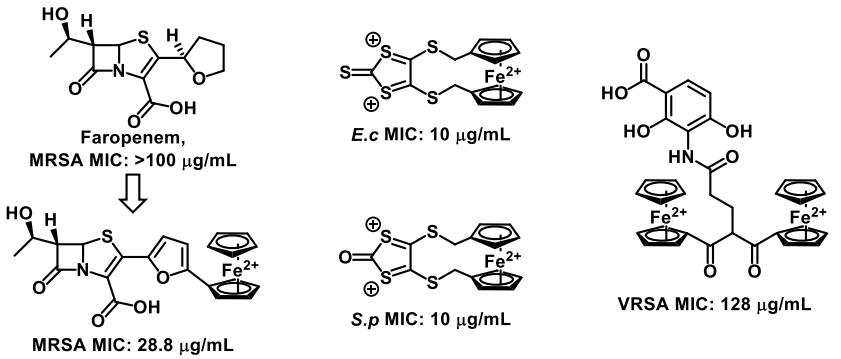

Figure 3.14 Ferrocene containing antibacterial compounds. MRSA = methicillin-resistant *S. aureus*, *E.c* = *E. coli*, *S.p* = *S. pyogenes*, VRSA = vancomycin-resistant *S. aureus*.

Similarly to Fetroja, several other antibiotics have been developed that use a ferrocene moiety to increase antibacterial activity (**Figure 3.14**).[75] Ferrocene was attached to a penem to generate a variety of analogs, the most active of which had decreased MICs against gram positive pathogens such as MRSA by four-fold. The MICs against gram negative bacteria were decreased by a more modest two-fold.[76] Ferrocene could also be appended to novel scaffolds for excellent antibacterial activity, such as the addition of ferrocene to dithiothione and dithioketone scaffolds that had excellent MICs against *E. coli* and *S. pyogenes*.[77] Additionally, a ferrocene could be appended to natural product platensimycin to give modest antibacterial activities against vancomycin-resistant *S. aureus*.[78]

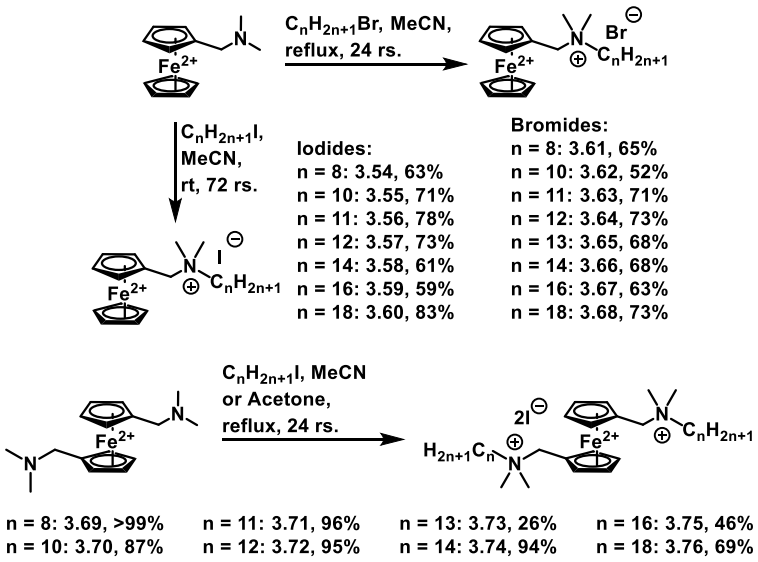

Scheme 3.3 Synthesis of the ferrocene mono- and bisQACs. MeCN = acetonitrile.

Given the promising background of ferrocene containing antibacterial compounds, the Minbiole lab undertook the synthesis of a library of ferrocene containing QACs that had both mono- and bisQACs (**Scheme 3.3**).[79] Ferrocene was chosen as it is commercially available for a relatively affordable price and has ferrous iron that could potentially be taken up by ferrous iron and divalent metal transporters. Starting with commercially available (dimethylaminomethyl) ferrocene, the monoQAC series was made via refluxing the substrate with long chain alkyl bromides or iodides in acetonitrile. Using similar 1,1'-bis(dimethylaminomethyl)ferrocene, a similar procedure was applied by refluxing the substrate with long chain alkyl iodides in either acetone or acetonitrile to yield the bisQAC series (**Scheme 3.3**). The long chain halogens ranged from 8 to 18 carbons for both series.

Minimum Inhibitory Concentration (μM)							
Compound	**MSSA**	**HA-MRSA**	**CA-MRSA**	***P. aeruginosa***	***E. coli***	***E. faecalis***	**$Lysis_{20}$**
BAC (**3.1**)	2	8	2	125	32	250	32
CPC (**3.2**)	1	1	1	125	32	125	8
3.54	32	125	32	>250	>250	>250	250
3.55	4	16	63	>250	63	>250	250
3.56	4	8	32	250	63	250	63
3.57	2	63	16	63	1	4	32
3.58	1	2	8	250	8	250	16
3.59	2	2	32	>250	63	>250	16
3.60	4	4	2	>250	125	250	32
3.61	32	125	32	>250	>250	>250	250
3.62	4	16	63	>250	125	>250	250
3.63	2	4	32	125	32	125	125
3.64	1	4	8	63	16	63	32
3.65	1	4	1	>250	8	>250	32
3.66	2	2	8	250	8	250	16
3.67	2	2	2	250	63	125	16
3.68	2	125	125	250	63	4	32
3.69	8	32	32	>250	63	>250	32
3.70	1	2	2	32	4	32	63
3.71	1	1	2	8	2	8	16
3.72	2	2	2	32	4	32	8
3.73	2	4	4	63	32	63	8
3.74	2	2	2	125	32	125	8
3.75	4	4	32	250	63	125	8
3.76	8	8	63	125	125	125	16

Table 3.4 MIC and $hemolysis_{20}$ values for ferrocene-containing mono- and bisQACs **3.54**-**3.76** against clinically relevant bacteria and sheep's blood. MSSA = methicillin-susceptible *S. aureus*, MRSA = methicillin-resistant *S. aureus*, HA = hospital acquired, CA = community-acquired.

Having synthesized the complimentary ferrocene containing mono- and bisQACs, the Minbiole sent the compounds to be tested in the Wuest lab. We then conducted the typical MIC and hemolysis assays for these compounds, using the same clinical pathogens as before (**Table 3.4**). For the monoQACs, we did not observe any counterion dependent trend, as both the bromide and iodide salts had similar MICs (within a dilution if not the same). The bisQACs were typically more active than their monoQAC counterparts, especially against gram negative bacteria. As per usual, we did see a dependence on chain length, as compounds with 11-12 carbons had the best activity. When compared to commercial QACs **3.1** and **3.2**, the best ferrocene containing QACs were typically four-fold more active for gram negative pathogens and either comparable or two-

Minimum Inhibitory Concentration (μM)										
Compound	**MSSA**	**1289**	**G-1891**	**G-382**	**123**	**120336**	**CA11**	**EUH 13**	**115**	**221**
BAC (**3.1**)	2-4	8	4	8	8	8	8	8	8	4
3.70	1-2	2	2	2	4	2	2	2	2	2
3.71	1-2	4	4	4	4	4	4	4	8	4
3.72	2	4	4	4	4	4	4	4	4	4
3.75	4	4	4	8	4	4	4	4	4	8

Table 3.5 MIC and hemolysis$_{20}$ values for ferrocene-containing mono- and bisQACs **3.70-3.72** and **3.75** against methicillin-resistant *S. aureus* clinical isolates. MSSA = methicillin-susceptible *S. aureus*.

fold better activity for the gram positive pathogens. For hemolysis, the bisQACs tended to be more lytic than the monoQACs, but all compounds tested were less hemolytic than commercially available **3.2**. The best compounds (**3.70**-**3.72**, **3.75**) were also tested against a panel of clinical MRSA isolates and compared to **3.1** (**Table 3.5**). These QACs were either on par or had two- to four-fold better activity than **3.1**, again demonstrating the improved activity of bisQACs over monoQACs. This work successfully utilized a trojan horse approach to the development of antibacterial QACs with improved efficacy over commercial QACs that could potentially be trafficked into the cell via metal ion uptake pathways.

3.5 Trivalent Sulfonium Compounds versus Quaternary Ammonium Compounds

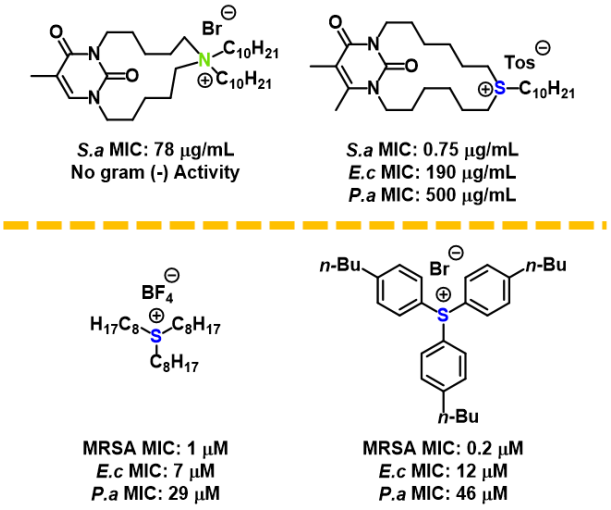

Figure 3.5 Efficacy of uracil derived QAC (green) and TSC (blue) (top) and trialkyl- and triphenyl-TSCs (bottom). *S.a* = *S. aureus*, *E.c* = *E. coli*, *P.a* = *P. aeruginosa*, MRSA = methicillin-resistant *S. aureus*.

The synthesis of these compounds was completed by members of the Minbiole lab. MIC and hemolysis assays were completed by Ryan A. Allen and Cassandra L. Schrank in equal contribution. Citation: Feliciano, J. A., Leitgeb, A. J., Schrank, C. L., **Allen, R. A.**, Minbiole, K. P. C., Wuest, W. M., Carden, R. G. Trivalent Sulfonium Compounds (TSCs): Tetrahydrothiophene-based amphiphiles exhibit similar antimicrobial activity to analogous ammonium-based amphiphiles. *Bioorg. Med. Chem. Lett.* **2021** *37* 127809.

In order to broaden the scope of amphiphilic disinfectants from just positively charged nitrogens to other positively charged heteroatoms, trivalent sulfonium compounds

(TSCs) were explored.[80] Although ubiquitous in nature as methyl transfer reagents, trivalent sulfonium compounds have been underexplored in antibacterial development. One study compared the activity of uracil-QAC macrocycles versus uracil-TSC macrocycles, finding that the TSCs had comparable and sometimes better activity when appended with a long alkyl chain, much like typical QACs (**Figure 3.15**).[81] Additionally, trialkyl- and triphenyl-TSCs have been developed and found to have good to great activity against both gram-positive and -negative pathogens (**Figure 3.15**). Moreover, the mechanism of action of these TSCs was analyzed for membrane perturbations, and they were found to act similarly to QACs, causing membrane disruption and lysis as visualized by transmission and scanning electron microscopy. These TSCs were also found to be minimally toxic in acute dermal and oral toxicity studies, thereby making them excellent candidates for typically corrosive QACs.[82–84]

To assess the potency and toxicity of novel TSCs as compared to their QAC counterparts, the Minbiole lab synthesized a range of pyrrolidine and tetrahydrothiophene amphiphiles via refluxing the heterocycle in acetonitrile (QACs) or trifluoroacetic acid (TSCs) with the corresponding long chain alkyl bromide (**Scheme 3.4**).[80] In addition to the monocationic amphiphiles, the Minbiole lab also synthesized "bola" amphiphiles,

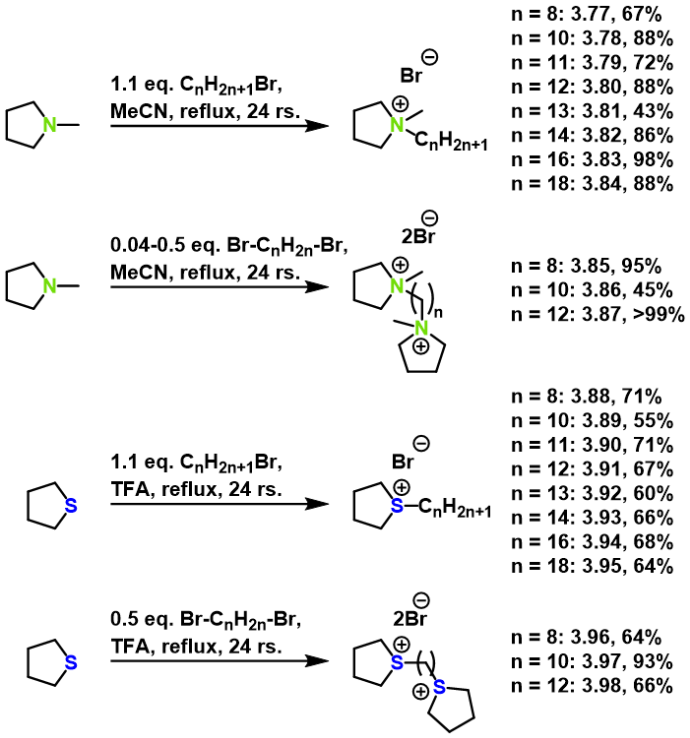

Scheme 3.4 Synthesis of the mono- and bis-QACs and -TSCs, with QACs highlighted in green and TSCs highlighted in blue. TFA = Trifluoroacetic acid.

Minimum Inhibitory Concentration (μM)							
Compound	**MSSA**	**HA-MRSA**	**CA-MRSA**	***P. aeruginosa***	***E. coli***	***E. faecalis***	**$Lysis_{20}$**
BAC (**3.1**)	2	8	2	125	32	250	32
CPC (**3.2**)	1	1	1	125	32	125	8
3.77	>250	>250	>250	>250	>250	>250	125
3.78	>250	>250	>250	>250	>250	>250	125
3.79	125	>250	32	>250	>250	>250	125
3.80	32	125	32	>250	>250	>250	32
3.81	8	63	16	>250	>250	>250	63
3.82	4	16	8	>250	250	>250	32
3.83	4	8	2	>250	125	>250	16
3.84	2	8	4	250	63	>250	16
3.85	>250	>250	>250	>250	>250	>250	125
3.86	>250	>250	>250	>250	>250	>250	125
3.87	>250	>250	>250	>250	>250	>250	125
3.88	>250	>250	>250	>250	>250	>250	125
3.89	250	>250	250	>250	>250	>250	125
3.90	125	250	250	>250	>250	>250	125
3.91	16	125	16	>250	>250	>250	125
3.92	8	125	32	>250	>250	>250	63
3.93	4	32	4	>250	250	>250	16
3.94	2	8	4	>250	125	>250	16
3.95	1	8	4	250	63	250	16
3.96	>250	>250	>250	>250	>250	>250	125
3.97	250	>250	250	>250	>250	>250	125
3.98	250	>250	250	>250	>250	>250	250

Table 3.6 MIC and $hemolysis_{20}$ values for mono- and bis-QACs and -TSCs **3.77-3.98** against clinically relevant bacteria and sheep's blood. MSSA = methicillin-susceptible *S. aureus*, MRSA = methicillin-resistant *S. aureus*, HA = hospital acquired, CA = community-acquired.

or two cationic centers connected by a long alkyl chain, in a similar fashion (**Scheme 3.4**).

Once prepared, the compounds were once again shipped to the Wuest lab for MIC and hemolysis assays (**Table 3.6**). From the data collected, the TSCs had approximately equal activity to their QAC counterpart (within one to two dilutions). This trend also carried over to the hemolytic values of these compounds, were the TSCs were as hemolytic as the QACs. Further toxicity studies, such as dermal and oral studies, would need to be conducted to determine if the TSCs are less toxic than the QACs. Additionally, these amphiphiles differed from previously made QACs insofar as they were mostly only active against gram positive bacteria and the optimal chain length was found to be 18 carbons long instead of 11 to 13 carbons in length. Moreover, the bola amphiphiles were almost completely inactive against all strains tested. The best of these

compounds was two sulfoniums connected by a 12-carbon linker, where it had an MIC of 250 μM against MSSA and CA-MRSA and was inactive against all other strains. The best TSCs were active against HA- and CA-MRSA, which may indicate that they may be able to evade resistance mechanisms; however, further compounds and studies would be needed to determine this, such as active bisTSCs and resistance selection assays. Taken together, this work expanded the breadth of trivalent sulfonium compounds and compared them to their QAC counterparts, demonstrating they are equipotent and have a platform for future studies on resistance evasion.

3.6 Exploring Amphiphilic Disinfectant Resistance in Clinical Isolates

The synthesis of these compounds was completed by members of the Minbiole lab. MIC assays were completed by Ryan A. Allen, Kelly R. Morrison-Lewis, Marina E. Michaud, and Savannah J. Post in equal contribution. The resistance selection assay was completed by Marina E. Michaud and Savannah J. Post in equal contribution. Ryan A. Allen aided in the resistance selection assay spontaneously when needed. The MBEC assay was completed by Marina E. Michaud and Christian A. Sanchez in equal contribution. Citation: Michaud, M. E., **Allen, R. A.**, Morrison-Lewis, K. R., Sanchez, C. A., Minbiole, K. P. C., Post, S. J., Wuest, W. M. *ACS Infect. Dis.* **2022** *8* (11) 2307-14.

As previously mentioned, QACs are ubiquitously used in hospital and clinical settings to disinfect common surfaces and furniture. Given the rise of antibiotic resistant bacteria coincides with rise of QAC resistance, the Minbiole-Wuest collaboration decided to determine the efficacy of four commercially used QACs against a panel of extensively to pan drug resistant clinical isolates obtained from the Department of Defense (DoD). These isolates were of *A. baumannii* (AB) and *P. aeruginosa* (PA), two pathogens known to

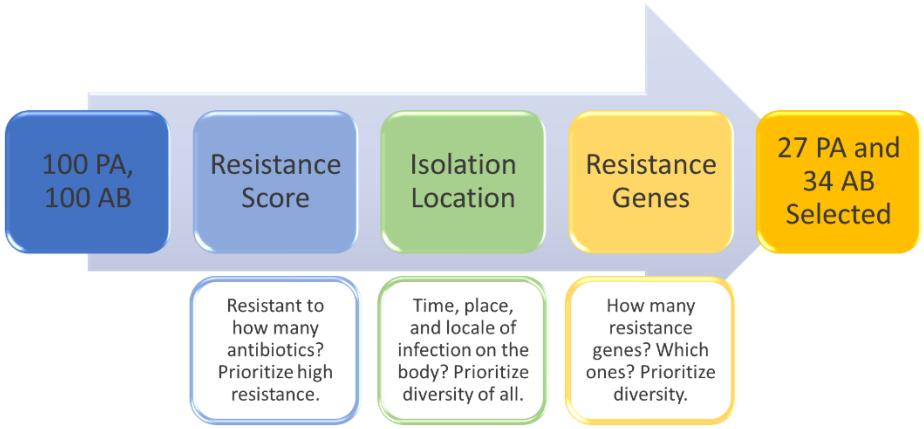

Figure 3.16 Workflow for selecting which clinical isolates to test against the best-in-class and commercial QACs.

cause nosocomial infections in compromised patients. PA specifically is known to colonize the airways of patients with cystic fibrosis and lead to poor outcomes.[85] AB is known to cause nosocomial pneumonia, bacteremia, and skin and soft tissue infections in compromised patients.[86] These bacteria are particularly troublesome in a hospital setting not only because they are gram negative, which are notoriously harder to kill, but also because of their genomes' plasticity, or ability to transfer and receive new genetic material and adapt to changes in the environment.[87–89] Moreover, these pathogens are known to form biofilms in hospital settings that allow for their continued resistance to disinfectants and transmission even after a surface has been cleaned.[90–92] Therefore, we sought to use this library to better understand the mechanisms of amphiphilic resistance and susceptibility and their relation to antibiotic resistance in clinical isolates.

The library of clinical isolates we received from the DoD contained 100 strains of each type of bacteria, along with resistance data to 14 clinically used antibiotics, resistance genes harbored, isolation location, and year of isolation. To streamline the MIC assays, the list of bacteria

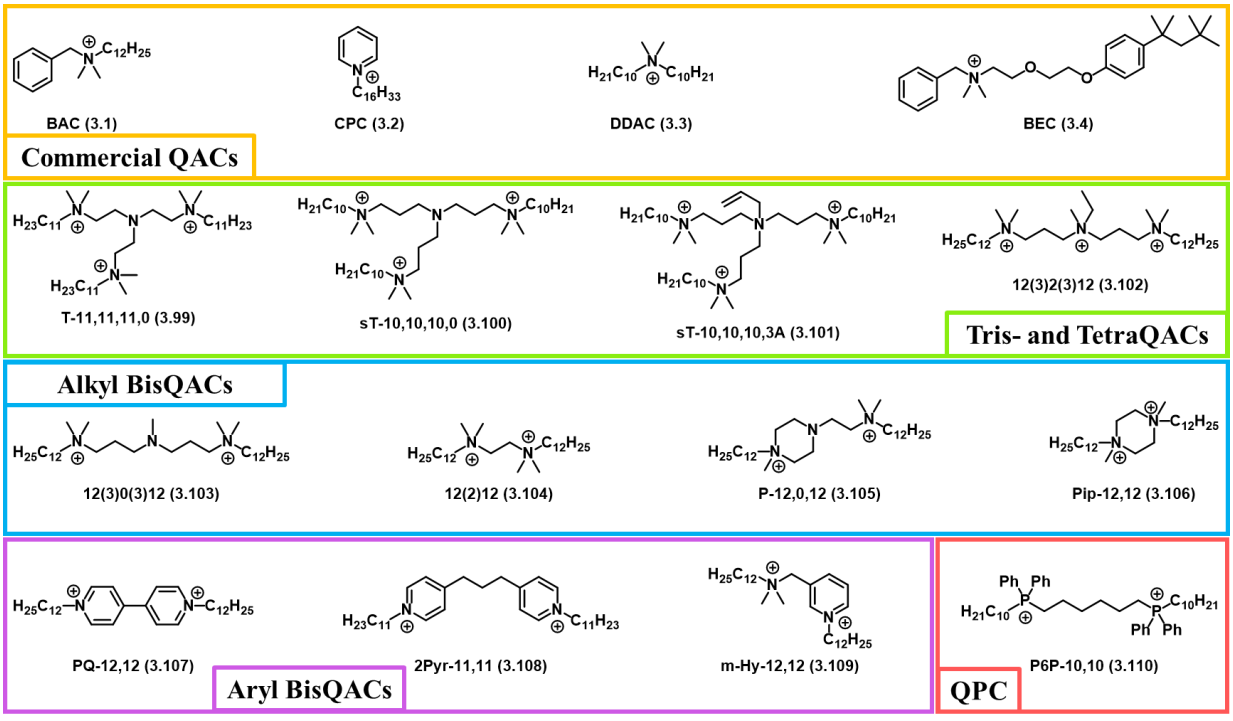

Figure 3.17 Structures of the commercial QACs and "best-in-class" QACs and QPC.

was shortened to a more manageable size that still allowed for diversity of resistance to antibiotics, different resistance genes harbored, and isolation location and year (**Figure 3.16**). The bacteria were each first given a resistance score, which is the total number of antibiotics they are resistant to. We chose bacteria that were resistant to the most antibiotics and had unique resistance profiles to allow for the greatest diversity possible. Next, we sorted the bacteria by isolation year and location, again looking to maximize bacteria from different geographic areas as they likely have different genomes and mechanisms of resistance. We then parsed through the genetic resistance determinants that each bacterium harbored, eliminating duplicates where possible. This led us to a library of 27 isolates of PA and 34 isolates of AB to test against the selected amphiphiles.

The amphiphiles for this study were selected as the mast active, or "best-in-class", from the vast library of over 800 compounds that the Minbiole lab has synthesized over the years (**Figure 3.17**). As discussed in *Section 3.1.3.3*, these QACs have been proven more active that commercial QACs, as well as less likely to induce resistance. The newly discovered yet impressively active QPC P6P-10,10 was also included in this study to explore the resistance profile of this compound and compare it to the QACs.

3.6.1 A. baumannii

The resistance profiles of the selected AB strains are depicted in **Table 3.7**, followed by the obtained MIC and IC_{90} values in **Table 3.8**. The resistance genes harbored by each isolate is displayed in **Supplementary Table 4.1**. IC_{90} was used as a proxy for activity in these strains as many of them displayed growth of small colonies after the breakpoint, a known phenotype of heteroresistance (**Figure 3.18**). This is made clear by the difference between the MIC and IC_{90} for many compounds. Gratifyingly, the next-

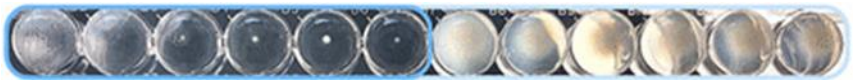

Figure 3.18 Persistence of microcolonies after the breakpoint observed during routine MIC measurements.

generation amphiphiles displayed increased activity compared to three of the commercial QACs tested: BAC, CPC, and BEC. The other commercial QAC, DDAC, exhibited on par or decreased activity when compared to the best of the best QAC and the QPC tested. Also noteworthy, the pan resistant strain that is resistant to colistin (MRSN 17493) was completely resistant to every QAC tested. This is likely because colistin resistance is typically attributed to two-component systems, such as PhoPQ and PmrAB, that append cationic ethanolamines or 4-amino-L-arabinose to the

	Antibiotic Susceptibility													
Strain	Aminoglycosides			Cephalosporin			β-Lactam	Carbapenem		Quinolone		Tetracycline	Combo	Polymyxin
	AMK	GEN	TOB	CAZ	FEB	CRO	SAM	IPM	MEM	CIP	LVX	TET	SXT	CST
ATCC 19606	S	S	S	S	S	S	S	S	S	S	S	S	S	S
MRSN 114427	R	R	R	R	R	R	R	R	R	R	R	S	R	S
MRSN 21681	R	R	R	R	R	R	R	R	R	R	R	R	R	S
MRSN 21660	R	R	R	R	R	R	R	R	R	R	R	R	R	S
MRSN 11224	R	R	R	R	R	R	R	R	R	R	R	R	R	S
MRSN 32866	R	R	S	R	R	R	R	S	S	R	R	R	R	S
MRSN 4943	R	R	R	R	R	R	R	S	S	R	R	R	R	S
MRSN 7521	R	R	R	R	R	R	S	R	R	R	R	R	R	S
MRSN 17493	R	R	R	R	R	R	R	R	R	R	R	R	R	R
MRSN 334	S	R	S	R	R	R	R	R	R	R	R	R	R	S
MRSN 29908	S	R	R	R	R	R	R	R	R	R	R	R	R	S
MRSN 918	R	R	S	R	R	R	R	R	R	R	R	R	R	S
MRSN 32915	S	R	R	R	R	R	R	R	R	R	R	R	R	S
MRSN 1174	R	R	R	R	R	R	S	R	R	R	R	R	R	S
MRSN 423159	R	R	R	R	R	R	R	R	R	R	R	S	R	S
MRSN 489669	R	R	R	R	R	R	R	R	R	R	R	S	S	S
MRSN 480622	R	R	R	R	R	R	R	R	R	R	R	R	S	S
MRSN 25547	R	R	R	R	R	R	R	R	R	R	R	R	R	S
MRSN 4484	R	R	R	R	R	R	R	R	R	R	R	R	R	S
MRSN 337038	R	R	R	R	R	R	R	R	R	R	R	S	R	S
MRSN 7067	S	R	R	R	R	R	S	S	S	R	R	R	R	S
MRSN 31196	R	R	R	R	R	R	R	R	R	R	R	R	R	S
MRSN 959	R	R	R	R	R	R	R	R	R	R	R	S	R	S
MRSN 1311	S	R	S	R	R	R	R	R	R	R	R	R	R	R
MRSN 14193	R	R	R	R	R	R	R	R	R	R	R	R	R	S
MRSN 15049	R	R	S	R	R	R	R	R	R	R	R	R	R	S
MRSN 960	R	R	S	R	R	R	R	R	R	R	R	R	R	S
MRSN 11695	R	R	R	R	R	R	R	R	R	R	R	R	R	S
MRSN 11703	R	R	R	R	R	R	R	R	R	R	R	R	R	S
MRSN 30000	R	R	R	R	R	R	S	S	S	R	R	R	R	S
MRSN 11663	R	R	R	R	R	R	R	R	R	R	R	R	R	S
MRSN 3874	R	R	R	R	R	R	R	R	R	R	R	S	R	S
MRSN 19482	R	R	R	R	R	R	S	R	R	R	R	S	R	S
MRSN 480561	R	R	R	R	R	R	R	R	R	R	R	S	R	S
MRSN 32104	R	R	R	R	R	R	R	R	R	R	R	R	R	S
MRSN 1437	R	R	R	R	R	R	R	R	R	R	R	R	R	S

Table 3.7 Antibiotic susceptibility profiles of the tested *A. baumannii* clinical isolates. ATCC is a lab strain of *A. baumannii*. AMK = amikacin, GEN = gentamycin, TOB = tobramycin, CAZ = ceftazidime, FEB = cefepime, CRO = ceftriaxone, SAM = ampicillin-sulbactam, IPM = imipenem, MEM = meropenem, CIP = ciprofloxacin, LVX = levofloxacin, TET = tetracycline, SXT = trimethoprim-sulfamethoxazole, CST = colistin sulfate.

phospholipid heads of LPS, thereby replacing the negative charge with a positive one at physiological pH.[93–95] This inhibits the binding of polycationic colistin via charge repulsion, which is likely occurring with the cationic QACs. Intriguingly, the QPC tested did not seem to be perturbed by this pan resistant isolate, as it had an IC_{90} of 3μM. This is an extremely important piece of evidence that indicates QPCs may be acting with a different mode of action than QACs as they are able to evade mechanisms of resistance that they should not be able to. Additionally, we tested the ability of the best QAC and QPC, along with BAC, DDAC, and a 94:100 mixture of BAC and DDAC against the biofilms of a lab strain of AB and two extensively drug resistant clinical isolate in a minimum biofilm eradication concentration (MBEC) assay (**Table 3.9**). The mixture of the two QACs is based on the commercially used disinfectant Virex 256. The pan

	Amphiphilic Disinfectant Susceptibility IC_{90} (μM)															
Strain	Commercial QACs				Tris- and TetraQACs				Alkyl BisQACs				Aryl BisQACs			QPC
	3.1	3.2	3.3	3.4	3.99	3.100	3.101	3.102	3.103	3.104	3.105	3.106	3.107	3.108	3.109	3.110
ATCC 19606	23	6	6	57	4	14	6	6	6	3	3	12	5	3	3	1
MRSN 114427	35	33	0.4	34	4	18	8	45	8	4	4	19	8	3	1	1
MRSN 21681	64	49	3	82	4	10	6	20	4	4	2	12	4	4	4	2
MRSN 21660	32	37	8	31	8	23	15	29	26	4	4	9	8	4	7	7
MRSN 11224	36	34	0.4	34	4	15	8	25	9	4	4	17	15	6	1	1
MRSN 32866	33	32	6	32	4	8	6	10	4	4	4	8	8	8	4	1
MRSN 4943	61	20	10	70	4	15	6	7	3	2	2	13	53	3	2	3
MRSN 7521	32	31	0.5	31	10	17	8	18	8	4	4	17	8	3	1	2
MRSN 17493	>250	>250	>250	>250	>250	>250	>250	>250	>250	>250	>250	>250	>250	>250	>250	3
MRSN 334	39	16	7	45	7	15	14	18	8	17	3	31	18	5	8	1
MRSN 29908	100	33	6	93	4	8	3	37	11	4	4	19	7	3	7	3
MRSN 918	32	31	6	33	4	8	9	18	8	4	4	16	8	4	8	4
MRSN 32915	33	33	7	32	4	8	4	8	7	4	4	8	13	3	4	2
MRSN 1174	38	36	6	46	6	12	12	3	26	8	12	58	12	5	6	7
MRSN 423159	38	36	6	46	4	8	7	91	4	69	2	>250	7	3	56	2
MRSN 489669	34	30	13	31	9	15	7	16	7	4	4	15	8	6	16	2
MRSN 480622	81	35	6	91	4	9	8	110	20	102	80	>250	18	41	16	1
MRSN 25547	105	108	13	140	5	19	14	80	42	5	4	>250	188	5	8	1
MRSN 4484	104	146	0.4	119	8	17	4	30	15	6	5	>250	36	5	117	1
MRSN 337038	36	30	6	32	4	7	7	17	4	4	4	8	8	4	4	2
MRSN 7067	37	16	3	16	5	4	4	8	5	2	2	5	4	2	4	1
MRSN 31196	35	77	4	44	4	8	38	32	11	4	4	71	32	4	10	1
MRSN 959	33	30	7	28	7	15	14	15	7	4	3	16	14	3	15	1
MRSN 1311	32	32	6	32	4	8	11	8	8	4	4	17	14	3	8	1
MRSN 14193	32	32	0.4	32	4	15	16	16	8	4	4	16	15	3	2	1
MRSN 15049	65	32	1	65	9	17	15	18	8	4	4	43	15	4	1	3
MRSN 960	55	28	7	25	8	15	13	16	8	8	7	7	15	3	7	2
MRSN 11695	34	32	0.4	35	4	4	4	4	4	5	3	8	4	4	0.4	1
MRSN 11703	34	33	0.2	70	12	8	4	9	8	4	4	17	16	4	1	1
MRSN 30000	36	17	4	34	4	4	8	9	4	4	4	8	8	3	8	1
MRSN 11663	33	32	0.2	32	4	8	4	8	8	4	4	14	8	3	4	1
MRSN 3874	44	121	0.4	64	8	8	12	28	7	4	4	46	7	4	0.4	1
MRSN 19482	83	145	11	121	8	41	17	36	40	11	16	>250	96	12	24	2
MRSN 480561	35	16	3	33	4	8	8	8	6	4	3	8	7	3	4	1
MRSN 32104	34	17	3	>250	84	8	8	170	4	54	5	217	16	4	9	3
MRSN 1437	34	23	0.4	33	39	18	9	103	9	5	4	18	8	4	>250	3

Table 3.8 Susceptibility of clinical isolates to commercial QAC disinfectants and best-in-class QACs and QPC. See **Figure 3.18** for structures of each compound. White = Low IC_{90}, bacterium less resistant. Orange = High IC_{90}, bacterium more resistant. ATCC 19606 is a lab strain of *A. baumannii*.

resistant strain was attempted in this assay, but it was unable to form mature and robust biofilms. Extensively drug-resistant AB have been shown to be poor biofilm formers previously.[91] The results showed once again that the QPC was better than the QACs, and the Virex imitation and DDAC tended to be better than the best-in-class QAC tested by about a dilution.

	MBEC (µM)				
Strain	**3.1**	**3.3**	**3.1+3.3**	**3.108**	**3.11**
ATCC 19606	500	125	125	250	63
MRSN 4484	500	63	125	250	32
MRSN 29908	500	125	250	500	63

Table 3.9 Minimum biofilm eradication concentration (MBEC) of the top commercial QACs, a clinically used combination of the two (**3.1** + **3.3**), and the most efficacious best-in-class QAC and QPC. ATCC 19606 is a lab strain of *A. baumannii*. White = low MBEC, orange = high MBEC.

In order to determine how resistance to these disinfectants may be occurring, we performed a resistance selection assay on wild-type lab strain ATCC 19606 with the best-in-class QAC and QPC, as well as the best commercial QACs, BAC and DDAC (**Table 3.10**). During the 100 serial passages, no resistance was observed for the QPC; however, the isolate that survived the 100 days at sub-MIC concentrations did have the most mutations of any resistant isolate, indicating the bacterium tried to overcome the QPC treatment but these mutations were futile. Resistance was

Mutant Strain	Disinfectant MIC (µM)						Resistance Mutations											
	Commercial QACs				Best-in-Class QACs		AdeB	HypEP	RpoC	PpsA	YahK	PpiB	ArgF	AstC	TynA	MlaA	AtoC	HypTR
	3.1	3.2	3.3	3.4	3.108	3.11												
ATCC 19606 (WT)	32	8	4	63	4	2												
2X MIC BAC	63	8	8	63	32	2	H84D	L160L	P39T			L118fs				Trp128*		
2X MIC DDAC	32	8	8	63	8	2	H84D					L118fs						V121F
2X MIC 3.108	32	8	4	63	8	2	H84D											
4X MIC 3.108	63	8	8	125	16	2	H84D						E227fs					
8X MIC 3.108	63	8	8	63	32	2	H84D					L118fs						
1X MIC 3.110	32	8	4	63	16	2	H84D			V121del	G7R	L118fs		G162G	A518V		P365L	

Mutant Strain	Antibiotic MICs (µM)													
	Aminoglycosides			Cephalosporins			β-Lactam	Carbapenem		Quinolones		Tetracycline	Combo	Polymyxin
	AMK	GEN	TOB	CAZ	FEP	CRO	SAM	IPM	MEM	CIP	LVX	TET	SMX	CST
ATCC 19606 (WT)	8	16	2	16	16	125	8	2	2	4	1	8	>250	0.25
2X MIC BAC	8	16	4	16	16	63	8	1	1	8	1	16	>250	0.25
2X MIC DDAC	2	8	2	32	32	63	8	1	2	4	1	8	>250	0.25
2X MIC 3.108	8	16	4	16	32	125	8	4	2	4	1	16	>250	0.50
4X MIC 3.108	8	16	4	16	32	125	8	4	2	2	1	16	>250	0.50
8X MIC 3.108	1	2	1	8	8	63	8	4	4	4	2	8	>250	0.50
1X MIC 3.110	8	16	4	16	16	63	8	1	2	4	1	8	>250	0.25

Table 3.10 Disinfectant and antibiotic susceptibility profiles of the resistance mutants and the mutations they accrued during exposure. ATCC is a wild-type lab strain of *A. baumannii*. AMK = amikacin, GEN = gentamycin, TOB = tobramycin, CAZ = ceftazidime, FEB = cefepime, CRO = ceftriaxone, SAM = ampicillin-sulbactam, IPM = imipenem, MEM = meropenem, CIP = ciprofloxacin, LVX = levofloxacin, TET = tetracycline, SXT = trimethoprim-sulfamethoxazole, CST = colistin sulfate.

seen for the three QACs, with a two-fold increase for the commercial BAC and DDAC and three resistant strains with two-, four-, and eight-fold increases for the best-in-class QAC.

Gene	Function
AdeB	Multidrug efflux pump
HypEP	PltJ-like ABC family transporter
RpoC	DNA-directed RNA polymerase subunit β
PpsA	Phosphoenolpyruvate synthase
YahK	Zinc-dependent alcohol dehydrogenase
PpiB	Peptidyl-prolyl cis-trans isomerase B
ArgF	Ornithine carbamoyltransferase
AstC	Succinylornithine transaminase
TynA	Tyramine oxidase
MlaA	Phospholipid-binding lipoprotein
AtoC	Putative sigma-54 dependent transcriptional regulator
HypTR	Hypothetical transcriptional regulator

Table 3.11 Expanded functions of the mutated genes discovered in the resistance selection assay.

Next generation whole genome sequencing of the resistant isolates returned mutations in efflux pumps (hypothesized and known), as well as primary metabolism and membrane biosynthesis (**Table 3.10**). Expanded functions of each protein are displayed in **Table 3.11**. Interestingly, a point mutation in the RND multidrug efflux pump AdeB (His84Asp) was seen in all resistant mutants generated. This efflux pump has been previously implicated in effluxing a variety of antibiotics and cationic disinfectants such as ethidium bromide and methyltriphenylphosphonium.[96] The change from neutral to positively charged histidine to negatively charged aspartate may help this efflux pump electrostatically eject these cations from the cell. Additionally, two proteins in arginine biosynthesis and degradation (ArgF and AstC, respectively) that are necessary for cell wall formation were mutated in some isolates.[97,98] Mutations in MlaA, a protein involved in outer membrane biogenesis, were also prevalent in some of the resistant mutants.[99] Additionally, serial passaging with DDAC and the QPC led to strains that had mutations in putative transcriptional regulators, which points towards amphiphilic disinfectant resistance being related to altered gene expression. Some mutants also had changes to their transcription and translation machinery, namely RpoC and PpiB, respectively. This may point to the bacterium overcoming cationic amphiphilic exposure via stabilization of the proteome, as reported by Knauf.[28] Specifically, PpiB is known to assist with and accelerate protein folding.[100,101]

The same frameshift mutation was present in four of the six mutants, indicating it is a generally beneficial mutation to accrue during amphiphile treatment.

The strains were also tested for cross-resistance to the tested amphiphiles as well as the 14 clinically relevant antibiotics the clinical isolates were originally screened against. No cross-resistance was observed with the antibiotics and the resistant mutants, but there was some observed between the amphiphiles (**Table 3.10**). Most notably, the best-in-class QAC was typically more sensitive to the resistance gained in the resistance selection assay, whereas the other amphiphiles were much less perturbed by the resistance mechanisms employed by these strains. The differential resistance seen by the best-in-class QAC also indicates that these bacteria are likely resisting the amphiphiles in different ways, possibly through differences in upregulation of efflux pumps or modulation of other genes.

Herein, we were able to delve deeper into the correlation between amphiphile and antibiotic resistance. We demonstrated that colistin resistance confers resistance to QACs, whereas the newly investigated QPC as able to evade this resistance. We also demonstrated that this QPC is more adept at eradicating biofilms than its QAC counterparts, and likewise does not induce resistance. On the other hand, the tested commercial and best in class QACs were susceptible to resistance selection and were not as able to eradicate biofilms. Additionally, the best in class QAC tested against the generated resistant isolates was susceptible to cross resistance generated by the other QACs. Taken together, these results demonstrate the need for innovation in disinfectant practices in hospital settings to ensure the eradication of MDR, XDR, and PDR gram negative bacteria.

3.6.2 P. aeruginosa

The synthesis of these compounds was completed by members of the Minbiole lab. MIC and hemolysis assays were completed by Ryan A. Allen, Savannah J. Post, and Kelly R. Morrison-Lewis. Continuing research on this topic is being undertaken by Christian A. Sanchez.

Strain	Antibiotic Susceptibility													
	Aminoglycosides			Cephalosporin			β-Lactam		Carbapenem		Quinolone		Trimethoprim	Combo
	AMK	GEN	TOB	CAZ	FEB	CRO	AZT	SAM	IPM	MEM	CIP	LVX	TRI	PTC
MRSN 4841	R	R	I	S	R	R	R	R	S	S	R	R	R	S
MRSN 1739	S	R	R	R	I	R	R	R	R	R	R	R	R	S
MRSN 3705	S	S	S	R	R	R	R	R	S	S	R	R	R	R
MRSN 321	S	S	S	R	R	R	R	R	R	S	S	S	R	R
MRSN 1938	S	R	R	S	S	R	S	R	R	I	R	R	R	S
MRSN 2444	R	R	R	S	S	R	R	R	R	R	R	R	R	S
MRSN 994	S	S	S	R	R	R	R	R	R	R	R	R	R	R
MRSN 5498	S	R	R	S	R	R	R	R	R	R	R	R	R	R
MRSN 5508	S	S	R	S	R	R	NT	R	R	R	R	R	R	R
MRSN 5524	S	R	R	I	R	R	R	R	R	R	R	R	R	S
MRSN 6220	R	R	R	R	R	R	R	R	R	R	R	R	R	R
MRSN 8130	R	S	R	S	R	R	R	R	R	R	R	R	R	R
MRSN 8914	R	R	R	R	R	R	R	R	R	R	R	R	R	R
MRSN 6695	S	S	S	R	R	R	R	R	R	R	R	R	R	R
MRSN 8136	S	R	S	R	R	R	R	R	R	R	R	R	R	R
MRSN 5539	S	R	S	R	R	R	R	R	R	R	R	R	R	R
MRSN 8912	S	R	R	S	R	R	R	R	R	R	R	R	R	S
MRSN 6241	S	R	R	R	R	R	R	R	R	R	R	R	R	R
MRSN 8141	S	R	R	R	R	R	R	R	R	R	R	R	R	R
MRSN 6678	S	R	R	R	R	R	R	R	R	R	R	R	R	R
MRSN 8915	R	R	R	S	I	R	S	R	R	I	R	R	R	R
MRSN 9873	S	R	R	R	R	R	S	R	R	R	S	S	R	S
MRSN 409937	S	S	S	R	R	R	R	R	S	S	R	R	R	R
MRSN 23861	S	S	I	R	R	R	R	R	R	R	R	R	R	S
MRSN 12914	R	R	R	R	R	R	R	R	R	R	R	R	R	S
MRSN 11536	S	R	R	S	S	R	R	R	R	R	R	R	R	S
MRSN 390231	S	R	S	R	R	R	R	R	S	S	R	R	R	S

Table 3.12 Antibiotic susceptibility profiles of the tested *P. aeruginosa* clinical isolates. NT = not tested, I = intermediate resistance, AMK = amikacin, GEN = gentamycin, TOB = tobramycin, CAZ = ceftazidime, FEB = cefepime, CRO = ceftriaxone, AZT = aztreonam, SAM = ampicillin-sulbactam, IPM = imipenem, MEM = meropenem, CIP = ciprofloxacin, LVX = levofloxacin, TRI = trimethoprim, PTC = piperacillin-tazobactam.

In a similar approach, we started with a thoughtfully tailored group of resistant PA (**Table 3.12**). We then determined the MICs of the selected best in class QACs and commercial QACs against this panel (**Table 3.13**). IC_{90}'s were not performed for these strains as they exhibited less microcolony formation and three consistent trials were able to be acquired. The clearest trend from this data is that the commercially available QACs are far less active than the best-in-class QACs. When it comes to the most active best in class QACs, 2-Pyr-11 was again one of the most active QACs in the group, along with 12(3)0(3)12, demonstrating that 11 to 12 carbon chains are more active than their 10 carbon chain counterparts. It was also apparent that there was a preference for bisQACs over tris- or monoQACs. Future work on these strains will include resistance selection and MBEC assays, as well as testing the strains against **3.110**.

3.7 Developing Novel QAC Scaffolds from a Natural Product: Quaternization of Ianthelliformisamine C

Strain	Amphiphilic Disinfectant Susceptibility MIC (μM)														
	Commercial QACs				Tris- and TetraQACs				Alkyl BisQACs				Aryl BisQACs		
	3.1	3.2	3.3	3.4	3.99	3.100	3.101	3.102	3.103	3.104	3.105	3.106	3.107	3.108	3.109
MRSN 4841	>250	250	125	>250	32	125	>250	63	63	32	63	>250	4	16	250
MRSN 1739	>250	250	125	>250	16	125	16	63	8	63	125	>250	8	16	8
MRSN 3705	125	250	32	125	32	16	16	32	8	8	16	8	8	16	16
MRSN 321	>250	125	32	>250	>250	>250	>250	>250	125	250	>250	>250	>250	8	63
MRSN 1938	>250	125	250	>250	32	250	16	63	63	16	63	16	16	16	125
MRSN 2444	>250	250	125	>250	32	16	16	63	8	32	63	8	16	8	32
MRSN 994	250	125	125	250	32	16	>250	63	8	125	63	8	8	16	16
MRSN 5498	>250	125	125	>250	63	>250	>250	125	125	8	125	>250	>250	>250	16
MRSN 5508	>250	125	63	>250	16	8	8	4	8	16	8	>250	>250	16	32
MRSN 5524	>250	250	125	250	16	16	16	16	8	16	8	8	8	16	32
MRSN 6220	250	125	32	125	16	16	16	8	4	8	4	8	8	16	8
MRSN 8130	>250	250	250	>250	63	125	>250	16	8	125	8	>250	>250	>250	250
MRSN 8914	>250	125	63	>250	63	32	>250	8	8	8	8	8	>250	8	8
MRSN 6695	>250	125	63	>250	>250	>250	>250	125	63	32	63	16	32	32	>250
MRSN 8136	>250	125	125	125	16	16	16	16	8	16	16	8	16	16	32
MRSN 5539	>250	>250	250	>250	32	16	8	63	250	32	250	16	32	16	125
MRSN 8912	250	250	63	125	32	125	>250	63	8	63	63	8	8	16	125
MRSN 6241	>250	250	63	>250	63	>250	>250	125	125	16	250	8	8	>250	125
MRSN 8141	>250	250	>250	>250	16	63	16	125	4	250	8	>250	8	16	32
MRSN 6678	>250	250	125	>250	250	>250	>250	250	250	250	250	>250	16	>250	250
MRSN 8915	250	125	63	>250	63	250	>250	125	63	32	63	>250	>250	16	125
MRSN 9873	>250	250	250	>250	63	250	>250	125	63	250	125	>250	>250	>250	32
MRSN 409937	250	125	32	125	32	125	16	32	26	16	32	16	>250	32	125
MRSN 23861	>250	250	250	>250	125	16	16	16	8	63	32	16	16	32	32
MRSN 12914	>250	250	250	>250	16	16	16	8	8	16	16	16	16	16	16
MRSN 11536	250	250	125	250	32	32	16	16	16	32	16	16	32	16	32
MRSN 390231	250	125	125	250	63	250	63	63	4	32	4	8	4	4	250

Table 3.13 MIC values for the tested *P. aeruginosa* clinical isolates against the commercially available QACs and the best-in-class QACs. White = low MIC, high activity. Orange = high MIC, low activity.

The synthesis of these compounds was completed by Ryan A. Allen and Caroline McCormack in equal contribution. The MIC, DISC, nitrocefin hydrolysis, and propidium iodide assays were completed by Ryan A. Allen and Caroline McCormack in equal contribution. A manuscript is in preparation to be submitted to ChemMedChem with the title "Transformation of Ianthelliformisamine C into a Novel Quaternary Ammonium Compound Decreases its Antibacterial Activity". Authors: Ryan A. Allen, Caroline McCormack, William M. Wuest.

3.7.1 Activity of the Ianthelliformisamines and Potential for Polypharmacological Development

As previously mentioned in chapter 1, development of polypharmacological antibiotics is a viable strategy for preventing the eventual rise of resistance. We therefore sought to apply this strategy to the generation of a QAC, hypothesizing that a QAC with multiple targets would not generate resistance as quickly when leaked into the environment. We initially chose the ianthelliformisamines A and C (**Figure 3.19**) for this approach as they have previously reported

activity as protonophores in *P. aeruginosa* (MIC of 25 μg/mL) and inhibiting human carbonic anhydrase IX, as well as other human carbonic anhydrases, with nanomolar inhibitory activity (270 nM).[102,103] A quick BLASTp search of the PA and *S. aureus* (SA) genomes revealed that both organisms have an analogous enzyme.[104] The SA enzyme aligned with a score of 61.2 and an identity of 40.26%, while the alignment for PA gave a score of 99.4 and 30.47% identity. Moreover, ianthelliformisamine C was found to inhibit *M. tuberculosis* β-carbonic anhydrase with 10 μM inhibition.[105] The BLASTp results from the SA and PA genomes revealed similar proteins in both bacteria, with a score of 111 and identity of 45.93% for SA and a score of 69.7 and identity of 30.77% for PA.[106] Carbonic anhydrases are viewed as new targets for antibiotic development as they are necessary for bacterial survival.[105,107] Additionally, pulmonarin B, a trimethyl QAC with a similar structure to the ianthelliformisamines, was found to be a potent acetylcholinesterase inhibitor in humans (**Figure 3.19)**.[108] A BLASTp search of the SA and PA genomes revealed similar carboxylesterase and lipase enzymes with good alignment (SA: 143 score and 36.44% identity, PA: score of 49 and 55.24% identity).[109] Therefore, it is reasonable to assume that in addition to being protonophores, these molecules, specifically ianthelliformisamine C, likely inhibit the carbonic anhydrases of SA and PA and its QAC derivative may inhibit carboxylesterases or lipases.

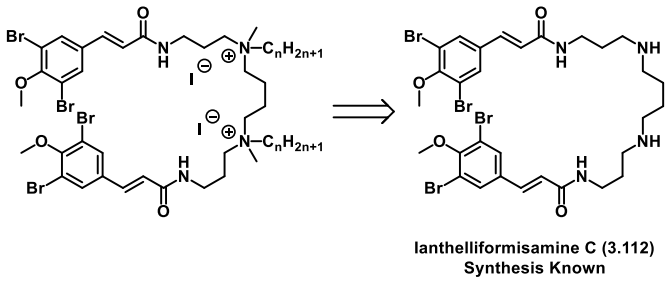

Scheme 3.5 Retrosynthesis of the ianthelliformisamine C QAC analogs. Total synthesis of **3.112** had already been completed by others.

3.7.2 Total Synthesis of Ianthelliformisamine C and QAC Analogs

Given the proven activity of ianthelliformisamine C, we decided to move forward with development of it as a potential QAC with polypharmacological properties (**Scheme 3.5**). The QACs could be easily made using already known procedures from **3.112**, namely a reductive amination followed by an alkylation.[53] This strategy gave us the option to do the reductive amination on with etither the long chains or formaldehyde to give the methyl groups, then alkylation with the opposite alkyl bromide. We started by using the total synthesis originally developed by Pieri and coworkers, which starts with a Wittig on 3,5-dibromo-4-hydroxybenaldehyde, which gives the E-isomer exclusively (**Scheme 3.6**).[102] After methylation of free phenol and hydrolysis of ester, acid is primed for coupling to spermine. Unfortunately, the literature reported procedure for the amide coupling with dicyclohexylcarbodiimide (DCC) and hydroxybenzotriazole (HOBt) did not go as smoothly as the rest of the synthesis. When these conditions were attempted, we obtained C in 29% yield, albeit with some small impurities. We reattempted this reaction several times with varying success (**Table 3.14**). We attribute the variable yields mainly to the purification process of this molecule. The reaction itself has multiple byproducts, including dicyclohexylurea, HOBt, excess starting acid, excess DCC, and monomer ianthelliformisamine A. The reaction also does not go to completion, adding DCC-coupled starting acid and HOBt-coupled starting acid to the mixture. We tried to circumvent this by running the reaction for longer; however, this did not yield more product. We also ran the reaction at a

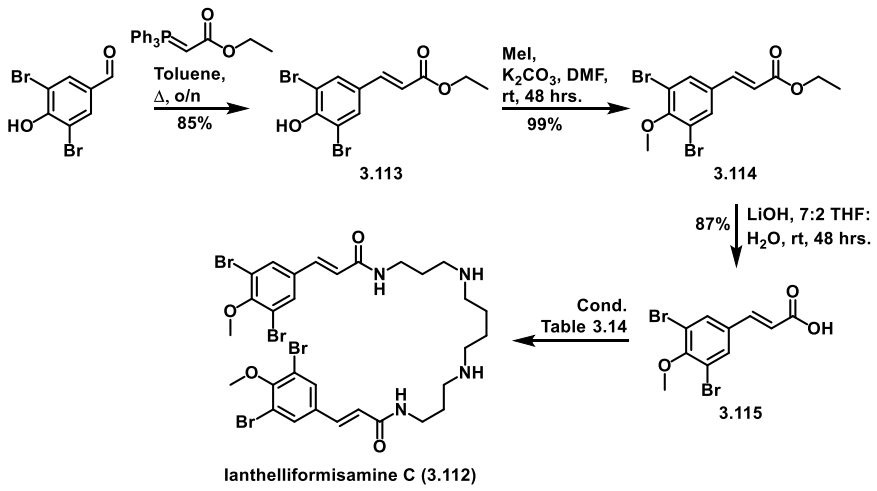

Scheme 3.6 Synthetic scheme towards the total synthesis of **3.112**.

higher temperature to consume more starting materials, which only led to the isolation of acid and activated esters. The variety of intermediates and side products made the columns particularly difficult to run and get good separation. Moreover, the columns had to be run in a gradient of DCM:methanol:NH_4OH, with concentrations going up to 5:5:1 DCM:methanol: NH_4OH. This is an issue as silica gel starts to shear when concentrations go above 10% methanol in DCM, which meant we also collected silica with our desired material.

To circumvent this troublesome column, we attempted a variety of different purification techniques. First, we tried doing an extraction procedure, in which we would first quench the reaction with 0.5 M HCl in water, then extract the organic layer multiple times with the same solvent.. This protonates the free amines on C, thereby extracting it from the organic layer and leaving the starting material acid, HOBt, and any coupled intermediates in the organic layer. The aqueous layers would then be basified with 1 M NaOH, combined, and extracted multiple times with 5% methanol in DCM. The base would deprotonate the free amines, allowing them to dissolve in the organic layer more efficiently. After the last extraction and drying with sodium sulfate, the

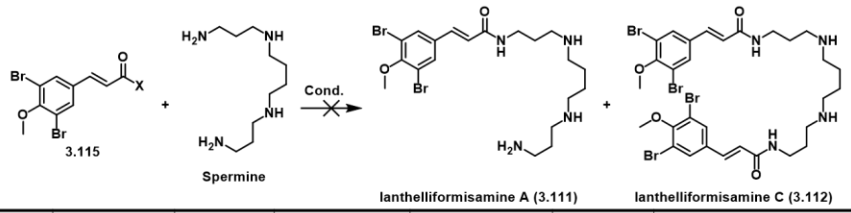

X	Coupling Reagent	Activator?	Solvent	Base	Temp.	Time	Result
-OH	DCC	HOBt	DCM	none	rt	24 hrs.	29% **3.112**
-OH	DCC	HOBt	DCM	none	rt	24 hrs.	14% **3.111**, 3% **3.112**
-OH	DCC	NHP	Dioxane	TEA	rt	17 hrs.	Both observed in crude, unable to purify
-OH	HATU	none	MeCN	DIPEA	rt	19 hrs.	HATU coupled starting material
-OH	HATU	none	DCM	TEA	rt	19 hrs.	20% **3.112**
-OH	T3P	none	EtOAc	TEA	0˚C to 65˚C	2 days	Coupling to T3P, partially hydrolyzed T3P
-OH	$SOCl_2$	none	DCM	TEA, DMAP	0˚C to rt	o/n	T1: 28% **3.112**, T2: 6% **3.112**
-OH	$SOCl_2$	none	DCM	TEA	0˚C to rt	o/n	Both observed in crude, unable to purify
-OEt	none	TBD	DCM	none	rt	o/n	Starting materials
-OEt	none	none	MeOH	none	reflux	42 hrs.	Starting materials
-OEt	none	none	THF	none	reflux	70 hrs.	1,4-addition to α,β-unsaturated ester

Table 3.14 Coupling conditions attempted to make ianthelliformisamine C (**3.112**). DCC = dicyclohexylcarbodiimide, HOBt = 1-hydroxybenzotriazole, NHP = *N*-hydroxythalimide, HATU = hexafluorophosphate azabenzotriazoletetramethyluronium, T3P = propanephosphonic anhydride.

combined organic layers were filtered, concentrated, and analyzed via NMR. To our chagrin, there were always some residual peaks from starting materials and byproducts, as the extraction process was never completely efficient at removing them. We then attempted running a reverse phase column. This procedure would allow for us to use a silica gel that would not shear under the solvent conditions, and would allow for easy purification of the somewhat aqueous soluble C. Unfortunately, these columns took over 8 hours to run and did not give separation. We then sought to use HPLC instead of a hand column for our reverse phase approach. This approach gave back starting material, so we hypothesized that our material was degrading on the column because of the acidic aqueous conditions. However, even when we used ammonium hydroxide in place of formic acid in the solvents, we still saw only starting material acid come off the column. Knowing from the crude NMR that C was most likely in the mixture, we hypothesized that despite the basic conditions, we were either degrading our desired product or it was in quantities too low to detect

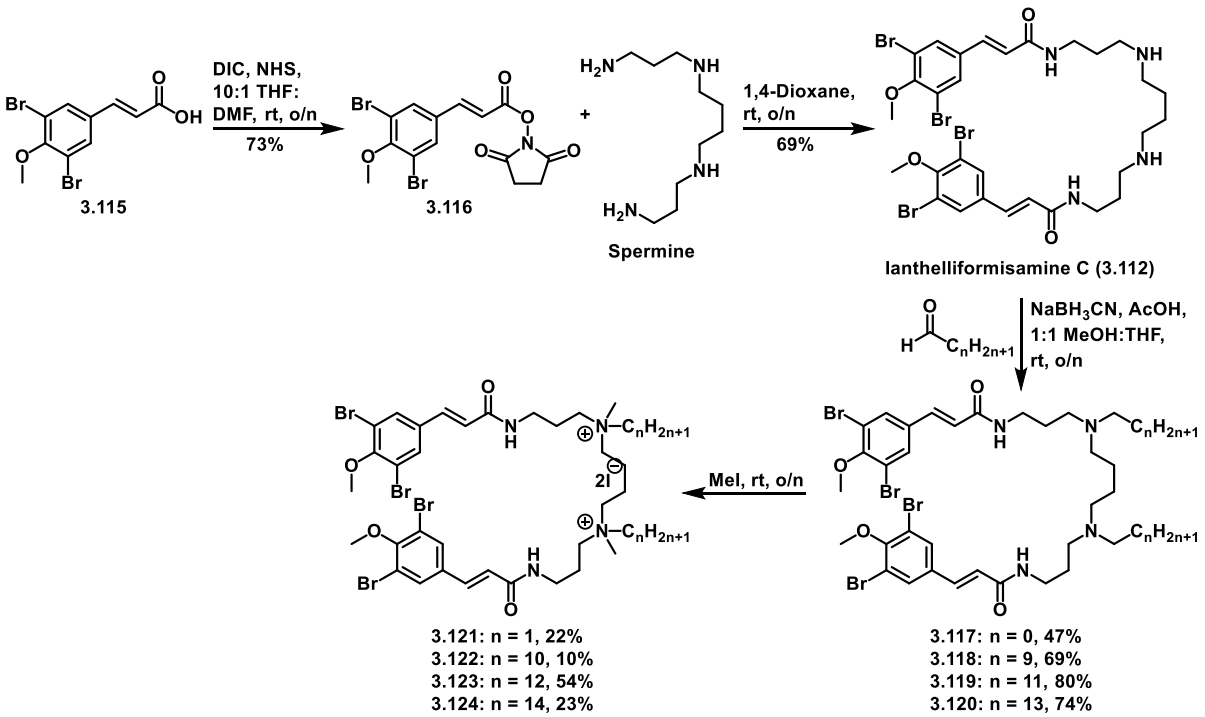

Scheme 3.6 Total synthesis of the desired QAC analogs **3.121**-**3.124**. DIC = diisopropylcarbodiimide, NHS = *N*-hydroxysuccinimide.

with the UV detector on the instrument. Despite our best efforts, the column appeared to be the best solution to our purification problem as it still gave the best separation.

In attempt to optimize the amide coupling, we tried a variety of different coupling conditions (**Table 3.14**). We tried switching out the HOBt for *N*-hydroxythalimide, as HOBt comes as a hydrate salt and we hypothesized this water could be responsible for consumption of the DCC activated ester and returning of starting materials. This worked better than the HOBt at producing product; however, we were unable to separate A and C from one another, nor from the triethylamine (TEA) base. When HATU was used as the coupling reagent, we initially did not produce any product in the reaction. When we switched the solvent and base from acetonitrile and diisopyopylethylamine (DIPEA) to DCM and TEA, we were able to isolate C in 20% yield. T3P gave no product even though no starting material acid was detected in the mixture via TLC. We hypothesize that the intermediate was forming and either partially hydrolyzing to make the ester less activated or the ester intermediate was not electrophilic enough to tempt spermine to react. Seeing as the acid is conjugated to an electron rich aryl ring via the alkene, it is likely not as electrophilic as typical acids in amide couplings. In an attempt to make the carbonyl more electrophilic, we formed acyl chloride *in situ*, then added it to a solution of spermine. We were able to produce C in 28% yield using this procedure; however, the yields were irreproducible. This can again be attributed to the challenging purifications, especially since product usually coeluted with TEA. We also attempted several direct amidations from the ethyl ester intermediate; however, these reactions either gave no product or, in the case of when THF was used as the solvent, Michael addition to the α,β-unsaturated ester. This occurred either through Michael addition of spermine or water from the THF or spermine that attacked that position.

Gratifyingly, we were able to make C via a two step amide coupling procedure (**Scheme 3.6**). By first activating the ester with diisopropylcarbodiimide (DIC) to obtain the activated *N*-hydroxysuccinimide (NHS) ester, we were able to cleanly purify it from the byproducts and side products to allow for the clean addition of spermine into ester. Because the only side product was NHS, this reaction was easy to purify either by column chromatography or by extraction via the previously described procedure. We were then able to obtain pure C in 69% yield.

With the worst of our woes behind us, we were able to do a reductive amination of long chain aldehydes as well as formaldehyde onto the core scaffold (**Scheme 3.6**). These reactions proceeded in moderate to good yields and were simple to purify via column chromatography. With alkylated amines in hand, we were then able to methylate the amines with methyl iodide to furnish the QACs in poor yields. The yields for these reactions are low because the purification required trituration with hot ethyl acetate to extract out the impurities, which dissolves a small amount of the product as well. We also attempted to reverse the order of alkylation by first methylating with a reductive amination, then alkylating with long chain bromides. These reactions did not produce product, even when refluxed in acetonitrile or heated with sodium iodide in DMF.

3.7.3 Biological Activity of Ianthelliformisamine C and its QAC Derivatives

With the long sought after C and QACs in hand, we turned our gazes towards assessing their biological activity. We started with an MIC assay against eight strains of biologically

	MIC (μg/mL)					
Strain	**3.1 (BAC)**	**3.112**	**3.117**	**3.121**	**3.123**	**3.124**
MSSA	2	2	8	8	>250	>250
HA-MRSA	2	2	63	32	>250	>250
CA-MRSA	2	2	63	8	>250	>250
E. faecalis	8	16	32	63	>250	>250
E. coli	8	16	32	63	>250	>250
A. baumanii	8	125	63	32	>250	>250
***P. aeruginosa* (PAO1)**	32	16	>250	63	>250	>250
***P. aeruginosa* (PA14)**	32	125	>250	125	>250	>250
Lysis20	16	125	32	125	32	16

Table 3.15 MICs of ianthelliformisamine C and QAC analogs against gram- positive and -negative strains, as well as hemolysis$_{20}$ concentrations. MSSA = methicillin-susceptible *S. aureus*, HA-MRSA = hospital-acquired methicillin-resistant *S. aureus*, CA-MRSA = community-acquired methicillin-resistant *S. aureus*.

relevant pathogens, using commercial QAC BAC (**3.1**) as a control (**Table 3.15**). The bisdecyl QAC **3.122** was not tested as it was unable to be purified and retain its purity. To our dismay, the only QAC that was active was dimethyl QAC **3.121**. The long chain QACs **3.123** and **3.124** were likely inactive as they did not dissolve in the 10% DMSO in water solution. **3.112** tended to be the most active against all pathogens tested, with **3.121** and **3.117** having slightly diminished activity. *N*-methyl natural product **3.117** being less active than the natural product itself is interesting as it implies that either the methyl groups make C a worse protonophore, or the additional methyl groups interfere with binding to β-carbonic anhydrase or other potential protein targets. Additionally, **3.121** was likely active because the phenolic amide is acting like a long alkyl chain and intercalating into the membrane.

We then did a preliminary assessment of toxicity via hemolysis$_{20}$ assay (**Table 3.15**). Despite being inactive against bacteria, the long chain QACs were able to lyse red blood cells with activity that is on par with commercially available BAC. C, N-methyl C, and dimethyl QAC C were all relatively nonlytic to red blood cells, giving them a good therapeutic index. Surprisingly, the long chain QACs were able to lyse red blood cells, indicating they are soluble in high enough quantities to lyse red blood cells but not bacterial cells.

3.8 Conclusions

This work explored and expanded upon the classes QACs and bacterial resistance to them. Starting with appending QACs to antibiotic polymyxin B, we were able to broaden its scope from just gram-negative to include gram-positive bacteria as well. We also completed further investigations into rigidity-activity relationships, we were able to corroborate previous findings indicating that antibacterial activity is improved when the positively charged nitrogens are closer to one another, possibly through cooperative binding. We additionally explored trivalent sulfonium

compounds (TSCs) as replacements for nitrogenous QACs. We also utilized the ferrocene moiety containing QAC as a trojan horse strategy, aiming to use the iron as a pass for easier access to the cytosol. The best of these compounds had single digit micromolar activity against all strains tested, and even against clinical MRSA isolates. We discovered that the TSCs had comparable activity to their QAC counterparts, and they could potentially evade resistance mechanisms to QACs. We also explored the mechanisms of QAC resistance in clinical isolates of *A. baumannii*, finding a correlation between QAC resistance and colistin resistance. We also identified novel quaternary phosphonium compounds (QPCs) as potent antibacterial agents against these extensively and pan drug resistant isolates. Through a resistance selection assay, we were able to discover a mutation in the efflux pump AdeB that corresponds to QAC resistance; however, even with this mutation, the bacteria were still susceptible to the tested QPC. Additionally, QPCs were more potent biofilm eradicators than any of the commercial or best-in-class QACs tested. We also tested our best-in-class compounds against clinical isolates of *P. aeruginosa*, finding that commercial QACs that are currently being used in hospitals are ineffective against these highly resistant pathogens. We also discovered a slight preference for bisQACs with 11 to 12 carbon chain lengths for the best activity. To expand upon polypharmacology in QACs, we undertook the total synthesis of ianthelliformisamine C and it quaternization. Through this study, we were able to determine one of the mechanisms of action of these compounds, namely that of membrane depolarization for C and membrane permeabilization for the QAC. Taken together, this work broadens the scope of QACs, novel derivatives thereof, and the mechanisms of resistance that endanger their continued efficacy.

3.9 Chapter 3 References

(1) Bureš, F. Quaternary Ammonium Compounds: Simple in Structure, Complex in Application. *Top Curr Chem (Cham)* **2019**, *377* (3), 14. https://doi.org/10.1007/s41061-019-0239-2.

(2) S, M.; Vk, T. Esterquats: The Novel Class of Cationic Fabric Softeners. *Journal of oleo science* **2007**, *56* (6). https://doi.org/10.5650/jos.56.269.
(3) Zhu, M.-M.; Fang, Y.; Chen, Y.-C.; Lei, Y.-Q.; Fang, L.-F.; Zhu, B.-K.; Matsuyama, H. Antifouling and Antibacterial Behavior of Membranes Containing Quaternary Ammonium and Zwitterionic Polymers. *J Colloid Interface Sci* **2021**, *584*, 225–235. https://doi.org/10.1016/j.jcis.2020.09.041.
(4) Gerba, C. P. Quaternary Ammonium Biocides: Efficacy in Application. *Appl Environ Microbiol* **2015**, *81* (2), 464–469. https://doi.org/10.1128/AEM.02633-14.
(5) Sanz, M.; Serrano, J.; Iniesta, M.; Santa Cruz, I.; Herrera, D. Antiplaque and Antigingivitis Toothpastes. *Monogr Oral Sci* **2013**, *23*, 27–44. https://doi.org/10.1159/000350465.
(6) Bapat, R. A.; Parolia, A.; Chaubal, T.; Yang, H. J.; Kesharwani, P.; Phaik, K. S.; Lin, S. L.; Daood, U. Recent Update on Applications of Quaternary Ammonium Silane as an Antibacterial Biomaterial: A Novel Drug Delivery Approach in Dentistry. *Front Microbiol* **2022**, *13*, 927282. https://doi.org/10.3389/fmicb.2022.927282.
(7) Denyer, S. P.; Stewart, G. S. A. B. Mechanisms of Action of Disinfectants. *International Biodeterioration & Biodegradation* **1998**, *41* (3), 261–268. https://doi.org/10.1016/S0964-8305(98)00023-7.
(8) McDonnell, G.; Russell, A. D. Antiseptics and Disinfectants: Activity, Action, and Resistance. *Clinical Microbiology Reviews* **1999**, *12* (1), 147–179. https://doi.org/10.1128/CMR.12.1.147.
(9) Lambert, P. A.; Hammond, S. M. Potassium Fluxes, First Indications of Membrane Damage in Micro-Organisms. *Biochemical and Biophysical Research Communications* **1973**, *54* (2), 796–799. https://doi.org/10.1016/0006-291X(73)91494-0.
(10) Denyer, S. P. Mechanisms of Action of Biocides. *International Biodeterioration* **1990**, *26* (2), 89–100. https://doi.org/10.1016/0265-3036(90)90050-H.
(11) Kwaśniewska, D.; Chen, Y.-L.; Wieczorek, D. Biological Activity of Quaternary Ammonium Salts and Their Derivatives. *Pathogens* **2020**, *9* (6), 459. https://doi.org/10.3390/pathogens9060459.
(12) Jiao, Y.; Niu, L.; Ma, S.; Li, J.; Tay, F. R.; Chen, J. Quaternary Ammonium-Based Biomedical Materials: State-of-the-Art, Toxicological Aspects and Antimicrobial Resistance. *Prog Polym Sci* **2017**, *71*, 53–90. https://doi.org/10.1016/j.progpolymsci.2017.03.001.
(13) Fredell, D. L. Biological Properties and Applications of Cationic Surfactants. In *Cationic Surfactants*; CRC Press, 1994.
(14) Jacobs, W. A. THE BACTERICIDAL PROPERTIES OF THE QUATERNARY SALTS OF HEXAMETHYLENETETRAMINE. *J Exp Med* **1916**, *23* (5), 563–568.
(15) Dogmak, G. Eine Neue Klasse von Desinfektionsmitteln. *Dtsch. Med. Wochenschr.* **1935**, *61* (21), 829–832.
(16) Morrison, K. R.; Allen, R. A.; Minbiole, K. P. C.; Wuest, W. M. More QACs, More Questions: Recent Advances in Structure Activity Relationships and Hurdles in Understanding Resistance Mechanisms. *Tetrahedron Letters* **2019**, *60* (37), 150935. https://doi.org/10.1016/j.tetlet.2019.07.026.
(17) Forman, M. E.; Jennings, M. C.; Wuest, W. M.; Minbiole, K. P. C. Building a Better Quaternary Ammonium Compound (QAC): Branched Tetracationic Antiseptic Amphiphiles. *ChemMedChem* **2016**, *11* (13), 1401–1405. https://doi.org/10.1002/cmdc.201600176.
(18) EPA. *Disinfectants Pesticides*. https://cfpub.epa.gov/wizards/disinfectants/ (accessed 2023-04-04).
(19) Zheng, G.; Webster, T. F.; Salamova, A. Quaternary Ammonium Compounds: Bioaccumulation Potentials in Humans and Levels in Blood before and during the Covid-19 Pandemic. *Environ. Sci. Technol.* **2021**, *55* (21), 14689–14698. https://doi.org/10.1021/acs.est.1c01654.
(20) Zheng, G.; Filippelli, G. M.; Salamova, A. Increased Indoor Exposure to Commonly Used Disinfectants during the COVID-19 Pandemic. *Environ. Sci. Technol. Lett.* **2020**, *7* (10), 760–765. https://doi.org/10.1021/acs.estlett.0c00587.
(21) Li, X.; Brownawell, B. J. Quaternary Ammonium Compounds in Urban Estuarine Sediment Environments - A Class of Contaminants in Need of Increased Attention? *Environ. Sci. Technol.* **2010**, *44* (19), 7561–7568. https://doi.org/10.1021/es1011669.
(22) Hora, P. I.; Arnold, W. A. Photochemical Fate of Quaternary Ammonium Compounds in River Water. *Environ. Sci.: Processes Impacts* **2020**, *22* (6), 1368–1381. https://doi.org/10.1039/D0EM00086H.
(23) Lowbury, E. J. L. Contamination of Cetrimide and Other Fluids with Pseudomonas Pyocyanea. *Br J Ind Med* **1951**, *8* (1), 22–25. https://doi.org/10.1136/oem.8.1.22.
(24) Plotkin, S. A.; Austrian, R. Bacteremia Caused by Pseudomonas Sp. Following the Use of Materials Stored in Solutions of a Cationic Surface-Active Agent. *Am J Med Sci* **1958**, *235* (6), 621–627. https://doi.org/10.1097/00000441-195806000-00001.

(25) Malizia, W. F.; Gangarosa, E. J.; Goley, A. F. Benzalkonium Chloride as a Source of Infection. *New England Journal of Medicine* **1960**, *263* (16), 800–802. https://doi.org/10.1056/NEJM196010202631608.
(26) Adair, F. W.; Geftic, S. G.; Gelzer, J. Resistance of Pseudomonas to Quaternary Ammonium Compounds. I. Growth in Benzalkonium Chloride Solution. *Applied Microbiology* **1969**, *18* (3), 299–302. https://doi.org/10.1128/am.18.3.299-302.1969.
(27) McBain, A. J.; Ledder, R. G.; Moore, L. E.; Catrenich, C. E.; Gilbert, P. Effects of Quaternary-Ammonium-Based Formulations on Bacterial Community Dynamics and Antimicrobial Susceptibility. *Appl Environ Microbiol* **2004**, *70* (6), 3449–3456. https://doi.org/10.1128/AEM.70.6.3449-3456.2004.
(28) Knauf, G. A.; Cunningham, A. L.; Kazi, M. I.; Riddington, I. M.; Crofts, A. A.; Cattoir, V.; Trent, M. S.; Davies, B. W. Exploring the Antimicrobial Action of Quaternary Amines against *Acinetobacter Baumannii*. *mBio* **2018**, *9* (1), e02394-17. https://doi.org/10.1128/mBio.02394-17.
(29) Heredia, R. M.; Boeris, P. S.; Biasutti, M. A.; López, G. A.; Paulucci, N. S.; Lucchesi, G. I. Coordinated Response of Phospholipids and Acyl Components of Membrane Lipids in Pseudomonas Putida A (ATCC 12633) under Stress Caused by Cationic Surfactants. *Microbiology* **2014**, *160* (12), 2618–2626. https://doi.org/10.1099/mic.0.081943-0.
(30) Srinivasan, V. B.; Rajamohan, G.; Gebreyes, W. A. Role of AbeS, a Novel Efflux Pump of the SMR Family of Transporters, in Resistance to Antimicrobial Agents in Acinetobacter Baumannii. *Antimicrob Agents Chemother* **2009**, *53* (12), 5312–5316. https://doi.org/10.1128/AAC.00748-09.
(31) Li, X.-Z.; Poole, K.; Nikaido, H. Contributions of MexAB-OprM and an EmrE Homolog to Intrinsic Resistance of Pseudomonas Aeruginosa to Aminoglycosides and Dyes. *Antimicrob Agents Chemother* **2003**, *47* (1), 27–33. https://doi.org/10.1128/AAC.47.1.27-33.2003.
(32) Huang, L.; Wu, C.; Gao, H.; Xu, C.; Dai, M.; Huang, L.; Hao, H.; Wang, X.; Cheng, G. Bacterial Multidrug Efflux Pumps at the Frontline of Antimicrobial Resistance: An Overview. *Antibiotics (Basel)* **2022**, *11* (4), 520. https://doi.org/10.3390/antibiotics11040520.
(33) Wand, M. E.; Sutton, J. M. Efflux-Mediated Tolerance to Cationic Biocides, a Cause for Concern? *Microbiology (Reading)* **2022**, *168* (11). https://doi.org/10.1099/mic.0.001263.
(34) Jensen, S. O.; Apisiridej, S.; Kwong, S. M.; Yang, Y. H.; Skurray, R. A.; Firth, N. Analysis of the Prototypical Staphylococcus Aureus Multiresistance Plasmid PSK1. *Plasmid* **2010**, *64* (3), 135–142. https://doi.org/10.1016/j.plasmid.2010.06.001.
(35) Baines, S. L.; Jensen, S. O.; Firth, N.; Gonçalves da Silva, A.; Seemann, T.; Carter, G. P.; Williamson, D. A.; Howden, B. P.; Stinear, T. P. Remodeling of PSK1 Family Plasmids and Enhanced Chlorhexidine Tolerance in a Dominant Hospital Lineage of Methicillin-Resistant Staphylococcus Aureus. *Antimicrob Agents Chemother* **2019**, *63* (5), e02356-18. https://doi.org/10.1128/AAC.02356-18.
(36) Brown, M. H.; Skurray, R. A. Staphylococcal Multidrug Efflux Protein QacA. *J Mol Microbiol Biotechnol* **2001**, *3* (2), 163–170.
(37) Firth, N.; Skurray, R. A. Mobile Elements in the Evolution and Spread of Multiple-Drug Resistance in Staphylococci. *Drug Resistance Updates* **1998**, *1* (1), 49–58. https://doi.org/10.1016/S1368-7646(98)80214-8.
(38) Jennings, M. C.; Forman, M. E.; Duggan, S. M.; Minbiole, K. P. C.; Wuest, W. M. Efflux Pumps May Not Be the Major Drivers of QAC Resistance in Methicillin-Resistant Staphylococcus Aureus. *Chembiochem* **2017**, *18* (16), 1573–1577. https://doi.org/10.1002/cbic.201700233.
(39) Martínez-Suárez, J. V.; Ortiz, S.; López-Alonso, V. Potential Impact of the Resistance to Quaternary Ammonium Disinfectants on the Persistence of Listeria Monocytogenes in Food Processing Environments. *Front Microbiol* **2016**, *7*, 638. https://doi.org/10.3389/fmicb.2016.00638.
(40) Zubris, D. L.; Minbiole, K. P. C.; Wuest, W. M. Polymeric Quaternary Ammonium Compounds: Versatile Antimicrobial Materials. *Curr Top Med Chem* **2017**, *17* (3), 305–318. https://doi.org/10.2174/1568026616666160829155805.
(41) Uppu, D. S. S. M.; Haldar, J. Lipopolysaccharide Neutralization by Cationic-Amphiphilic Polymers through Pseudoaggregate Formation. *Biomacromolecules* **2016**, *17* (3), 862–873. https://doi.org/10.1021/acs.biomac.5b01567.
(42) Hoque, J.; Akkapeddi, P.; Ghosh, C.; Uppu, D. S. S. M.; Haldar, J. A Biodegradable Polycationic Paint That Kills Bacteria in Vitro and in Vivo. *ACS Appl. Mater. Interfaces* **2016**, *8* (43), 29298–29309. https://doi.org/10.1021/acsami.6b09804.
(43) Ghosh, S.; Mukherjee, R.; Mahajan, V. S.; Boucau, J.; Pillai, S.; Haldar, J. Permanent, Antimicrobial Coating to Rapidly Kill and Prevent Transmission of Bacteria, Fungi, Influenza, and SARS-CoV-2. *ACS Appl. Mater. Interfaces* **2022**, *14* (37), 42483–42493. https://doi.org/10.1021/acsami.2c11915.

(44) Geng, Z.; Finn, M. G. Fragmentable Polycationic Materials Based on Anchimeric Assistance. *Chem. Mater.* **2016**, *28* (1), 146–152. https://doi.org/10.1021/acs.chemmater.5b03445.
(45) Geng, Z.; Finn, M. G. Thiabicyclononane-Based Antimicrobial Polycations. *J. Am. Chem. Soc.* **2017**, *139* (43), 15401–15406. https://doi.org/10.1021/jacs.7b07596.
(46) Wu, Z.-C.; Isley, N. A.; Boger, D. L. N-Terminus Alkylation of Vancomycin: Ligand Binding Affinity, Antimicrobial Activity, and Site-Specific Nature of Quaternary Trimethylammonium Salt Modification. *ACS Infect. Dis.* **2018**, *4* (10), 1468–1474. https://doi.org/10.1021/acsinfecdis.8b00152.
(47) LaDow, J. E.; Warnock, D. C.; Hamill, K. M.; Simmons, K. L.; Davis, R. W.; Schwantes, C. R.; Flaherty, D. C.; Willcox, J. A. L.; Wilson-Henjum, K.; Caran, K. L.; Minbiole, K. P. C.; Seifert, K. Bicephalic Amphiphile Architecture Affects Antibacterial Activity. *European Journal of Medicinal Chemistry* **2011**, *46* (9), 4219–4226. https://doi.org/10.1016/j.ejmech.2011.06.026.
(48) Black, J. W.; Jennings, M. C.; Azarewicz, J.; Paniak, T. J.; Grenier, M. C.; Wuest, W. M.; Minbiole, K. P. C. TMEDA-Derived Biscationic Amphiphiles: An Economical Preparation of Potent Antibacterial Agents. *Bioorganic & Medicinal Chemistry Letters* **2014**, *24* (1), 99–102. https://doi.org/10.1016/j.bmcl.2013.11.070.
(49) Paniak, T. J.; Jennings, M. C.; Shanahan, P. C.; Joyce, M. D.; Santiago, C. N.; Wuest, W. M.; Minbiole, K. P. C. The Antimicrobial Activity of Mono-, Bis-, Tris-, and Tetracationic Amphiphiles Derived from Simple Polyamine Platforms. *Bioorganic & Medicinal Chemistry Letters* **2014**, *24* (24), 5824–5828. https://doi.org/10.1016/j.bmcl.2014.10.018.
(50) Mitchell, M. A.; Iannetta, A. A.; Jennings, M. C.; Fletcher, M. H.; Wuest, W. M.; Minbiole, K. P. C. Scaffold-Hopping of Multicationic Amphiphiles Yields Three New Classes of Antimicrobials. *ChemBioChem* **2015**, *16* (16), 2299–2303. https://doi.org/10.1002/cbic.201500381.
(51) Jennings, M. C.; Buttaro, B. A.; Minbiole, K. P. C.; Wuest, W. M. Bioorganic Investigation of Multicationic Antimicrobials to Combat QAC-Resistant Staphylococcus Aureus. *ACS Infect Dis* **2015**, *1* (7), 304–309. https://doi.org/10.1021/acsinfecdis.5b00032.
(52) Grenier, M. C.; Davis, R. W.; Wilson-Henjum, K. L.; LaDow, J. E.; Black, J. W.; Caran, K. L.; Seifert, K.; Minbiole, K. P. C. The Antibacterial Activity of 4,4′-Bipyridinium Amphiphiles with Conventional, Bicephalic and Gemini Architectures. *Bioorganic & Medicinal Chemistry Letters* **2012**, *22* (12), 4055–4058. https://doi.org/10.1016/j.bmcl.2012.04.079.
(53) Al-Khalifa, S. E.; Jennings, M. C.; Wuest, W. M.; Minbiole, K. P. C. The Development of Next-Generation Pyridinium-Based MultiQAC Antiseptics. *ChemMedChem* **2017**, *12* (4), 280–283. https://doi.org/10.1002/cmdc.201600546.
(54) Schallenhammer, S. A.; Duggan, S. M.; Morrison, K. R.; Bentley, B. S.; Wuest, W. M.; Minbiole, K. P. C. Hybrid BisQACs: Potent Biscationic Quaternary Ammonium Compounds Merging the Structures of Two Commercial Antiseptics. *ChemMedChem* **2017**, *12* (23), 1931–1934. https://doi.org/10.1002/cmdc.201700597.
(55) Kontos, R. C.; Schallenhammer, S. A.; Bentley, B. S.; Morrison, K. R.; Feliciano, J. A.; Tasca, J. A.; Kaplan, A. R.; Bezpalko, M. W.; Kassel, W. S.; Wuest, W. M.; Minbiole, K. P. C. An Investigation into Rigidity–Activity Relationships in BisQAC Amphiphilic Antiseptics. *ChemMedChem* **2019**, *14* (1), 83–87. https://doi.org/10.1002/cmdc.201800622.
(56) Sommers, K. J.; Michaud, M. E.; Hogue, C. E.; Scharnow, A. M.; Amoo, L. E.; Petersen, A. A.; Carden, R. G.; Minbiole, K. P. C.; Wuest, W. M. Quaternary Phosphonium Compounds: An Examination of Non-Nitrogenous Cationic Amphiphiles That Evade Disinfectant Resistance. *ACS Infect. Dis.* **2022**, *8* (2), 387–397. https://doi.org/10.1021/acsinfecdis.1c00611.
(57) Ongwae, G. M.; Morrison, K. R.; Allen, R. A.; Kim, S.; Im, W.; Wuest, W. M.; Pires, M. M. Broadening Activity of Polymyxin by Quaternary Ammonium Grafting. *ACS Infect Dis* **2020**, *6* (6), 1427–1435. https://doi.org/10.1021/acsinfecdis.0c00037.
(58) Vaara, M. Polymyxin Derivatives That Sensitize Gram-Negative Bacteria to Other Antibiotics. *Molecules* **2019**, *24* (2), 249. https://doi.org/10.3390/molecules24020249.
(59) Leitgeb, A. J.; Feliciano, J. A.; Sanchez, H. A.; Allen, R. A.; Morrison, K. R.; Sommers, K. J.; Carden, R. G.; Wuest, W. M.; Minbiole, K. P. C. Further Investigations into Rigidity-Activity Relationships in BisQAC Amphiphilic Antiseptics. *ChemMedChem* **2020**, *15* (8), 667–670. https://doi.org/10.1002/cmdc.201900662.
(60) Lau, C. K. Y.; Krewulak, K. D.; Vogel, H. J. Bacterial Ferrous Iron Transport: The Feo System. *FEMS Microbiology Reviews* **2016**, *40* (2), 273–298. https://doi.org/10.1093/femsre/fuv049.
(61) Contreras, H.; Chim, N.; Credali, A.; Goulding, C. W. Heme Uptake in Bacterial Pathogens. *Current Opinion in Chemical Biology* **2014**, *19*, 34–41. https://doi.org/10.1016/j.cbpa.2013.12.014.
(62) Richard, K. L.; Kelley, B. R.; Johnson, J. G. Heme Uptake and Utilization by Gram-Negative Bacterial Pathogens. *Frontiers in Cellular and Infection Microbiology* **2019**, *9*.

(63) Choby, J. E.; Skaar, E. P. Heme Synthesis and Acquisition in Bacterial Pathogens. *Journal of Molecular Biology* **2016**, *428* (17), 3408–3428. https://doi.org/10.1016/j.jmb.2016.03.018.
(64) Khasheii, B.; Mahmoodi, P.; Mohammadzadeh, A. Siderophores: Importance in Bacterial Pathogenesis and Applications in Medicine and Industry. *Microbiological Research* **2021**, *250*, 126790. https://doi.org/10.1016/j.micres.2021.126790.
(65) Page, M. G. P. The Role of Iron and Siderophores in Infection, and the Development of Siderophore Antibiotics. *Clin Infect Dis* **2019**, *69* (Suppl 7), S529–S537. https://doi.org/10.1093/cid/ciz825.
(66) Porcheron, G.; Garenaux, A.; Proulx, J.; Sabri, M.; Dozois, C. Iron, Copper, Zinc, and Manganese Transport and Regulation in Pathogenic Enterobacteria: Correlations between Strains, Site of Infection and the Relative Importance of the Different Metal Transport Systems for Virulence. *Frontiers in Cellular and Infection Microbiology* **2013**, *3*.
(67) Rajasekaran, M. B.; Hussain, R.; Siligardi, G.; Andrews, S. C.; Watson, K. A. Crystal Structure and Metal Binding Properties of the Periplasmic Iron Component EfeM from Pseudomonas Syringae EfeUOB/M Iron-Transport System. *Biometals* **2022**, *35* (3), 573–589. https://doi.org/10.1007/s10534-022-00389-2.
(68) Makui, H.; Roig, E.; Cole, S. T.; Helmann, J. D.; Gros, P.; Cellier, M. F. M. Identification of the Escherichia Coli K-12 Nramp Orthologue (MntH) as a Selective Divalent Metal Ion Transporter. *Molecular Microbiology* **2000**, *35* (5), 1065–1078. https://doi.org/10.1046/j.1365-2958.2000.01774.x.
(69) Cao, J.; Woodhall, M. R.; Alvarez, J.; Cartron, M. L.; Andrews, S. C. EfeUOB (YcdNOB) Is a Tripartite, Acid-Induced and CpxAR-Regulated, Low-PH Fe2+ Transporter That Is Cryptic in Escherichia Coli K-12 but Functional in E. Coli O157:H7. *Molecular Microbiology* **2007**, *65* (4), 857–875. https://doi.org/10.1111/j.1365-2958.2007.05802.x.
(70) Poole, K.; Neshat, S.; Heinrichs, D. Pyoverdine-Mediated Iron Transport in Pseudomonas Aeruginosa: Involvement of a High-Molecular-Mass Outer Membrane Protein. *FEMS Microbiol Lett* **1991**, *62* (1), 1–5.
(71) Worst, D. J.; Otto, B. R.; de Graaff, J. Iron-Repressible Outer Membrane Proteins of Helicobacter Pylori Involved in Heme Uptake. *Infect Immun* **1995**, *63* (10), 4161–4165.
(72) Wolf, S. L.; Hogan, J. S.; Smith, K. L. Iron Uptake by Escherichia Coli Cultured with Antibodies from Cows Immunized with High-Affinity Ferric Receptors. *Journal of Dairy Science* **2004**, *87* (7), 2103–2107. https://doi.org/10.3168/jds.S0022-0302(04)70028-4.
(73) Wu, J. Y.; Srinivas, P.; Pogue, J. M. Cefiderocol: A Novel Agent for the Management of Multidrug-Resistant Gram-Negative Organisms. *Infect Dis Ther* **2020**, *9* (1), 17–40. https://doi.org/10.1007/s40121-020-00286-6.
(74) *Fetroja® (cefiderocol) | Overcoming carbapenem-resistance*. Fetroja® (cefiderocol) HCP Website. https://www.fetroja.com/overcoming-carbapenem-resistance (accessed 2023-04-04).
(75) Ludwig, B. S.; Correia, J. D. G.; Kühn, F. E. Ferrocene Derivatives as Anti-Infective Agents. *Coordination Chemistry Reviews* **2019**, *396*, 22–48. https://doi.org/10.1016/j.ccr.2019.06.004.
(76) Long, B.; He, C.; Yang, Y.; Xiang, J. Synthesis, Characterization and Antibacterial Activities of Some New Ferrocene-Containing Penems. *European Journal of Medicinal Chemistry* **2010**, *45* (3), 1181–1188. https://doi.org/10.1016/j.ejmech.2009.12.045.
(77) Chohan, Z. H. Antibacterial and Antifungal Ferrocene Incorporated Dithiothione and Dithioketone Compounds. *Applied Organometallic Chemistry* **2006**, *20* (2), 112–116. https://doi.org/10.1002/aoc.1018.
(78) Patra, M.; Gasser, G.; Wenzel, M.; Merz, K.; Bandow, J. E.; Metzler-Nolte, N. Synthesis and Biological Evaluation of Ferrocene-Containing Bioorganometallics Inspired by the Antibiotic Platensimycin Lead Structure. *Organometallics* **2010**, *29* (19), 4312–4319. https://doi.org/10.1021/om100614c.
(79) Sommers, K. J.; Bentley, B. S.; Carden, R. G.; Post, S. J.; Allen, R. A.; Kontos, R. C.; Black, J. W.; Wuest, W. M.; Minbiole, K. P. C. Metallocene QACs: The Incorporation of Ferrocene Moieties into MonoQAC and BisQAC Structures. *ChemMedChem* **2021**, *16* (3), 467–471. https://doi.org/10.1002/cmdc.202000605.
(80) Feliciano, J. A.; Leitgeb, A. J.; Schrank, C. L.; Allen, R. A.; Minbiole, K. P. C.; Wuest, W. M.; Carden, R. G. Trivalent Sulfonium Compounds (TSCs): Tetrahydrothiophene-Based Amphiphiles Exhibit Similar Antimicrobial Activity to Analogous Ammonium-Based Amphiphiles. *Bioorg Med Chem Lett* **2021**, *37*, 127809. https://doi.org/10.1016/j.bmcl.2021.127809.
(81) Nikolaev, A. E.; Semenov, V. É.; Voloshina, A. D.; Kulik, N. V.; Reznik, V. S. Synthesis and Antimicrobial Activity of Pyrimidinophanes Containing a Uracil Moiety and a Bridging Sulfur Atom. *Pharmaceutical chemistry journal* **2010**.
(82) Hirayama, M. The Antimicrobial Activity, Toxicity and Antimicrobial Mechanism of a New Type of Tris(Alkylphenyl)Sulfonium. *Biocontrol Science* **2012**, *17* (1), 27–35. https://doi.org/10.4265/bio.17.27.
(83) Hirayama, M. The Antimicrobial Activity, Hydrophobicity and Toxicity of Sulfonium Compounds, and Their Relationship. *Biocontrol Science* **2011**, *16* (1), 23–31. https://doi.org/10.4265/bio.16.23.

(84) Hirayama, M. The Antimicrobial Activity, Hydrophobicity and Toxicity of Tri(<I>n</I>-Alkyl)Sulfoniums and Tris(<I>n</I>-Alkylphenyl) Sulfoniums, and Their Relationships. *Biocontrol Science* **2011**, *16* (4), 149–158. https://doi.org/10.4265/bio.16.149.
(85) Murray, T. S.; Egan, M.; Kazmierczak, B. I. Pseudomonas Aeruginosa Chronic Colonization in Cystic Fibrosis Patients. *Curr Opin Pediatr* **2007**, *19* (1), 83–88. https://doi.org/10.1097/MOP.0b013e3280123a5d.
(86) Almasaudi, S. B. Acinetobacter Spp. as Nosocomial Pathogens: Epidemiology and Resistance Features. *Saudi J Biol Sci* **2018**, *25* (3), 586–596. https://doi.org/10.1016/j.sjbs.2016.02.009.
(87) Shen, K.; Sayeed, S.; Antalis, P.; Gladitz, J.; Ahmed, A.; Dice, B.; Janto, B.; Dopico, R.; Keefe, R.; Hayes, J.; Johnson, S.; Yu, S.; Ehrlich, N.; Jocz, J.; Kropp, L.; Wong, R.; Wadowsky, R. M.; Slifkin, M.; Preston, R. A.; Erdos, G.; Post, J. C.; Ehrlich, G. D.; Hu, F. Z. Extensive Genomic Plasticity in Pseudomonas Aeruginosa Revealed by Identification and Distribution Studies of Novel Genes among Clinical Isolates. *Infection and Immunity* **2006**, *74* (9), 5272–5283. https://doi.org/10.1128/IAI.00546-06.
(88) Imperi, F.; Antunes, L. C. S.; Blom, J.; Villa, L.; Iacono, M.; Visca, P.; Carattoli, A. The Genomics of Acinetobacter Baumannii: Insights into Genome Plasticity, Antimicrobial Resistance and Pathogenicity. *IUBMB Life* **2011**, *63* (12), 1068–1074. https://doi.org/10.1002/iub.531.
(89) Dobrindt, U.; Hacker, J. Whole Genome Plasticity in Pathogenic Bacteria. *Current Opinion in Microbiology* **2001**, *4* (5), 550–557. https://doi.org/10.1016/S1369-5274(00)00250-2.
(90) Lineback, C. B.; Nkemngong, C. A.; Wu, S. T.; Li, X.; Teska, P. J.; Oliver, H. F. Hydrogen Peroxide and Sodium Hypochlorite Disinfectants Are More Effective against Staphylococcus Aureus and Pseudomonas Aeruginosa Biofilms than Quaternary Ammonium Compounds. *Antimicrob Resist Infect Control* **2018**, *7* (1), 1–7. https://doi.org/10.1186/s13756-018-0447-5.
(91) Upmanyu, K.; Haq, Q. Mohd. R.; Singh, R. Factors Mediating Acinetobacter Baumannii Biofilm Formation: Opportunities for Developing Therapeutics. *Curr Res Microb Sci* **2022**, *3*, 100131. https://doi.org/10.1016/j.crmicr.2022.100131.
(92) Frolov, N.; Detusheva, E.; Fursova, N.; Ostashevskaya, I.; Vereshchagin, A. Microbiological Evaluation of Novel Bis-Quaternary Ammonium Compounds: Clinical Strains, Biofilms, and Resistance Study. *Pharmaceuticals (Basel)* **2022**, *15* (5), 514. https://doi.org/10.3390/ph15050514.
(93) Ly, N. S.; Yang, J.; Bulitta, J. B.; Tsuji, B. T. Impact of Two-Component Regulatory Systems PhoP-PhoQ and PmrA-PmrB on Colistin Pharmacodynamics in Pseudomonas Aeruginosa. *Antimicrob Agents Chemother* **2012**, *56* (6), 3453–3456. https://doi.org/10.1128/AAC.06380-11.
(94) Barrow, K.; Kwon, D. H. Alterations in Two-Component Regulatory Systems of PhoPQ and PmrAB Are Associated with Polymyxin B Resistance in Clinical Isolates of Pseudomonas Aeruginosa. *Antimicrob Agents Chemother* **2009**, *53* (12), 5150–5154. https://doi.org/10.1128/AAC.00893-09.
(95) Miller, A. K.; Brannon, M. K.; Stevens, L.; Johansen, H. K.; Selgrade, S. E.; Miller, S. I.; Høiby, N.; Moskowitz, S. M. PhoQ Mutations Promote Lipid A Modification and Polymyxin Resistance of Pseudomonas Aeruginosa Found in Colistin-Treated Cystic Fibrosis Patients. *Antimicrobial Agents and Chemotherapy* **2011**, *55* (12), 5761–5769. https://doi.org/10.1128/AAC.05391-11.
(96) Xu, C.; Bilya, S. R.; Xu, W. AdeABC Efflux Gene in Acinetobacter Baumannii. *New Microbes New Infect* **2019**, *30*, 100549. https://doi.org/10.1016/j.nmni.2019.100549.
(97) Xu, Y.; Liang, Z.; Legrain, C.; Rüger, H. J.; Glansdorff, N. Evolution of Arginine Biosynthesis in the Bacterial Domain: Novel Gene-Enzyme Relationships from Psychrophilic Moritella Strains (Vibrionaceae) and Evolutionary Significance of N-α-Acetyl Ornithinase. *J Bacteriol* **2000**, *182* (6), 1609–1615.
(98) Cunin, R.; Glansdorff, N.; Piérard, A.; Stalon, V. Biosynthesis and Metabolism of Arginine in Bacteria. *Microbiol Rev* **1986**, *50* (3), 314–352.
(99) Nasu, H.; Shirakawa, R.; Furuta, K.; Kaito, C. Knockout of MlaA Increases Escherichia Coli Virulence in a Silkworm Infection Model. *PLoS One* **2022**, *17* (7), e0270166. https://doi.org/10.1371/journal.pone.0270166.
(100) Bzdyl, N. M.; Scott, N. E.; Norville, I. H.; Scott, A. E.; Atkins, T.; Pang, S.; Sarovich, D. S.; Coombs, G.; Inglis, T. J. J.; Kahler, C. M.; Sarkar-Tyson, M. Peptidyl-Prolyl Isomerase PpiB Is Essential for Proteome Homeostasis and Virulence in Burkholderia Pseudomallei. *Infect Immun* **2019**, *87* (10), e00528-19. https://doi.org/10.1128/IAI.00528-19.
(101) Skagia, A.; Zografou, C.; Venieraki, A.; Fasseas, C.; Katinakis, P.; Dimou, M. Functional Analysis of the Cyclophilin PpiB Role in Bacterial Cell Division. *Genes Cells* **2017**, *22* (9), 810–824. https://doi.org/10.1111/gtc.12514.
(102) Pieri, C.; Borselli, D.; Di Giorgio, C.; De Méo, M.; Bolla, J.-M.; Vidal, N.; Combes, S.; Brunel, J. M. New Ianthelliformisamine Derivatives as Antibiotic Enhancers against Resistant Gram-Negative Bacteria. *J. Med. Chem.* **2014**, *57* (10), 4263–4272. https://doi.org/10.1021/jm500194e.

(103) Davis, R. A.; Vullo, D.; Supuran, C. T.; Poulsen, S.-A. Natural Product Polyamines That Inhibit Human Carbonic Anhydrases. *Biomed Res Int* **2014**, *2014*, 374079. https://doi.org/10.1155/2014/374079.

(104) *Protein [Internet]. Bethesda (MD): National Library of Medicine (US), National Center for Biotechnology Information; [1988] - Accession No. Q16790, Homo Sapiens Carbonic Anhydrase IX, Protein; [Cited 2023 03 26]. Avaialbe from: Https://Blast.Ncbi.Nlm.Nih.Gov/Blast.Cgi?PROGRAM=blastp&PAGE_TYPE=BlastSearch&LINK_LOC=blasthome.*

(105) Gnielinski, N. von; Nienaber, L.; Mason, L.; Ellis, S.; Triccas, J. A.; Davis, R. A.; Hofmann, A. Non-Classical β-Carbonic Anhydrase Inhibitors-towards Novel Anti-Mycobacterials. *Med. Chem. Commun.* **2014**, *5* (10), 1563–1566. https://doi.org/10.1039/C4MD00310A.

(106) *Protein [Internet]. Bethesda (MD): National Library of Medicine (US), National Center for Biotechnology Information; [1988] - Accession No. P9WPJ9, Mycobacterium Tuberculosis Carbonic Anhydrase 2, Carbonate Dehydratase 2, Protein; [Cited 2023 03 26]. Avaialbe from: Https://Blast.Ncbi.Nlm.Nih.Gov/Blast.Cgi?PROGRAM=blastp&PAGE_TYPE=BlastSearch&LINK_LOC=blasthome.*

(107) Nocentini, A.; Capasso, C.; Supuran, C. T. Carbonic Anhydrase Inhibitors as Novel Antibacterials in the Era of Antibiotic Resistance: Where Are We Now? *Antibiotics (Basel)* **2023**, *12* (1), 142. https://doi.org/10.3390/antibiotics12010142.

(108) Cheng, Z.-Q.; Song, J.-L.; Zhu, K.; Zhang, J.; Jiang, C.-S.; Zhang, H. Total Synthesis of Pulmonarin B and Design of Brominated Phenylacetic Acid/Tacrine Hybrids: Marine Pharmacophore Inspired Discovery of New ChE and Aβ Aggregation Inhibitors. *Mar Drugs* **2018**, *16* (9), 293. https://doi.org/10.3390/md16090293.

(109) *Protein [Internet]. Bethesda (MD): National Library of Medicine (US), National Center for Biotechnology Information; [1988] - Accession No. P22303, Homo Sapiens Acetylcholiesterase, Protein; [Cited 2023 03 26]. Avaialbe from: Https://Blast.Ncbi.Nlm.Nih.Gov/Blast.Cgi?PROGRAM=blastp&PAGE_TYPE=BlastSearch&LINK_LOC=blasthome.*

Chapter 4: Discussion

Using the Wuest Lab approach, the total synthesis and biological investigation of previously unexplored mindapyrroles was undertaken in the search for novel mechanisms of action that can target drug resistant bacteria. These molecules, recently discovered in 2019, have an unexplored mechanism of action that could potentially be polypharmacological. Originally hypothesized to be ionophores, similar molecules have been proven to act as protonophores that depolarize the membrane in addition to inhibiting a variety of protein targets. To allow for further investigation of their mechanism of action, I completed the second total synthesis of mindapyrrole A and the first total synthesis of mindapyrrole B by initially designing three routes to access these molecules. I also expanded upon the chemistry of resorcinol and γ-resorcylic acid dimers, as well as 2-acylpyrroles. Additionally, I confirmed the antibacterial activity of these compounds through minimum inhibitory concentration (MIC) assays. I also demonstrated the inability for *S. aureus* to develop resistance to pyoluteorin over a 24 day period.

In an effort to return disinfectant activity against previously resistant bacteria, a variety of collaborations were leveraged towards the investigation of novel and particularly active amphiphilic surfactants against both lab strains and extensively and pan drug resistant bacteria, wherein I and fellow members of the Wuest lab acted as the microbiologists. To explore the effect of grafting a quaternary ammonium warhead onto polymyxin B, the Pires lab at the University of Virginia undertook the synthesis of a library of QAC-containing analogs that we were able to switch the activity of this molecule from solely gram-negative to both gram-negative and -positive. To expand the current knowledge on rigidity-activity relationships in quaternary ammonium compounds (QACs), the Minbiole lab at Villanova University synthesized a library of novel QACs of varying structures that I and several other members of the Wuest lab tested in MIC and

hemolysis assays. A series of bispyridinium QACs with ethyl linkers of varying rigidity (alkane, alkene, and alkyne) were tested to expand the activity-rigidity relationships know for QACs. Through MMIC assays, we were able to demonstrate the decreased activity of the more rigid alkyne-linked bispyridinium compounds, likely due to decreased cooperative binding. To exploit the iron acquisition systems of bacteria, the Minbiole lab synthesized a series of ferrocene-containing mono- and bisQACs that we tested against a library of lab strains as well as MRSA clinical isolates. We were able to show that the best synthesized analogs were more active than commercially available QAC disinfectant benzalkonium chloride. The expand the classes of amphiphilic disinfectants, the Minbiole lab synthesized a series of trivalent sulfonium compounds (TSCs) that we tested for antibacterial activity. Comparing them to structurally similar QACs, we were able to show the TSCs had similar activity and less toxicity than commercially available cetylpyridinium chloride. To explore disinfectant resistance in multidrug- and pan-resistant *A. baumannii* and *P. aeruginosa* clinical isolates, we tested the antibacterial activity of the best-in-class cationic surfactants synthesized by the Minbiole lab and compared them to commercial disinfectants that are currently being used to disinfectant hospitals. We were able to show that the tested quaternary phosphonium compound (QPC) tested was the most efficacious against all *A. baumannii* tested, and it was effective at eradicating biofilms. Additionally, resistance selections assays revealed a variety of mutations that helped a lab strain of *A. baumannii* overcome QAC treatment, such as mutations to phospholipid synthesis and chaperone-like enzymes. To synthesize QACs with the potential for polypharmacological properties, undergraduate research student Caroline McCormack and I undertook the total synthesis of ianthelliformisamine C and QAC analogs via quaternization of the internal amines. Through this synthesis and MIC assays, we were able to show that methylation and quaternization of the internal amines decreased activity against

all bacteria tested. These efforts expand the variety of amphiphilic disinfectants structures and confirm their activity, explore the efficacy of commercially available and best-in-class amphiphilic disinfectants against clinical isolates, discovered novel mutations acquired in response to QAC treatment, and generated disinfectants with the possibility of having polypharmacological properties.

Chapter 5: Experimental Details

5.1 General Information

5.1.1 General Chemical Materials and Methods

NMR spectra were collected using the following instruments: Varian INOVA400, VNMR400, Bruker NEO400, Varian INOVA500, Varian INOVA600, and Bruker AVANCA III HD 600. All NMRs were collected at ambient temperature. The collected spectra were normalized to the corresponding solvent in which the sample was dissolved (^{1}H: δ = 7.26 ppm and ^{13}C: δ = 77.2 ppm for chloroform, ^{1}H: δ = 3.31 ppm and ^{13}C: δ = 49.0 ppm for methanol, ^{1}H: δ = 2.05 ppm and ^{13}C: δ = 29.8 ppm for acetone, ^{1}H: δ = 2.50 ppm and ^{13}C: δ = 39.5 ppm for dimethyl sulfoxide). Trace amounts of water in each solvent was accounted for as follows (^{1}H: δ = 1.56 ppm for chloroform, ^{1}H: δ = 4.87 ppm for methanol, ^{1}H: δ = 2.84 ppm for acetone, ^{1}H: δ = 3.33 ppm for dimethyl sulfoxide). The abbreviations used to describe the coupling patterns are as follows: s (singlet), d (doublet), t (triplet), q (quartet), m (multiplet), b (broad singlet), dd (doublet of doublets), dt (doublet of triplets), etc.

Accurate mass spectra were obtained on a Thermo LTQ-FTMS using either APCI or ESI techniques.

Infrared spectra were obtained neat using a Thermoscientific Nicolet with an attenuated total reflectance (ATR) with a germanium crystal. Peaks were recorded in cm-1 and described as either weak (w), strong (s), or broad (b).

Non-aqueous reactions were performed under an atmosphere of argon in flame-dried glassware. Solvents used were either HPLC grade solvents dried by passage through alumina or were DrySolv solvents purchased from VWR. Amine bases were distilled over calcium hydride when indicated. Otherwise, amine bases were used without further purification. Brine refers to saturated solution of sodium chloride. Purification via flash chromatography describes purification via Biotage Isolera One Automated Column. Reactions monitored via thin-layer chromatography (TLC) using aluminum-backed silica gel 60 F_{254} TLC plates obtained from Millipore-Sigma Supelco. Products purified via reverse phase high performance liquid chromatography (HPLC) were purified using an Agilent 1260 Infinity II LC System. Solvents used were HPLC grade water and acetonitrile each spiked with 0.1% formic acid.

5.1.2 General Biological Materials and Methods

For all biological assays, bacteria were grown overnight in 5 mL of Mueller-Hinton broth (MHB) at 37˚C with shaking from freezer stocks made from 0.6 mL of stationary phase bacterial culture and 0.6 mL of sterile filtered 50% glycerol in water.

5.1.2.1 Minimum Inhibitory Concentrations (MIC) Assay

Compounds were serially diluted two-fold from 1 mM or 1 mg/mL stock solutions (10% DMSO in water) to yield twelve test concentrations in round bottom or flat bottom 96-well plates, each well containing 100 μL of solution. Overnight cultures were diluted to ca. 106 cfu/mL in MHB and regrown to exponential phase as determined by optical density recorded at 600 nm (OD600). All cultures were then diluted again to ca. 106 cfu/mL in MHB (CLSI Standards) and 100 μL were inoculated into each well. Plates were incubated statically at 37˚C for 24 hours (mindapyrroles and ianthelliformisamines) or 72 hours (quaternary ammonium compounds), at which point they were evaluated visually for bacterial growth. The MIC was determined as the lowest concentration of compound resulting in no bacterial growth visible to the naked eye, based on three independent trials. In the case of IC_{90} values, the OD's were measured on a plate reader to determine inhibition at 90%. Aqueous 10% DMSO was used as a negative control, and the appropriate antibacterial compound was used as a positive control (mindapyrroles: oxacillin sodium salt, quaternary ammonium compounds and ianthelliformisamines: benzalkonium chloride (70% benzyldimethyldodecylammonium chloride, 30% benzyl dimethyltetradecyl ammonium chloride)).

5.1.2.2 Hemolysis$_{20}$ Assay

Mechanically defibrinated sheep's blood (1.5 mL) was centrifuged in a sterile Eppendorf tube at 10,000 rpm for 10 minutes at ambient temperature. The supernatant was discarded, and the cells pellet was resuspended in 1.0 mL of sterile filtered phosphate buffered solution (PBS). These steps of centrifugation followed by resuspension were repeated until the supernatant was no longer red and was clear. The pellet was resuspended in 1.0 mL of PBS, then diluted into 29 mL of PBS. In round bottom plates, 100 μL of a 1 mM or 1 mg/mL solution of compound was serially diluted across the plate to give twelve test concentrations. PBS was used as a negative control 0% lysis) and a 1% solution of Triton-X was used as a positive control (100% lysis). Then, 100 μL of diluted red blood cells were added to each well. The plates were incubated at 37˚C with shaking for one hour, then centrifuged at 3,700 rpm for ten minutes. The supernatant was then carefully pipetted from the well and added to a 96-well flat bottom plate. The absorbance at 540 nm was then read using a plate reader. The 0% lysis was then subtracted from the 100% lysis, and 20% of that normalized number was used as the benchmark for 20% hemolysis. Concentrations above this number were considered hemolytic.

5.2 Synthetic Procedures

5.2.1 Chapter 2

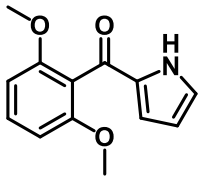

2-(2',6'-dimethoxybenzoyl)pyrrole (2.7): A flame dried flask under argon at 0˚C was charged with thionyl chloride (0.677 mL, 9.33 mmol, 3.4 equiv.). To this was added 2,6-dimethoxybenzoic acid (507.2 mg, 2.74 mmol, 1.0 equiv.) in portions. The reaction was then warmed to room temp and stirred for 1 hour before excess thionyl chloride was removed under reduced pressure. The resulting yellow oil was dissolved in DCM (4.0 mL, 0.69 M) and cooled to 0˚C in a water-ice bath. To this solution was added dropwise freshly distilled pyrrole (0.190 mL, 2.74 mmol, 1.0 equiv.) dissolved in DCM (4.0 ml, 0.69 M). After addition, the solution was stirred at ambient temperature for 3 hours, then 1 M sulfuric acid (4.12 mL, 4.12 mmol, 1.5 equiv.) was added. The biphasic solution was stirred for 20 minutes before the layers were separated. The aqueous layer was extracted twice with DCM, then the combined organic layers were washed twice with a saturated sodium bicarbonate solution, twice with brine, dried with MgSO4, filtered, concentrated under reduced pressure, and purified via flash column chromatography (silica gel, 20% ethyl acetate in hexanes) to yield **2.7** (0.3700 g, 1.60 mmol, 58%) as a white solid. Spectra matched those previously reported.1,2

^{1}H NMR: (600 MHz, , (CD3)2CO) δ 10.97 (b, 1H), 7.34 (t, J = 8.4 Hz, 1H), 7.14 (td, J = 2.5 Hz, 1.5 Hz, H), 6.71 (d, J = 8.4, 2H), 6.42-6.40 (m, 1H), 6.17 (td, J = 2.4 Hz, 3.8 Hz, 1H), 3.70 (s, 6H).

^{13}C-NMR: (100.6 MHz, $(CD_3)_2CO$) δ 183.1, 158.6, 134.7, 131.2, 125.6, 119.6, 118.5, 110.7, 105.0, 56.1.

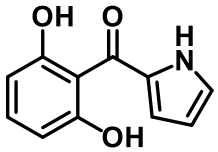

2-(2',6'-dihydroxybenzoyl)pyrrole (2.8): In a flame dried flask under argon was suspended **2.7** (0.8952 g, 3.86 mmol, 1.0 equiv.) in DCM (6.2 mL, 0.62 M). The suspension was cooled to -78˚C, then boron tribromide (1.0 M, 30.9 mL, 30.9 mmol, 8.0 equiv.) was added via syringe pump (0.67 mL/minute). The reaction was slowly warmed to -40˚C over 4 hours, then warmed to ambient temperature and stirred for 2 days. The reaction was then cooled to 0˚C in a water-ice bath, and the reaction was quenched via slow addition of ice cubes. The aqueous phase was the extracted thrice with ethyl acetate. The combined organic layers were then washed once with brine, dried with MgSO4, filtered, concentrated under reduced pressure, and purified via flash column chromatography (40% ethyl acetate with 0.1% acetic acid in hexanes) to yield yellow solid **2.8** (0.7423 g, 3.66 mmol, 94% yield). Spectra matched those previously reported.[1]

^{1}H-NMR: (400 MHz, $(CD_3)_2SO$) δ 11.79 (s, 1H), 9.37 (s, 2H), 7.07-7.05 (m, 1H), 6.97 (t, *J* = 8.1 Hz, 1H), 6.39-6.36 (m, 1H), 6.34 (d, *J* = 8.2 Hz, 2H), 6.10 (dt, *J* = 3.8, 2.2 Hz, 1H)

^{13}C-NMR: (100.6 MHz, $(CD_3)_2SO$) δ

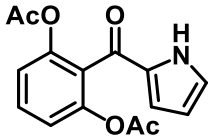

2-(2',6'-dihydroxybenzoyl)pyrrole O,O-diacetate (2.9): In a flame dried flask under argon was dissolved **2.8** (0.1282 g, 0.63 mmol, 1.0 equiv.) in ethyl acetate (6.3 mL, 0.1 M). To this was added triethylamine (0.195 mL, 1.39 mmol, 2.2 equiv.), and the reaction was stirred at ambient temperature for ten minutes. The reaction was then cooled to 0˚C in a water-ice bath, then acetyl chloride (91 μL, 1.26 mmol, 2.0 equiv.) was added, causing the clear orange solution to turn a chunky yellow. The reaction was allowed to slowly warm to ambient temperature overnight, then quenched the next day with ca. 0.5 M HCl. The aqueous layer was extracted twice with ethyl acetate, then the combined organic layers were washed once with brine, dried with MgSO4, filtered, concentrated under reduced pressure, and purified via flash column chromatography (15% ethyl acetate in hexanes) to yield **2.9** (0.1645 g, 0.57 mmol, 91% yield) as a yellow oil. Spectra matched those previously reported.[1,3]

^{1}H-NMR: (600 MHz, $CDCl_3$) δ 9.37 (b, 1H), 7.48 (t, *J* = 8.4 Hz, 1H), 7.11 (d, *J* = 8.3 Hz, 2H), 7.11-7.09 (m, 1H), 6.68-6.62 (m, 1H), 6.28-6.26 (m, *J* = 3.9, 1H), 2.03 (s, 6H).

^{13}C-NMR: (100.6 MHz, $(CD_3)_2SO$) δ

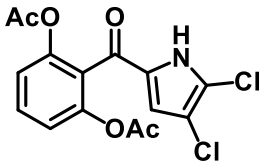

4,5-dichloro-2-(2',6'-dihydroxybenzoyl)pyrrole *O,O*-diacetate (2.10): In a flame dried flask under argon was dissolved **2.9** (0.1645 g, 0.57 mmol, 1.0 equiv.) in chloroform (1.55 mL, 0.37M). To this was added *N*-chlorosuccinimide (0.1547 g, 1.15 mmol, 2.01 equiv.) of N-chlorosuccinimide. The reaction was then heated to reflux for 18 hours. Once cooled, the reaction was quenched with a saturated sodium bicarbonate solution. The aqueous layer was extracted twice with ethyl acetate, then the combined organic phases were washed once with brine, dried with $MgSO_4$, filtered, concentrated under reduced pressure, and purified via flash column chromatography (15% ethyl acetate in hexanes) to yield a yellow solid (0.1581 g, 0.44 mmol, 78% yield). Spectra matched those previously reported.[1,3]

^{1}H-NMR: (400 MHz, $(CD_3)_2SO$) δ 9.39 (s, 1H), 7.50 (t, *J* = 8.2 Hz, 1H), 7.12 (d, *J* = 8.3 Hz, 2H), 6.59 (s, 1H), 2.10 (s, 6H).

^{13}C-NMR: (100.6 MHz, $(CD_3)_2SO$) δ

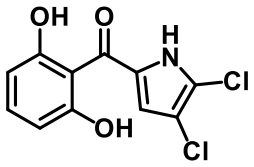

Pyoluteorin (2.1): In a vial was dissolved **2.10** (0.2120 g, 0.60 mmol, 1.0 eq.) in methanol (3.31 mL, 0.18 M), then a drop of concentrated hydrochloric acid was added. The reaction was heated at 60˚C for 3 hours, then the mixture was concentrated and triturated with deionized water to yield **2.1** (0.1642 g, 0.60 mmol, quantitative yield) as a yellow solid. Spectra matched those previously reported.[1–3]

^{1}H-NMR: (500 MHz, $(CD_3)_2SO$) δ 13.13 (d, *J* = 1.7 Hz, 1H), 9.50 (s, 2H), 7.01 (d, *J* = 6.5 Hz, 1H), 6.40 (d, *J* = 2.2 Hz, 1H), 6.34 (d, *J* = 6.5 Hz, 2H).

^{13}C-NMR: (126 MHz, $(CD_3)_2SO$) δ 182.81, 155.69, 130.99, 130.32, 119.32, 116.55, 114.48, 109.20, 106.42.

HRMS ($APCI^-$): $C_{11}H_7NO_3Cl_2$ [M^-] requires 271.98758; Found: 271.98775.

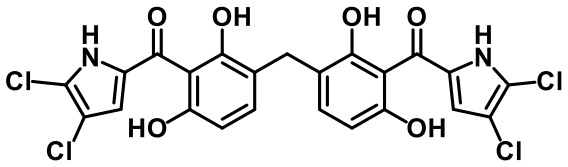

Mindapyrrole A (2.2): In a flame dried flask under argon was dissolved dimethoxymethane (2.60 μL, 29.4 μmol, 1.00 equiv.) and aluminum (III) chloride (6.2 mg, 47.0 μmol, 1.60 equiv.) in acetonitrile (1.0 mL, 0.03 M). To this was added **2.1** (28.8 mg, 106 μmol, 3.60 equiv.), and the reaction was stirred at reflux for 16 hours. The reaction was then quenched with deionized water, and the aqueous phase was extracted thrice with ethyl acetate. The combined organic layers were washed once with brine, dried with magnesium sulfate, filtered, concentrated under reduced pressure, and purified via flash column chromatography (silica gel, 25% to 45% ethyl acetate with 0.1% acetic acid in hexanes) to yield **2.2** (13.2 mg, 81% yield) as a yellow solid. The yellow solid was further purified via HPLC (30% to 95% acetonitrile in water with 0.1% formic acid). Spectra matched those previously reported.[2,4]

^{1}H-NMR: (400 MHz, CD_3OD) δ 7.03 (d, *J* = 8.4 Hz, 2H), 6.68 (s, 2H), 6.37 (d, *J* = 8.4 Hz, 1H), 3.78 (s, 2h).

^{13}C-NMR: (106 MHz, CD_3OD) δ 185.8, 156.3, 155.8, 134.5, 131.9, 121.6, 120.7, 119.3, 114.7, 111.9, 108.4, 29.7.

HRMS (ESI^-): $C_{23}H_{12}N_2O_6Cl_4$ [M^-] requires 552.95332; Found: 552.95496.

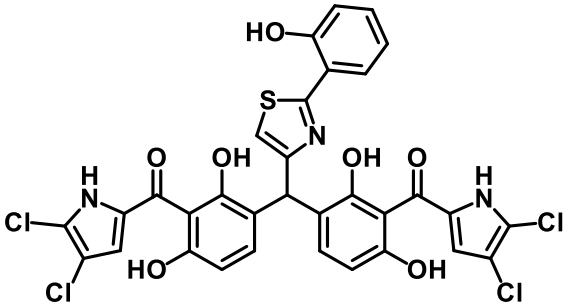

Mindapyrrole B (2.3): In a flame dried flask under argon was dissolved aeruginaldehyde (**2.5**) (6.1 mg, 30 μmol, 1.00 equiv.) and aluminum (III) chloride (12.7 mg, 95.3 μmol, 3.20 equiv.) in acetonitrile 1.6 mL, 0.02 M). The yellow reaction was stirred for 10 minutes before **2.1** (25.5 mg, 93.7 μmol, 3.20 equiv.) was added. The reaction was heated to reflux for 16 hours, then cooled to

ambient temperature and quenched with deionized water. The aqueous phase was extracted thrice with ethyl acetate, then the combined organic layers were washed once with brine, dried with magnesium sulfate, filtered, concentrated under reduced pressure, and purified via flash column chromatography (silica gel, 25% to 45% ethyl acetate with 0.1% acetic acid in hexanes) to yield **2.3** (7.1 mg, 9.7 μmol, 33% yield) as a yellow solid. The yellow solid was further purified via HPLC (30% to 95% acetonitrile in water with 0.1% formic acid). The spectra matched those previously reported.[4]

^{1}H-NMR: (600 MHz, CD_3OD) δ 7.72 (dd, *J* = 7.8, 1.44 Hz, 1H), 7.28 (td, *J* = 8.6, 1.56 Hz, 1H), 6.95-6.89 (m, 5H), 6.79 (s, 2H), 6.37 (d, *J* = 8.5 Hz, 2H), 6.13 (s, 1H).

^{13}C-NMR: (106 MHz, $(CD_3)_2CO$) δ 184.8, 172.0, 169.2, 158.4, 157.6, 156.8, 134.6, 132.6, 131.4, 127.9, 122.1, 120.9, 120.4, 119.0, 118.3, 117.9, 115.5, 117.7, 111.5, 108.0, 40.1.

HRMS (ESI^+): $C_{32}H_{20}N_3O_7Cl_4S$ [M^+] requires 729.97706; Found: 729.97689.

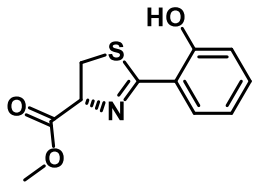

Methyl-(R)-2-(2-hydroxyphenyl)-4,5-dihydrothiazole-4-carboxylate (2.63): In a flame dried flask under argon was suspended 2-hydroxybenzonitrile (1.53460 g, 12.88 mmol, 1.00 equiv.) and L-cysteine methyl ester hydrochloride (8.8282 g, 51.43 mmol, 3.99 equiv.) in methanol (12.6 mL, 1.02 M). The reaction was heated to reflux overnight, then quenched the next morning with deionized water at ambient temperature. The aqueous phase was extracted twice with diethyl ether, then the combined organic layers were washed once with brine, dried with magnesium sulfate, filtered, concentrated under reduced pressure, and purified via flash column chromatography (silica gel, 15% to 25% ethyl acetate in hexanes) to yield **2.63** (2.4852 g, 10.47 mmol, 81% yield) as a white solid. Spectra matched those previously reported.[5]

^{1}H-NMR: (600 MHz, $CDCl_3$) δ 7.42 (dd, *J* = 7.9, 1.62 Hz, 1H), 7.38 (td, *J* = 8.9, 1.62 Hz, 1H), 7.03 (d, *J* = 8.3 Hz, 1H), 6.89 (td, *J* = 7.9, 3.6 Hz, 1H), 5.36 (dd, *J* = 9.4, 8.0 Hz, 1H), 3.83 (s, 3H), 3.69 (dd, *J* = 11.2, 7.9 Hz, 1H), 3.61 (dd, *J* = 11.7, 9.5 Hz, 1H).

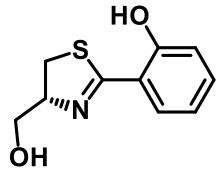

(R)-2-(4-(hydroxymethyl)-4,5-dihydrothiazol-2-yl)phenol (2.64): In a flame dried flask under argon was dissolved **2.63** (2.3416 g, 9.87 mmol, 1.00 equiv.) in ethanol (50 mL, 0.2 M). To this was added sodium borohydride (1.0532 g, 27.8 mmol, 2.82 equiv.) in portions, waiting for the bubbling to subside before adding the next portion. After the addition, the reaction was stirred at ambient temperature for 3.5 hours, then quenched with ethyl acetate and a saturated aqueous solution of sodium bicarbonate. The aqueous layer was extracted twice with ethyl acetate, then the combined organic layers were washed once with brine, dried with magnesium sulfate, filtered,

concentrated under reduced pressure, and purified via flash column chromatography (silica gel, 25% ethyl acetate in hexanes) to yield **2.64** (2.4852 g, 10.47 mmol, 81% yield) as a yellow solid. Spectra matched those previously reported.[5]

^{1}H-NMR: (400 MHz, $CDCl_3$) δ 7.42 (dd, *J* = 7.8, 1.6 Hz, 1H), 7.37 (td, *J* = 8.4, 1.64 Hz, 1H), 7.01 (dd, *J* = 8.3, 0.88 Hz, 1H), 6.89 (td, *J* = 7.8, 1.16 Hz, 1H), 4.89 (ddt, *J* = 13.4, 8.64, 4.9 Hz, 1H), 4.00 (dd, *J* = 11.2, 5.1 Hz, 1H), 3.85 (dd, *J* = 11.3, 4.8 Hz, 1H), 3.44 (dd, *J* = 10.9, 8.9 Hz, 1H), 3.36 (dd, *J* = 10.9, 8.2 Hz, 1H).

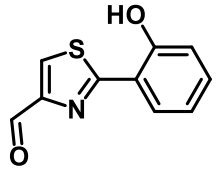

Aeruginaldehyde (2.5): In a flame dried flask under argon was dissolved 2.0 M oxalyl chloride in DCM (1.85 mL, 3.71 mmol, 2.22 equiv.) in DCM (42 mL, 0.15 M). The flask was cooled to -78˚C, then DMSO (0.450 mL, 6.28 mmol, 3.76 equiv.) was added slowly dropwise, causing the solution to bubble. The reaction was stirred for 20 minutes, then **2.64** (349.3 mg, 1.67 mmol, 1.00 equiv.) dissolved in DCM (43 mL, 0.039 M) was slowly added. The reaction was stirred for another 30 minutes, then triethylamine (2.80 mL, 20.0 mmol, 12.0 equiv.) was added slowly, turning the chunky white solution a clear yellow. The reaction was stirred for another 5 hours at -78˚C, then quenched with deionized water. The aqueous layer was acidified to a pH below 5 with 1 M HCl, then the aqueous layer was extracted twice with DCM. The combined organic layers were washed once with brine, dried with magnesium sulfate, filtered, concentrated under reduced pressure, and purified via flash column chromatography (silica gel, 0% to 15% ethyl acetate in hexanes) to yield **2.5** (342.6 mg, 0.98 mmol, 59% yield) as a pale-yellow solid. Spectra matched those previously reported.[5]

^{1}H-NMR: (600 MHz, $CDCl_3$) δ 11.61 (b, 1H), 10.07 (s, 1H), 8.14 (s, 1H), 7.64 (dd, *J* = 7.9, 1.56 Hz, 1H), 7.39 (td, *J* = 8.5, 1.56 Hz, 1H), 7.11 (dd, *J* = 8.4, 1.08 Hz, 1H), 6.96 (td, *J* = 7.9, 1.14 Hz, 1H).

^{13}C-NMR: (106 MHz, $(CD_3)_2CO$) δ 172.6, 159.8, 133.7, 131.2, 119.6, 117.5, 117.0, 79.2, 63.8, 33.3.

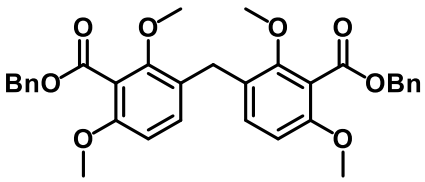

Dibenzyl 3,3'-methylenebis(2,6-dimethoxybenzoate) (2.12): In a flame dried flask under argon was dissolved dimethoxymethane (200 µL, 2.26 mmol, 1.0 equiv.) and aluminum (III) chloride (0.4813 g, 3.61 mmol, 1.6 equiv.) in acetonitrile (23 mL, 0.10 M). The reaction was stirred for 5 minutes, then benzyl-2,6-dimethoxybenzoate (1.5497 g, 5.69 mmol, 2.52 equiv.) was added. The reaction was heated to 45˚C for 3 hours, then quenched with deionized water. The aqueous layer was extracted twice with ethyl acetate, then the combined organic phases were washed once with brine, dried with MgSO4, filtered, concentrated under reduced pressure, and purified via flash

column chromatography (0% to 10% ethyl acetate in hexanes) to yield **2.12** (0.7790 g, 1.40 mmol, 62% yield) as a white solid.
^{1}H-NMR: (600 MHz, $CDCl_3$) δ 7.47-7.45 (m, 3H), 7.38-7.31 (m, 5H), 6.97 (d, *J* = 8.6 Hz, 2H), 6.59 (d, *J* = 8.5 Hz, 2H), 5.39 (s, 4H), 3.87 (s, 2H), 3.78 (s, 6H), 3.62 (s, 6H).

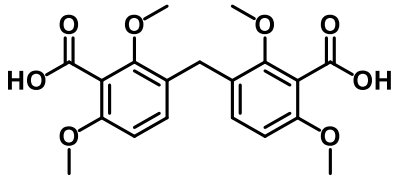

3,3'-methylenebis(2,6-dimethoxybenzoic acid) (2.13): In a flame dried vial under argon was dissolved **2.12** (0.3894 g, 0.70 mmol, 1.0 equiv.) in methanol (8.4 mL, 0.083 M). The solution was put under vacuum until bubbles started to form, then backfilled with argon four times to ensure no oxygen was present in the reaction mixture. Next, palladium on carbon (9.4 mg, 0.088 mmol, 0.13 equiv.) was added, then the mixture was put under vacuum until bubbles formed then backfilled with argon four times. Finally, the mixture was put under vacuum and backfilled with hydrogen gas five times to ensure a hydrogen full atmosphere. Hydrogen gas was then bubbled through the solution for 3 hours, then stirred under an atmosphere of hydrogen for another 3 hours. When TLC analysis had indicated the reaction had finished, the mixture was filtered over celite, yielding **2.13** (0.2626 g, 0.70 mmol, quantitative yield) as a white solid.
^{1}H-NMR: (600 MHz, CD_3OD) δ 7.07 (d, *J* = 8.6 Hz, 2H), 6.76 (d, *J* = 8.6 Hz, 2H), 3.91 (s, 2H), 3.81 (s, 6H), 3.77 (s, 6H).

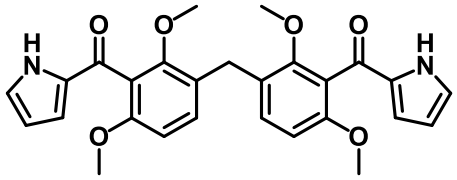

Methylenebis(2,6-dimethoxy-3,1-phenylene)bis((1H-pyrrol-2-yl)methanone) (2.14): In a flame dried flask under argon was suspended **2.13** (0.1011 g, 0.27 mmol, 1.0 equiv.) in 1,2-dichlorethane (3.0 mL, 0.09 M). To this was added thionyl chloride (45 µL, 0.59 mmol, 2.2 equiv.) at room temperature. The reaction then refluxed for 3.5 hours, yielding a brown solution. Once cooled to ambient temperature, the reaction cooled to 0°C and freshly distilled pyrrole (200 µL, 2.88 mmol, 10.7 equiv.) dissolved in DCM (10 mL, 0.29 M) were added in small portions (~0.5 mL). After addition, the reaction was allowed to warm to room temperature overnight, then quenched the next morning with saturated ammonium chloride. The aqueous phase extracted twice with ethyl acetate, then the combined organic layers were washed once with brine, dried with $MgSO_4$, filtered, concentrated under reduced pressure, and purified via flash column chromatography (15% to 30% ethyl acetate in hexanes) to yield **2.14** (0.0488 g, 0.27 mmol, 38% yield).
^{1}H-NMR: (600 MHz, $CDCl_3$) δ 9.41 (b, 2H), 7.09-7.07 (m, 4H), 6.67 (d, *J* = 8.6 Hz, 2H), 6.57(m, 2H), 6.25 (M, 2H), 3.95 (s, 2H), 3.73 (s, 6H), 3.65 (s, 6H).

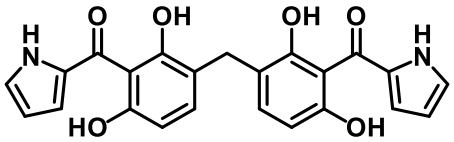

(Methylenebis(2,6-dihydroxy-3,1-phenylene))bis((1H-pyrrol-2-yl)methanone) (2.15): In a vial under argon was dissolved **2.14** (48.6 mg, 0.102 mmol, 1.0 equiv.) in DCM (2.05 mL, 0.05 M). The solution was cooled to -40˚C, then boron tribromide (0.62 mL, 0.615 mmol, 6.0 equiv.) was added slowly dropwise. The reaction was allowed to slowly warm to room temperature overnight, then cooled to 0˚C in a water-ice bath and quenched with ice cubes. The aqueous layer was then extracted thrice with 5% methanol in ethyl acetate, then the combined organic phases were washed once with brine, dried with MgSO4, filtered, concentrated under reduced pressure, and purified via flash column chromatography (silica gel, 20% to 45% ethyl acetate with 0.1% acetic acid in hexanes) to yield **2.15** (5.3 mg, 0.013 mmol, 12% yield).
^{1}H-NMR: (600 MHz, $(CD_3)_2CO$) δ 7.09-7.07 (m, 4H), 6.67 (d, *J* = 8.6 Hz, 2H), 6.57(m, 2H), 6.25 (M, 2H), 3.95 (s, 2H), 3.73 (s, 6H), 3.65 (s, 6H).

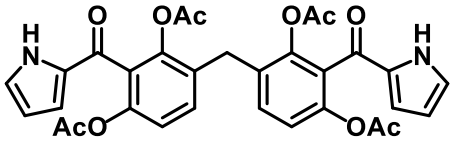

Methylenebis(2-(1H-pyrrole-2-carbonyl)benzene-4,1,3-triyl)tetraacetate (2.15-2.16): In a flame dried flask under argon was dissolved **2.15** (5.3 mg, 13 μmol, 1.0 equiv.) in ethyl acetate (0.63 mL, 0.02 M) and triethylamine (7.9 μL, 57 μmol, 4.5 equiv.). The reaction was stirred at ambient temperature for ten minutes, then cooled to 0˚C in a water ice bath. After cooling, acetyl chloride (3.7 μL, 52 μmol, 4.1 equiv.) was added, and the reaction was stirred at 0˚C for three hours. The reaction was then quenched with a saturated sodium bicarbonate solution, and the aqueous layer was extracted twice with ethyl acetate. The combined organic layers were washed once with brine, dried with MgSO4, filtered, concentrated under reduced pressure, and purified via flash column chromatography (silica gel, 15% ethyl acetate in hexanes) to yield **intermediate 2.15-2.16** (5.6 mg, 13 μmol, 75% yield).

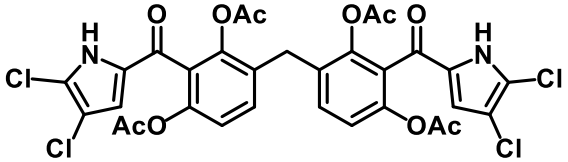

Methylenebis(2-(4,5-dichloro-1H-pyrrole-2-carbonyl)benzene-4,1,3-triyl)tetraacetate (2.16): In a flame dried vial under argon was dissolved intermediate 2.15-2.16 (5.6 mg, 9.5 μmol, 1.0 equiv.) in chloroform (0.9 mL, 0.01 M). To this was added N-chlorosuccinimide (5.1 mg, 38 μmol, 4.0 equiv.), and the reaction was stirred at 60˚C for 18 hours. The reaction was cooled to room temperature then quenched with an aqueous saturated sodium bicarbonate solution. The aqueous layer was extracted twice with ethyl acetate, then the combined organic layers were washed once with brine, dried with MgSO4, filtered, concentrated under reduced pressure, and

column purified (silica gel, 20% ethyl acetate in hexanes) to yield **2.16** (3.4 mg, 4.7 μmol, 49% yield).
1H-NMR: (600 MHz, CDCl3) δ 9.57 (b, 2H), 7.26-7.23 (m, 2H), 7.09 (d, *J* = 8.5 Hz, 2H), 6.62 (s, 2H), 3.78 (s, 2H), 2.05 (s, 12H).

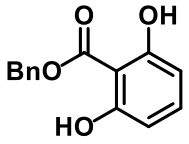

Benzyl 2,6-dihydroxybenzoate (2.18): In a flame dried flask under argon was dissolved 2,6-dihydroxybenzoic acid (519.1 mg, 3.37 mmol, 1.00 equiv.) in DMF (4.0 mL, 0.84 M). To this was added potassium bicarbonate (505.1 mg, 5.05 mmol, 1.50 equiv.), and the reaction was stirred for 10 minutes before benzyl bromide (600 μL, 5.04 mmol, 1.50 equiv.) was added. The reaction was heated to 40˚C for 5 days, then quenched with 1 M HCl. The aqueous phase was extracted twice with ethyl acetate, then the combined organic phases were washed thrice with brine, dried with magnesium sulfate, filtered, concentrated under reduced pressure, and purified via flash column chromatography (0% to 10% ethyl acetate with 0.1% acetic acid in hexanes) to yield **2.18** (537.0 mg, 2.20 mmol, 65% yield) as a white solid.
1H-NMR: (600 MHz, CDCl3) δ 9.71 (b, 1H), 7.46-7.38 (m, 5H), 7.31 (t, *J* = 8.4 Hz, 1H), 6.47 (d, *J* = 8.3 Hz, 2H), 5.50 (s, 2H).

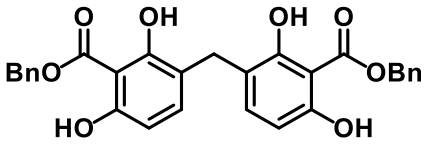

Dibenzyl 3,3'-methylenebis(2,6-dihydroxybenzoate) (2.19): In a flame dried flask under argon was dissolved dimethoxymethane (30.0 μL, 339 μmol, 1.0 equiv.) and aluminum (III) chloride (113.2 mg, 848 μmol, 2.50 equiv.) in acetonitrile (6.0 mL, 0.057 M). The reaction was stirred for 10 minutes before **2.18** (293.8 mg, 1.20 mmol, 3.55 equiv.). The reaction was stirred at ambient temperature for 4 hours, then quenched with 1 M HCl. The aqueous phase was extracted twice with ethyl acetate, then the combined organic phases were washed once with brine, dried with magnesium sulfate, filtered, concentrated under reduced pressure, and purified via flash column chromatography (15% to 30% ethyl acetate with 0.1% acetic acid in hexanes) to yield **2.19** (63.6 mg, 339 μmol, 38% yield) as a white solid.
1H-NMR: (600 MHz, $CDCl_3$) δ 10.07 (b, 2H), 9.45 (b, 2H), 7.45-7.37 (m, 10H), 7.18 (d, *J* = 8.5 Hz, 2H), 6.39 (d, *J* = 8.5 Hz, 2H), 5.50 (s, 2H) 3.77 (s, 2H).
^{13}C-NMR: (106 MHz, $CDCl_3$) δ 169.8, 159.3, 158.6, 138.0, 134.0, 129.4, 129.2, 129.0, 119.1, 107.7, 99.8, 68.3, 28.7.

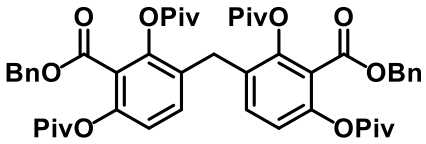

Methylenebis(2-((benzyloxy)carbonyl)benzene-4,1,3-triyl) tetrakis(2,2-dimethylpropanoate) (2.20): In a flame dried flask under argon was dissolved **2.19** (28.8 mg, 57.5 μmol, 1.00 equiv.) and triethylamine (50.0 μL, 359 μmol, 6.23 equiv.) in ethyl acetate (2.0 mL, 0.029 M). The reaction was stirred for 5 minutes before it was cooled to 0˚C in a water-ice bath, and pivaloyl chloride (50.0 μL, 406 μmol, 7.05 equiv.) was added slowly dropwise. The reaction was allowed to slowly warm to ambient temperature over 16 hours, then quenched with a saturated aqueous sodium bicarbonate solution. The aqueous phase was extracted twice with ethyl acetate, then the combined organic phases were washed once with brine, dried with magnesium sulfate, filtered, concentrated under reduced pressure, and purified via flash column chromatography (0% to 10% ethyl acetate in hexanes) to yield **2.20** (42.7 mg, 57.5 μmol, 89% yield) as a white solid.
1H-NMR: (600 MHz, $CDCl_3$) δ 7.39-7.29 (m, 10H), 7.07 (d, *J* = 8.5 Hz, 2H), 6.95 (d, *J* = 8.6 Hz, 2H), 5.25 (s, 2H) 3.70 (s, 2H), 1.20 (s, 9H), 1.17 (s, 9H).

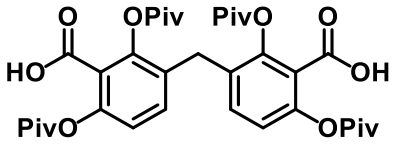

3,3'-methylenebis(2,6-bis(pivaloyloxy)benzoic acid) (2.21): In a flame dried vial under argon was dissolved **2.20** (42.7 mg, 51.0 μmol, 1.00 equiv.) in methanol (5.0 mL, 0.01 M). The vial was purged and backfilled with argon five times, then palladium on carbon (17.5 mg, 8.22 μmol, 0.16 equiv.) was added. The vial was purged and backfilled with argon five times, then purged and backfilled with hydrogen gas five times. Hydrogen gas was then bubbled through the solution for 3 hours, the stirred at ambient temperature for 16 hours. The reaction was then filtered over celite, then concentrated under reduced pressure to yield **2.21** (33.5 mg, 51.0 μmol, 100% yield) as a white solid.
1H-NMR: (600 MHz, $CDCl_3$) δ 7.10 (d, *J* = 8.6 Hz, 2H), 6.95 (d, *J* = 8.4 Hz, 2H), 3.71 (s, 2H), 1.33 (s, 9H), 1.29 (s, 9H).

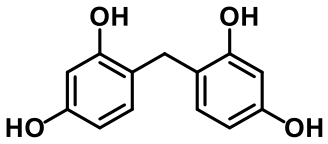

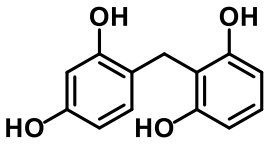

4,4'-methylenebis(benzene-1,3-diol) (2.23) and **2-(2,4-dihydroxybenzyl)benzene-1,3-diol (2.24):** In a flame dried flask under argon was dissolved dimethoxymethane (100 μL, 1.13 mmol, 1.00 equiv.) and aluminum (III) chloride (229.0 mg, 1.72 mmol, 1.52 equiv.) in acetonitrile (10 mL, 0.11 M). The reaction was stirred for 10 minutes, then resorcinol (909.9 mg, 8.26 mmol, 7.31 equiv.) was added. The reaction was stirred for 16 hours at ambient temperature, then the reaction was quenched with 1 M HCl. The aqueous phase was extracted twice with ethyl acetate, then the combined organic phases were washed once with brine, dried with magnesium sulfate, filtered, concentrated under reduced pressure, and purified via flash column chromatography (15% to 31% to 33% ethyl acetate with 0.1% acetic acid in hexanes) to yield **2.23** (178.1 mg, 767 μmol, 68%) and **2.24** (33.3 mg, 143 μmol, 13% yield), both as very pale orange solids.

2.23 1H-NMR: (500 MHz, $(CD_3)_2CO$) δ 8.34 (b, 3H), 7.96 (b, 1H), 6.92 (d, *J* = 8.2 Hz, 2H), 6.37 (d, *J* = 2.4 Hz, 2H), 6.27 (dd, *J* = 8.2, 2.5 Hz, 2H), 3.73 (s, 2H).
2.24 1H-NMR: (500 MHz, $(CD_3)_2CO$) δ 8.59 (b, 2H), 7.97 (b, 2H), 7.20 (d, *J* = 8.3 Hz, 1H), 6.84 (t, *J* = 8.1 Hz, 1H), 6.40 (d, *J* = 8.1 Hz, 2H), 6.33 (d, *J* = 2.5 Hz, 1H), 6.25 (dd, *J* = 8.3, 2.5 Hz, 1H), 3.84 (s, 2H).

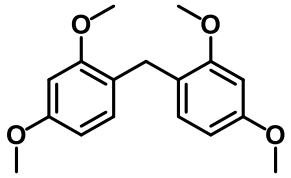

Bis(2,4-dimethoxyphenyl)methane (2.25): In a flame dried flask under argon was dissolved dimethoxymethane (100 μL, 1.13 mmol, 1.00 equiv.) and aluminum (III) chloride (234.8 mg, 1.76 mmol, 1.56 equiv.) in acetonitrile (10 mL, 0.11 M). The reaction was stirred for 10 minutes, then dimethoxybenzene (1.0 mL, 7.64 mmol, 6.76 equiv.) was added. The reaction was stirred for 16 hours, during which time it turned from clear to a light yellow. The reaction was then quenched with 1 M HCl. The aqueous phase was extracted twice with diethyl ether, then the combined organic phases were washed once with brine, dried with magnesium sulfate, filtered, concentrated under reduced pressure, and purified via flash column chromatography (0% to 4% to 6% ethyl acetate in hexanes) to yield **2.25** (188.2 mg, 653 μmol, 58%) as a white solid.
1H-NMR: (500 MHz, $CDCl_3$) δ 6.90 (d, *J* = 8.3 Hz, 2H), 6.46 (d, *J* = 2.4 Hz, 2H), 6.39 (dd, *J* = 8.3, 2.5 Hz, 2H), 3.80 (s, 6H), 3.78 (s, 6H), 3.75 (s, 2H).

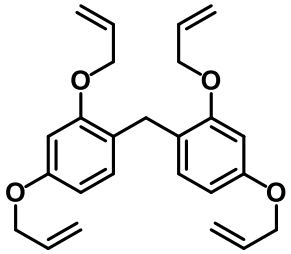

bis(2,4-bis(allyloxy)phenyl)methane (2.26): In a flame dried flask under argon was dissolved **2.23** (160.0 mg, 0.689 mmol, 1.00 equiv.) in acetone (2.0 mL, 0.34 M). This was added to a flame dried flask under argon charged with potassium carbonate (1.143 g, 8.27 mmol, 12.0 equiv.) suspended in 0.5 mL of acetone (16.5 M). The reaction was stirred at ambient temperature for 2 hours before allyl bromide (0.90 mL, 10.4 mmol, 15.1 equiv.) was added slowly dropwise. The reaction heated to reflux for 2 hours, then quenched with 1 M HCl. The aqueous phase was extracted twice with diethyl ether, then the combined organic phases were washed once with brine, dried with magnesium sulfate, filtered, concentrated under reduced pressure, and purified via flash column chromatography (0% to 4% to 6% ethyl acetate in hexanes) to yield **2.26** (63.2 mg, 161 μmol, 23%) as a white solid.
1H-NMR: (500 MHz, $CDCl_3$) δ 6.96 (d, *J* = 8.5 Hz, 2H), 6.47 (d, *J* = 2.3 Hz, 2H), 6.39 (dd, *J* = 8.3, 2.4 Hz, 2H), 6.10-5.99 (m, 4H), 5.43-5.35 (m, 4H), 5.29-5.21 (M, 4H), 4.52-4.48 (m, 8H), 3.88 (s, 2H).

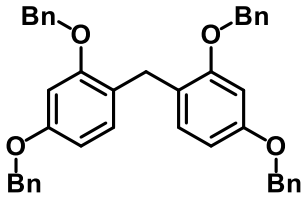

bis(2,4-bis(benzyloxy)phenyl)methane (2.27): In a flame dried reaction tube under argon was dissolved **2.23** (51.0 mg, 0.220 mmol, 1.00 equiv.) in DMF (2.1 mL, 0.10 M). Sodium hydride (43.2 mg, 1.08 mmol, 5.0 equiv.) was added, and the reaction was stirred at ambient temperature for 20 minutes before benzyl bromide (0.240 mL, 2.05 mmol, 9.5 equiv.) was added slowly dropwise. The reaction was the heated to 60˚C for 16 hours, then quenched with a saturated aqueous ammonium chloride solution. The aqueous phase was extracted twice with diethyl ether, then the combined organic phases were washed once with brine, dried with magnesium sulfate, filtered, concentrated under reduced pressure, and purified via flash column chromatography (0% to 4% to 6% ethyl acetate in hexanes) to yield **2.27** (88.6 mg, 149 μmol, 69%) as a white solid.
1H-NMR: (500 MHz, $CDCl_3$) δ 7.43-7.36 (m, 9H), 7.33-7.28 (m, 11H), 6.95 (d, *J* = 8.3 Hz, 2H), 6.58 (d, *J* = 2.4 Hz, 2H), 6.45 (dd, *J* = 8.3, 2.5 Hz, 2H), 3.95 (s, 2H).

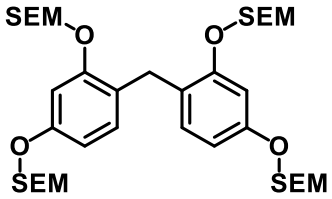

bis(2,4-bis((2-(trimethylsilyl)ethoxy)methoxy)phenyl)methane (2.28): In a flame dried reaction tube under argon was dissolved **2.23** (50.0 mg, 0.215 mmol, 1.00 equiv.) in DMF (2.1 mL, 0.10 M). Sodium hydride (42.6 mg, 1.07 mmol, 5.0 equiv.) was added, and the reaction was stirred at ambient temperature for 20 minutes before SEM-chloride (0.36 mL, 2.05 mmol, 9.5 equiv.) was added slowly dropwise. The reaction was stirred at ambient temperature for 16 hours, then quenched with a saturated aqueous ammonium chloride solution. The aqueous phase was extracted twice with diethyl ether, then the combined organic phases were washed once with brine, dried with magnesium sulfate, filtered, concentrated under reduced pressure, and purified via flash column chromatography (0% to 4% to 6% ethyl acetate in hexanes) to yield **2.28** (23.0 mg, 30.5 μmol, 14%) as a white solid.
1H-NMR: (500 MHz, $CDCl_3$) δ 6.93 (d, *J* = 8.4 Hz, 2H), 6.82 (d, *J* = 2.4 Hz, 2H), 6.45 (dd, *J* = 8.4, 2.4 Hz, 2H), 5.20 (s, 4H), 5.17 (s, 4H), 3.84 (s, 2H), 3.76-3.69 (m, 8H), 0.97-0.93 (m, 8H), 0.00 (s, 18H), -0.01 (18H).

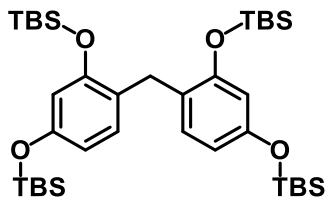

bis(2,4-bis((tert-butyldimethylsilyl)oxy)phenyl)methane (2.29): In a flame dried reaction tube under argon was dissolved **2.23** (50.6 mg, 0.218 mmol, 1.00 equiv.) in DMF (2.1 mL, 0.10 M). The reaction was cooled to 0˚C before DBU (0.23 mL, 1.51 mmol, 7.0 equiv.) was added, and the reaction was stirred at at this temperature for 20 minutes before TBS-chloride (0.3081 mg, 2.05 mmol, 9.5 equiv.) was added. The reaction was slowly warmed to room temperature over 16 hours, then quenched with a saturated aqueous ammonium chloride solution. The aqueous phase was extracted twice with diethyl ether, then the combined organic phases were washed once with brine, dried with magnesium sulfate, filtered, concentrated under reduced pressure, and purified via flash column chromatography (0% to 4% to 6% ethyl acetate in hexanes) to yield **2.29** (128.8 mg, 187 μmol, 87%) as a white solid.
1H-NMR: (500 MHz, $CDCl_3$) δ 6.68 (d, *J* = 8.2 Hz, 2H), 6.34 (dd, *J* = 8.2, 2.4 Hz, 2H), 6.31 (d, *J* = 2.4 Hz, 2H), 3.75 (s, 2H), 0.97 (s, 18H), 0.91 (s, 18H), 0.18 (s, 12H), 0.17 (s, 12H).

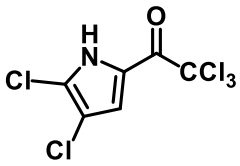

4,5-Dichloro-2-trichloroacetylpyrrole (2.30): In a flame dried flask under argon was suspended 2-trichloroacetylpyrrole (1.1050g, 5.20 mmol, 1.00 equiv.) in DCM (15 mL, 0.35 M). To this was slowly added sulfuryl dichloride (0.95 mL, 11.8 mmol, 2.26 equiv.). Reaction stirred for 16 hours, then quenched with saturated sodium bicarbonate The aqueous phase was extracted twice with ethyl acetate, then the combined organic phases were washed once with brine, dried with magnesium sulfate, filtered, concentrated under reduced pressure, and purified via flash column chromatography (0% to 5% ethyl acetate in hexanes) to yield **2.30** (1.3126 g, 4.67 mmol, 90%) as a pale orange solid.
1H-NMR: (500 MHz, $CDCl_3$) δ 9.41 (s, 1H), 7.29 (s, 1H).

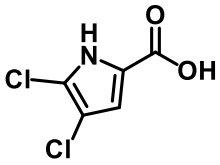

4,5-dichloro-1H-pyrrole-2carboxylic acid (2.31): In a flask was dissolved 2-trichloroacetyl pyrrole (302.5 mg 1.08 mmol, 1.00 equiv.) in DMSO (13.0 mL, 0.083 M). To this was slowly added an aqueous K_2CO_3 solution (50 ml, 2 M, 96.4 mmol, 90 equiv.). Reaction stirred at room temperature for 5 hours, then quenched with 3 M HCl until the aqueous layer pH was less than 2. The aqueous layer was extracted twice with ethyl acetate, then the combined organic layers were washed once with brine, dried with magnesium sulfate, concentrated and purified via flash column chromatography (10% to 25% ethyl acetate with 0.1% acetic acid in hexanes) to yield **2.31** (190.5 mg, 1.058 mmol, 98%) as a pale tan solid.
1H-NMR: (600 MHz, CD_3OD) δ 6.77 (s, 1H).

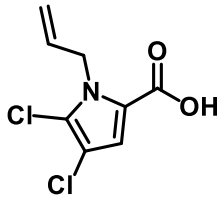

***N*-allyl-4,5-dichloro-pyrrole-2-carboxylic acid (2.33):** In a flame dried flask under argon was dissolved **2.30** (195.8 mg, 0.696 mmol, 1.00 equiv.) in DMF (4.0 mL, 0.17 M). It was cooled to 0°C, then sodium hydride (35.8 mg, 0.895 mmol, 1.29 equiv.) was added portion wise, causing the solution to bubble. Reaction stirred for 10 minutes, then allyl bromide (0.10 mL, 1.16 mmol, 1.66 equiv.) was added slowly dropwise. Reaction allowed to slowly warm to room temp overnight, then quenched by dumping into an aqueous solution of K_2CO_3 (13.0 mL, 2.0 M, 26.0 mmol, 37.4 equiv.) and transferred with DMSO (15 mL) and acetone (10 mL). Reaction heated to 36°C for 4 hours, then quenched by acidifying the aqueous layer to below 4 with 3M HCl. The aqueous layer was extracted twice with ethyl acetate, then the combined organic layers were washed once with brine, dried with magnesium sulfate, concentrated and purified via flash column chromatography (5% to 10% ethyl acetate with 0.1% acetic acid in hexanes) to yield **2.33** (113.3 mg, 0.515 mmol, 74%) as a pale-yellow solid.
1H-NMR: (400 MHz, $CDCl_3$) δ 11.75 (b, 1H), 7.09 (s, 1H), 5.91 (ddt, *J* = 15.4, 10.2, 5.1 Hz, 1H), 5.17 (d, *J* = 10.3 Hz, 1H), 5.04 (d, *J* = 5.1 Hz, 1H), 4.95 (d, *J* = 17.7 Hz, 1H).
^{13}C-NMR: (106 MHz, $CDCl_3$) δ 164.8, 132.5, 123.3, 119.5, 118.8, 117.4, 110.9, 48.7.

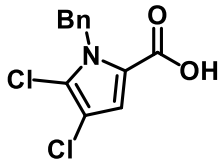

***N*-benzyl-4,5-dichloro-pyrrole-2-carboxylic acid (2.34):** In a flame dried flask under argon was dissolved **2.30** (256.4 mg, 0.911 mmol, 1.00 equiv.) and 18-crown-6 (256.8 mg, 0.972 mmol, 1.07 equiv.) in THF (2.0 mL, 0.5 M). The reaction was cooled to 0°C, then potassium *t*-butoxide (124.8 mg, 1.11 mmol, 1.22 equiv.) was added, causing the reaction to turn a dark brown. The reaction was stirred for 10 minutes before it was cannulated into a solution of benzyl bromide (0.18 mL, 1.51 mmol, 1.66 equiv.) in THF (2.0 mL, 0.75 M). Reaction allowed to slowly warm to room temp overnight. An additional 50 uL of benzyl bromide were added at 11am, then the reaction was quenched at 4pm by dumping it into an aqueous solution of potassium carbonate (16.0 mL, 2.0 M, 32.0 mmol, 35.1 equiv.). The flask was rinsed with DMSO (20 mL), then the new reaction mixture was heated to 35°C overnight. Reaction quenched the next morning with 3M HCl until the pH was below 2. The aqueous layer was extracted twice with ethyl acetate, then the combined organic layers were washed once with brine, dried with magnesium sulfate, concentrated and purified washing the crude solid dissolved in diethyl ether with deionized water 10 times to yield **2.34** (136.8 mg, 0.507 mmol, 56%) as a pale-yellow solid.
1H-NMR: (600 MHz, $CDCl_3$) δ 7.32-7.27 (m, 3H), 7.11 (s, 1H), 7.08 (d, *J* = 7.1 Hz, 2H), 5.66 (s, 2H).

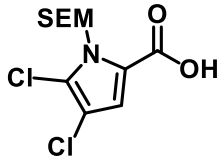

***N*-((2-(trimethylsilyl)ethoxy)methyl)-4,5-dichloro-pyrrole-2-carboxylic acid (2.35):** In a flame dried flask under argon was dissolved **2.30** (345.2 mg, 1.23 mmol, 1.00 equiv.) in DMF (3.5 mL, 0.05 M). It was cooled to 0°C, then sodium hydride (59.0 mg, 1.50 mmol, 1.2 equiv.) was added portion wise, causing the solution to bubble. Reaction stirred for 10 minutes, then SEM-chloride (0.33 mL, 1.84 mmol, 1.5 equiv.) was added slowly dropwise. Reaction allowed to slowly warm to room temp overnight, then quenched by dumping into an aqueous solution of K_2CO_3 (18.4 mL, 2.0 M, 36.8 mmol, 30.0 equiv.) and transferred with DMSO (8 mL) and acetone (8 mL). Reaction heated to 36°C for 4 hours, then quenched by acidifying the aqueous layer to below 4 with 3M HCl. The aqueous layer was extracted twice with ethyl acetate, then the combined organic layers were washed once with brine, dried with magnesium sulfate, concentrated and purified via flash column chromatography (0% to 8% ethyl acetate with 0.1% acetic acid in hexanes) to yield **2.35** (337.0 mg, 01.09 mmol, 89%) as a pale-yellow solid.
1H-NMR: (500 MHz, $CDCl_3$) δ 7.10 (s, 1H), 5.78 (s, 2H), 3.59 (dd, *J* = 8.3, 8.1 Hz, 2H), 0.91 (dd, *J* = 8.3, 8.0 Hz, 2H), -0.03 (s, 9H).

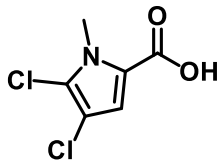

***N*-methyl-4,5-dichloro-pyrrole-2-carboxylic acid (2.36):** In a flame dried flask under argon was dissolved **2.30** (200.9 mg, 0.714 mmol, 1.00 equiv.) in DMF (4.0 mL, 0.18 M). It was cooled to 0°C, then sodium hydride (37.1 mg, 0.927 mmol, 1.3 equiv.) was added portion wise, causing the solution to bubble. Reaction stirred for 10 minutes, then methyl iodide (0.080 mL, 1.3 mmol, 1.8 equiv.) was added slowly dropwise. Reaction allowed to slowly warm to room temp overnight, then quenched by dumping into an aqueous solution of K_2CO_3 (13 mL, 2.0 M, 26.0 mmol, 36.4 equiv.) and transferred with DMSO (15 mL). Reaction heated to 36°C for 4 hours, then quenched by acidifying the aqueous layer to below 4 with 3M HCl. The aqueous layer was extracted twice with ethyl acetate, then the combined organic layers were washed once with brine, dried with magnesium sulfate, concentrated and purified via flash column chromatography (0% to 12% ethyl acetate with 0.1% acetic acid in hexanes) to yield **2.36** (118.2 mg, 0.609 mmol, 85%) as a pale-brown solid.
1H-NMR: (500 MHz, $CDCl_3$) δ 7.05 (s, 1H), 3.92 (s, 3H).

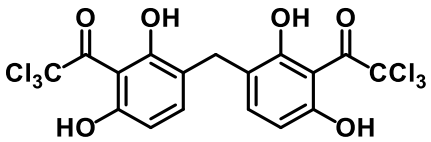

1,1'-(methylenebis(2,6-dihydroxy-3,1-phenylene))bis(2,2,2-trichloroethan-1-one) (2.37): In a flame dried flask under argon was dissolved **2.23** (26.4 mg, 0.114 mmol, 1.00 equiv.) in THF (1.1

mL, 0.1 M) and TEA (0.032 mL, 0.227 mmol, 2.0 equiv.). The reaction was stirred at room temp for 10 minutes, then **2.30** (68.3 mg, 0.243 mmol, 2.14 equiv.) was added. Reaction stirred at ambient temperature for 24 hours, then heated to 35˚C for 24 hours. The reaction was then quenched with 1 M HCl. The aqueous layer was extracted twice with ethyl acetate, then the combined organic layers were washed once with brine, dried with magnesium sulfate, concentrated and purified via flash column chromatography (0% to 12% ethyl acetate with 0.1% acetic acid in hexanes) to yield **2.36**.

1H-NMR: (500 MHz, $CDCl_3$) δ 7.98 (d, *J* = 8.8 Hz, 2H), 7.79 (d, *J* = 9.0 Hz, 2H), 4.08 (s, 2H).

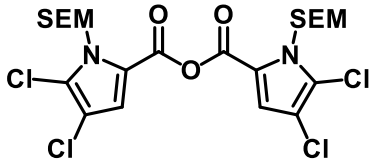

4,5-dichloro-1-((2-(trimethylsilyl)ethoxy)methyl)-1H-pyrrole-2-carboxylic anhydride (2.45): In a flame dried flask under argon was dissolved **2.35** (500.0 mg, 1.61 mmol, 1.00 equiv.) in freshly distilled TEA (0.52 mL, 3.73 mmol, 2.31 equiv.) and DCM (3.0 mL, 0.54 M). The reaction as cooled to 0˚C, then thionyl chloride (0.070 mL, 0.959 mmol, 0.595 equiv.) was added slowly dropwise. The reaction was allowed to warm to room temperature over 2.5 hours, then it was quenched with saturated sodium bicarbonate solution. The aqueous layer was extracted twice with diethyl ether, then the combined organic layers were washed once with brine, dried with magnesium sulfate, concentrated and purified via flash column chromatography (0% to 4% ethyl acetate in hexanes) to yield **2.45** (352.7 mg, 0.585 mmol, 73% yield).

1H-NMR: (600 MHz, $CDCl_3$) δ 7.11 (s, 1H), 5.80 (s, 2H), 3.62 (dd, *J* = 8.2, 8.1 Hz, 2H), 0.92 (dd, *J* = 8.3, 8.0 Hz, 2H), -0.02 (s, 9H).

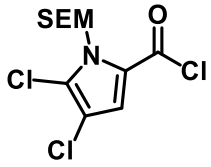

4,5-dichloro-1-((2-(trimethylsilyl)ethoxy)methyl)-1H-pyrrole-2-carbonyl chloride (2.46): In a flame dried flask under argon was dissolved **2.35** (852.1 mg, 2.75 mmol, 1.00 equiv.) in freshly distilled TEA (1.61 mL, 11.54 mmol, 4.2 equiv.) and THF (60 mL, 0.046 M). The reaction was stirred for 5 minutes, then cooled to 0˚C before thionyl chloride (0.450 mL, 6.17 mmol, 2.25 equiv.) was added slowly. The reaction was stirred at this temperature for 2 hours before it was quenched with saturated sodium bicarbonate. The aqueous layer was extracted twice with diethyl ether, then the combined organic layers were washed once with brine, dried with magnesium sulfate, concentrated and purified via flash column chromatography (0% to 4% ethyl acetate in hexanes) to yield **2.46** (900. mg, 2.74 mmol, 99.7% yield).

1H-NMR: (600 MHz, $CDCl_3$) δ 7.33 (s, 1H), 5.67 (s, 2H), 3.57 (dd, *J* = 8.2, 8.2 Hz, 2H), 0.90 (dd, *J* = 8.3, 8.0 Hz, 2H), -0.02 (s, 9H).

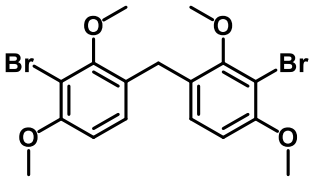

bis(3-bromo-2,4-dimethoxyphenyl)methane (2.49): In a flame dried flask under argon was dissolved paraformaldehyde (15.7 mg, 0.523 mmol, 1.00 equiv.) in acetonitrile (5.0 mL, 0.1 M). To this was added aluminum (III) and the reaction was stirred at room temperature for 10 minutes before 2-bromo-1,3-dimetheoxybenzene (1.1116 g, 2.12 mmol, 9.81 equiv.) and the reaction was heated to 40˚C for 16 hours. The reaction was then quenched with deionized water at room temperature. The aqueous layer was extracted twice with diethyl ether, then the combined organic layers were washed once with brine, dried with magnesium sulfate, concentrated and purified via flash column chromatography (0% to 15% diethyl ether in hexanes) to yield **2.49** (82.8 mg, 0.186 mmol, 36% yield).
1H-NMR: (500 MHz, $CDCl_3$) δ 6.95 (d, *J* = 8.6 Hz, 2H), 6.62 (d, *J* = 8.6 Hz, 2H), 3.96 (s, 2H), 3.87 (s, 6H), 3.80 (s, 6H).

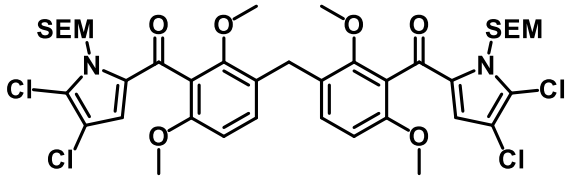

(methylenebis(2,6-dimethoxy-3,1-phenylene))bis((4,5-dichloro-1-((2-(trimethylsilyl)ethoxy) methyl)-1H-pyrrol-2-yl)methanone) (2.50): In a flame dried flask under argon was dissolved **2.49** (98.6 mg, 0.221 mmol, 1.00 equiv.) in THF (1.2 mL, 0.2 M) and TMEDA (0.083 mL, 0.553 mmol, 2.5 equiv.). The reaction was cooled to -78˚C, then *n*-buLi was slowly added dropwise. The reaction was stirred at this temperature for 1.5 hours, then **2.45** (399.5 mg, 0.663 mmol, 3.00 equiv.) dissolved in THF (1.2 mL, 0.55 M) was slowly added. The reaction was allowed to slowly warm to room temperature overnight, then the reaction was cooled to 0˚C and quenched with a saturated ammonium chloride solution. The aqueous layer was extracted twice with diethyl ether, then the combined organic layers were washed once with brine, dried with magnesium sulfate, concentrated and purified via flash column chromatography (0% to 20% diethyl ether in hexanes) to yield **2.50** (28.8 mg, 0.033 mmol, 15% yield).
1H-NMR: (500 MHz, $CDCl_3$) δ 7.06 (d, *J* = 8.6 Hz, 2H), 6.66 (d, *J* = 8.7 Hz, 2H), 6.43 (s, 2H), 6.00 (s, 4H), 3.93 (s, 2H), 3.73-3.70 (M, 10H), 3.66 (s, 6H), 3.80 (s, 6H), 0.95 (dd, *J* = 8.3,8.1 Hz, 4H), -0.01 (s, 18H).

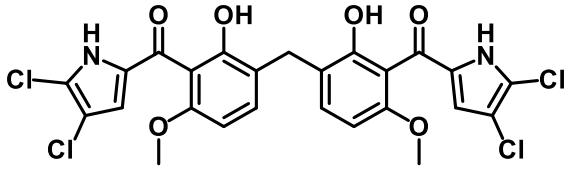

(methylenebis(2-hydroxy-6-methoxy-3,1-phenylene))bis((4,5-dichloro-1H-pyrrol-2-yl)methanone) (2.51): In a flame dried flask under argon was dissolved **2.50** (28.8 mg, 0.033

mmol, 1.00 equiv.) in DCM (0.20 mL, 0.17 M). The solution was cooled to 0˚C, then 1 M boron trichloride in DCM (0.20 mL, 0.20 mmol, 6.06 equiv.) was slowly added. The reaction was stirred for 10 minutes before tetrabutylammonium iodide (97.5 mg, 0.264 mmol, 8.0 equiv.) was added. The reaction was allowed to warm to room temperature over 5 hours, then quenched with saturated ammonium chloride at 0˚C. The aqueous layer was extracted twice with ethyl acetate, then the combined organic layers were washed once with brine, dried with magnesium sulfate, concentrated and purified via flash column chromatography (15% to 30% ethyl acetate with 0.1% acetic acid in hexanes) to yield **2.51** (5.1 mg, 8.7 µmol, 26% yield).
1H-NMR: (600 MHz, $CDCl_3$) δ 7.23 (d, *J* = 8.5 Hz, 2H), 6.70 (s, 2H), 6.57 (d, *J* = 8.6 Hz, 2H), 3.86 (s, 2H), 3.73 (s, 6H).

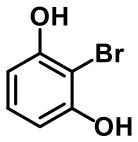

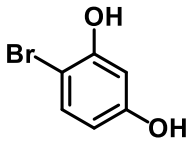

2-bromo-1,3-dihydroxybenzene (2.52) and 4-bromo-1,3-dihydroxybenzene (2.53): In a flame dried flask under argon was dissolved 2-bromo-1,3-dimethoxybenzene (159.2 mg, 0.733 mmol, 1.00 equiv.) in DCM (6.0 mL, 0.12 M). The reaction was cooled to 0˚C, then 1 M boron tribromide in DCM (3.5 mL, 3.5 mmol, 4.8 equiv.) was slowly added dropwise. The reaction was allowed to warm to room temperature slowly over 16 hours, then the reaction was quenched with a saturated ammonium chloride solution. The aqueous layer was extracted twice with ethyl acetate, then the combined organic layers were washed once with brine, dried with magnesium sulfate, concentrated and purified via flash column chromatography (15% to 30% ethyl acetate with 0.1% acetic acid in hexanes) to yield **2.52** and **2.53**. The products degraded before a yield could be obtained, but the NMRs were able to be collected. The collected spectra matched those previously reported.[6,7]
2.52 1H-NMR: (500 MHz, $CDCl_3$) δ 7.11 (d, *J* = 8.1 Hz, 1H), 6.60 (d, *J* = 8.2 Hz, 2H).
2.53 1H-NMR: (500 MHz, $(CD_3)CO$) δ 8.57 (b, 2H), 7.25 (d, *J* = 8.7 Hz, 1H), 6.53 (d, *J* = 2.7 Hz, 1H), 6.32 (d, *J* = 8.7, 2.8 Hz, 1H).

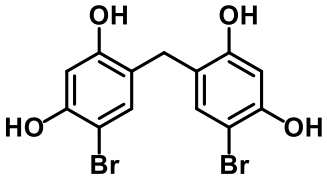

6,6'-methylenebis(4-bromobenzene-1,3-diol) (2.54): In a flame dried flask under argon was dissolved **2.23** (111.1 mg, 0.478 mmol, 1.00 equiv.) in acetonitrile (4.0 mL, 0.12 M). The reaction was cooled to 0˚C, then *N*-bromosuccinimide was added, causing the reaction to turn bright yellow. Reaction allowed to allowed to slowly warm to room temperature over 16 hours, then it was quenched with ca. 0.5 M HCl. The aqueous layer was extracted twice with ethyl acetate, then the combined organic layers were washed once with brine, dried with magnesium sulfate, concentrated and purified via flash column chromatography (15% to 30% ethyl acetate with 0.1% acetic acid in hexanes) to yield **2.54** (73.5 mg, 0.188 mmol, 39% yield).
1H-NMR: (500 MHz, $(CD_3)CO$) δ 8.56 (b, 4H), 7.20 (s, 2H), 6.58(s, 2H), 3.75 (s, 2H).

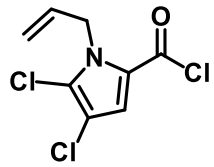

1-allyl-4,5-dichloro-1H-pyrrole-2-carbonyl chloride (2.55): In a flame dried flask under argon was dissolved **2.33** (196.2 mg, 0.892 mmol, 1.00 equiv.) in THF (20.0 mL, 0.045 M) and freshly distilled TEA (1.00 mL, 7.17 mmol, 8.05 equiv.). The reaction was cooled to 0˚C, then thionyl chloride (0.230 mL, 3.15 mmol, 3.53 equiv.) was slowly added dropwise. Reaction stirred at this temperature for 1.5 hours, then it was quenched with a saturated sodium bicarbonate solution. The aqueous layer was extracted twice with ethyl acetate, then the combined organic layers were washed once with brine, dried with magnesium sulfate, concentrated and purified via flash column chromatography (0% to 10% diethyl ether in hexanes) to yield **2.55** (204.4 mg, 0.857 mmol, 96% yield).
1H-NMR: (600 MHz, $CDCl_3$) 7.31 (s, 1H), 5.86 (ddt, *J* = 17.1, 10.4, 5.2, 1H), 5.21 (d, *J* = 10.3, 1H), 4.98 (d, *J* = 18.0, 1H), 4.96-4.94 (M, 2H).

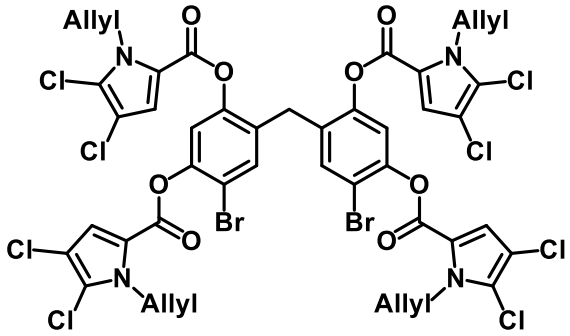

Methylenebis (6-bromobenzene-4,1,3-triyl) tetrakis(1-allyl-4,5-dichloro-1H-pyrrole-2-carboxylate) (2.56): In a flame dried vial under argon was dissolved **2.54** (28.8 mg, 0.074 mmol, 1.00 equiv.) and **2.55** (80.0 mg, 0.335 mmol, 4.54 equiv.) in acetonitrile (0.037 M). Cesium carbonate (131.8 mg, 0.405 mmol, 5.48 equiv.) was added, and the reaction was stirred at room temperature for 6 hours before it was quenched with 1 M HCl. The aqueous layer was extracted twice with DCM, then the combined organic layers were washed once with brine, dried with magnesium sulfate, concentrated and purified via flash column chromatography (0% to 8% ethyl acetate in hexanes) to yield **2.56** (67.7 mg, 0.057 mmol, 77% yield).
1H-NMR: (400 MHz, $CDCl_3$) 7.43 (s, 2H), 7.28 (s, 2H), 7.12 (s, 2H), 7.03 (s, 2H), 5.99-5.85 (m, 4H), 5.99-5.85 (m, 4H), 5.22-5.17 (m, 4H), 5.08-4.96 (m, 8H), 3.83 (s, 2H).

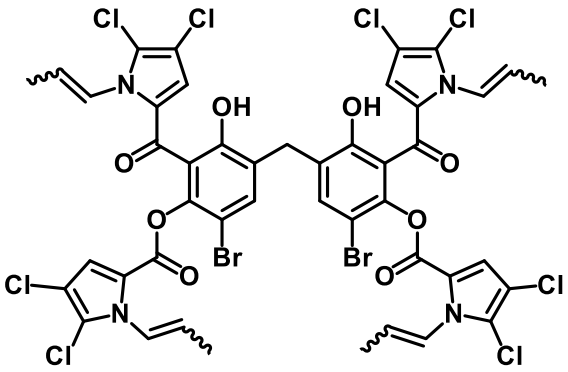

methylenebis(6-bromo-2-(4,5-dichloro-1-((E)-prop-1-en-1-yl)-1H-pyrrole-2-carbonyl)-3-hydroxy-4,1-phenylene) bis(4,5-dichloro-1-((E)-prop-1-en-1-yl)-1H-pyrrole-2-carboxylate) (2.57): In a flame dried vial under argon was dissolved **2.56** (5.1 mg, 4.3 μmol, 1.00 equiv.) in trifluoromethanesulfonic acid (0.30 mL, 0.014 M) at 0˚C, causing the reaction to turn bright yellow. The reaction was stirred at this temperature for 30 minutes before quenched via dumping into ice water. The aqueous layer was extracted twice with ethyl acetate, then the combined organic layers were washed once with brine, dried with magnesium sulfate, concentrated crude NMR confirmed the presence of **2.57**. A yield could not be obtained before the molecule degraded.
1H-NMR: (400 MHz, $(CD_3)CO$) 7.20 (s, 2H), 6.98 (s, 2H), 6.59 (s, 2H), 4.98-4.92 (m, 4H), 4.43-4.40 (m, 4H), 5.22-5.17 (m, 4H), 3.96-3.91 (m, 4H), 3.75 (s, 2H).

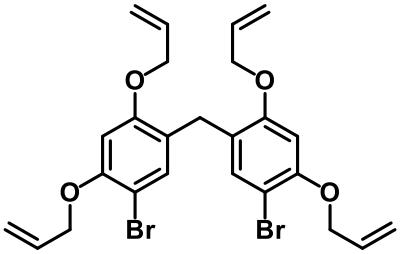

bis(2,4-bis(allyloxy)-5-bromophenyl)methane (2.58): In a flame dried flask under argon was dissolved **2.54** (39.3 mg, 0.101 mmol, 1.00 equiv.) in acetone (2.0 mL, 0.04 M). This was added to a slurry of potassium carbonate (165.3 mg, 1.20 mmol, 11.9 equiv.) in acetone (0.5 mL, 2.4 M). The reaction was stirred at room temperature for 2 hours before allyl bromide (0.13 mL, 1.50 mmol, 14.9 equiv.) was slowly added dropwise. The reaction was heated to reflux for 2 hours, then quenched with 1 M HCl. The aqueous layer was extracted twice with ethyl acetate, then the combined organic layers were washed once with brine, dried with magnesium sulfate, concentrated and purified via flash column chromatography (0% to 10% ethyl acetate in hexanes) to yield **2.58** (51.4 mg, 0.093 mmol, 93% yield).
1H-NMR: (500 MHz, $CDCl_3$) 7.27 (s, 2H), 6.45 (s, 2H), 6.09-5.99 (m, 4H), 5.49-5.45 (m, 2H), 5.40-5.36 (m, 2H), 5.32-5.28 (m, 4H), 3.79 (s, 2H).

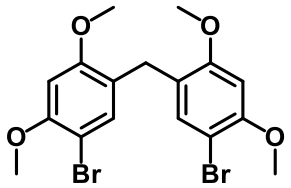

bis(5-bromo-2,4-dimethoxyphenyl)methane (2.60): In a flame dried vial under argon was dissolved **2.25** (254.5 mg, 0.883 mmol, 1.00 equiv.) in acetonitrile (5.0 mL, 0.18 M). The reaction was cooled to 0˚C, then NBS (316.4 mg, 1.78 mmol, 2.01 equiv.). The reaction was allowed to slowly warm to room temperature overnight, then quenched the following morning with ca, 0.5 M HCl. The aqueous layer was extracted twice with diethyl ether, then the combined organic layers were washed once with brine, dried with magnesium sulfate, concentrated and purified via flash column chromatography (0% to 10% ethyl acetate in hexanes) to yield **2.60** (205.0 mg, 0.460 mmol, 52% yield).
1H-NMR: (500 MHz, $CDCl_3$) 7.16 (s, 2H), 6.47 (s, 2H), 3.89 (s, 6H), 3.83 (s, 6H), 3.74 (s, 2H).

5.2.2 Chapter 3

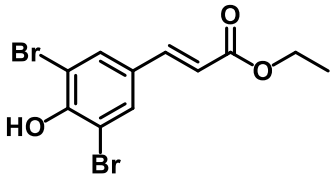

(E)-Ethyl 3-(3,5-dibromo-4-hydroxyphenyl)acrylate (3.113): In a flame dried flask under argon was dissolved 3,5-dibromo-4-hydroxybenzaldehyde (0.2510 g, 0.90 mmol, 1.00 equiv.) in toluene (5.0 mL, 0.18 M). To this was added Carbethoxymethylene triphenylphosphorane (413.6 mg, 1.19 mmol, 1.32 equiv.), causing the reaction to turn a light brown. The reaction was heated to 70˚C for 16 hours, then quenched via concentration under reduced pressure. The waxy brown solid was purified via flash column chromatography (0% to 50% diethyl ether in hexanes) to yield **3.113** (0.2951 g, 0.85 mmol, 94% yield) as a white solid. All spectra matched those previously reported.[8]
^{1}H-NMR: (400 MHz, $CDCl_3$) δ 7.61 (s, 2H), 7.47 (d, *J* = 16.0 Hz, 1H), 6.32 (d, *J* = 15.9 Hz, 1H), 4.25 (q, *J* = 7.1 Hz, 2H), 1.32 (t, 7.1 Hz, 3H).
^{13}C-NMR: (106 MHz, CD_3OD) δ 166.6, 151.0, 141.3, 131.7, 129.7, 118.7, 110.5, 60.83, 14.4.
HRMS ($APCI^+$): $C_{11}H_{11}O_3{}^{79}Br_2$ [M^+] requires 348.90695; Found: 348.90741.

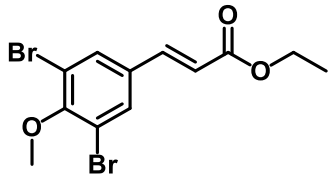

(E)-Ethyl-3-(3,5-dibromo-4-methoxypenyl)acrylate (3.114): A flame dried flask under argon was charged with potassium carbonate (2.1423 g, 15.5 mmol, 1.2 equiv.) and **3.113** (4.6626 g, 13.9 mmol, 1.00 equiv.). DMF (25 mL, 0.56 M) was added, followed by methyl iodide (1.05 mL, 16.9 mmol, 1.22 equiv.). The reaction was stirred at ambient temperature for 17 hours, during which

time a solid crashed out of solution. The reaction was quenched with 30 mL of 1 M sodium hydroxide, then stirred for an additional 20 minutes. The aqueous layer was then extracted twice with ethyl acetate, then the combined organic layers were washed once with 1 M NaOH, four times with brine, dried with $MgSO_4$, filtered, and concentrated under reduced pressure to yield **3.114** (4.6568 g, 12.8 mmol, 92% yield). The spectra matched those previously reported. All spectra matched those previously reported.[8]

^{1}H-NMR: (400 MHz, $CDCl_3$) δ 7.62 (s, 2H), 7.46 (d, *J* = 16.0 Hz, 1H), 6.32 (d, *J* = 15.9 Hz, 1H), 4.23 (q, *J* = 7.2 Hz, 2H), 3.87 (s, 3H), 1.30 (t, 7.1 Hz, 3H).

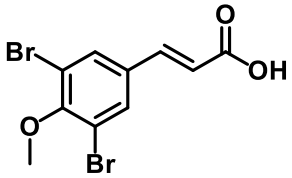

(E)-3-(3,5-dibromo-4-methoxypheyl)acrylic acid (3.115): In a flask was dissolved **3.114** (1.2208 g, 3.49 mmol, 1.00 equiv.) and lithium hydroxide (0.3343 g, 13.96 mmol, 4.00 equiv.) in THF (7 mL, 0.5 M) and deionized water (2.0 mL, 1.75 M). The reaction was stirred at ambient temperature for 28 hours, then quenched with 1 M HCl. The aqueous layer was extracted thrice with ethyl acetate, then the combined organic layers were washed once with brine, dried with $MgSO_4$, filtered, concentrated under reduced pressure, and purified via column chromatography (silica gel, 15% ethyl acetate with 0.1% acetic acid in hexanes) to yield **3.115** (0.9724 g, 2.89 mmol, 83% yield) as white powder. All spectra matched those previously reported.[8]

^{1}H-NMR: (400 MHz, CD_3OD) δ 7.83 (s, 2H), 7.52 (d, *J* = 16.0 Hz, 1H), 6.46 (d, *J* = 16.0 Hz, 1H), 3.88 (s, 3H).

^{13}C-NMR: (106 MHz, CD_3OD) δ 169.6, 156.7, 142.5, 134.9, 133.4, 121.7, 199.6, 61.2.

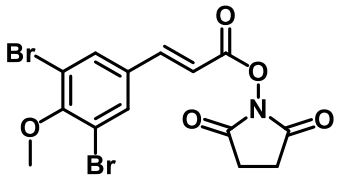

2,5-dioxopyrrolidin-1-yl (E)-3-(3,5-dibromo-4-methoxyphenyl)acrylate (3.116): In a flame dried flask under argon was dissolved **3.115** (2.5080 g, 7.46 mmol, 1.00 equiv.) in THF (30.0 mL, 0.25 M) and DMF (3.0 mL, 2.49 M). To this was added diisopropylcarbodiimide (1.1305 g, 8.96 mmol, 1.20 equiv.) and *N*-hydroxysuccinimide (1.1007 g, 9.56 mmol, 1.28 equiv.). The reaction was stirred at room temperature for 16 hours, during which time a white precipitate formed. The mixture was filtered, then the filtrate was concentrated under reduced pressure and purified via flash column chromatography (silica gel, 15% ethyl acetate in hexanes) to yield **3.116** (2.3580 g, 5.45 mmol, 73% yield) as a white powder. All spectra matched those previously reported.[8]

^{1}H-NMR: (400 MHz, $CDCl_3$) δ 7.72 (d, *J* = 16.0 Hz, 2H), 7.71 (s, 1H), 6.50 (d, *J* = 16.1 Hz, 1H), 3.92 (s, 3H), 2.87 (s, 4H).

^{13}C-NMR: (106 MHz, CD_3OD) δ 169.3, 161.6, 156.6, 146.3, 132.7, 132.1, 119.1, 113.6, 61.0, 25.7.

HRMS (ESI$^-$): $C_{14}H_{11}O_5N^{79}Br_2$ [M+Cl$^-$] requires 465.8698; Found: 465.86981.

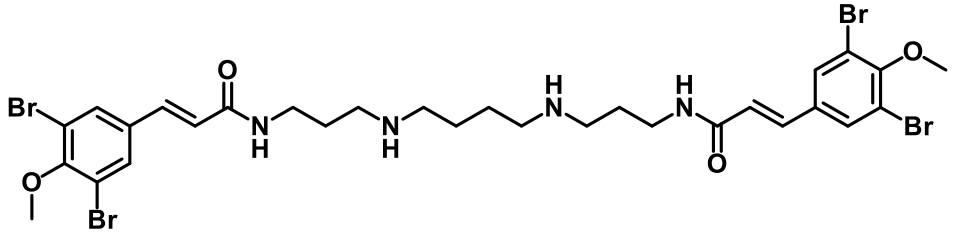

Ianthelliformisamine C (3.112): In a flame dried flask under argon was dissolved **3.116** (1.9978 g, 4.61 mmol, 2.31 equiv.) in 1,4-dioxane (20.0 mL, 0.23M). To this was added spermine (0.4034 g, 1.99 mmol, 1.00 equiv.), causing the clear, colorless solution to turn a chunky pale yellow. The reaction was stirred at ambient temperature for 24 hours, then quenched with a saturated aqueous sodium bicarbonate solution. The organic layer was diluted with DCM, then the organic layer was extracted thrice with the saturated aqueous sodium bicarbonate solution. The combined aqueous layers were basified to pH 14, then extracted 5 times with 10% methanol in DCM. The combined organic layers were dried over sodium sulfate, filtered, and concentrated under reduced pressure to yield **3.112** (1.1570 g, 1.3802 mmol, 69% yield) as a pale yellow solid. The title compound could also be purified via column chromatography (silica gel, 15% methanol with 10% ammonium hydroxide in DCM). The spectra matched those previously reported. All spectra matched those previously reported.[8]

^{1}H-NMR: (400 MHz, $CDCl_3$) δ 7.79 (s, 4H), 7.41 (d, *J* = 15.7 Hz, 2H), 6.50 (d, *J* = 15.7 Hz, 2H), 3.86 (s, 6H), 3.48-3.43 (m, 4H), 3.12-3.05 (m, 8H), 2.03-1.95 (m, 4H), 1.90-1.85 (m, 4H).

^{13}C-NMR: (106 MHz, CD_3OD) δ 164.3, 153.8, 134.8, 134.5, 131.5, 124.7, 118.0, 60.5, 49.4, 47.0, 37.1, 29.5, 27.6.

HRMS (ESI$^-$): $C30H39O_4N_4{}^{79}Br_4$ [M+Cl$^-$] requires 834.96993; Found: 834.97098.

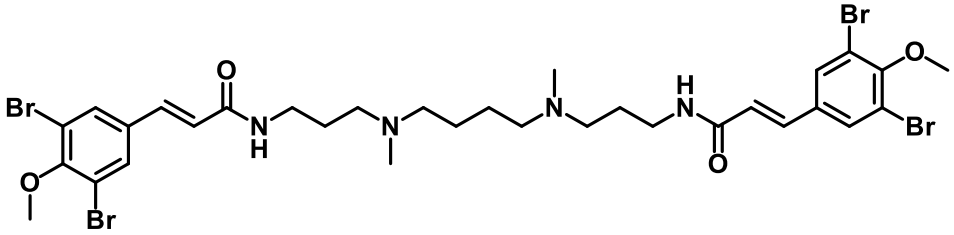

(2E,2'E)-N,N'-((butane-1,4-diylbis(methylazanediyl))bis(propane-3,1-diyl))bis(3-(3,5-dibromo-4-methoxyphenyl)acrylamide) (3.117): In a flame dried flask under argon was dissolved **3.112** (0.3323 g, 0.40 mmol, 1.00 equiv.) and 30% aqueous formaldehyde (73.8 μL, 0.99 mmol, 2.50 equiv.) in methanol (4.0 mL, 0.10 M). Acetic acid (113.5 μL, 1.98 mmol, 5.00 equiv.) was added, and the reaction was stirred for 30 minutes before sodium cyanoborohydride (52.4 mg, 0.83 mmol, 2.10 equiv.) was added in two portions, allowing for five minutes between each portion. The reaction was stirred at room temperature for 24 hours, then quenched with 1 M sodium hydroxide. The aqueous layer was extracted thrice with DCM, then the combined organic phases were dried over sodium sulfate, filtered, concentrated under reduced pressure, and purified via

flash column chromatography (silica gel, 7% methanol with 10% ammonium hydroxide in DCM) to yield **3.117** (0.1612 g, 186 μmol, 47% yield) as a white solid. After the column, the purified solid was dissolved in DCM and washed twice with 1 M NaOH to deprotonate the amines.
^{1}H-NMR: (600 MHz, CD_3OD) δ 7.77 (s, 4H), 7.37 (d, *J* = 15.7 Hz, 2H), 6.54 (d, *J* = 15.7 Hz, 2H), 3.86 (s, 6H), 3.34-3.32 (m, 4H), 2.50-2.42 (m, 8H), 2.27 (s, 6H) 1.79-1.73 (m, 4H), 1.54-1.51 (m, 4H).
^{13}C-NMR: (101 MHz, $CDCl_3$) δ 165.2, 154.9, 137.1, 134.0, 131.8, 123.2, 118.7, 60.9, 57.8, 56.9, 42.1, 39.9, 25.8, 25.3.
HRMS (ESI^+): $C_{32}H_{43}O_4N_4{}^{79}Br_4$ [M^+] requires 863.00123; Found: 863.00265.

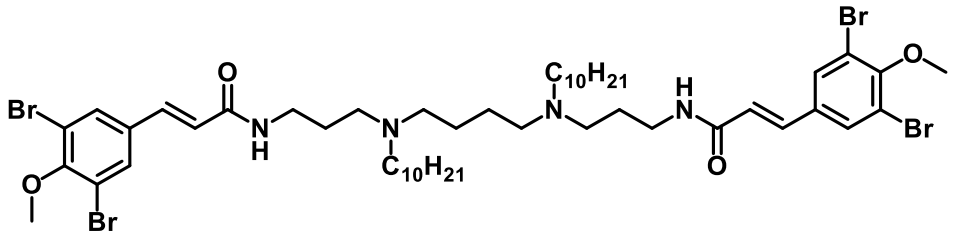

(2E,2'E)-N,N'-((butane-1,4-diylbis(decylazanediyl))bis(propane-3,1-diyl))bis(3-(3,5-dibromo-4-methoxyphenyl)acrylamide) (3.118): In a flame dried flask under argon was dissolved **3.112** (25.0 mg, 29.8 μmol, 1.00 equiv.) and decanal (30 μL, 0.16 mmol, 5.3 equiv.) in methanol (0.6 mL, 0.05 M). Acetic acid (10 μL, 0.17 mmol, 5.90 equiv.) was added, and the reaction was stirred for 30 minutes before sodium cyanoborohydride (12.8 mg, 204 μmol, 6.83 equiv.) was added in two portions, allowing for five minutes between each portion. The reaction was stirred at room temperature for 24 hours, then quenched with 1 M sodium hydroxide. The aqueous layer was extracted thrice with DCM, then the combined organic phases were dried over sodium sulfate, filtered, concentrated under reduced pressure, and purified via flash column chromatography (silica gel, 5% methanol with 10% ammonium hydroxide in DCM) to yield **3.118** (23.1 mg, 20.6 μmol, 69% yield) as a white solid. After the column, the purified solid was dissolved in DCM and washed twice with 1 M NaOH to deprotonate the amines.
^{1}H-NMR: (400 MHz, $CDCl_3$) δ 7.73-7.69 (m, 2H), 7.58 (s, 4H), 7.40 (d, *J* = 15.6 Hz, 2H), 6.29 (d, *J* = 15.6 Hz, 2H), 3.88 (s, 6H), 3.47-3.41 (m, 4H), 2.53-2.36 (m, 8H), 1.70-1.63 (m, 4H), 1.49-1.40 (m, 8H) 1.30-1.17 (m, 30H), 0.85 (t, *J* = 6.7 Hz, 6H).
^{13}C-NMR: (101 MHz, $CDCl_3$) δ 165.0, 154.9, 137.0, 133.9, 131.7, 123.2, 118.7, 60.9, 54.5, 54.2, 53.9, 40.3, 32.0, 29.8, 29.7, 29.4, 27.8, 27.4, 25.9, 22.8, 14.2.
HRMS (ESI^+): $C_{50}H_{79}O_4N_4{}^{79}Br_4$ [M^+] requires 1115.28293; Found: 1115.2847.

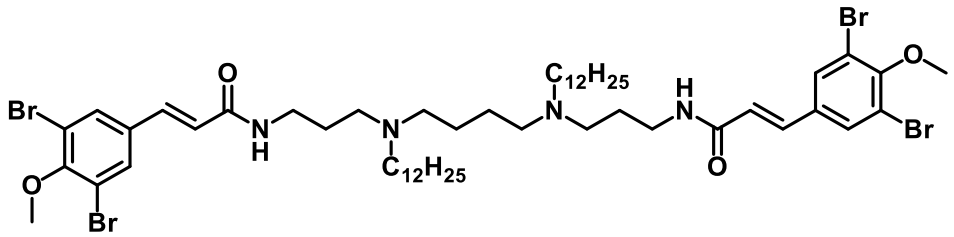

(2E,2'E)-N,N'-((butane-1,4-diylbis(dodecylazanediyl))bis(propane-3,1-diyl))bis(3-(3,5-dibromo-4-methoxyphenyl)acrylamide) (3.119): In a flame dried flask under argon was

dissolved **3.112** (48.6 mg, 58.0 μmol, 1.00 equiv.) and dodecanal (60 μL, 0.27 mmol, 4.70 equiv.) in methanol (0.6 mL, 0.10 M). Acetic acid (18 μL, 0.31 mmol, 5.42 equiv.) was added, and the reaction was stirred for 30 minutes before sodium cyanoborohydride (14.6 mg, 232 μmol, 4.00 equiv.) was added in two portions, allowing for five minutes between each portion. The reaction was stirred at room temperature for 24 hours, then quenched with 1 M sodium hydroxide. The aqueous layer was extracted thrice with DCM, then the combined organic phases were dried over sodium sulfate, filtered, concentrated under reduced pressure, and purified via flash column chromatography (silica gel, 5% methanol with 10% ammonium hydroxide in DCM) to yield **3.119** (54.3 mg, 46.2 μmol, 80% yield) as a white solid. After the column, the purified solid was dissolved in DCM and washed twice with 1 M NaOH to deprotonate the amines.

^{1}H-NMR: (600 MHz, $CDCl_3$) δ 7.78-7.74 (m, 2H), 7.57 (s, 4H), 7.39 (d, *J* = 15.5 Hz, 2H), 6.33 (d, *J* = 15.6 Hz, 2H), 3.87 (s, 6H), 3.45-3.41 (m, 4H), 2.56-2.52 (m, 4H), 2.47-2.39 (m, 8H), 1.72-1.66 (m, 4H), 1.50-1.40 (m, 8H) 1.29-1.17 (m, 36H), 0.85 (t, *J* = 6.9 Hz, 6H).

^{13}C-NMR: (101 MHz, $CDCl_3$) δ 165.0, 154.9, 136.9, 133.9, 131.7, 123.2, 118.7, 60.9, 60.5, 54.5, 54.2, 53.8, 40.2, 32.0, 29.81, 29.77, 29.75, 29.5, 27.8, 27.3, 25.9, 22.8, 21.1, 14.3, 14.2.

HRMS (ESI^+): $C_{54}H_{87}O_4N_4{}^{79}Br_4$ [M^+] requires 1171.34553; Found: 1171.34688.

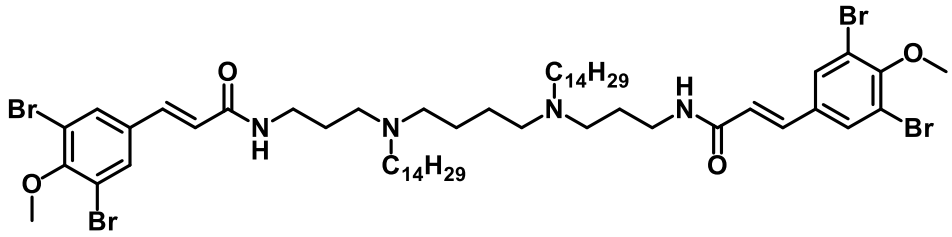

(2E,2'E)-N,N'-((butane-1,4-diylbis(tetradecylazanediyl))bis(propane-3,1-diyl))bis(3-(3,5-dibromo-4-methoxyphenyl)acrylamide) (3.120): In a flame dried flask under argon was dissolved **3.112** (50.6 mg, 60.4 μmol, 1.00 equiv.) and tetradecanal (55.5 mg, 261 μmol, 4.33 equiv.) in methanol (0.6 mL, 0.10 M) and THF (0.6 mL, 0.10 M). Acetic acid (18 μL, 0.31 mmol, 5.21 equiv.) was added, and the reaction was stirred for 30 minutes before sodium cyanoborohydride (15.2 mg, 241 μmol, 4.00 equiv.) was added in two portions, allowing for five minutes between each portion. The reaction was stirred at room temperature for 24 hours, then quenched with 1 M sodium hydroxide. The aqueous layer was extracted thrice with DCM, then the combined organic phases were dried over sodium sulfate, filtered, concentrated under reduced pressure, and purified via flash column chromatography (silica gel, 5% methanol with 10% ammonium hydroxide in DCM) to yield **3.120** (55.2 mg, 44.8 μmol, 74% yield) as a white solid. After the column, the purified solid was dissolved in DCM and washed twice with 1 M NaOH to deprotonate the amines.

^{1}H-NMR: (400 MHz, $CDCl_3$) δ 7.74-7.69 (m, 2H), 7.57 (s, 4H), 7.39 (d, *J* = 15.6 Hz, 2H), 6.29 (d, *J* = 15.6 Hz, 2H), 3.87 (s, 6H), 3.46-3.40 (m, 4H), 2.53-2.48 (m, 4H), 2.44-2.35 (m, 8H), 1.70-1.62 (m, 4H), 1.49-1.39 (m, 8H) 1.28-1.18 (m, 44H), 0.85 (t, *J* = 6.7 Hz, 6H).

^{13}C-NMR: (101 MHz, $CDCl_3$) δ 165.0, 154.9, 136.9, 133.9, 131.7, 123.2, 118.7, 60.9, 54.5, 54.2, 53.8, 40.2, 32.0, 29.81, 29.78, 29.5, 27.8, 27.3, 25.9, 22.8, 21.1, 14.2.

HRMS (ESI^+): $C_{58}H_{95}O_4N_4{}^{79}Br_4$ [M^+] requires 1227.40813; Found: 1227.41058.

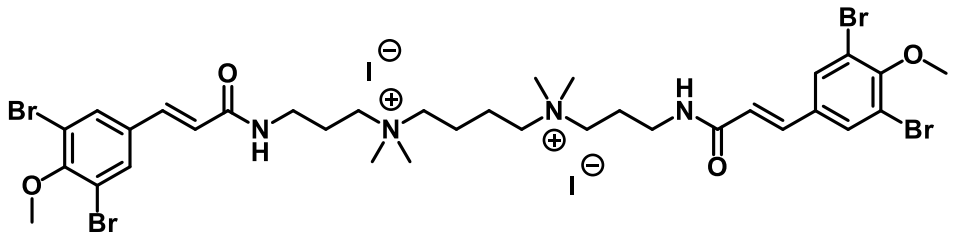

N1,N4-bis(3-((E)-3-(3,5-dibromo-4-methoxyphenyl)acrylamido)propyl)-N1,N1,N4,N4-tetramethylbutane-1,4-diaminium iodide (3.121): In a flame dried vial under argon was dissolved **3.117** (31.9 mg, 36.8 μmol, 1.00 equiv.) in methyl iodide (1.0 mL, 37 mM). The bright yellow solution slowly turned cloudy over 15 minutes. Reaction stirred at ambient temperature for 24 hours, then quenched via evaporation in the hood at atmospheric pressure. The crude solid was purified via trituration with hot ethyl acetate to yield **3.121** (9.4 mg, 8.2 μmol, 22% yield) as a white solid.

^{1}H-NMR: (400 MHz, $CDCl_3$) δ 7.81 (s, 4H), 7.41 (d, *J* = 15.8 Hz, 2H), 6.66 (d, *J* = 15.8 Hz, 2H), 3.87 (s, 6H), 3.54-3.40 (m, 12H), 3.16 (s, 12H), 2.15-2.06 (m, 4H), 1.95-1.88 (m, 4H).

^{13}C-NMR: (101 MHz, $CDCl_3$) δ 166.3, 155.1, 137.4, 133.9, 132.0, 123.1, 118.8, 60.9, 32.0, 29.5, 29.4, 29.2, 22.8, 14.3.

HRMS (ESI^+): $C_{34}H_{48}O_4N_4{}^{79}Br_4{}^{127}I$ [M^+] requires 1018.94483; Found: 1018.9446.
$C_{34}H_{48}O_4N_4{}^{79}Br_4$ [M^{2+}] requires 446.00372; Found: 446.00343.

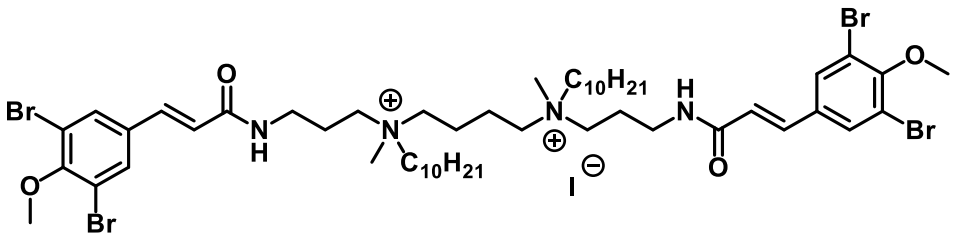

N1,N4-didecyl-N1,N4-bis(3-((E)-3-(3,5-dibromo-4-methoxyphenyl)acrylamido)propyl)-N1,N4-dimethylbutane-1,4-diaminium iodide (3.122): In a flame dried vial under argon was dissolved **3.117** (23.1 mg, 20.6 μmol, 1.00 equiv.) in methyl iodide (1.0 mL, 37 mM). The bright yellow solution slowly turned cloudy over 15 minutes. Reaction stirred at ambient temperature for 24 hours, then quenched via evaporation in the hood at atmospheric pressure. The crude solid was purified via trituration with hot ethyl acetate to yield **3.122** (4.1 mg, 20.6 μmol, 14% yield) as a white solid.

^{1}H-NMR: (400 MHz, $CDCl_3$) δ 7.89-7.84 (m,2H), 7.70 (s, 4H), 7.47 (d, *J* = 15.8 Hz, 2H), 6.73 (d, *J* = 15.7 Hz, 2H), 3.88 (s, 6H), 3.64-3.46 (m, 12H), 3.35-3.27 (m, 4H), 3.10 (s, 3H), 3.09 (s, 3H), 2.31-2.19 (m, 2H), 2.11-1.96 (m, 8H), 1.84-1.73 (m, 2H), 1.71-1.60 (m, 8H), 1.36-1.21 (m, 30H), 0.88 (t, *J* = 6.6, 6H).

^{13}C-NMR: (101 MHz, $CDCl_3$) δ 166.3, 155.1, 137.4, 133.9, 132.0, 123.1, 118.8, 64.2, 61.0, 60.9, 60.5, 59.1, 49.7, 35.7, 32.0, 29.6, 29.5, 29.4, 29.2, 26.5, 23.20, 23.16, 22.8, 22.7, 21.2, 19.6, 18.8, 14.34, 14.26.

HRMS (ESI^+): $C_{52}H_{84}O_4N_4{}^{79}Br_4{}^{127}I$ [M^+] requires 1271.22653; Found: 1271.22671.
$C_{34}H_{48}O_4N_4{}^{79}Br_4$ [M^{2+}] requires 572.16076; Found: 572.16037.

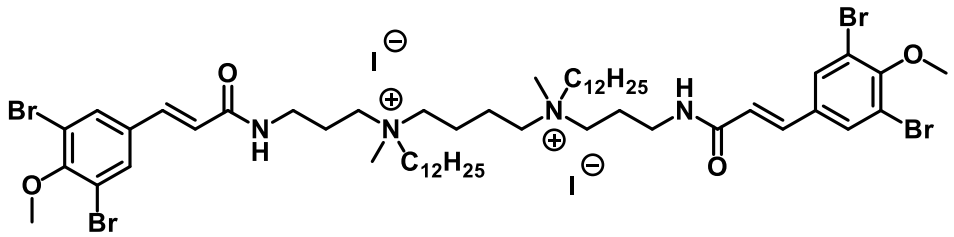

N1,N4-bis(3-((E)-3-(3,5-dibromo-4-methoxyphenyl)acrylamido)propyl)-N1,N4-didodecyl-N1,N4-dimethylbutane-1,4-diaminium iodide (3.123): In a flame dried vial under argon was dissolved **3.117** (50.9 mg, 43.3 μmol, 1.00 equiv.) in methyl iodide (2.0 mL, 22 mM). The bright yellow solution slowly turned cloudy over 15 minutes. Reaction stirred at ambient temperature for 24 hours, then quenched via evaporation in the hood at atmospheric pressure. The crude solid was purified via trituration with hot ethyl acetate to yield **3.123** (34.0 mg, 23.3 μmol, 54% yield) as a white solid.

^{1}H-NMR: (400 MHz, $CDCl_3$) δ 7.89-7.84 (m,2H), 7.67 (s, 4H), 7.43 (d, *J* = 15.6 Hz, 2H), 6.74 (d, *J* = 15.7 Hz, 2H), 3.86 (s, 6H), 3.78-3.63 (m, 2H), 3.58-3.49 (m, 4H), 3.41-3.32 (m, 4H), 3.24-3.07 (M, 10H), 2.28-1.97 (m, 10H), 1.80-1.61 (m, 4H), 1.71-1.60 (m, 8H), 1.34-1.17 (m, 36H), 0.86 (t, *J* = 6.6, 6H).

^{13}C-NMR: (101 MHz, $CDCl_3$) δ 166.2, 155.0, 137.3, 1333.8, 132.0, 123.1, 118.8, 63.9, 61.1, 60.9, 59.5, 59.4, 49.6, 35.9, 32.0, 29.69, 29.54, 29.50, 29.42, 29.24, 26.5, 23.1, 22.8, 22.7, 19.7, 19.6, 14.2.

HRMS (ESI^+): $C_{56}H_{92}O_4N_4{}^{79}Br_4{}^{127}I$ [M^+] requires 1327.289; Found: 1327.288.
$C_{34}H_{48}O_4N_4{}^{79}Br_4$ [M^{2+}] requires 600.19206; Found: 600.19162.

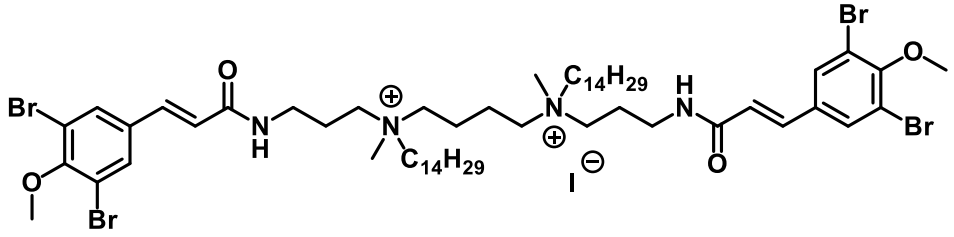

N1,N4-bis(3-((E)-3-(3,5-dibromo-4-methoxyphenyl)acrylamido)propyl)-N1,N4-dimethyl-N1,N4-ditetradecylbutane-1,4-diaminium iodide (3.124): In a flame dried vial under argon was dissolved **3.117** (52.8 mg, 42.9 μmol, 1.00 equiv.) in methyl iodide (2.0 mL, 21 mM). The bright yellow solution slowly turned cloudy over 15 minutes. Reaction stirred at ambient temperature for 24 hours, then quenched via evaporation in the hood at atmospheric pressure. The crude solid was purified via trituration with hot ethyl acetate to yield **3.124** (14.7 mg, 9.70 μmol, 23% yield) as a white solid.

^{1}H-NMR: (400 MHz, $CDCl_3$) δ 7.90-7.86 (m,2H), 7.70 (s, 4H), 7.47 (d, *J* = 15.7 Hz, 2H), 6.73 (d, *J* = 15.7 Hz, 2H), 3.88 (s, 6H), 3.81-3.48 (m, 6H), 3.43-3.24 (m, 6H), 3.11-3.08 (m, 6H), 2.33-1.92 (m, 8H), 1.84-1.61 (M, 6H), 1.37-1.18 (m, 42 H), 0.87 (t, *J* = 6.6 Hz, 6H).

^{13}C-NMR: (101 MHz, $CDCl_3$) δ 166.2, 155.1, 137.4, 133.8, 132.0, 123.1, 118.8, 64.1, 61.1, 60.9, 59.2, 49.7, 35.8, 32.0, 29.80, 29.77, 29.72, 29.56, 29.51, 29.48, 29.25, 26.5, 23.1, 22.8, 22.7, 19.6, 14.2.
HRMS (ESI^+): $C_{60}H_{100}O_4N_4{}^{79}Br_4{}^{127}I$ [M^+] requires 1383.35173; Found: 1383.35046.
$C_{34}H_{48}O_4N_4{}^{79}Br_4$ [M^{2+}] requires 628.22336; Found: 628.2229.

5.3 Characterization

5.3.1 Chapter 2

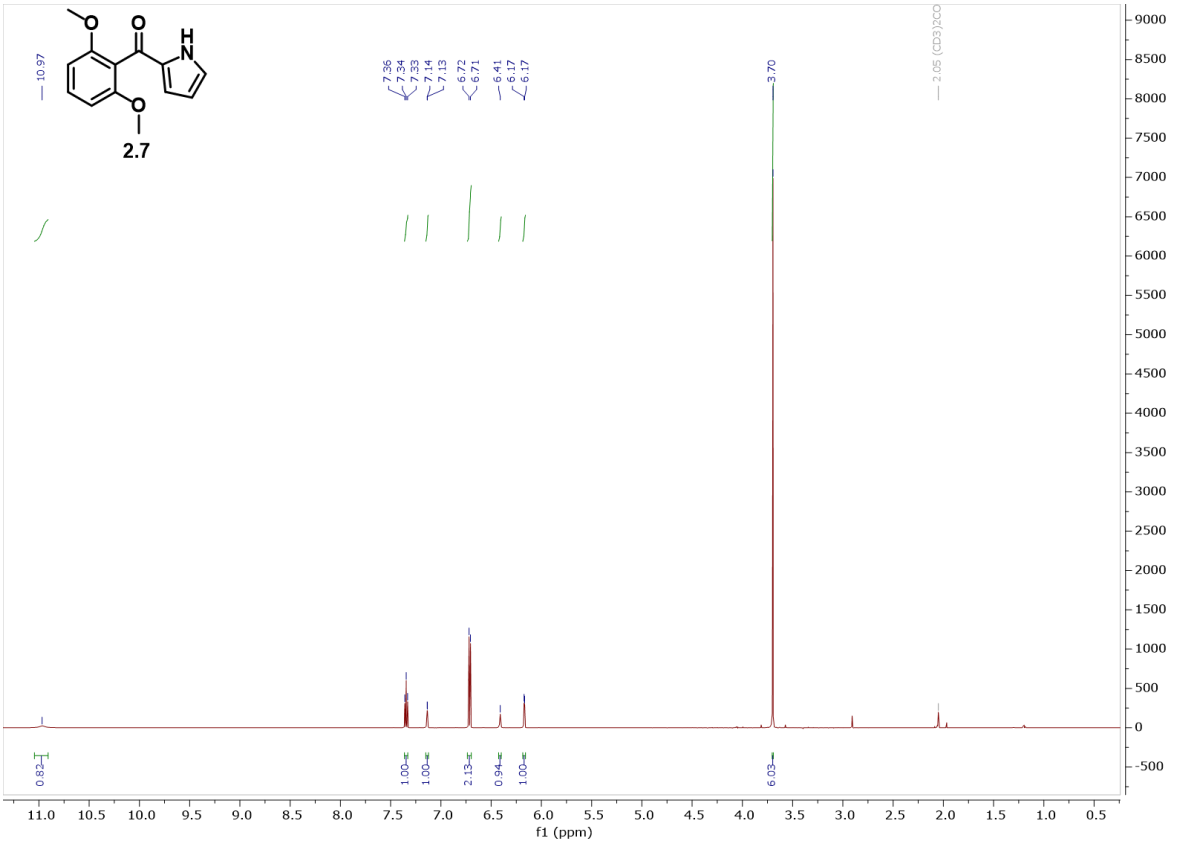
10.97
7.36
7.34
7.33
7.14
7.13
6.72
6.71
6.41
6.17
6.17
3.70
2.05 (CD3)2CO
0.82
1.00
1.00
2.13
0.94
1.00
6.03
f1 (ppm)

2.7

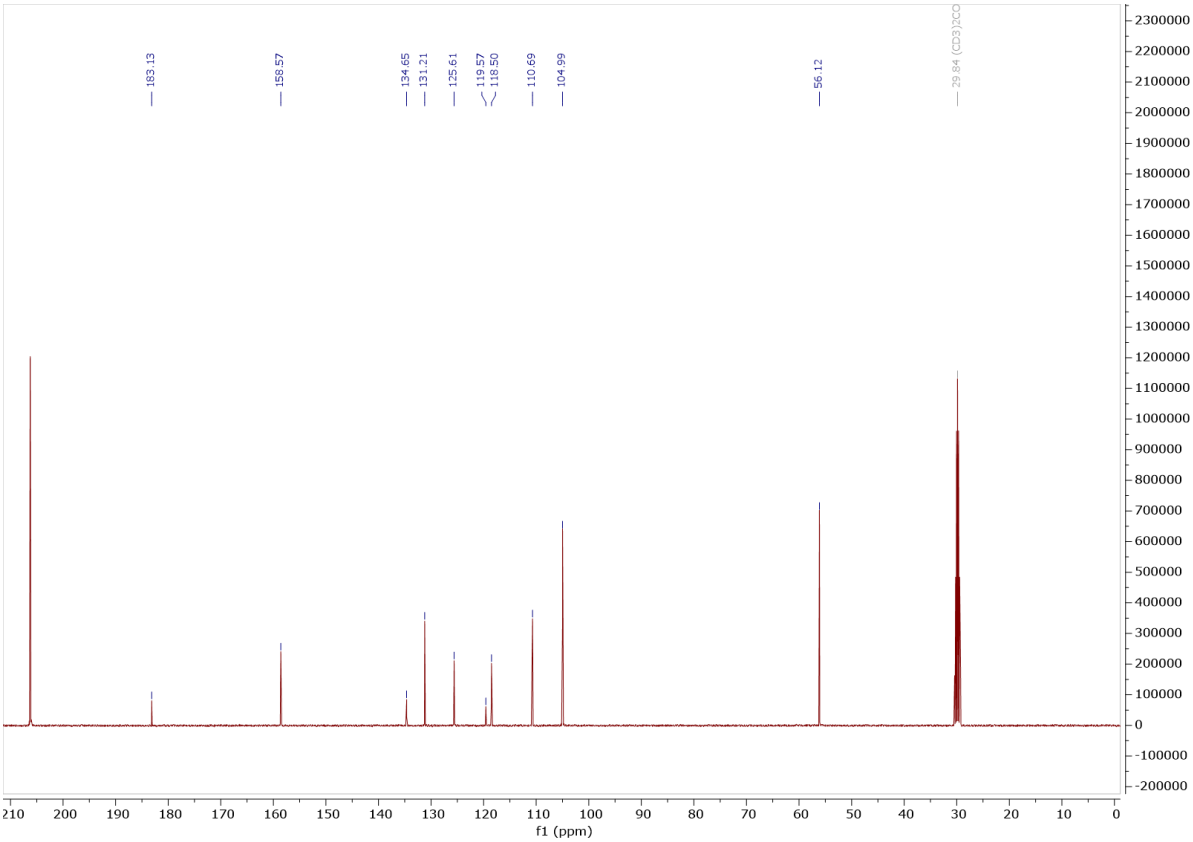
183.13
158.57
134.65
131.21
125.61
119.57
118.50
110.69
104.99
56.12
29.84 (CD3)2CO
f1 (ppm)

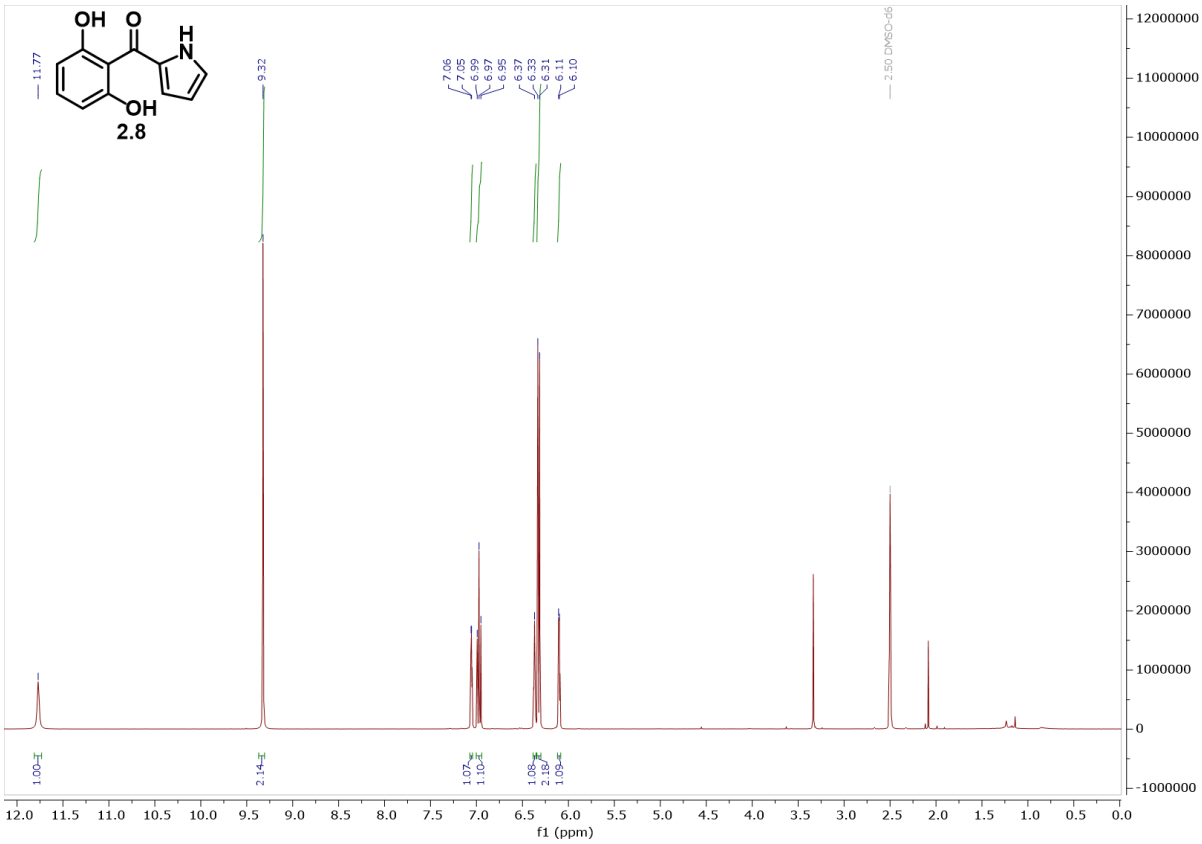
OH
O
H
N
OH
2.8
11.77
9.32
7.06
7.05
6.99
6.97
6.95
6.37
6.33
6.31
6.11
6.10
2.50 DMSO-d6
1.00
2.14
1.07
1.10
1.08
2.18
1.09
f1 (ppm)

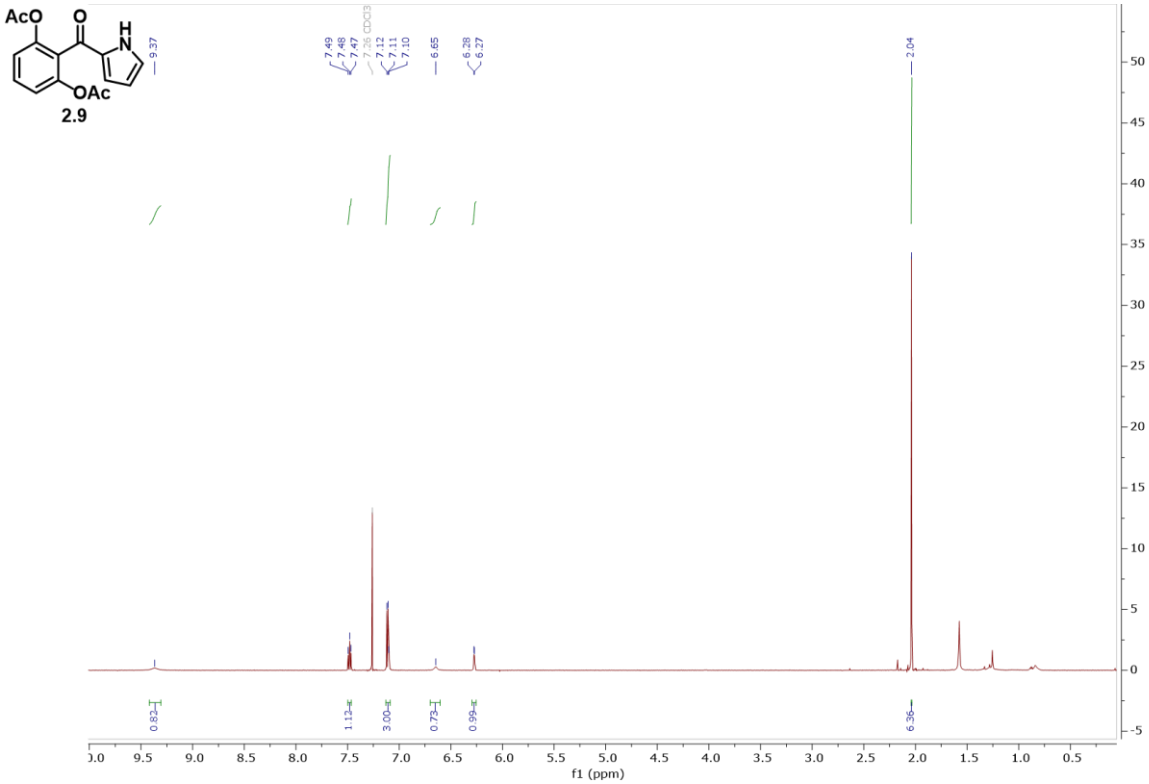
AcO
O
H
N
OAc
2.9
9.37
7.49
7.48
7.47
7.26
CDCl3
7.12
7.11
7.10
6.65
6.28
6.27
2.04
0.82
1.12
3.00
0.73
0.99
6.36
f1 (ppm)

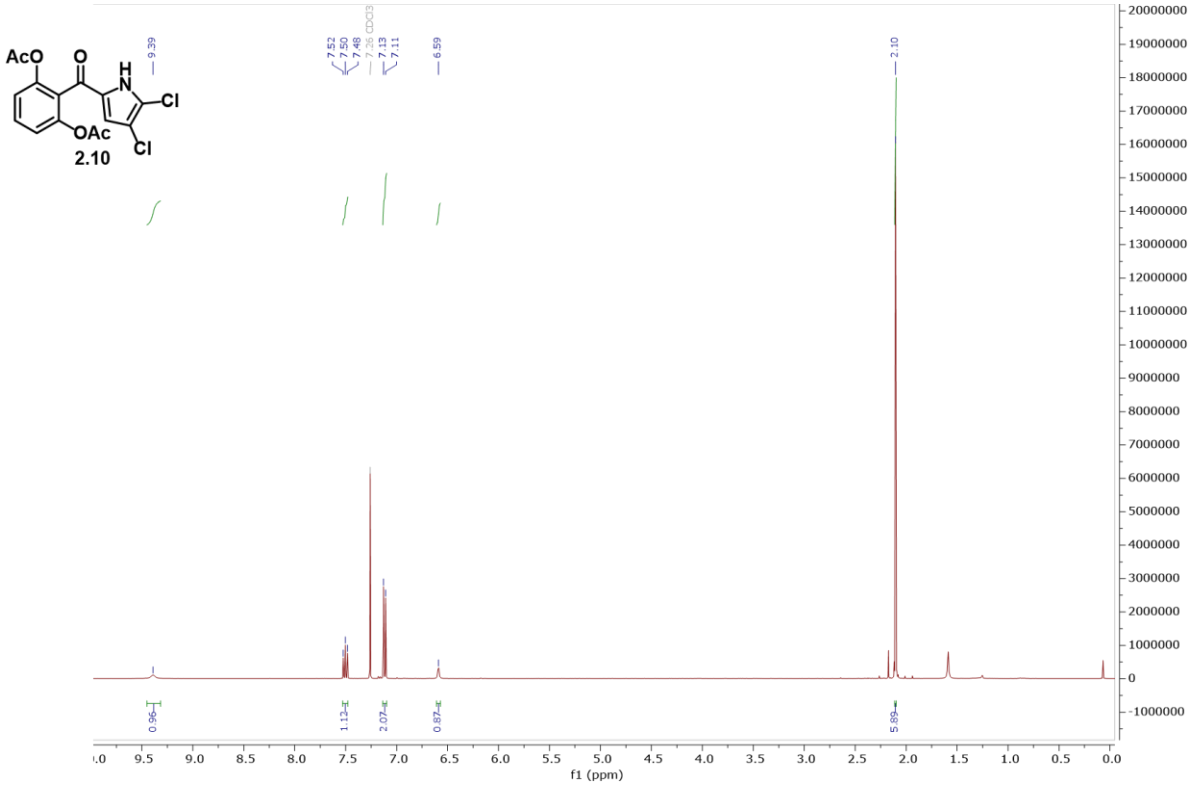
AcO
O
H
N
Cl
OAc
Cl
2.10
9.39
7.52
7.50
7.48
7.35
7.13
7.11
6.59
2.10
CDCl3
0.96
1.12
2.07
0.87
5.89
f1 (ppm)

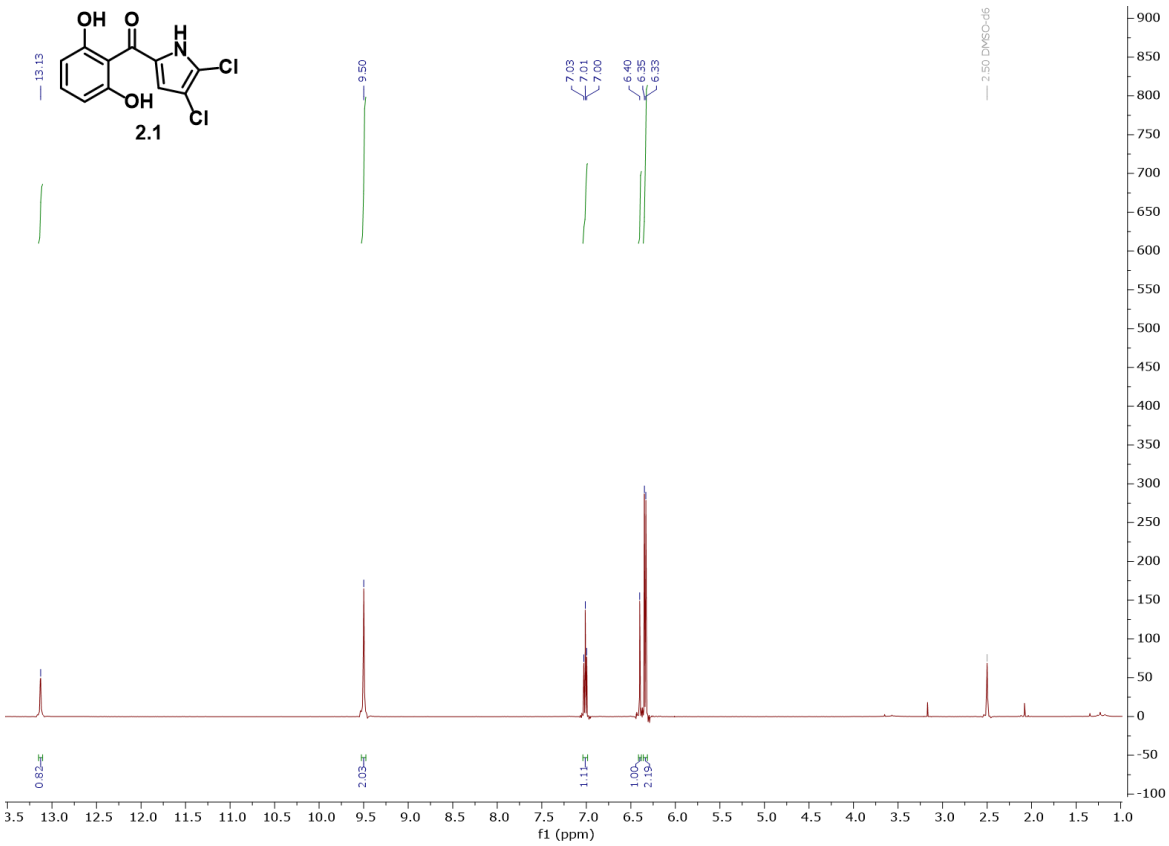
OH
O
H
N
Cl
OH
Cl
2.1
13.13
9.50
7.03
7.01
7.00
6.40
6.35
6.33
2.50 DMSO-d6
0.82
2.03
1.11
1.00
2.19
f1 (ppm)

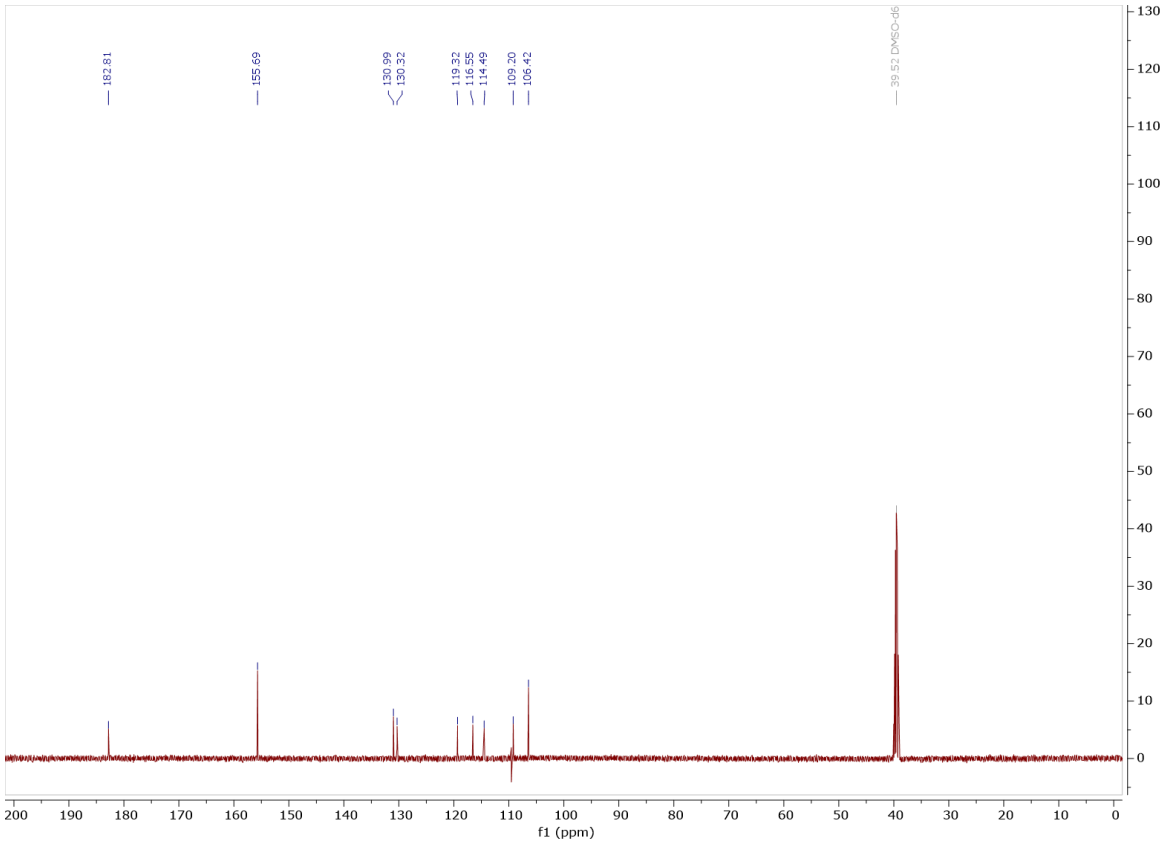
182.81
155.69
130.99
130.32
119.32
116.55
114.49
109.20
106.42
39.52 DMSO-d6
f1 (ppm)

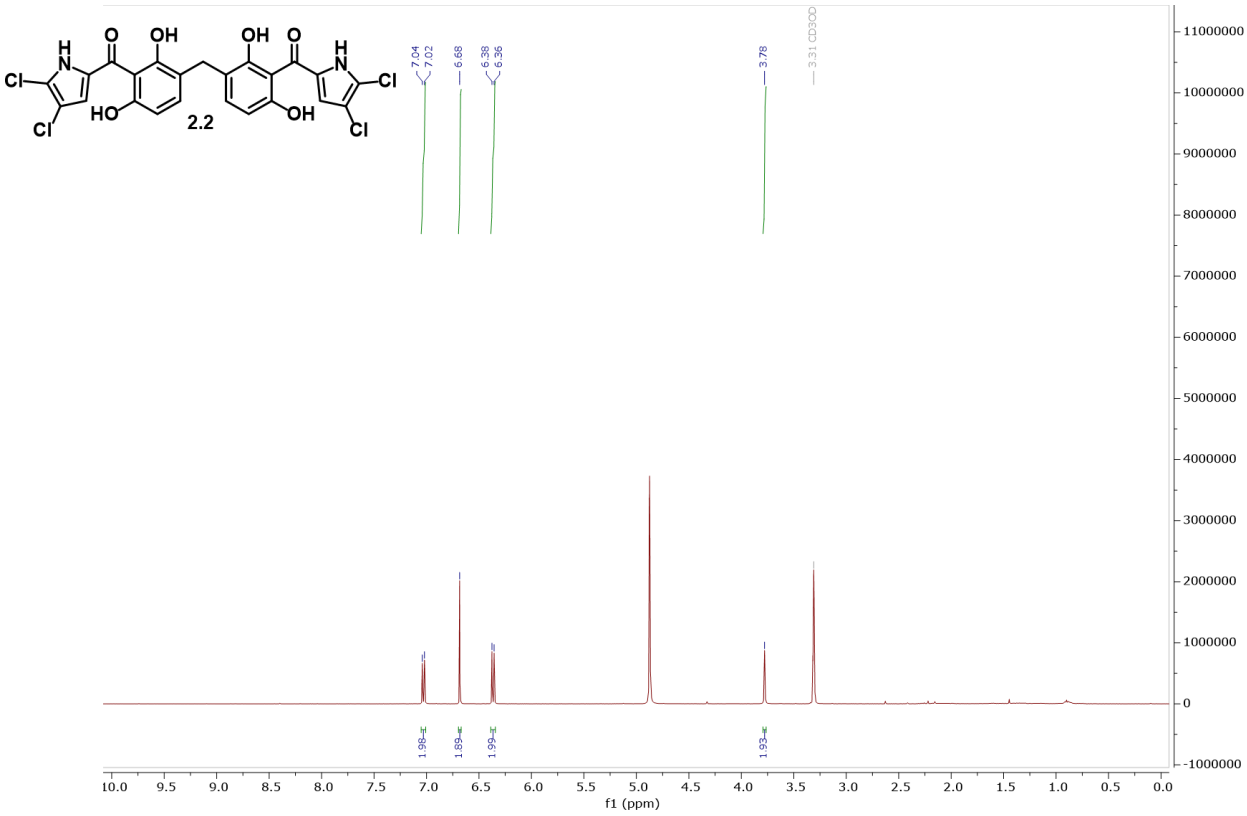
2.2
7.04
7.02
6.68
6.38
6.36
3.78
3.31 CD3OD
1.98
1.89
1.99
1.93
f1 (ppm)

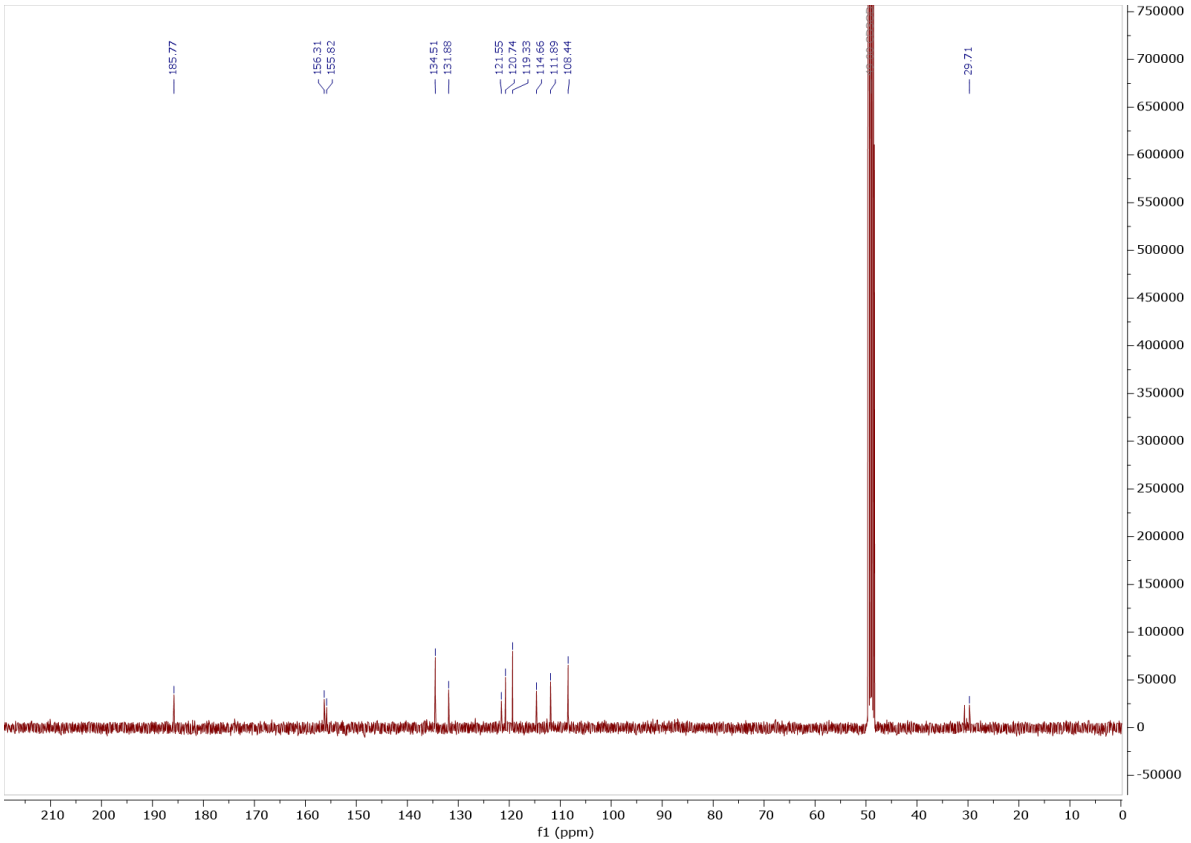
185.77
156.31
155.82
134.51
131.88
121.55
120.74
119.33
114.66
111.89
108.44
29.71
f1 (ppm)

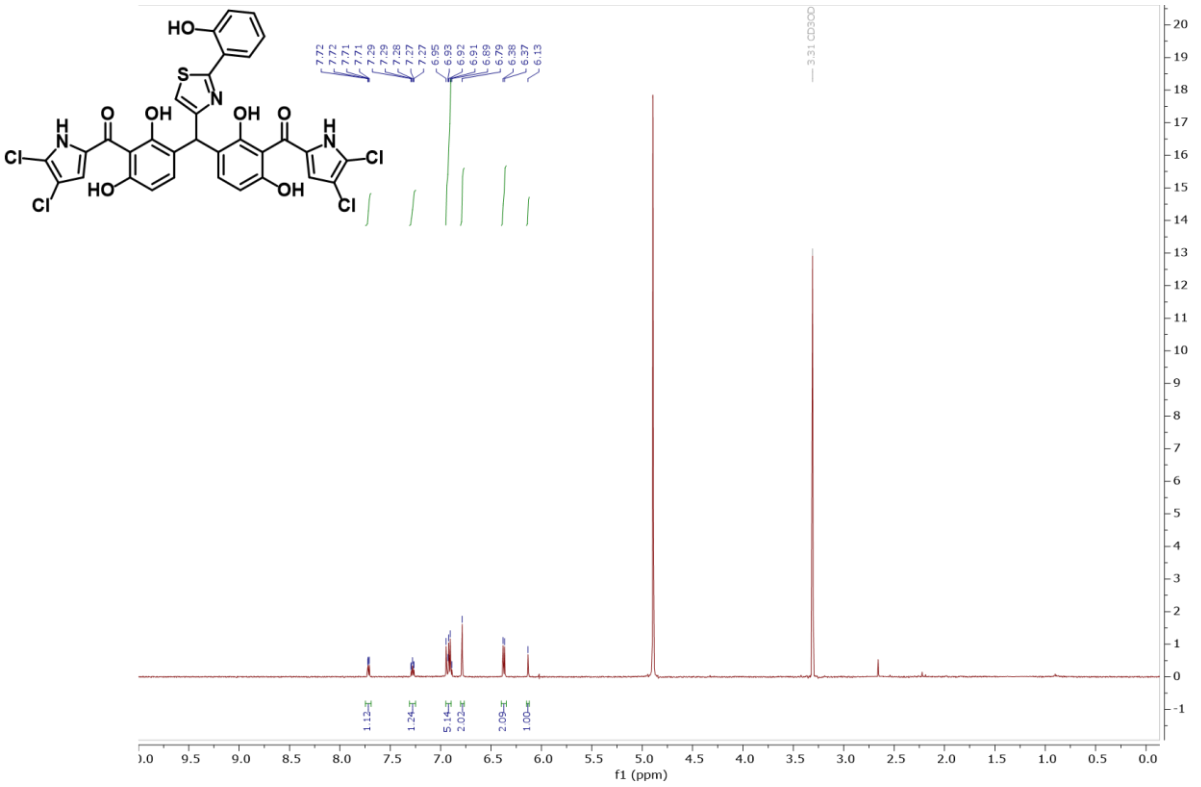
HO
S
N
H
N
O
OH
OH
O
H
N
Cl
Cl
HO
OH
Cl
Cl
7.72
7.72
7.71
7.71
7.29
7.29
7.28
7.27
7.27
6.95
6.93
6.92
6.91
6.89
6.79
6.38
6.37
6.13
3.31
1.13
1.24
5.14
2.03
2.09
1.00
f1 (ppm)

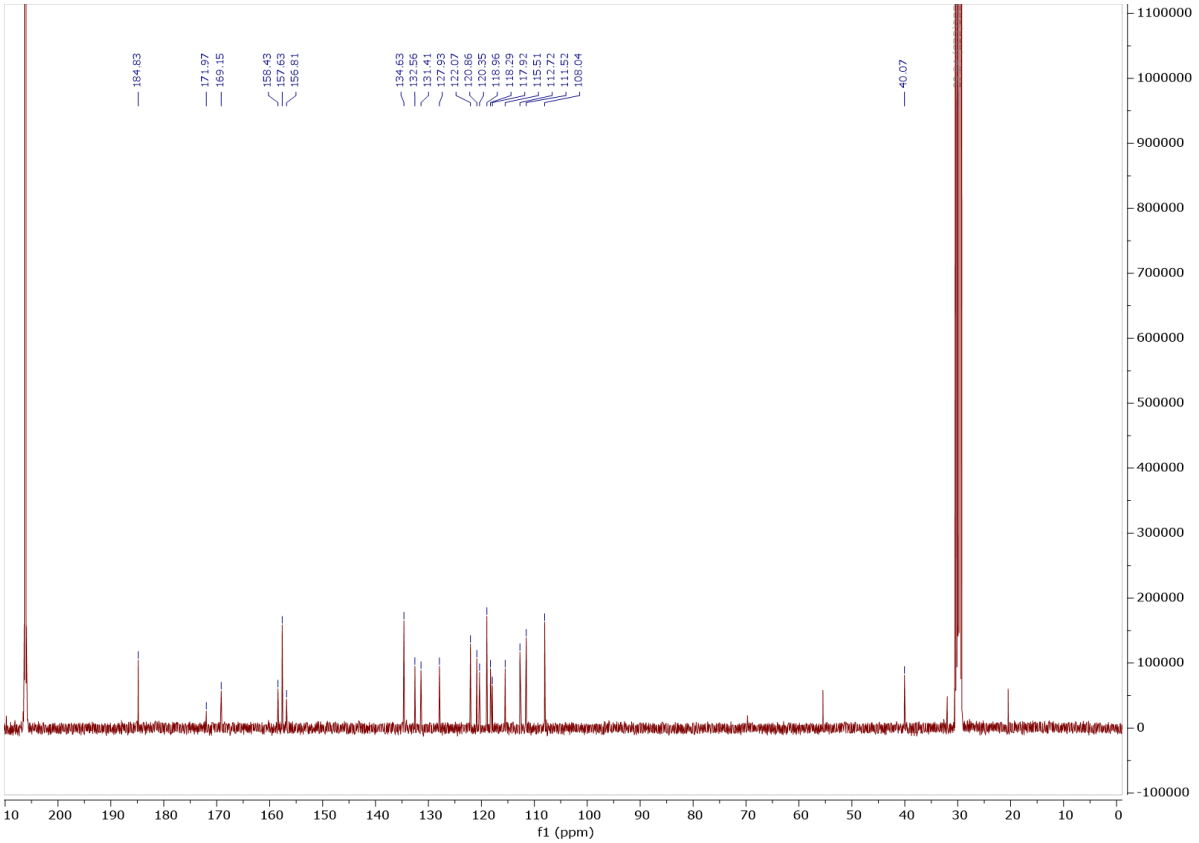
184.83
171.97
169.15
158.43
157.63
156.81
134.63
132.56
131.41
127.93
122.07
120.86
120.35
118.96
118.29
117.92
115.51
112.72
111.52
108.04
40.07
f1 (ppm)

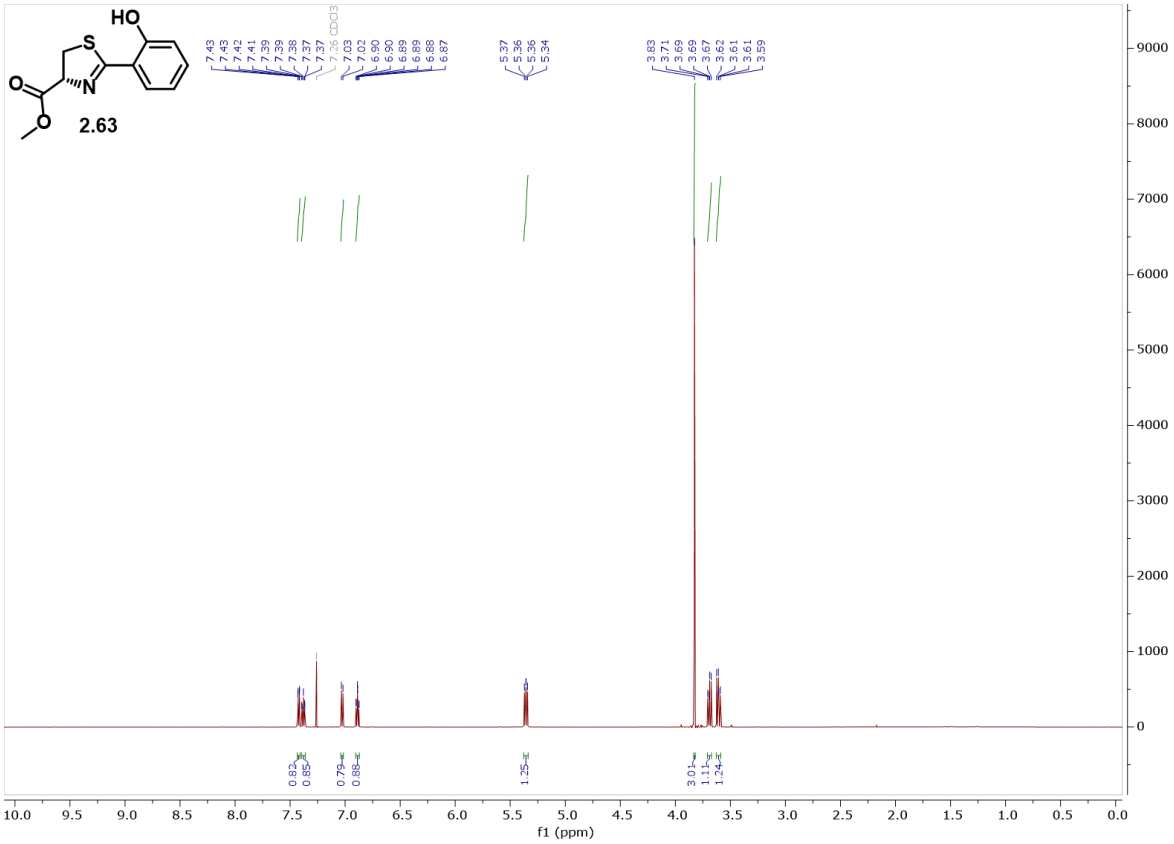
HO
S
N
O
O
2.63
7.43
7.43
7.42
7.41
7.39
7.39
7.38
7.37
7.37
7.26 CDCl3
7.03
7.02
6.90
6.90
6.89
6.89
6.88
6.87
5.37
5.36
5.36
5.34
3.83
3.71
3.69
3.69
3.67
3.62
3.61
3.61
3.59
0.82
0.85
0.79
0.88
1.25
3.01
1.11
1.24
f1 (ppm)

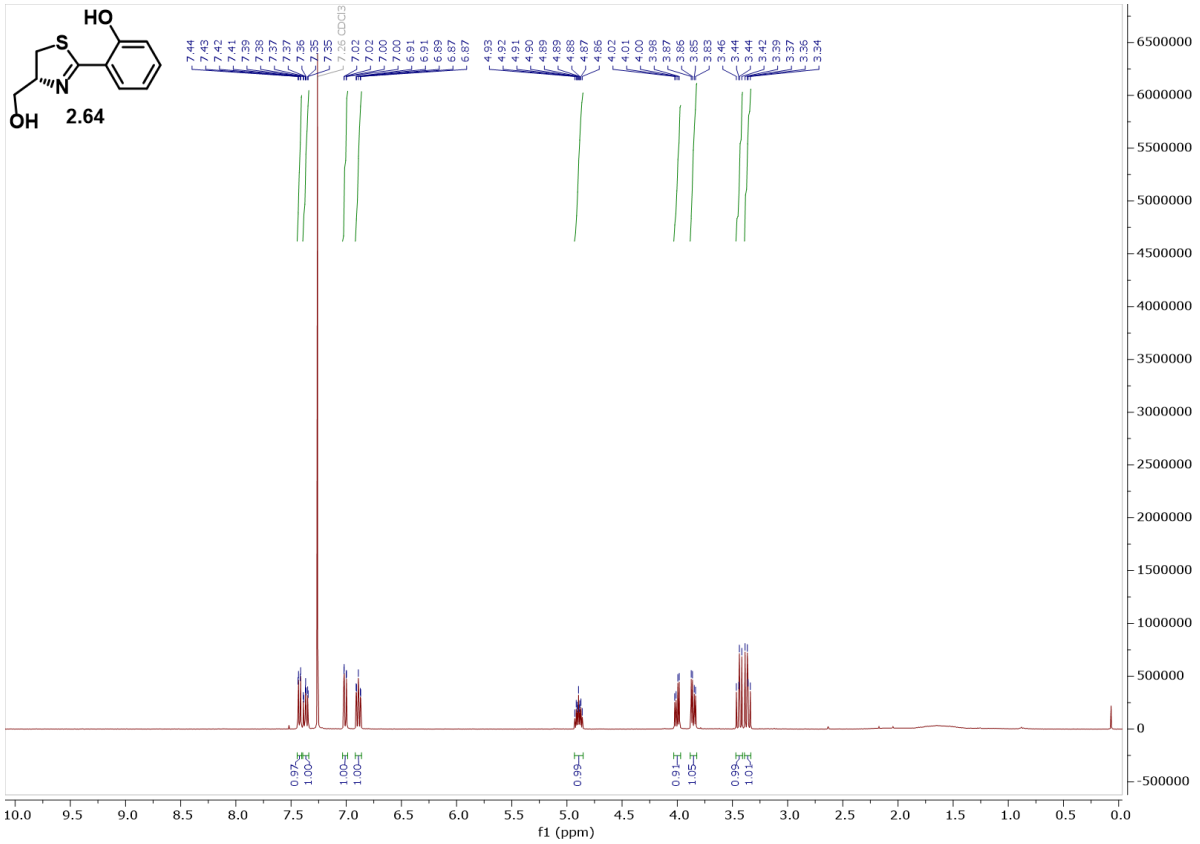
HO
S
N
OH
2.64
7.44
7.43
7.42
7.41
7.39
7.38
7.37
7.37
7.36
7.35
7.35
7.26 CDCl3
7.02
7.02
7.00
7.00
6.91
6.91
6.89
6.87
6.87
4.93
4.92
4.91
4.90
4.89
4.89
4.88
4.87
4.86
4.02
4.01
4.00
3.98
3.87
3.86
3.85
3.83
3.46
3.44
3.44
3.42
3.39
3.37
3.36
3.34
0.97
1.00
1.00
1.00
0.99
0.91
1.05
0.99
1.01
f1 (ppm)

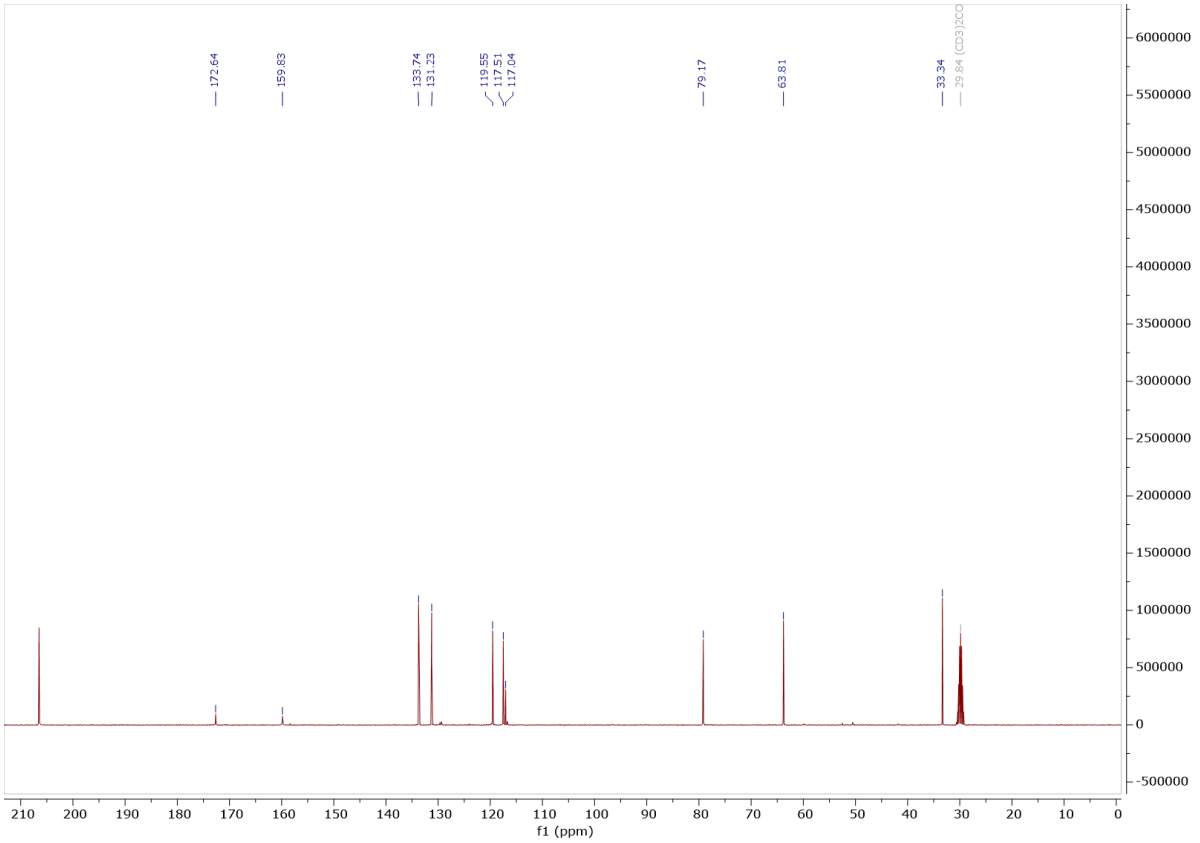
172.64
159.83
133.74
131.23
119.55
117.51
117.04
79.17
63.81
33.34
29.84 (CD3)2CO
f1 (ppm)

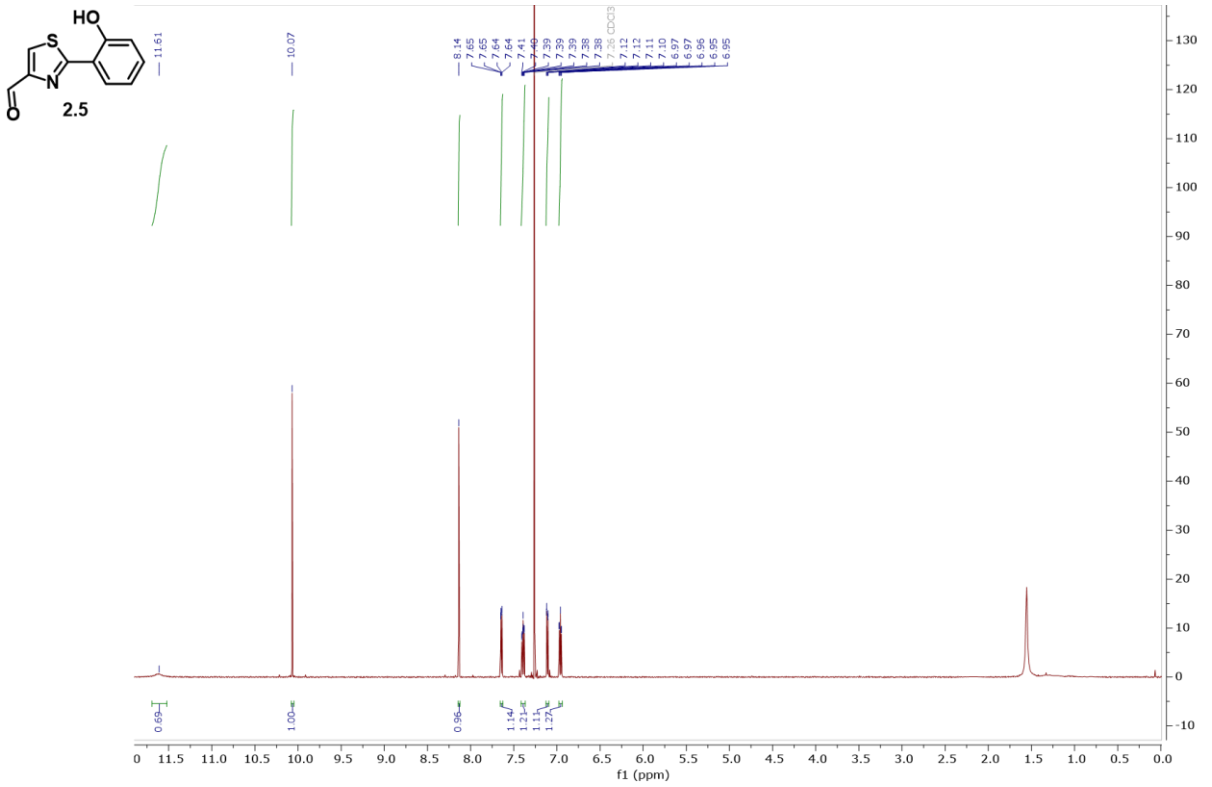
HO
S
N
O
2.5
11.61
10.07
8.14
7.65
7.65
7.64
7.64
7.41
7.40
7.39
7.39
7.39
7.38
7.38
7.26 CDCl3
7.12
7.12
7.11
7.10
6.97
6.97
6.96
6.95
6.95
0.69
1.00
0.96
1.14
1.12
1.11
1.12
1.12
f1 (ppm)

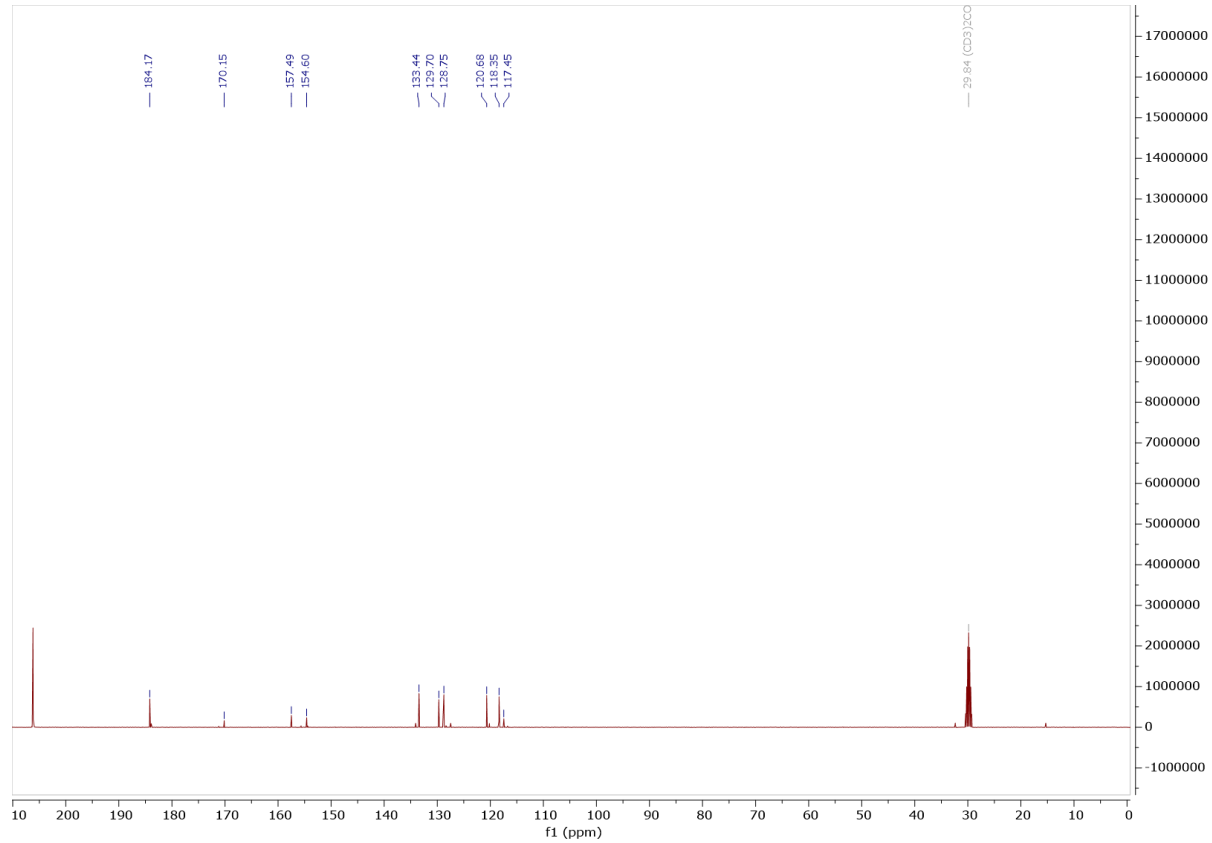
184.17
170.15
157.49
154.60
133.44
129.70
128.75
120.68
118.35
117.45
29.84 (CD3)2CO
f1 (ppm)

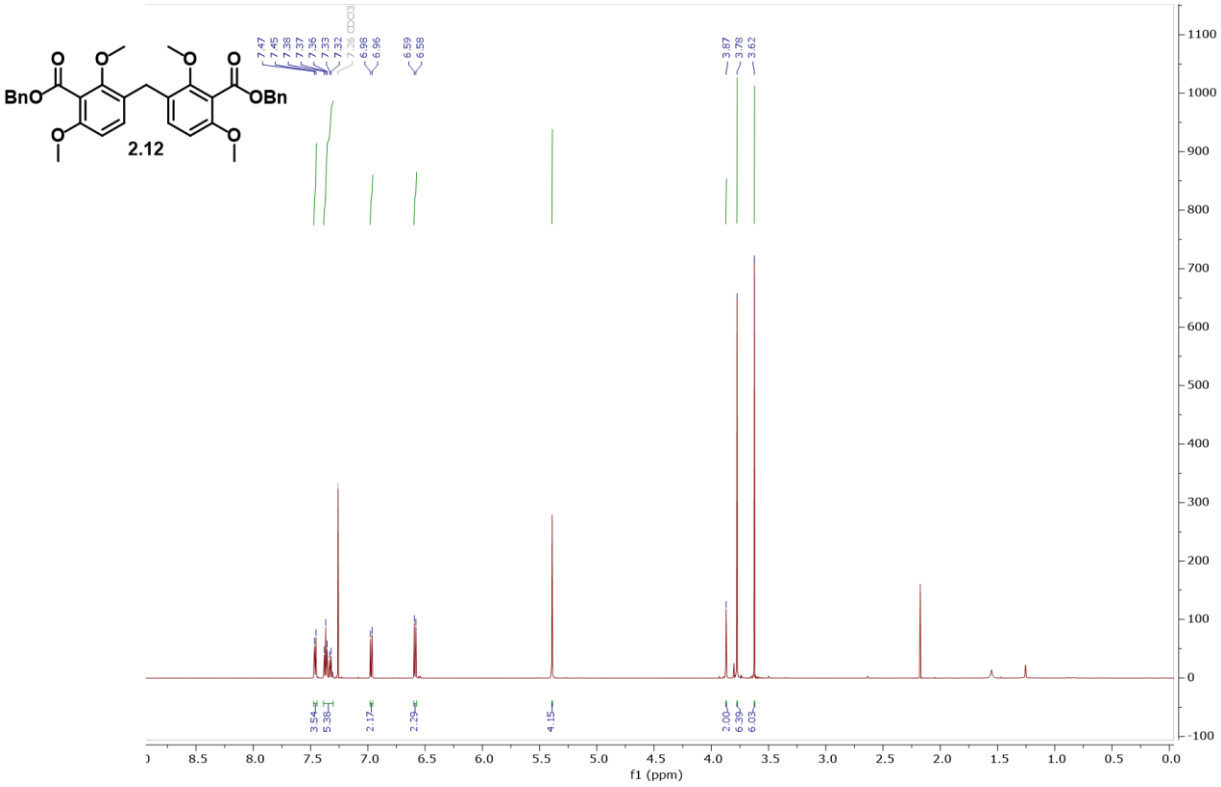
BnO
OBn
2.12
7.47
7.45
7.38
7.37
7.36
7.33
7.32
7.26 CDCl3
6.98
6.96
6.59
6.58
3.87
3.78
3.62
3.54
5.38
2.17
2.29
4.15
2.00
6.39
6.03
f1 (ppm)

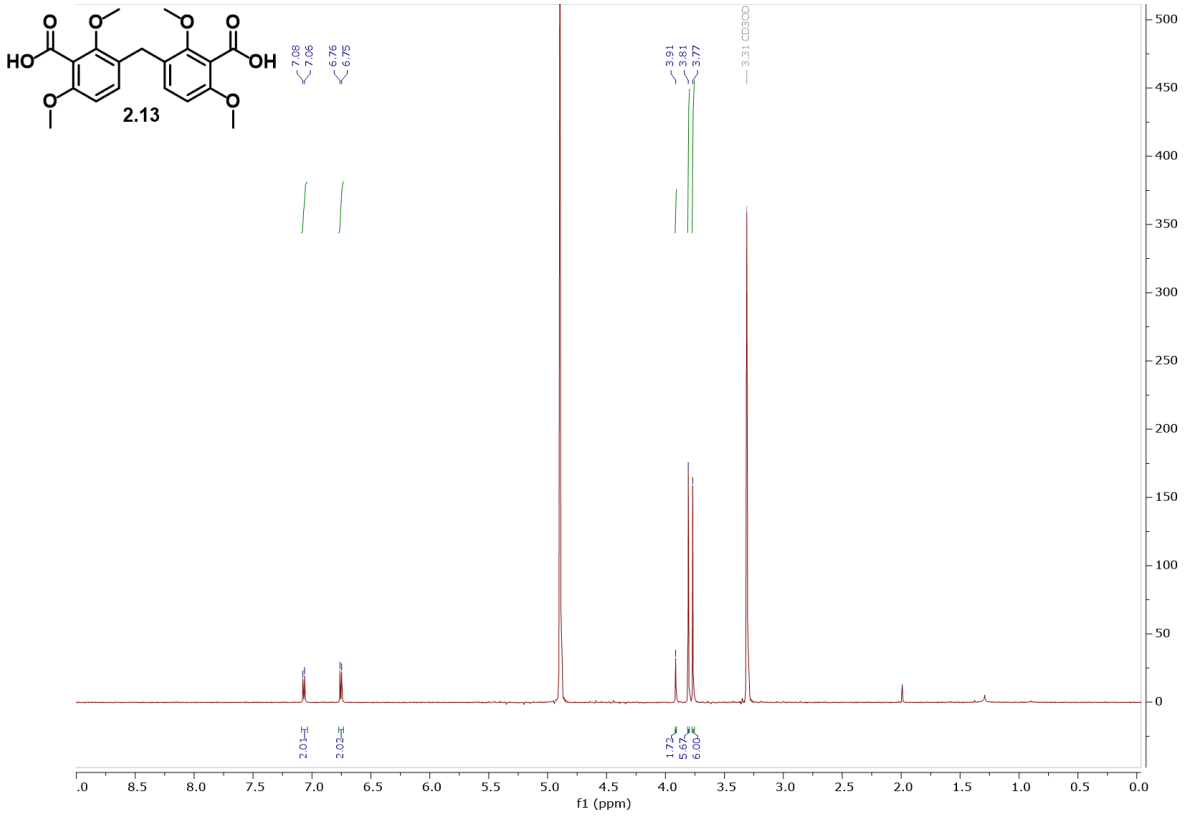
HO
OH
2.13
7.08
7.06
6.76
6.75
3.91
3.81
3.77
3.31 CD3OD
2.01
2.02
1.72
5.67
6.00
f1 (ppm)

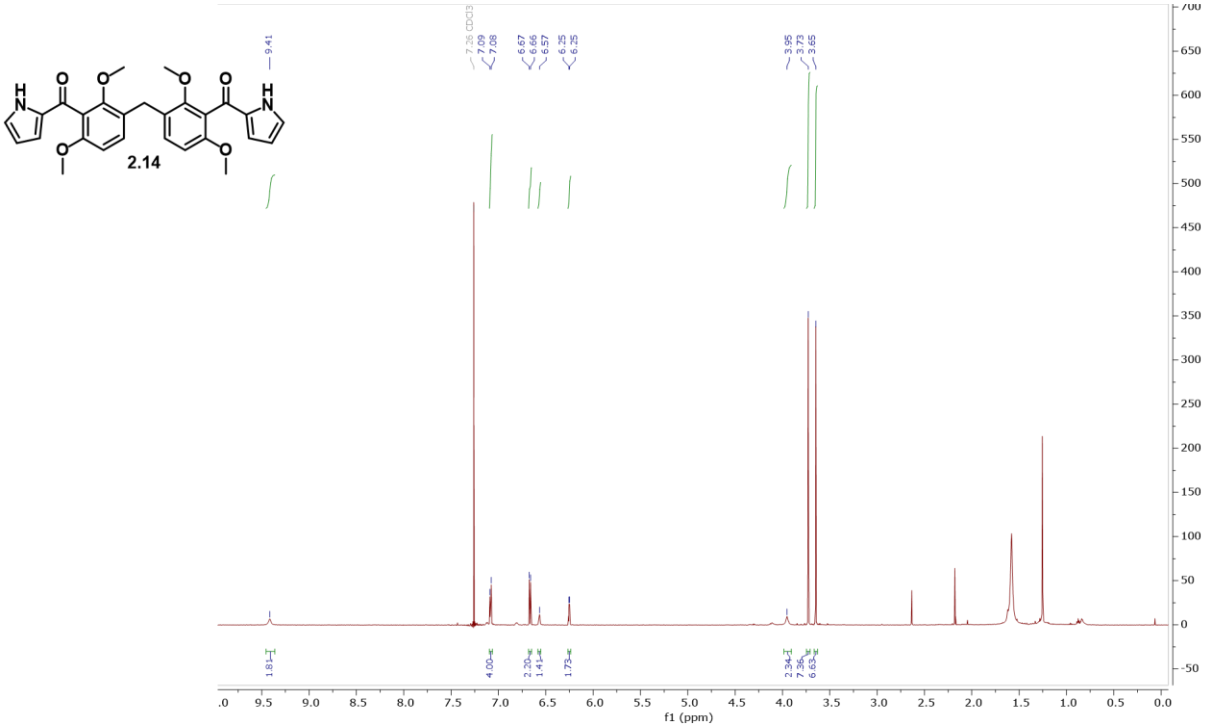
2.14
f1 (ppm)

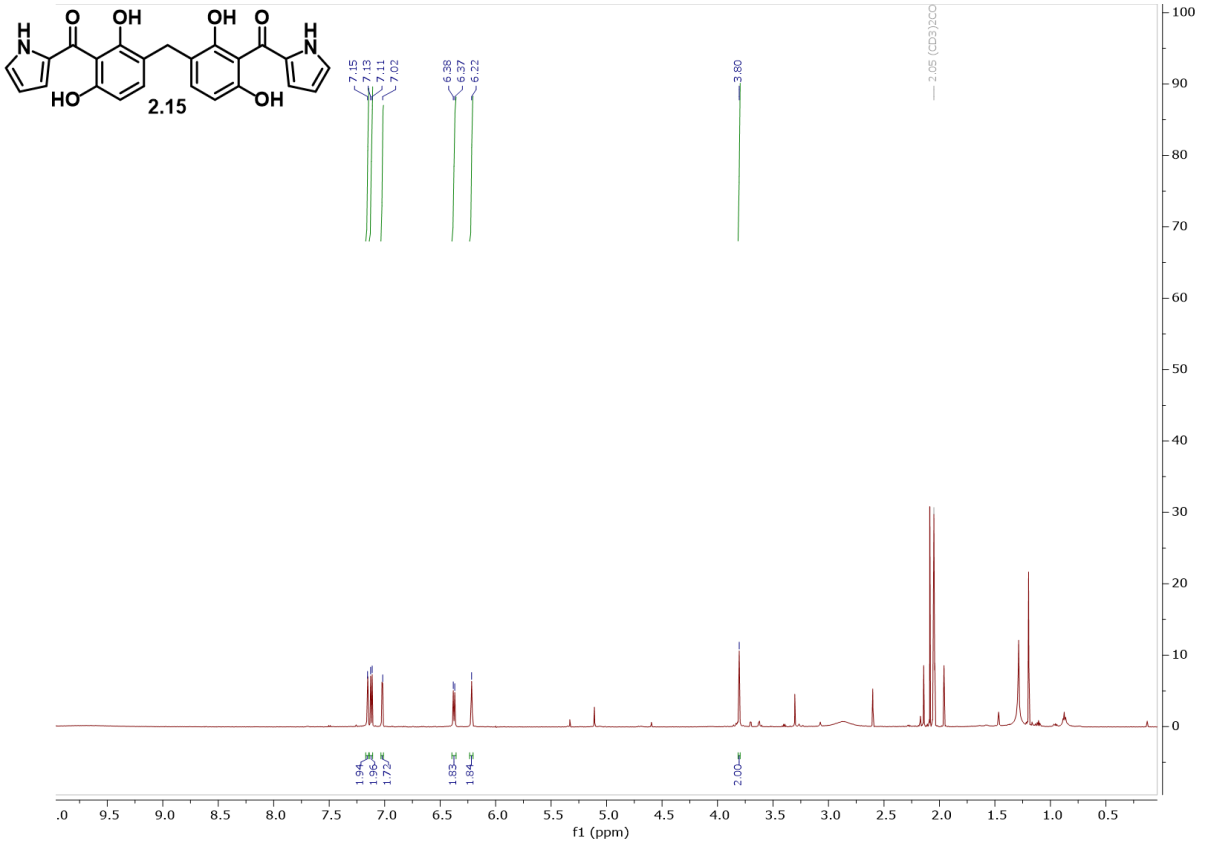
2.15
f1 (ppm)

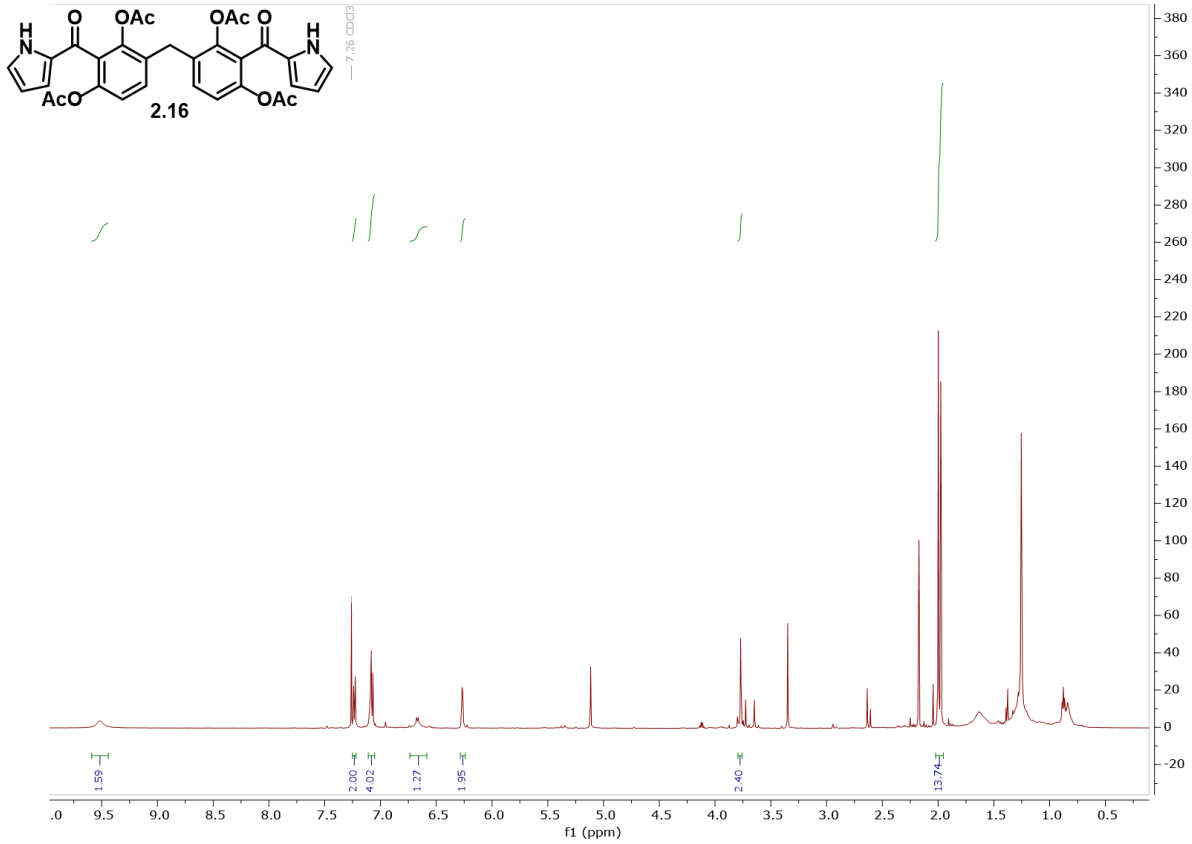
2.16
7.26 CDCl3
1.59
2.00
4.02
1.27
1.95
2.40
13.74
f1 (ppm)

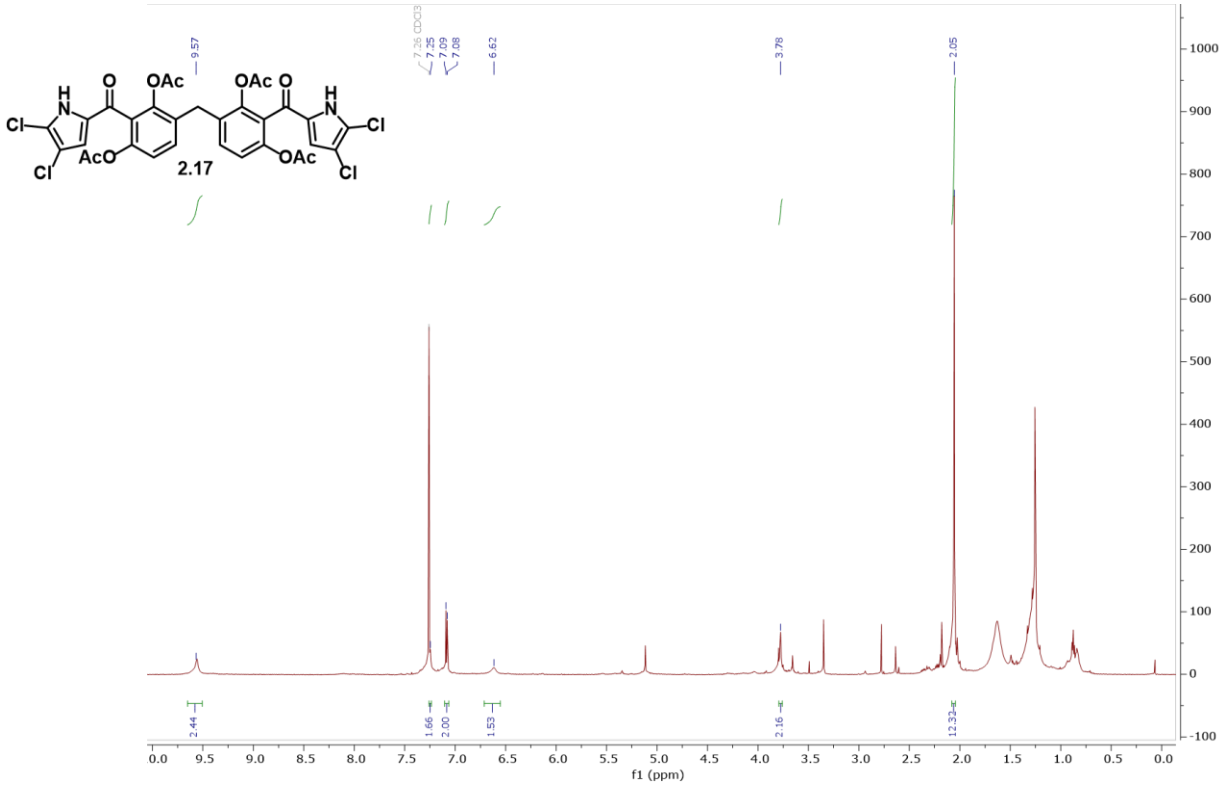
2.17
9.57
7.26 CDCl3
7.25
7.09
7.08
6.62
3.78
2.05
2.44
1.66
2.00
1.53
2.16
12.33
f1 (ppm)

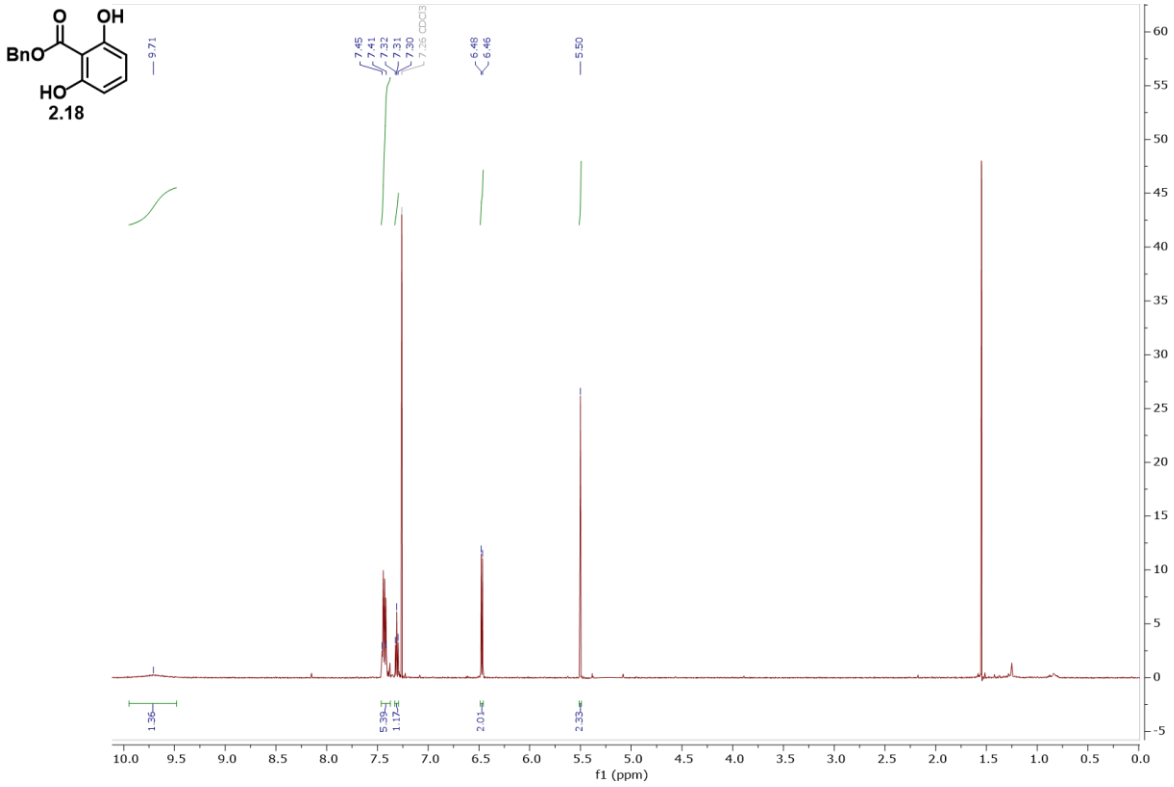
BnO
O
OH
HO
2.18
9.71
7.45
7.41
7.32
7.31
7.30
7.26 CDCl3
6.48
6.46
5.50
1.36
5.39
1.17
2.01
2.33
f1 (ppm)

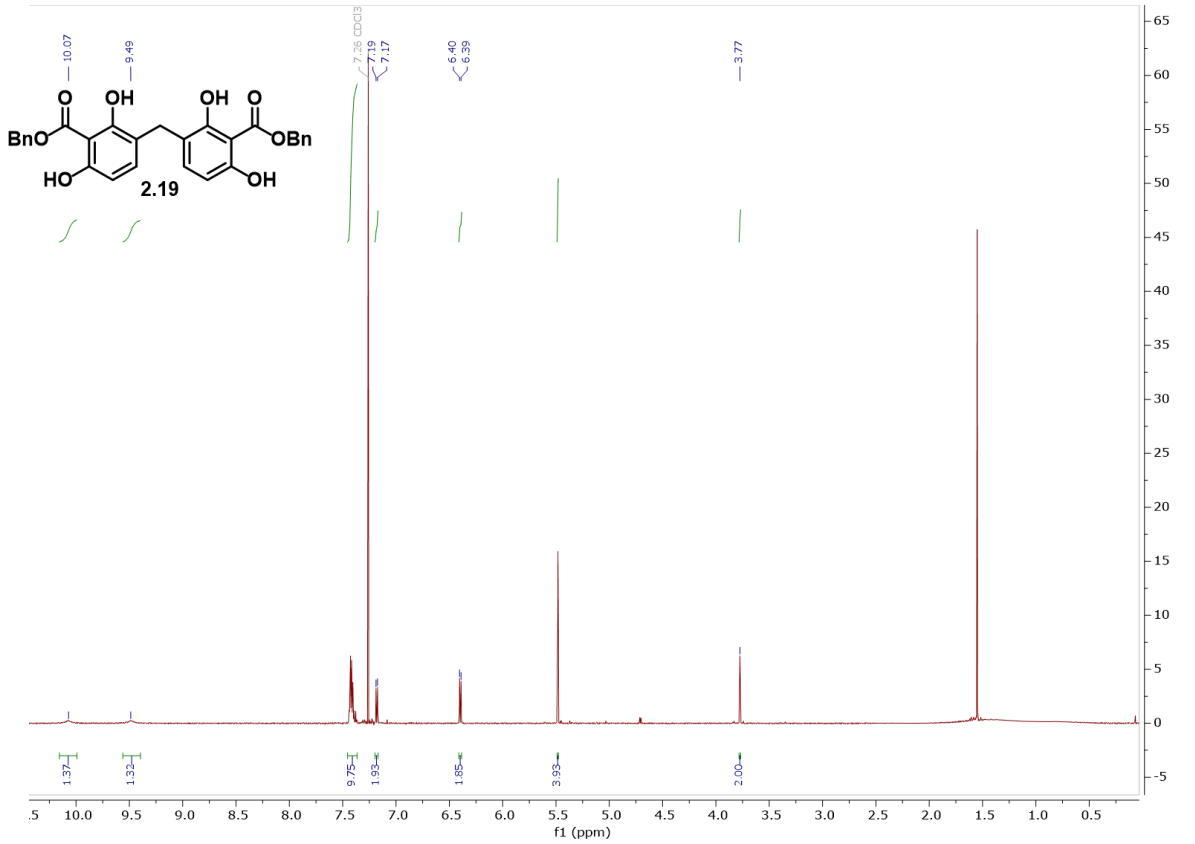
10.07
9.49
7.26 CDCl3
7.19
7.17
6.40
6.39
3.77
BnO
OH
OH
O
OBn
HO
OH
2.19
1.37
1.32
9.75
1.93
1.85
3.93
2.00
f1 (ppm)

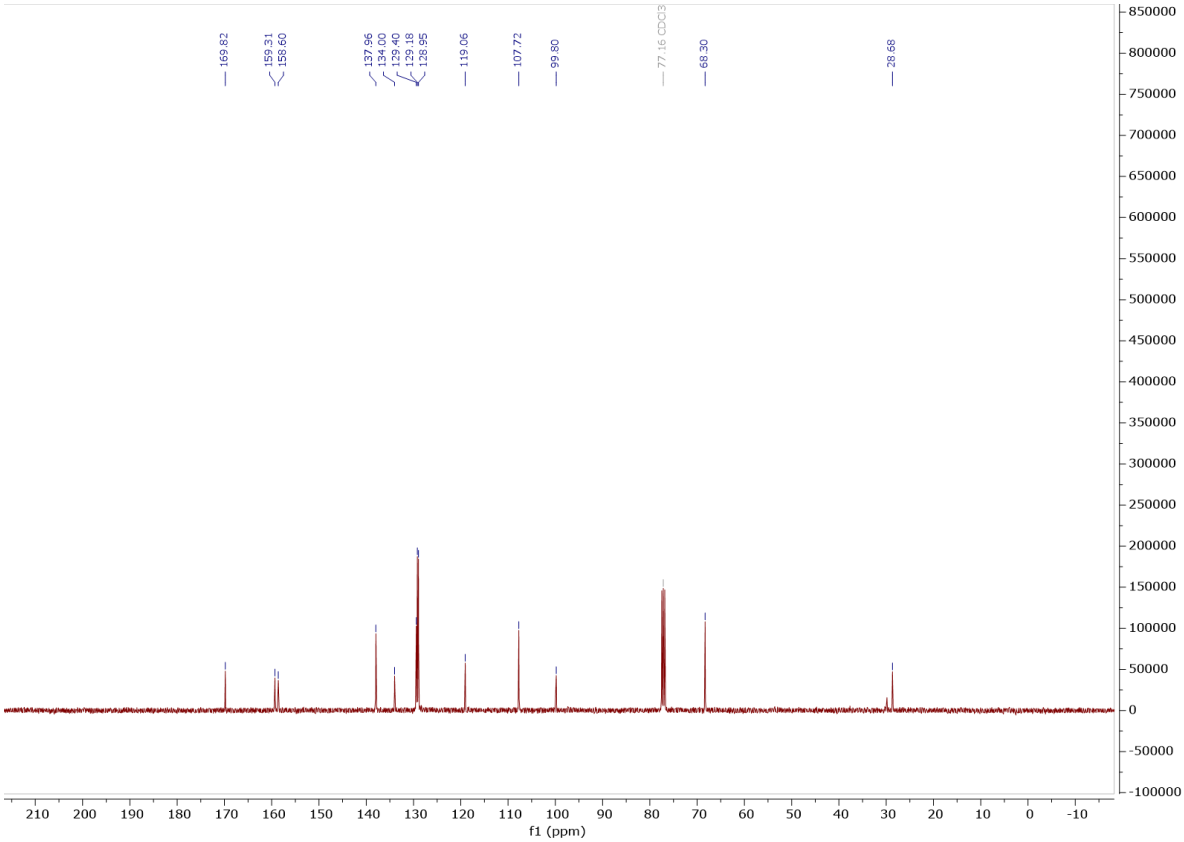
169.82
159.31
158.60
137.96
134.00
129.40
129.18
128.95
119.06
107.72
99.80
77.16 CDCl3
68.30
28.68
f1 (ppm)

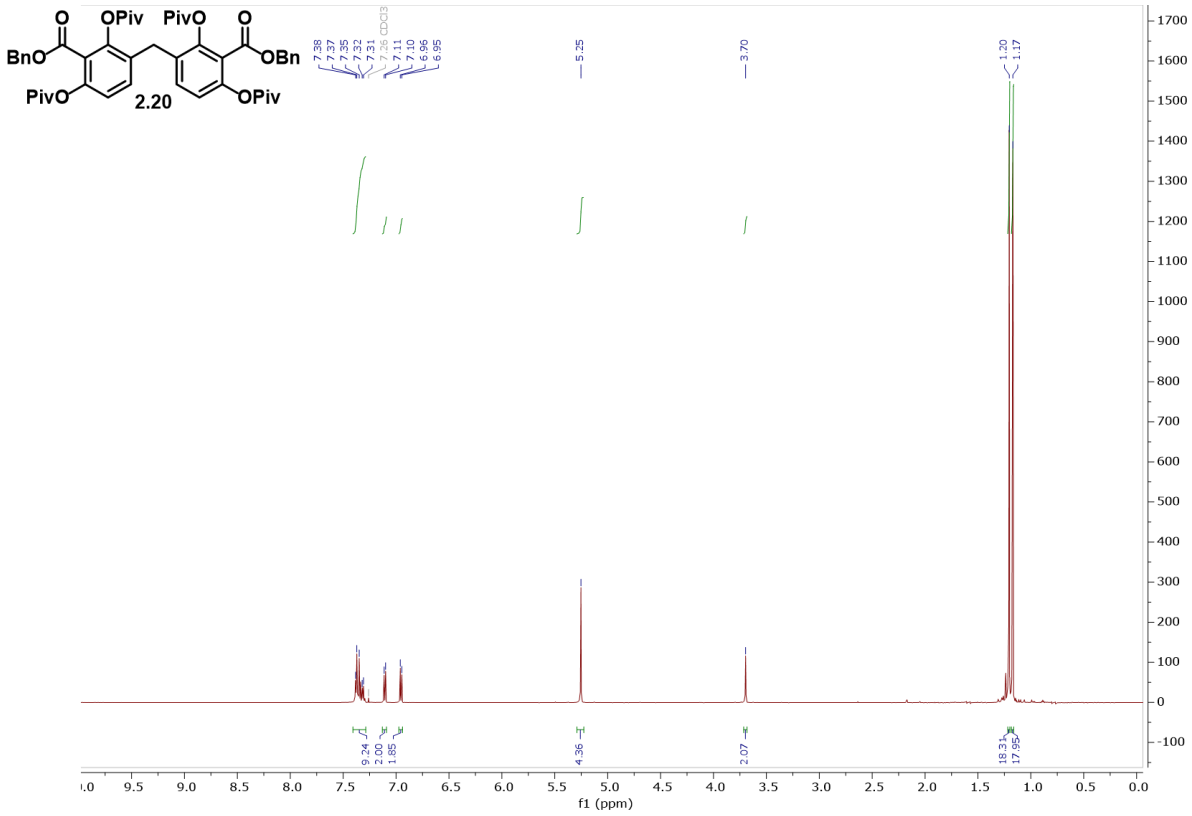
BnO
OPiv
PivO
O
OBn
PivO
OPiv
2.20
7.38
7.37
7.35
7.32
7.31
7.26 CDCl3
7.11
7.10
6.96
6.95
5.25
3.70
1.20
1.17
9.24
2.00
1.85
4.36
2.07
18.31
17.95
f1 (ppm)

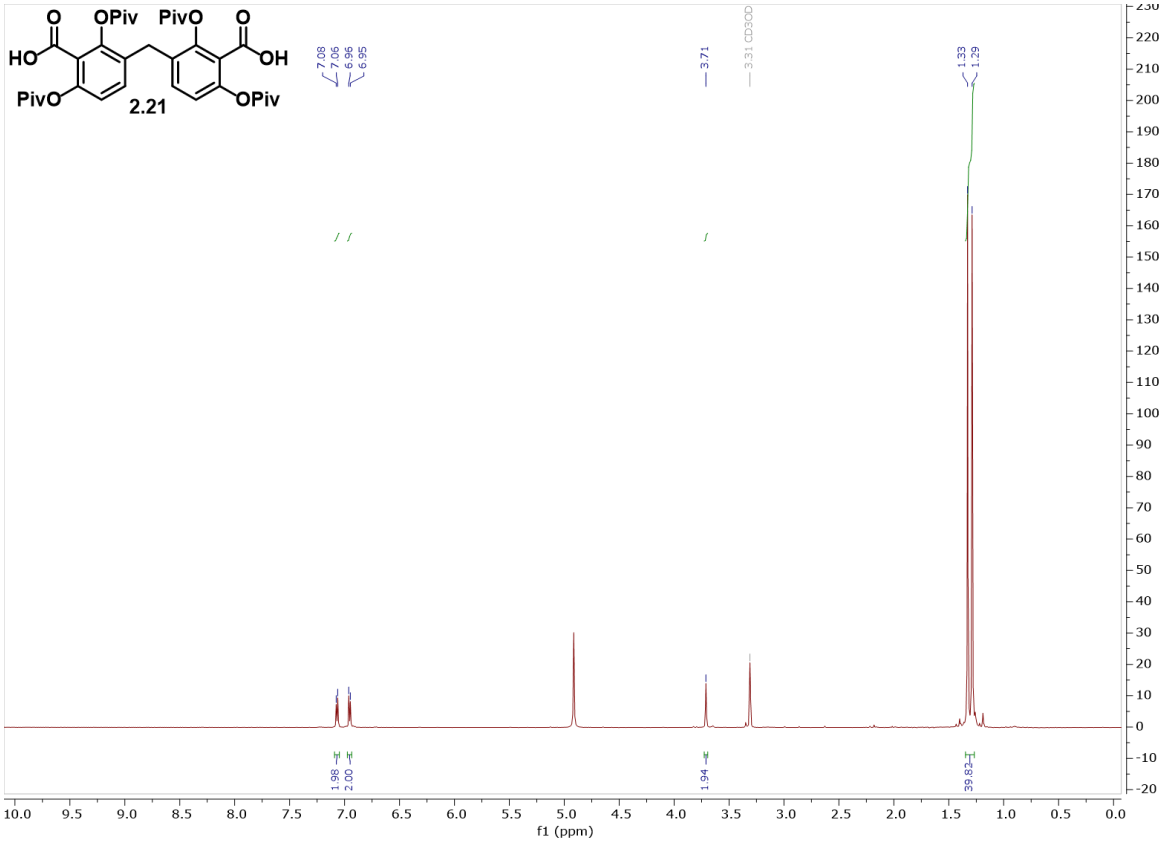
HO
OPiv
PivO
O
OH
PivO
OPiv
2.21
7.08
7.06
6.96
6.95
3.71
3.31 CD3OD
1.33
1.29
1.98
2.00
1.94
39.82
f1 (ppm)

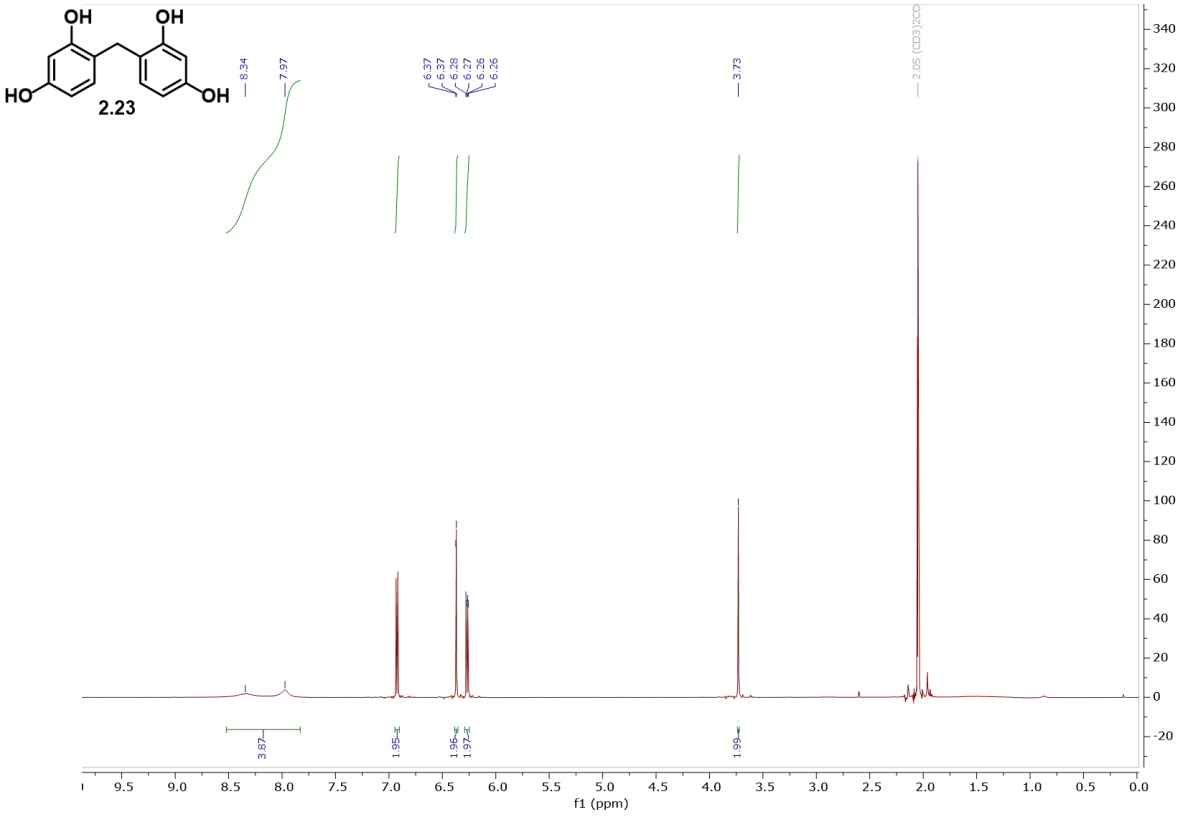
OH
OH
HO
OH
2.23
8.34
7.97
6.37
6.37
6.28
6.27
6.26
6.26
3.73
2.05 (CD3)2CO
3.87
1.95
1.96
1.97
1.99
f1 (ppm)

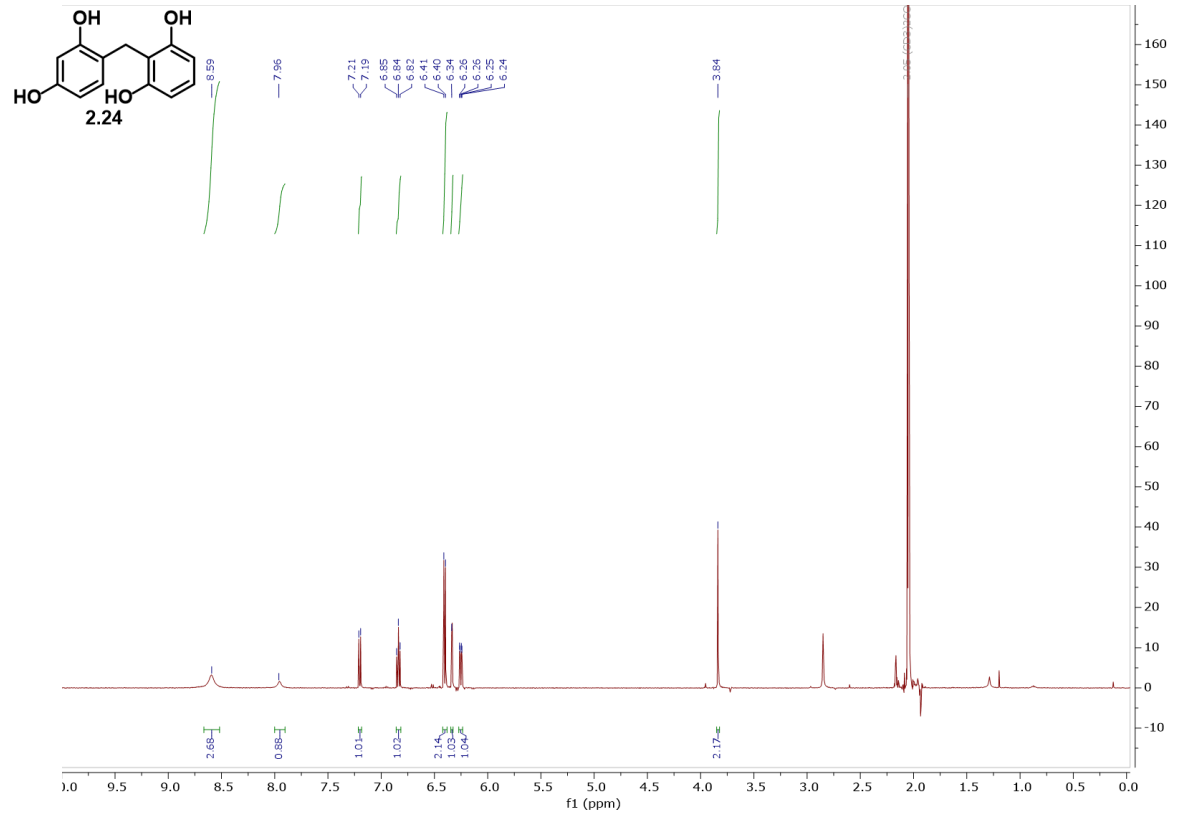
OH
OH
HO
HO
2.24
8.59
7.96
7.21
7.19
6.85
6.84
6.82
6.41
6.40
6.34
6.26
6.25
6.24
3.84
2.68
0.88
1.01
1.03
2.14
1.03
1.04
2.17
f1 (ppm)

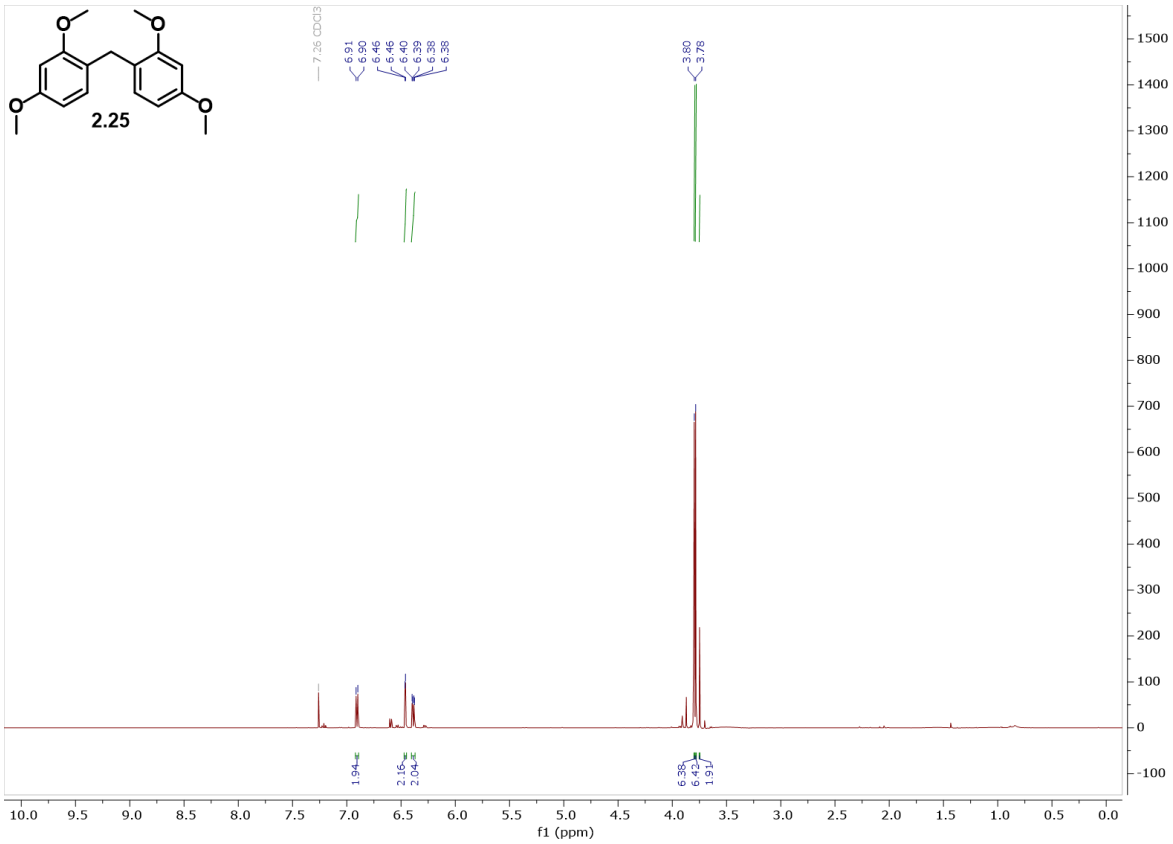
2.25
7.26 CDCl3
6.91
6.90
6.46
6.46
6.40
6.39
6.38
6.38
3.80
3.78
1.94
2.16
2.04
6.38
6.42
1.91
f1 (ppm)

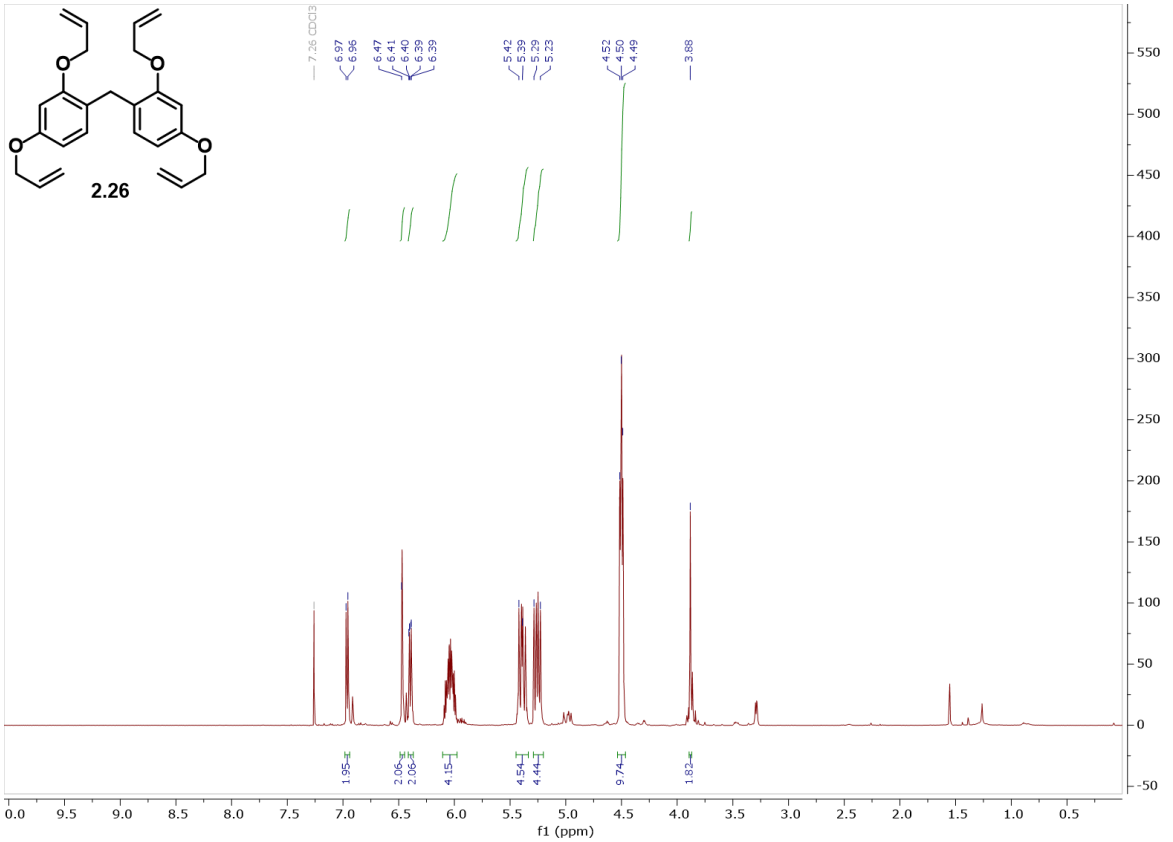
2.26
7.26 CDCl3
6.97
6.96
6.47
6.41
6.40
6.39
6.39
5.42
5.39
5.29
5.23
4.52
4.50
4.49
3.88
1.95
2.06
2.06
4.15
4.54
4.44
9.74
1.82
f1 (ppm)

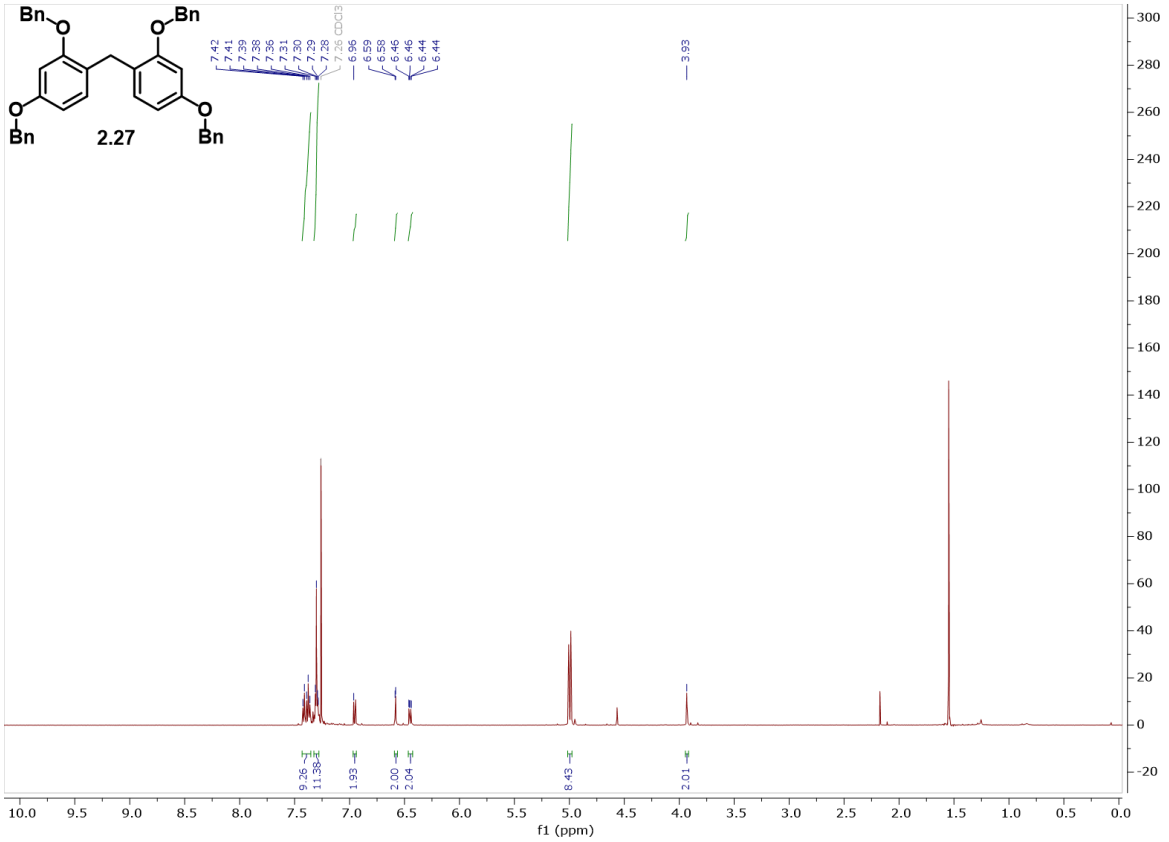
Bn
Bn
Bn
Bn
2.27
f1 (ppm)

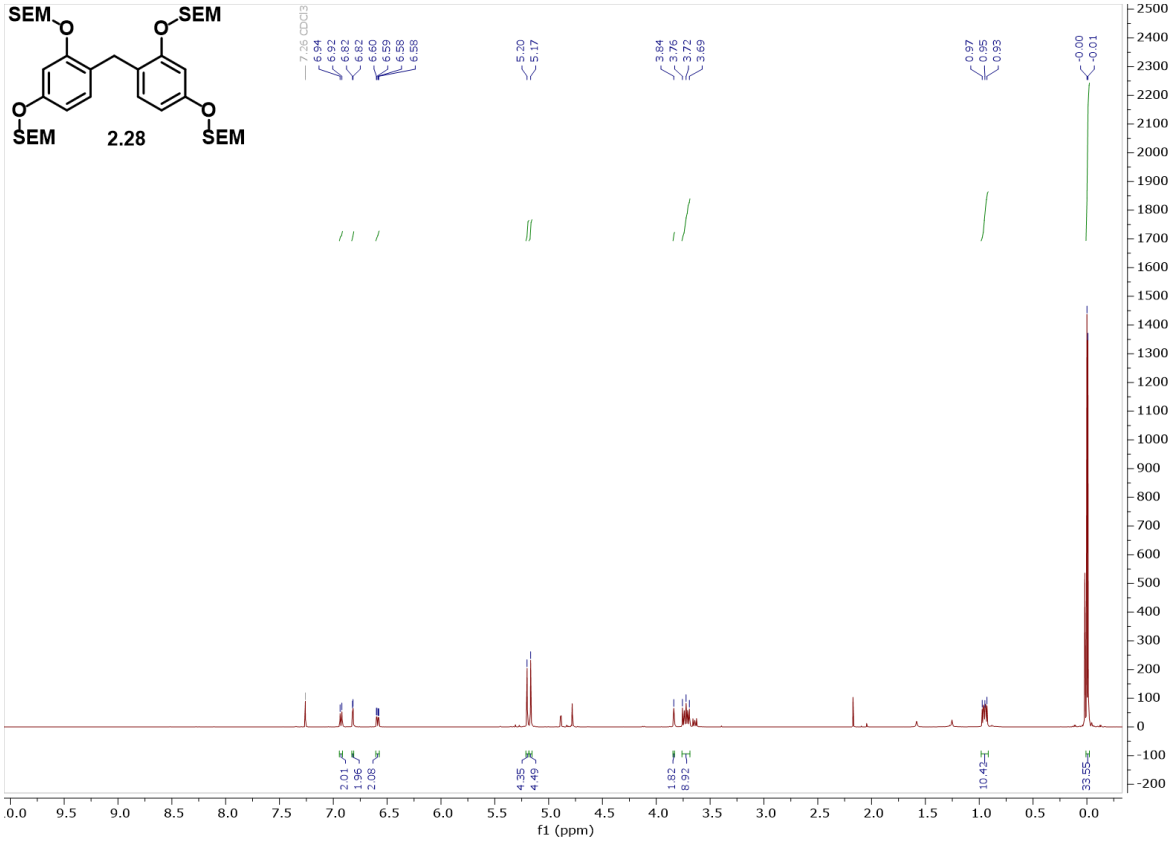
SEM
SEM
SEM
SEM
2.28
f1 (ppm)

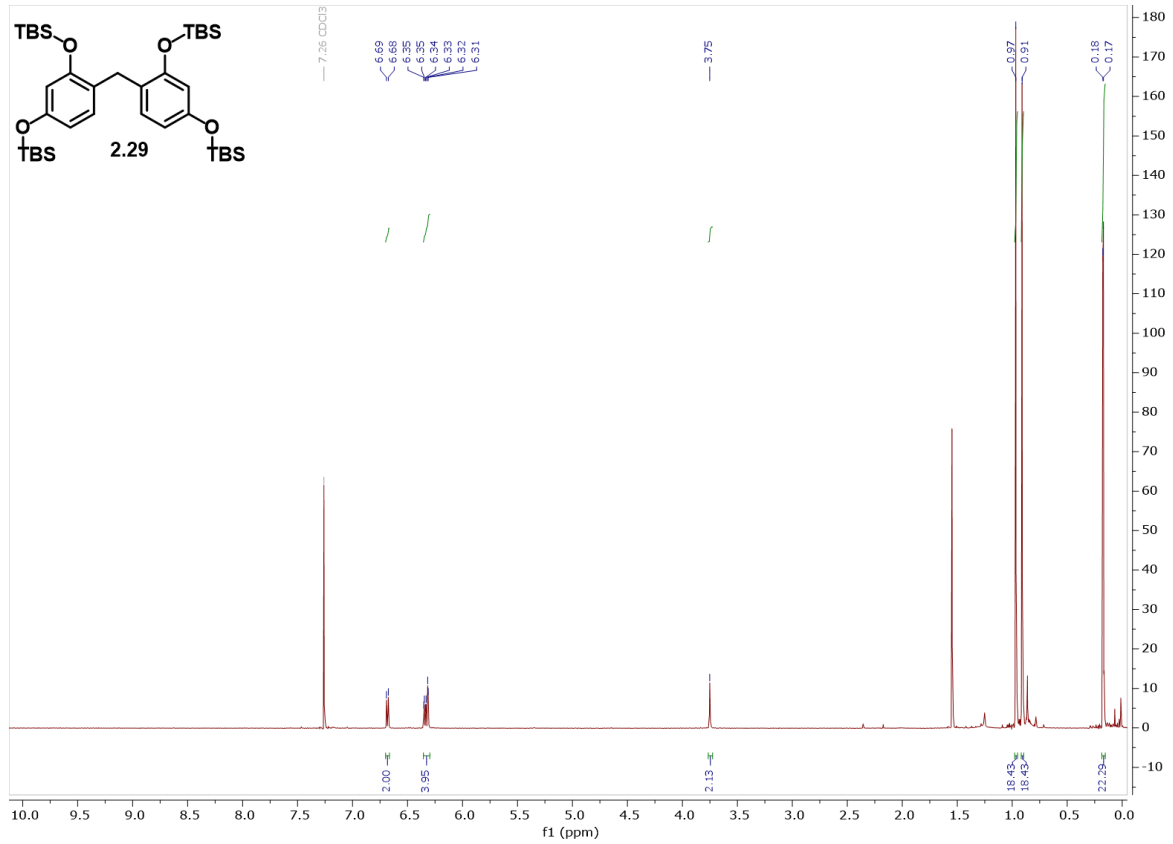
TBS
TBS
TBS
TBS
2.29
7.26 CDCl3
6.69
6.68
6.35
6.35
6.34
6.33
6.32
6.31
3.75
0.97
0.91
0.18
0.17
2.00
3.95
2.13
18.45
18.43
22.29
f1 (ppm)

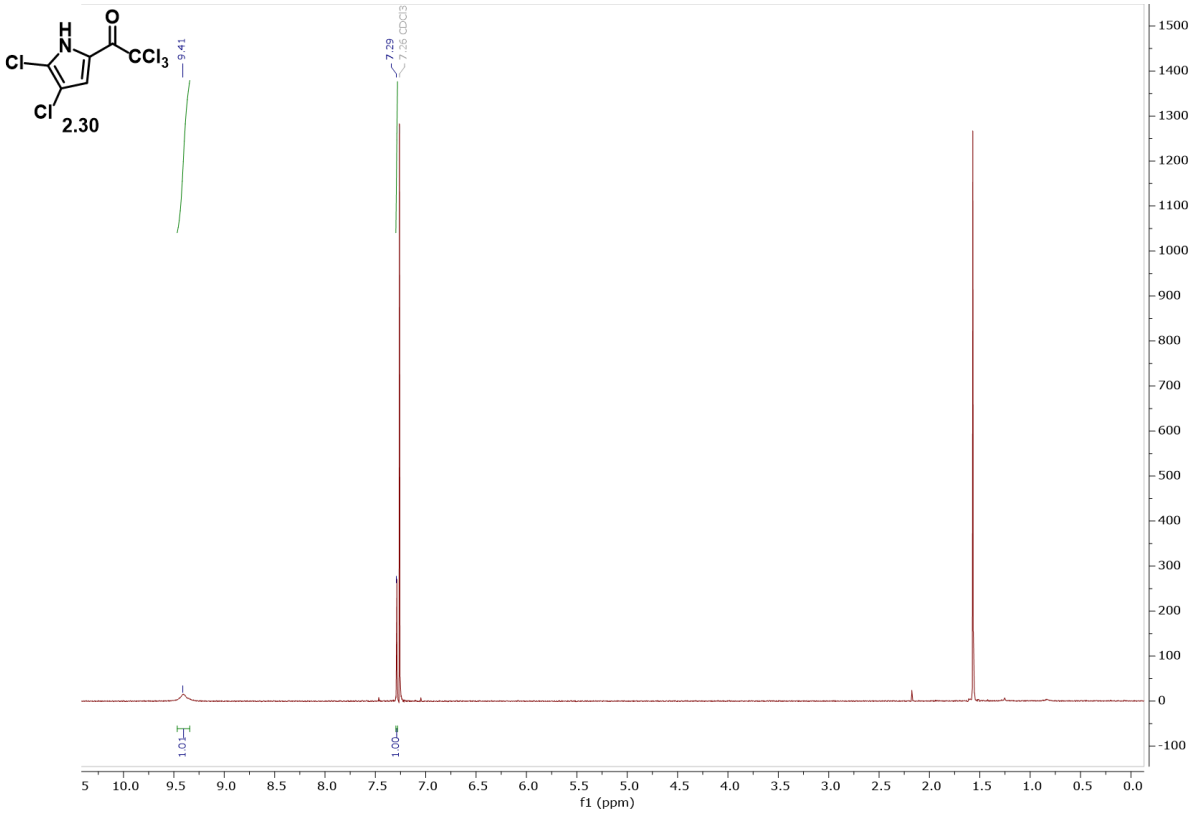
H
N
O
CCl3
Cl
Cl
2.30
9.41
7.29
7.26 CDCl3
1.01
1.00
f1 (ppm)

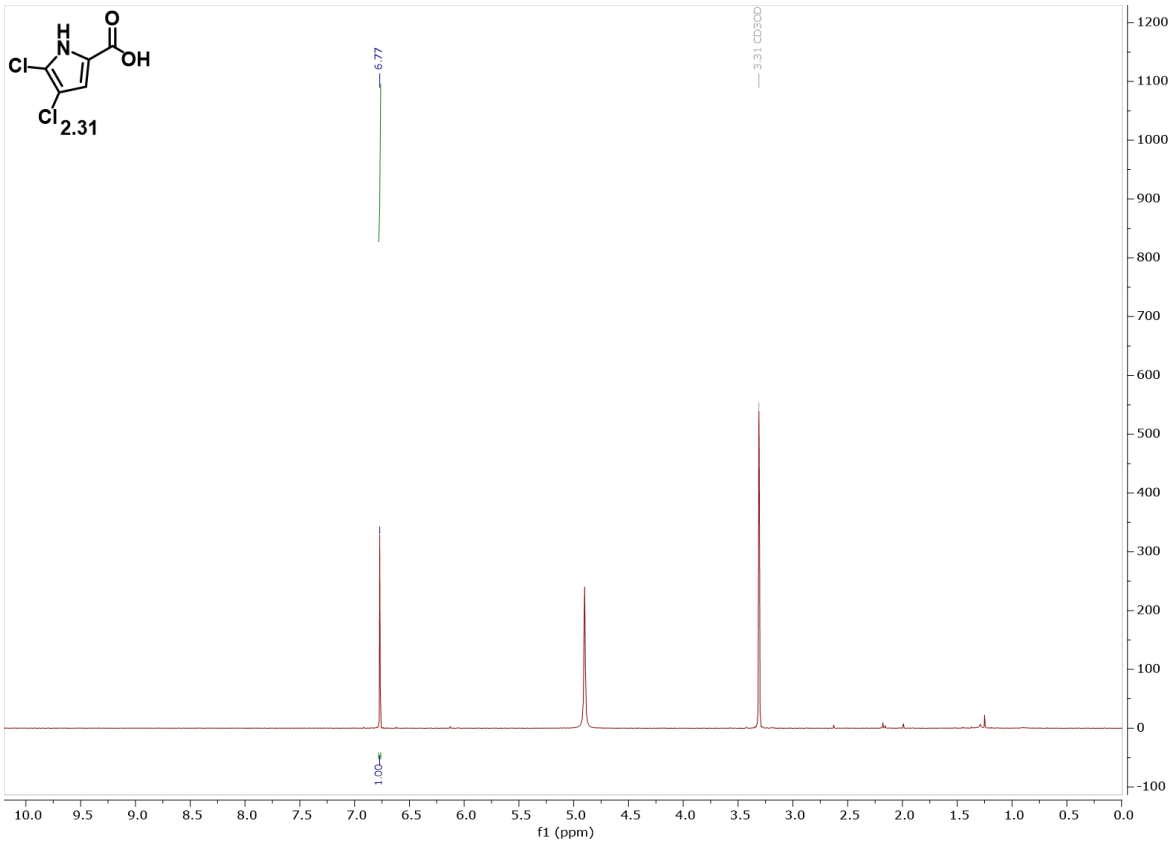
H
N
O
OH
Cl
Cl
2.31
6.77
3.31 CD3OD
1.00
1200
1100
1000
900
800
700
600
500
400
300
200
100
0
-100
10.0
9.5
9.0
8.5
8.0
7.5
7.0
6.5
6.0
5.5
5.0
4.5
4.0
3.5
3.0
2.5
2.0
1.5
1.0
0.5
0.0
f1 (ppm)

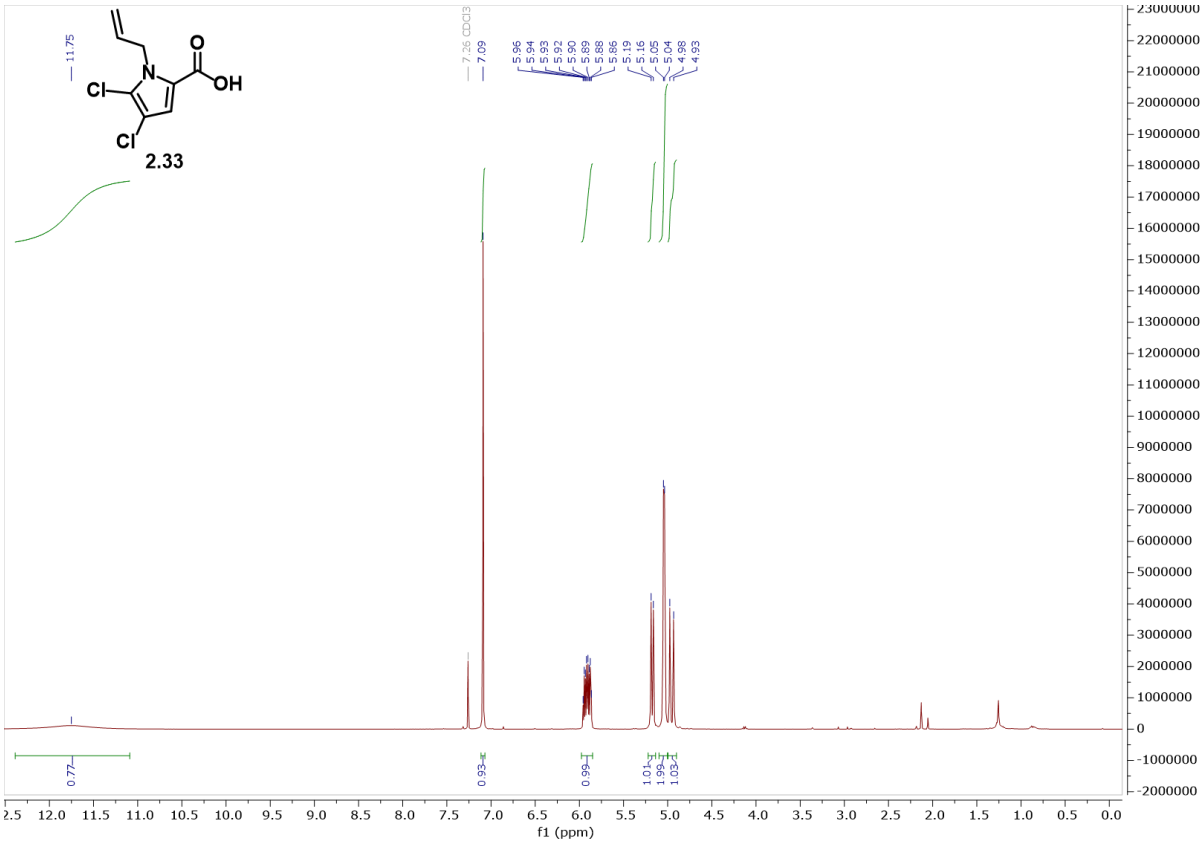
11.75
7.26 CDCl3
7.09
5.96
5.94
5.93
5.92
5.90
5.89
5.88
5.86
5.19
5.15
5.05
5.04
4.98
4.93
Cl
N
O
OH
Cl
2.33
0.77
0.93
0.99
1.01
1.99
1.03
f1 (ppm)

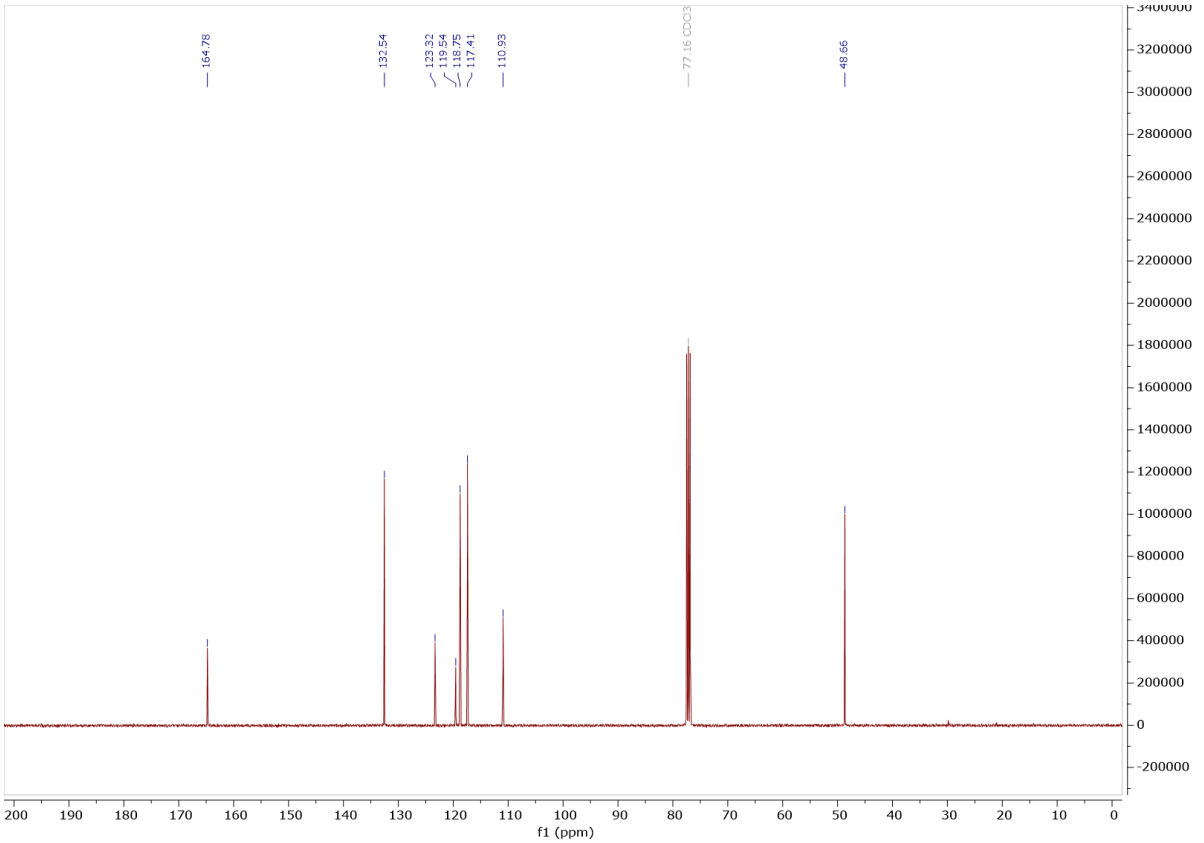
164.78
132.54
123.32
119.54
118.75
117.41
110.93
77.16 CDCl3
48.66
f1 (ppm)

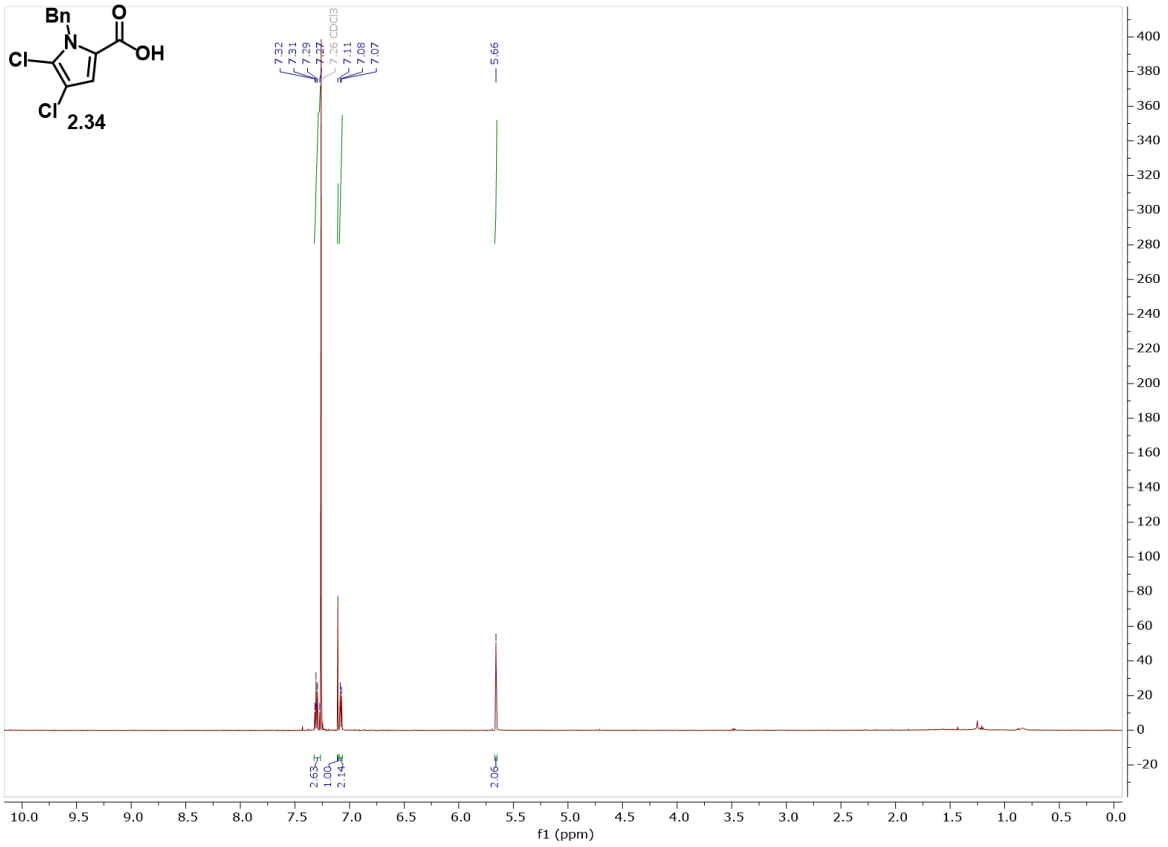
Bn
N
O
OH
Cl
Cl
2.34
7.32
7.31
7.29
7.27
7.26 CDCl3
7.11
7.08
7.07
5.66
2.63
1.00
2.14
2.06
f1 (ppm)

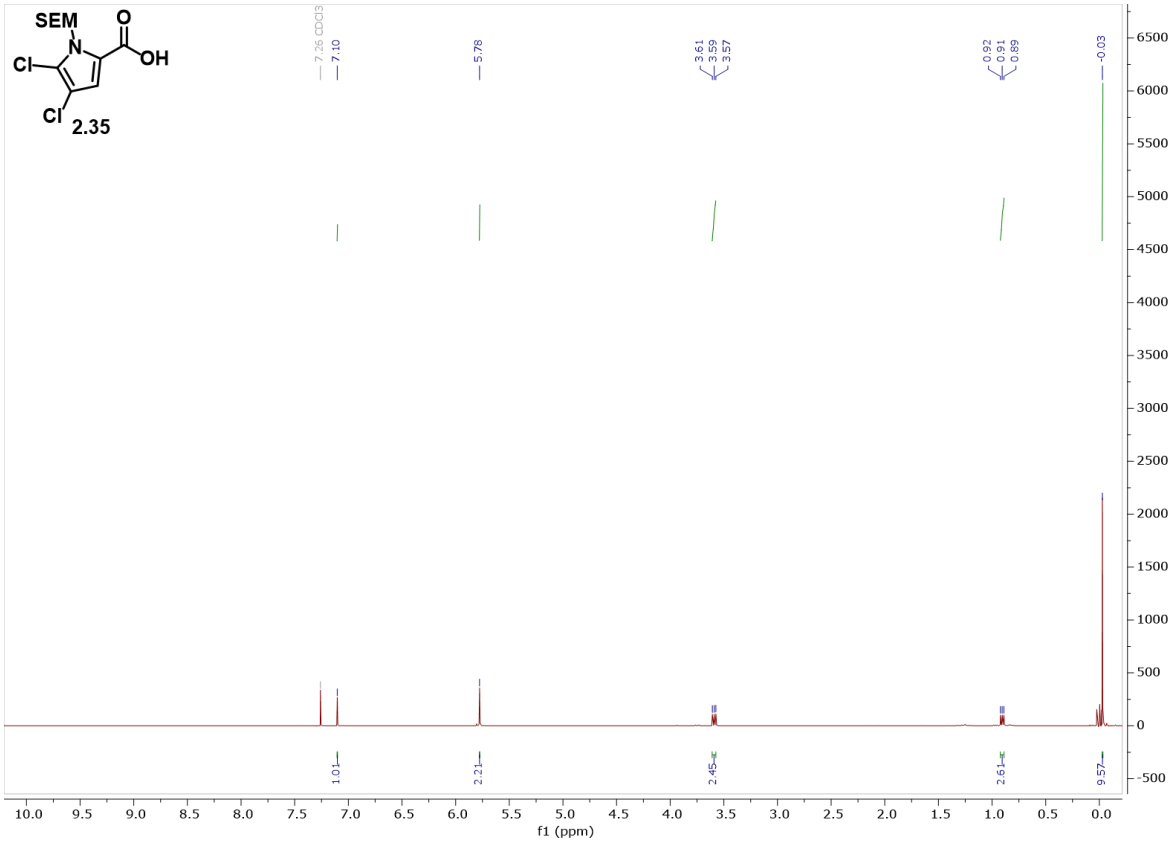
SEM
N
O
OH
Cl
Cl
2.35
7.26 CDCl3
7.10
5.78
3.61
3.59
3.57
0.92
0.91
0.89
-0.03
1.01
2.21
2.45
2.61
9.57
f1 (ppm)

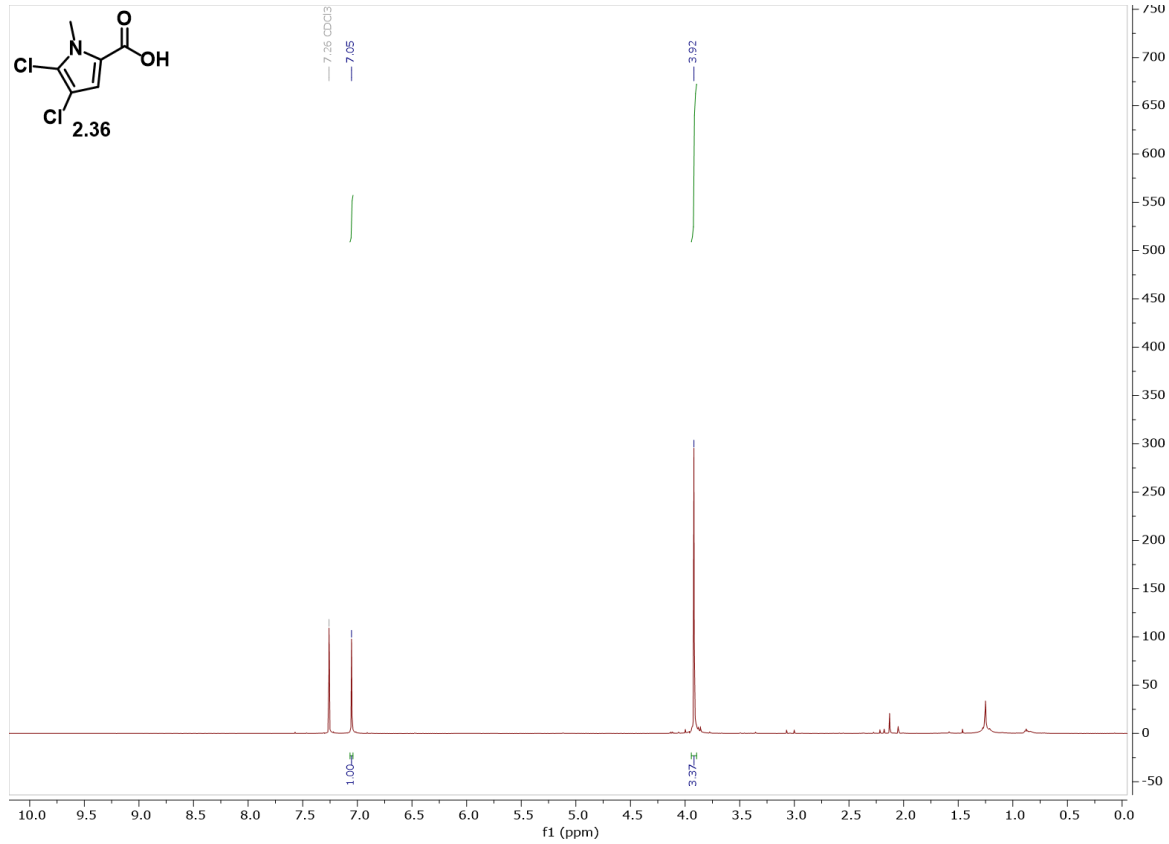
Cl
N
O
OH
Cl
2.36
7.26 CDCl3
7.05
3.92
1.00
3.37
f1 (ppm)

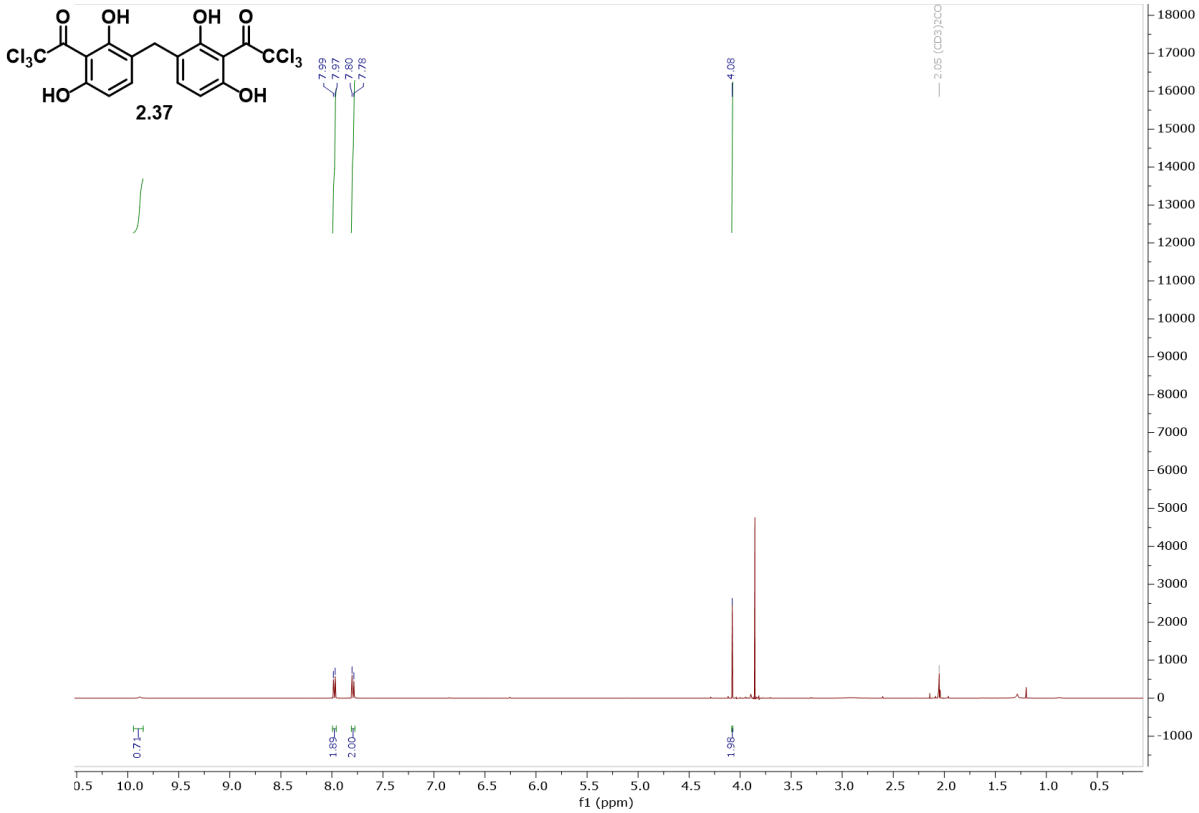
Cl3C
O
OH
OH
O
CCl3
HO
OH
2.37
7.99
7.97
7.80
7.78
4.08
2.05 (CD3)2CO
0.71
1.89
2.00
1.98
f1 (ppm)

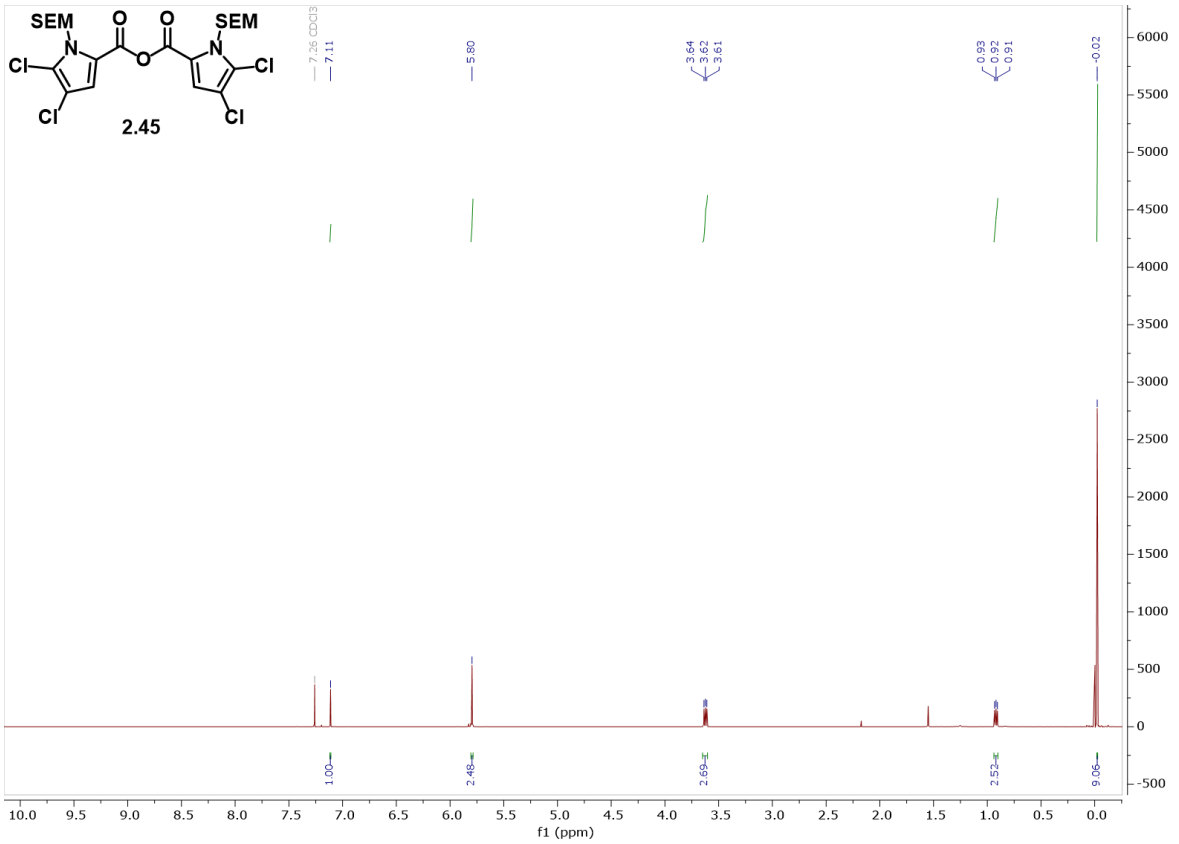
SEM
O
O
SEM
N
N
Cl
Cl
Cl
Cl
O
2.45
7.26 CDCl3
7.11
5.80
3.64
3.62
3.61
0.93
0.92
0.91
-0.02
1.00
2.48
2.69
2.52
9.06
f1 (ppm)

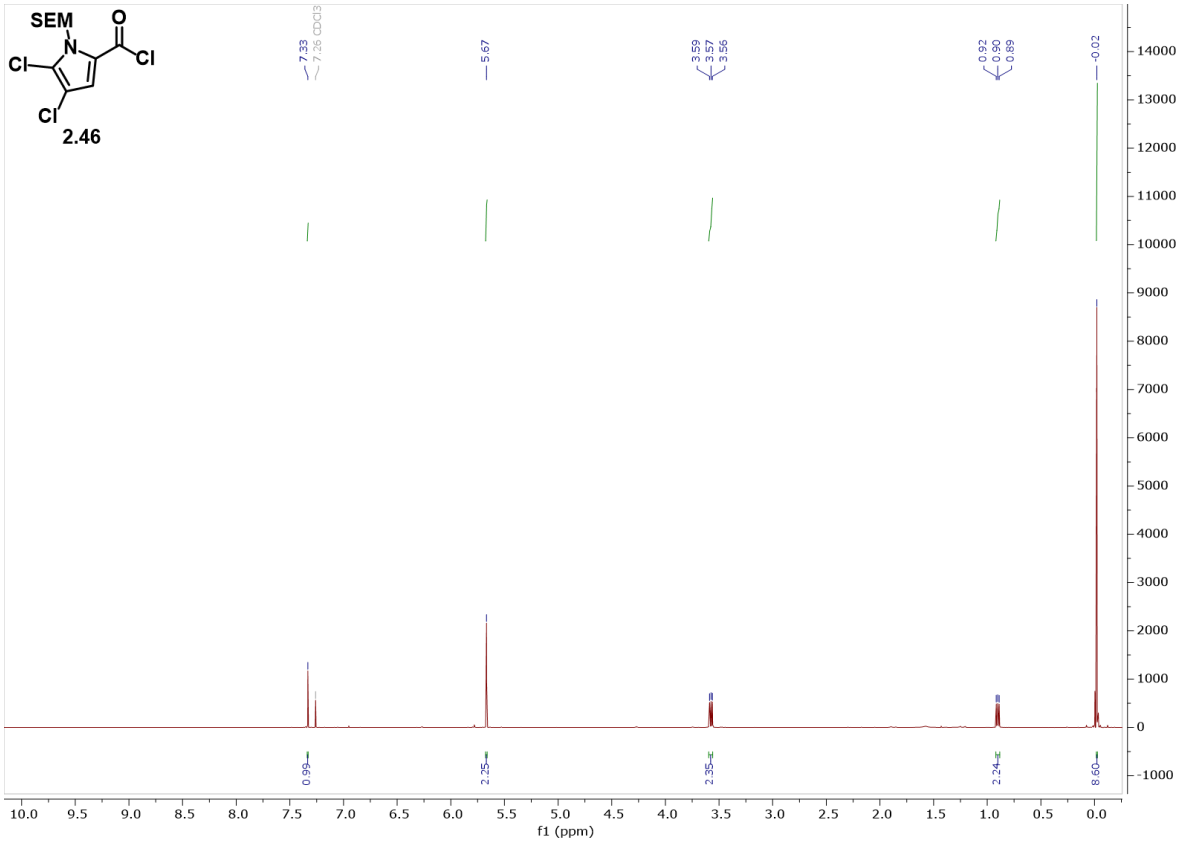
SEM
O
N
Cl
Cl
Cl
2.46
7.33
7.26 CDCl3
5.67
3.59
3.57
3.56
0.92
0.90
0.89
-0.02
0.99
2.25
2.35
2.24
8.60
f1 (ppm)

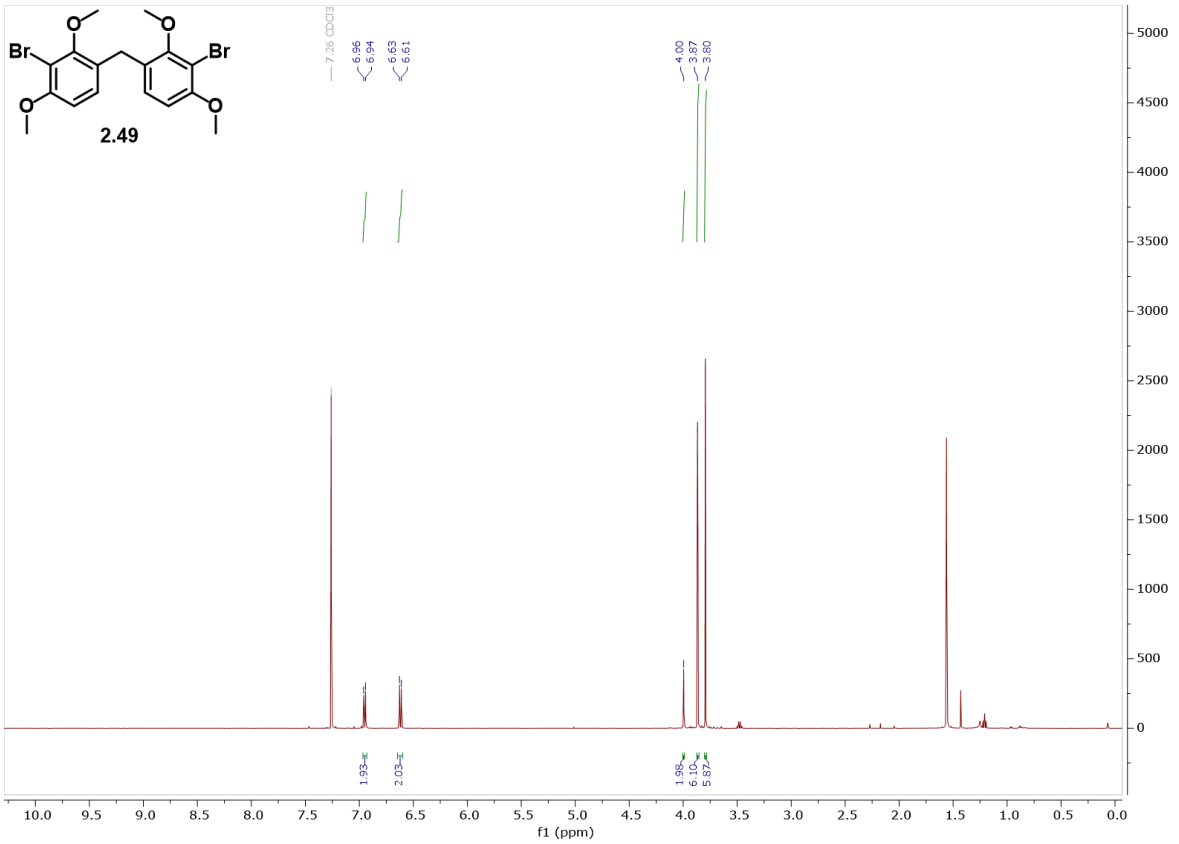
Br
Br
O
O
O
O
2.49
7.26 CDCl3
6.96
6.94
6.63
6.61
4.00
3.87
3.80
1.93
2.03
1.98
6.10
5.87
f1 (ppm)

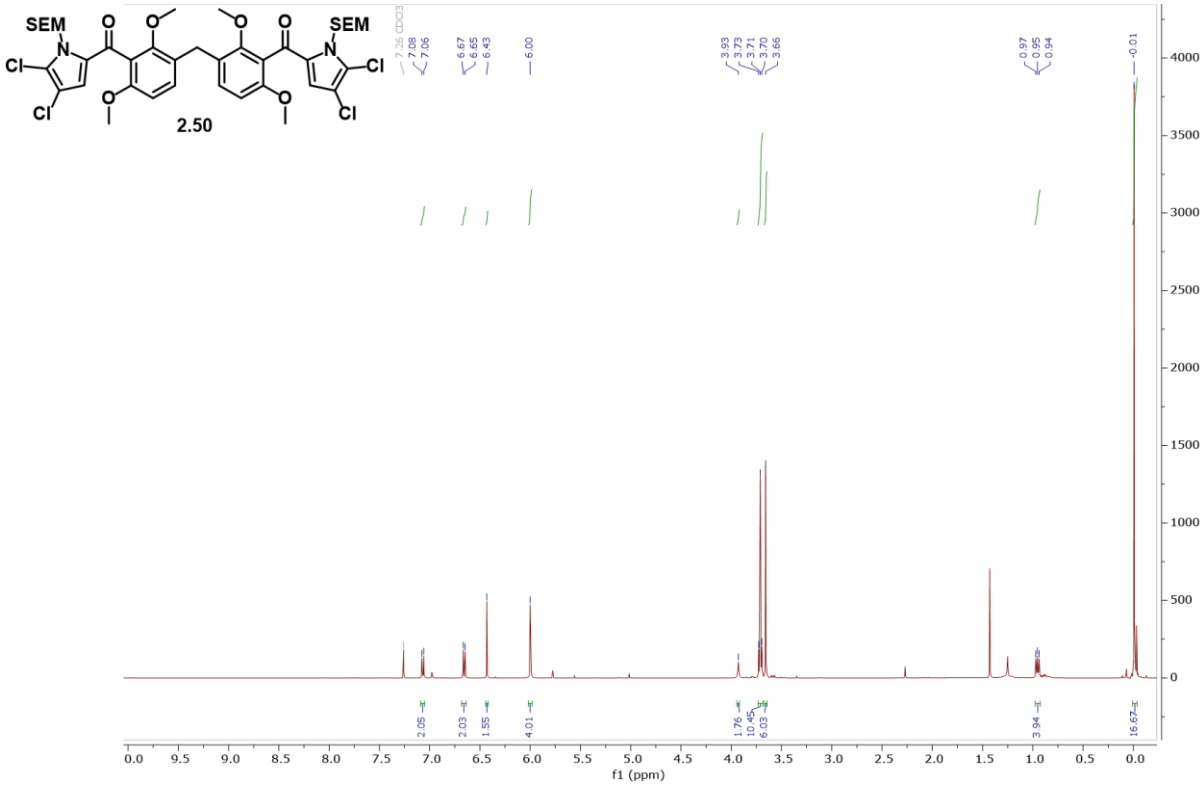
SEM
SEM
Cl
Cl
Cl
Cl
O
O
O
O
O
O
2.50
7.26 CDCl3
7.08
7.06
6.67
6.65
6.43
6.00
3.93
3.73
3.71
3.70
3.66
0.97
0.95
0.94
0.01
2.05
2.03
1.55
4.01
1.76
10.45
6.03
3.94
16.67
f1 (ppm)

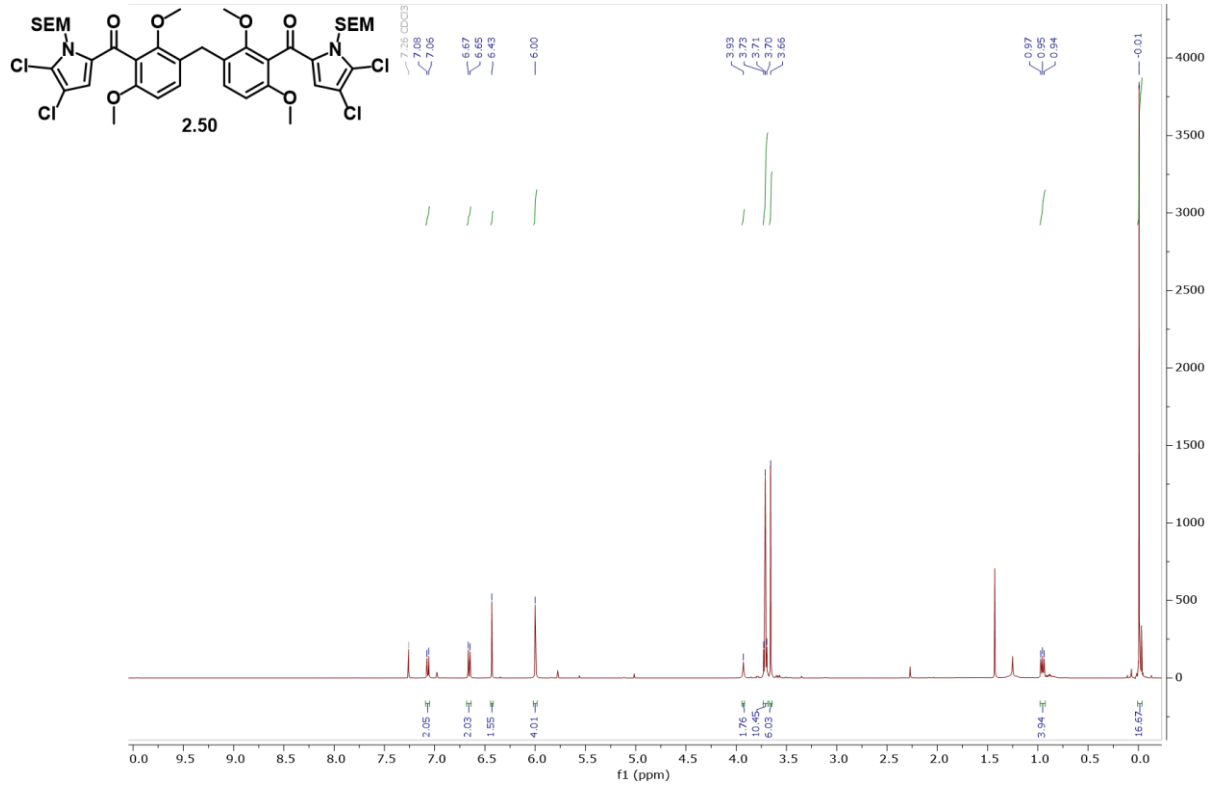
SEM
SEM
Cl
Cl
Cl
Cl
O
O
O
O
O
O
N
N
2.50
7.26 CDCl3
7.08
7.06
6.67
6.65
6.43
6.00
3.93
3.73
3.71
3.70
3.66
0.97
0.95
0.94
-0.01
2.05
2.03
1.55
4.01
1.76
10.45
6.03
3.94
16.67
f1 (ppm)

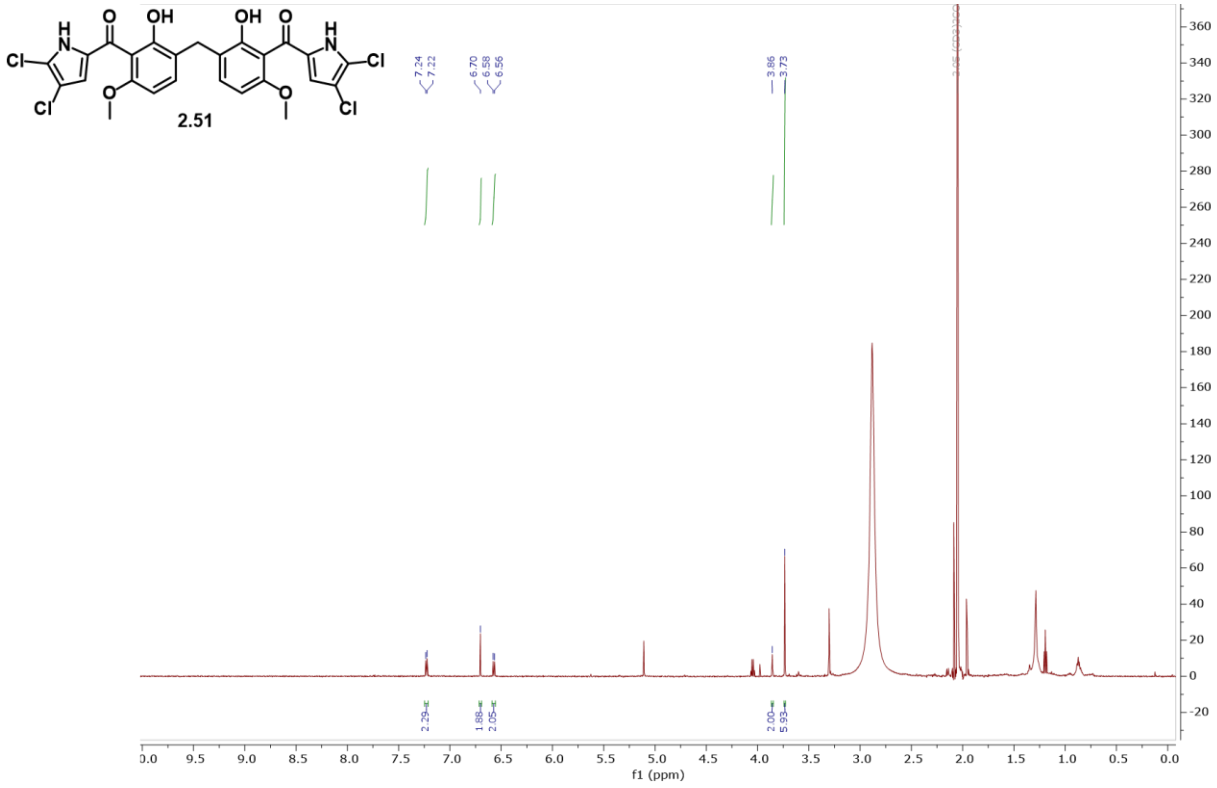
H
H
Cl
Cl
Cl
Cl
O
OH
OH
O
O
O
N
N
2.51
7.24
7.22
6.70
6.58
6.56
3.86
3.73
2.29
1.88
2.05
2.00
5.93
f1 (ppm)

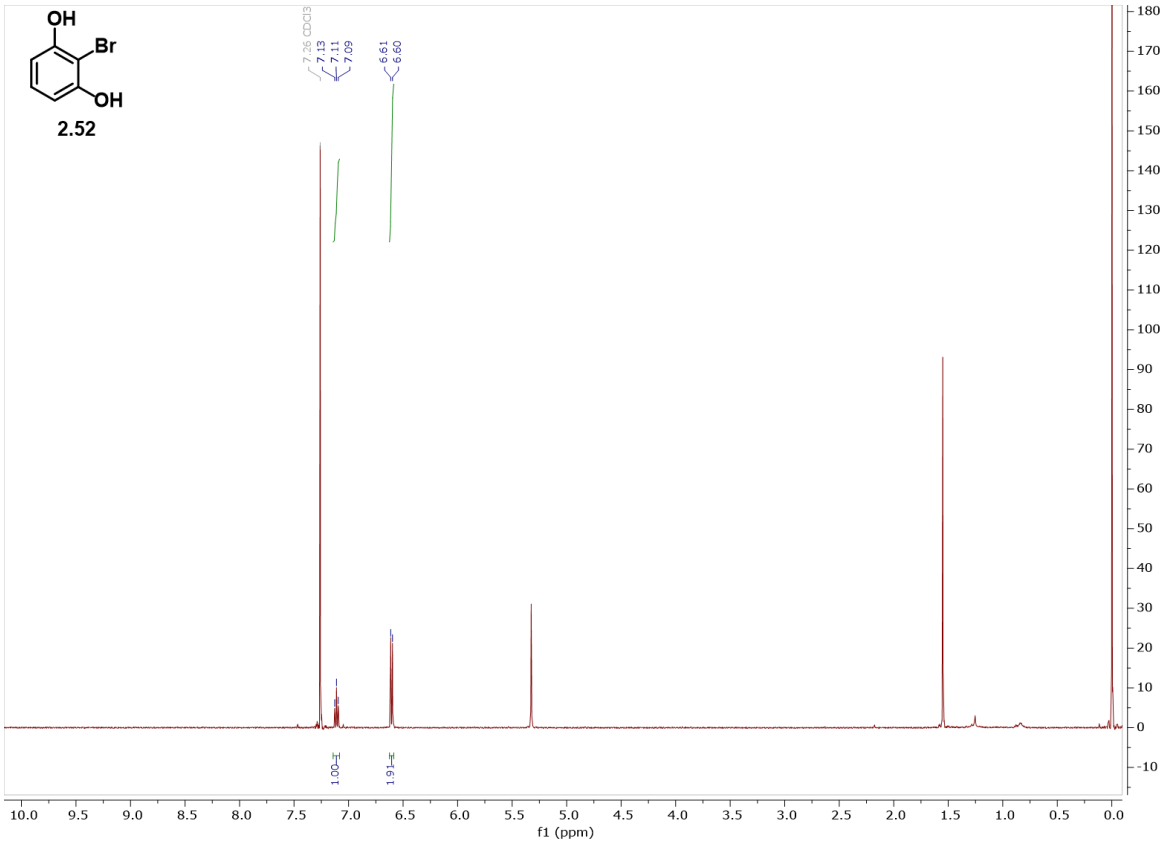
OH
Br
OH
2.52
7.26 (CDCl3
7.13
7.11
7.09
6.61
6.60
1.00
1.91
f1 (ppm)

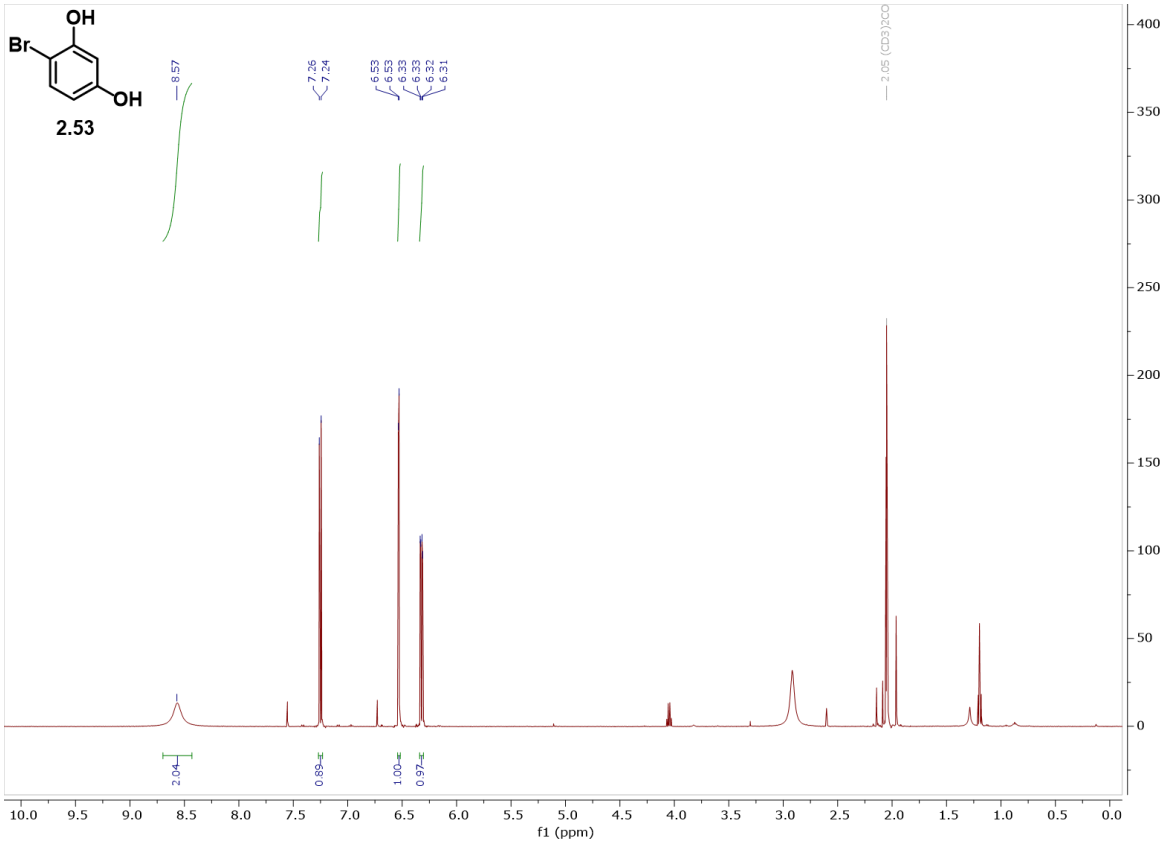
OH
Br
OH
2.53
8.57
7.26
7.24
6.53
6.53
6.33
6.33
6.32
6.31
2.05 (CD3)2CO
2.04
0.89
1.00
0.97
f1 (ppm)

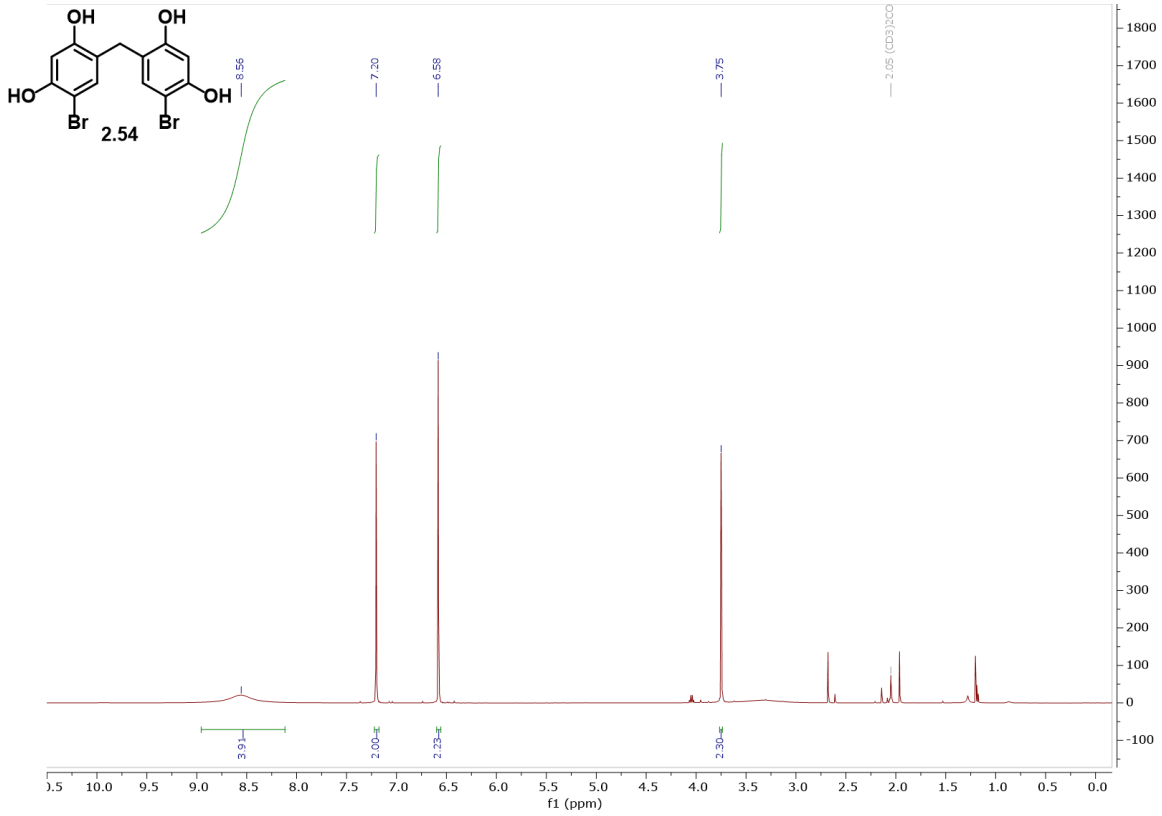
OH
OH
HO
OH
Br
Br
2.54
8.56
7.20
6.58
3.75
2.05 (CD3)2CO
3.91
2.00
2.23
2.30
f1 (ppm)

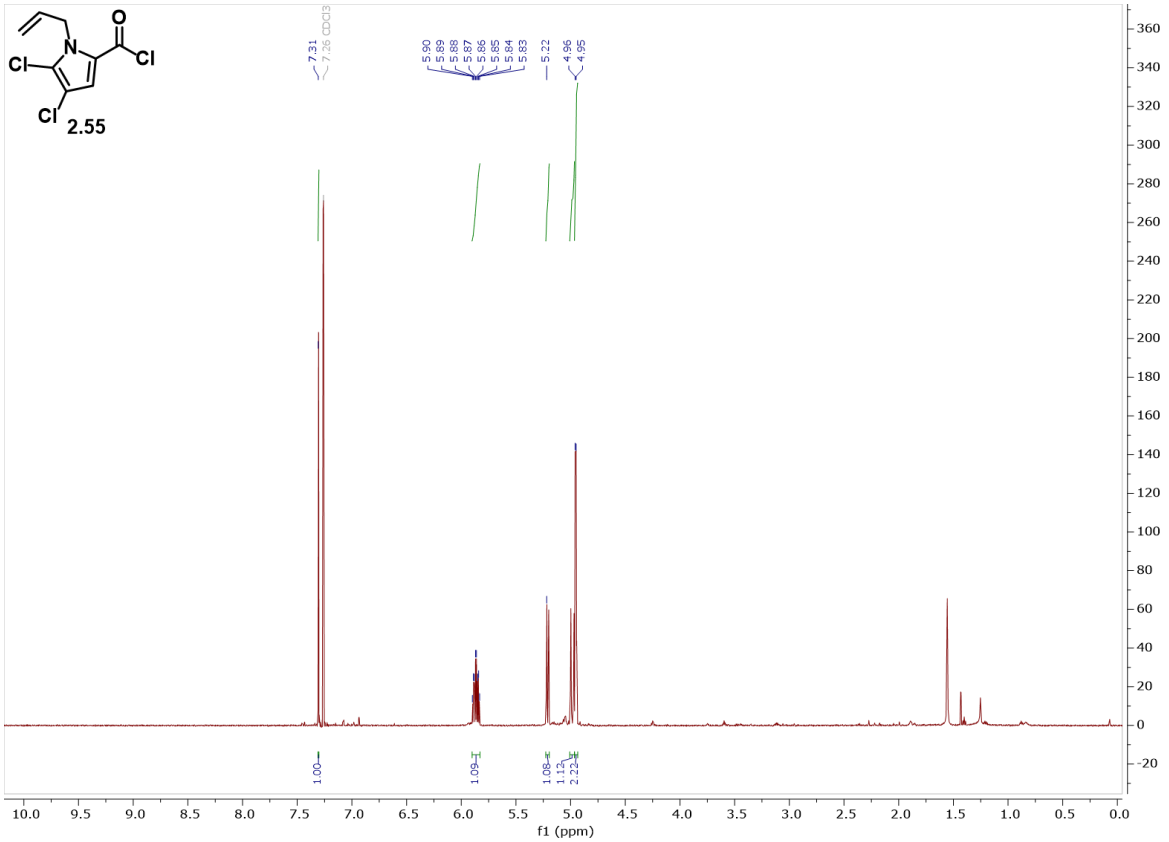
O
N
Cl
Cl
Cl
2.55
7.31
7.26 CDCl3
5.90
5.89
5.88
5.87
5.86
5.85
5.84
5.83
5.22
4.96
4.95
1.00
1.09
1.08
1.12
2.22
f1 (ppm)

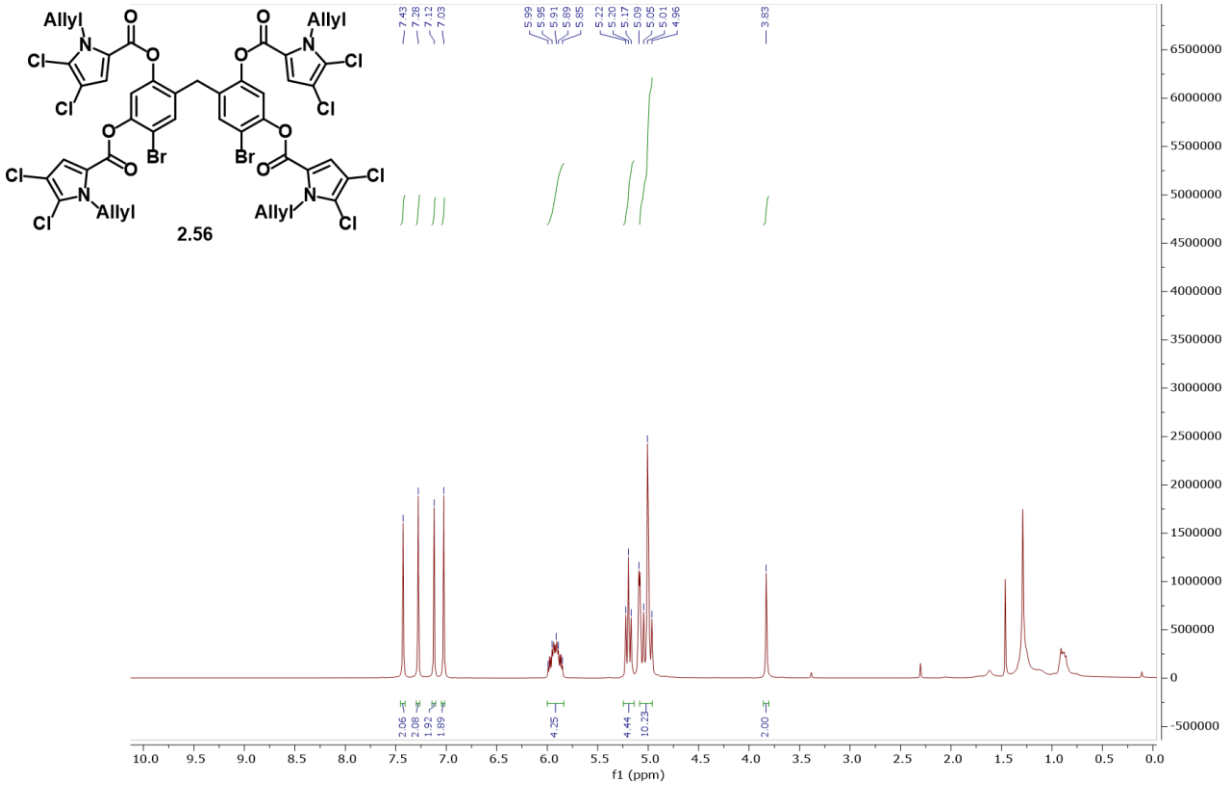
Allyl
Cl
Br
O
N
2.56
7.43
7.38
7.12
7.03
5.99
5.95
5.91
5.89
5.85
5.22
5.20
5.17
5.09
5.05
5.01
4.96
3.83
2.06
2.08
1.92
1.89
4.25
4.44
10.23
2.00
f1 (ppm)

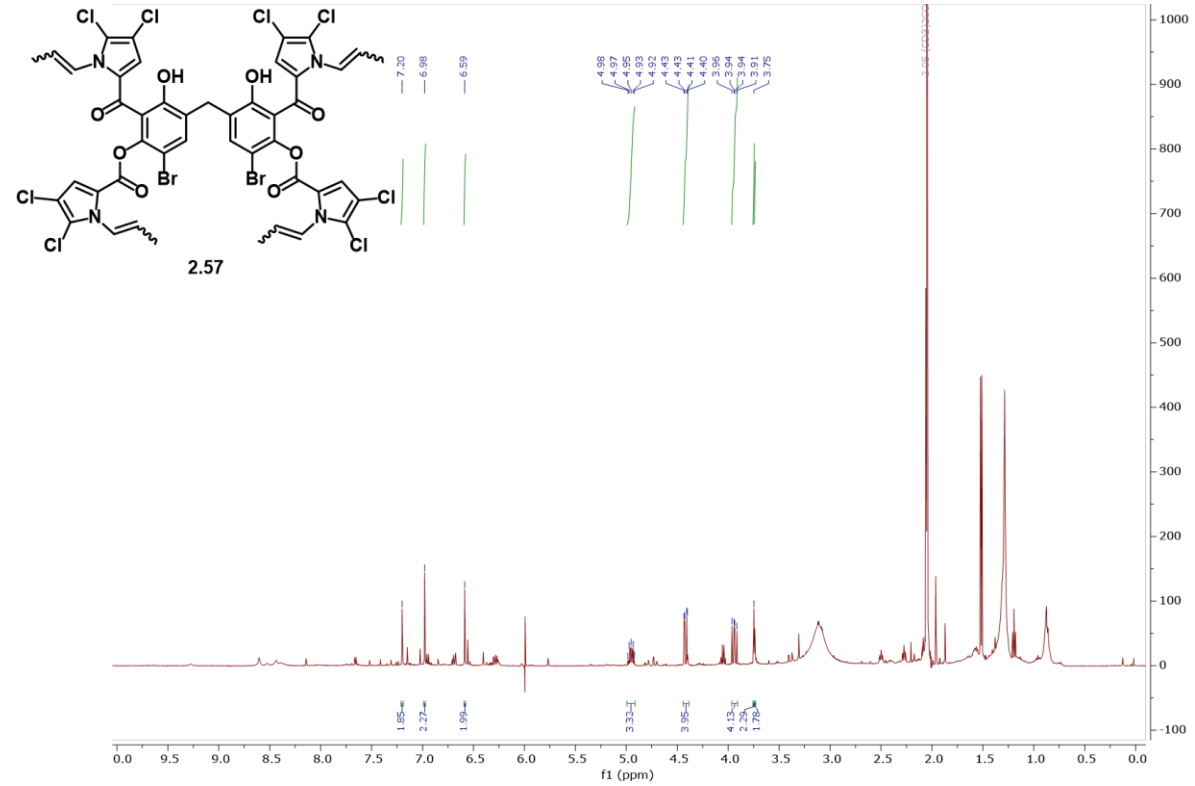
Cl
OH
Br
O
N
2.57
7.20
6.98
6.59
4.98
4.97
4.95
4.93
4.92
4.43
4.41
4.40
3.96
3.94
3.94
3.91
3.75
1.85
2.27
1.99
3.33
3.95
4.13
2.29
1.78
f1 (ppm)

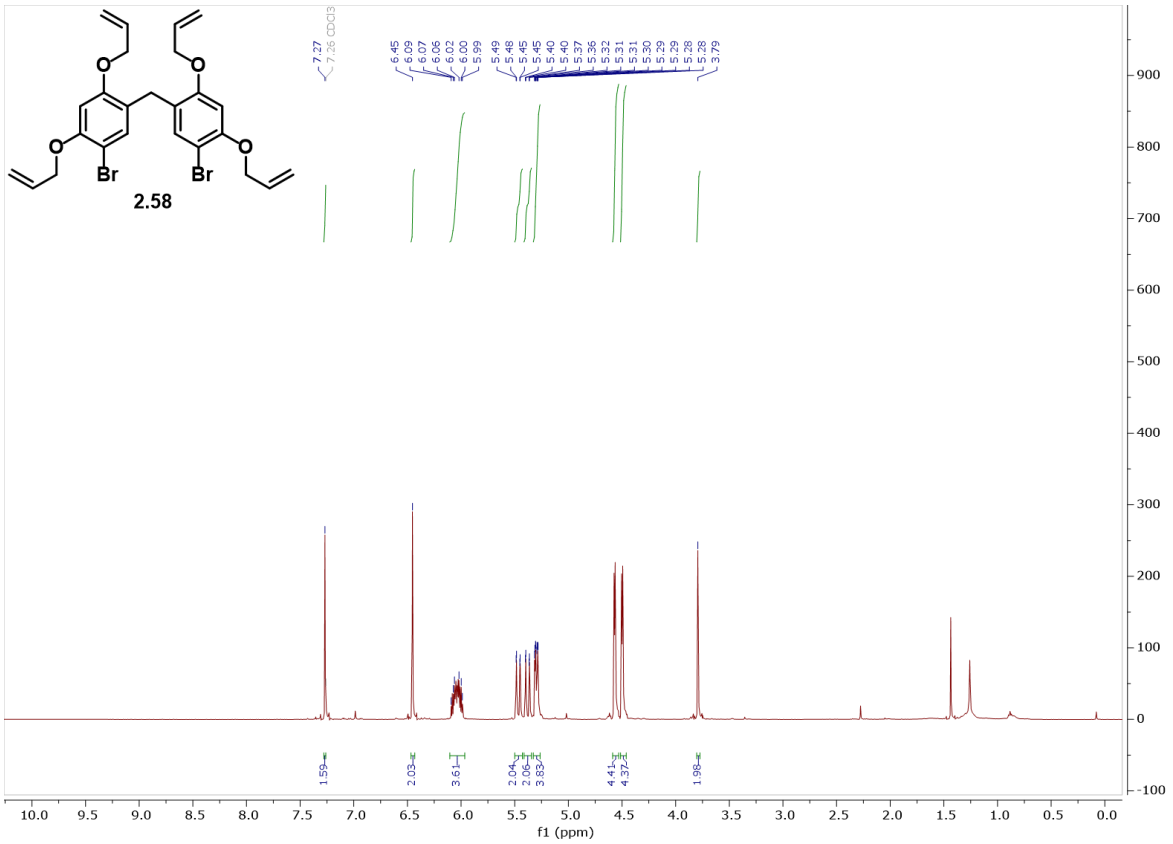
2.58
Br
Br
O
7.27
7.26 CDCl3
6.45
6.09
6.07
6.06
6.02
6.00
5.99
5.49
5.48
5.45
5.45
5.40
5.40
5.37
5.36
5.32
5.31
5.31
5.30
5.29
5.29
5.28
5.28
3.79
1.59
2.03
3.61
2.04
2.06
3.83
4.41
4.37
1.98
f1 (ppm)

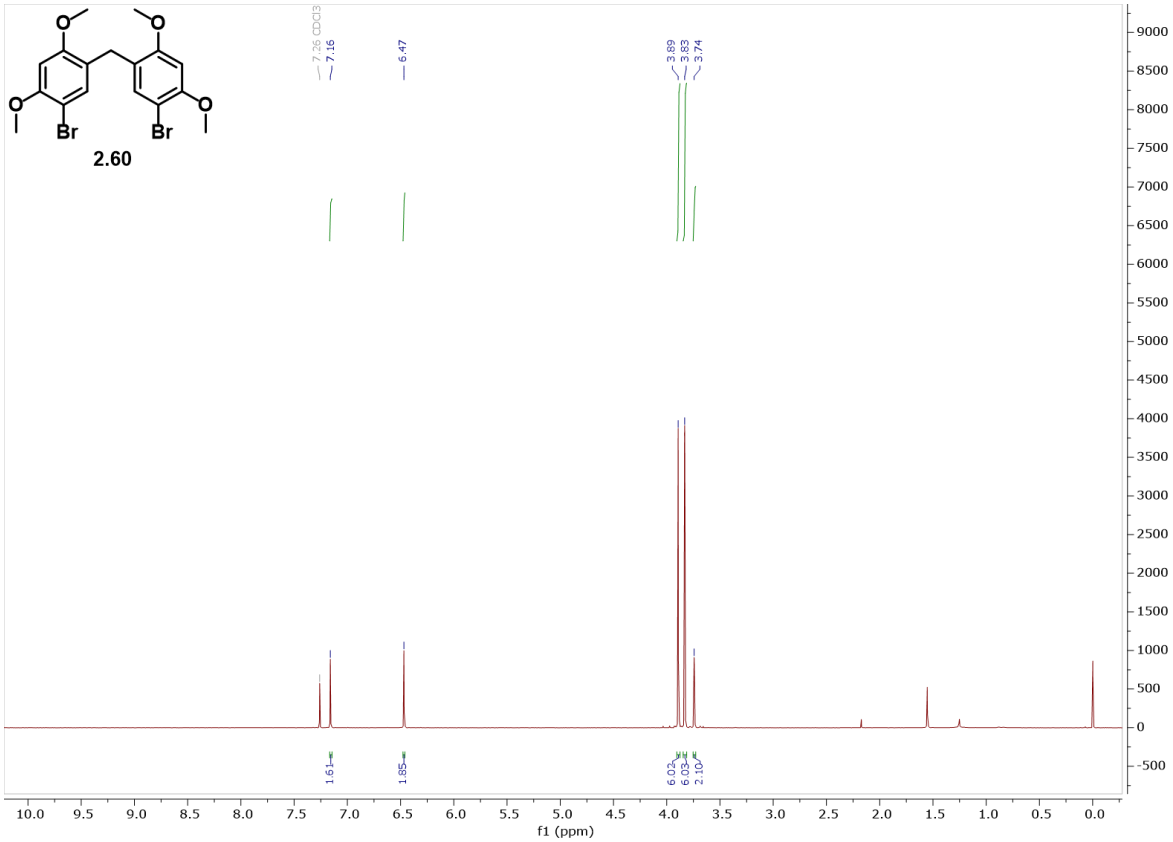
2.60
Br
Br
O
7.26 CDCl3
7.16
6.47
3.89
3.83
3.74
1.61
1.85
6.02
6.03
2.10
f1 (ppm)

5.3.2 Chapter 3

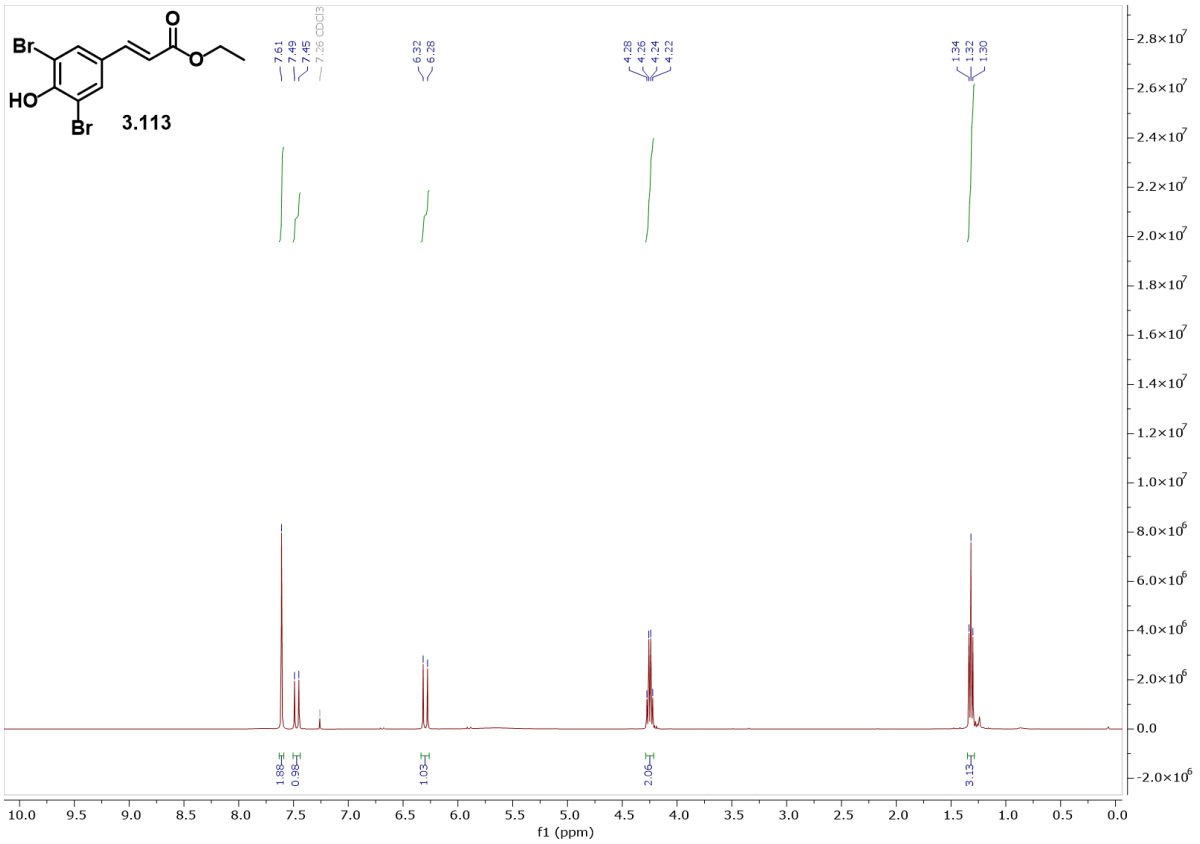
Br
HO
Br
O
O
3.113
7.61
7.49
7.45
7.26 CDCl3
6.32
6.28
4.28
4.26
4.24
4.22
1.34
1.32
1.30
1.88
0.98
1.03
2.06
3.13
f1 (ppm)

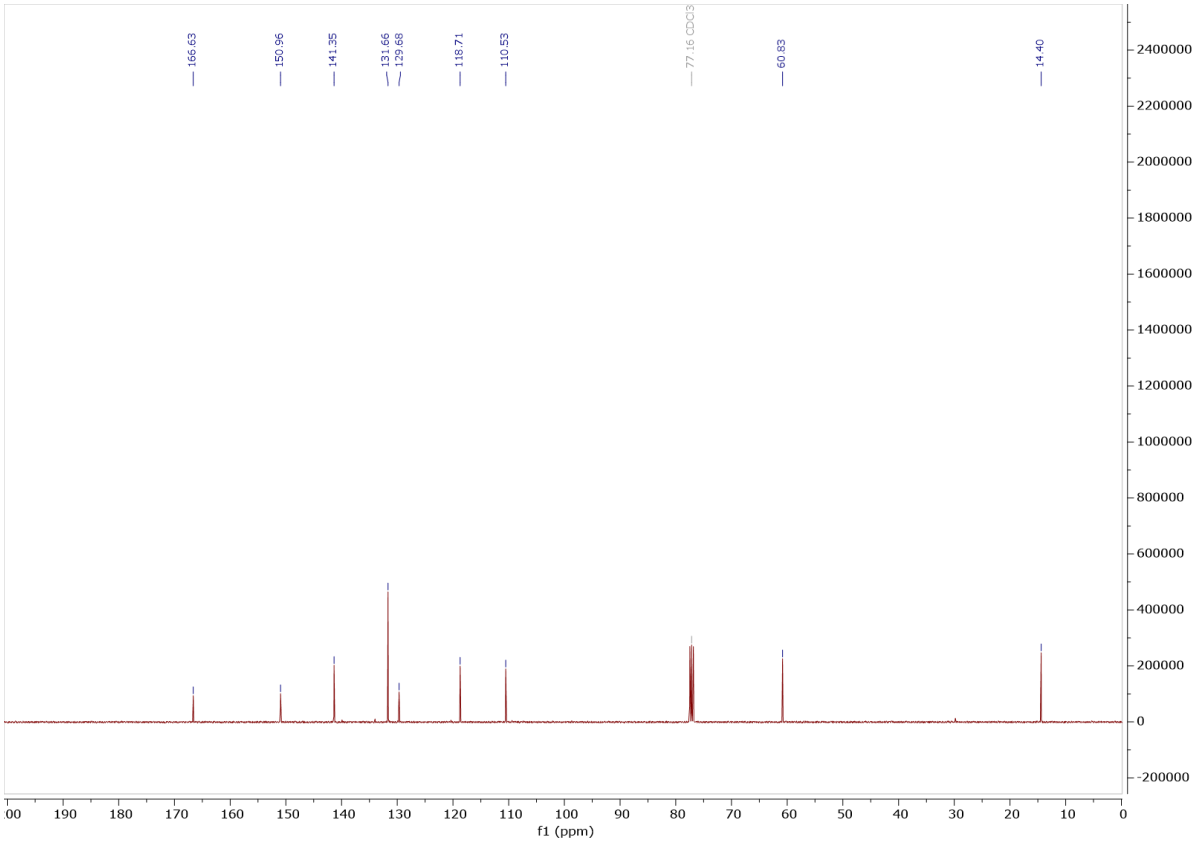
166.63
150.96
141.35
131.66
129.68
118.71
110.53
77.16 CDCl3
60.83
14.40
f1 (ppm)

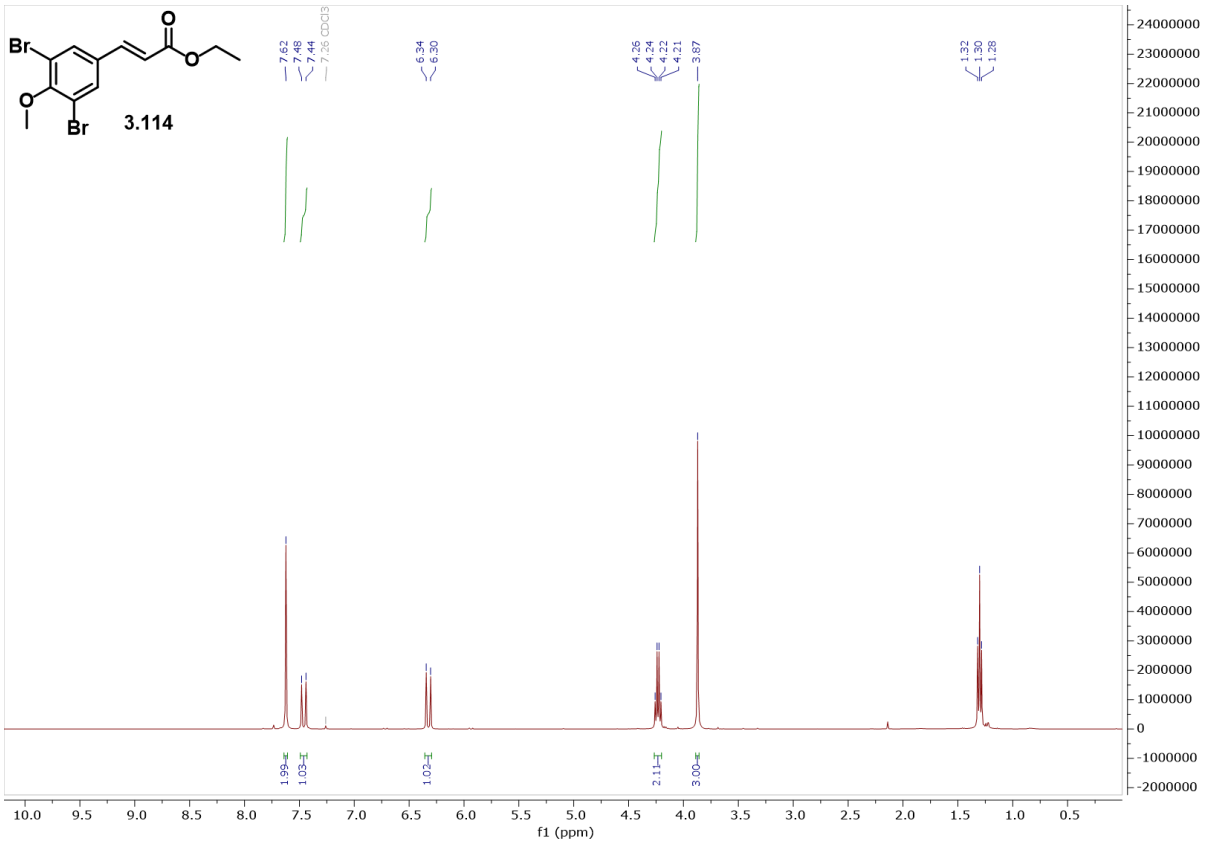
3.114
7.62
7.48
7.44
7.26 CDCl3
6.34
6.30
4.26
4.24
4.22
4.21
3.87
1.32
1.30
1.28
1.99
1.03
1.02
2.11
3.00
f1 (ppm)

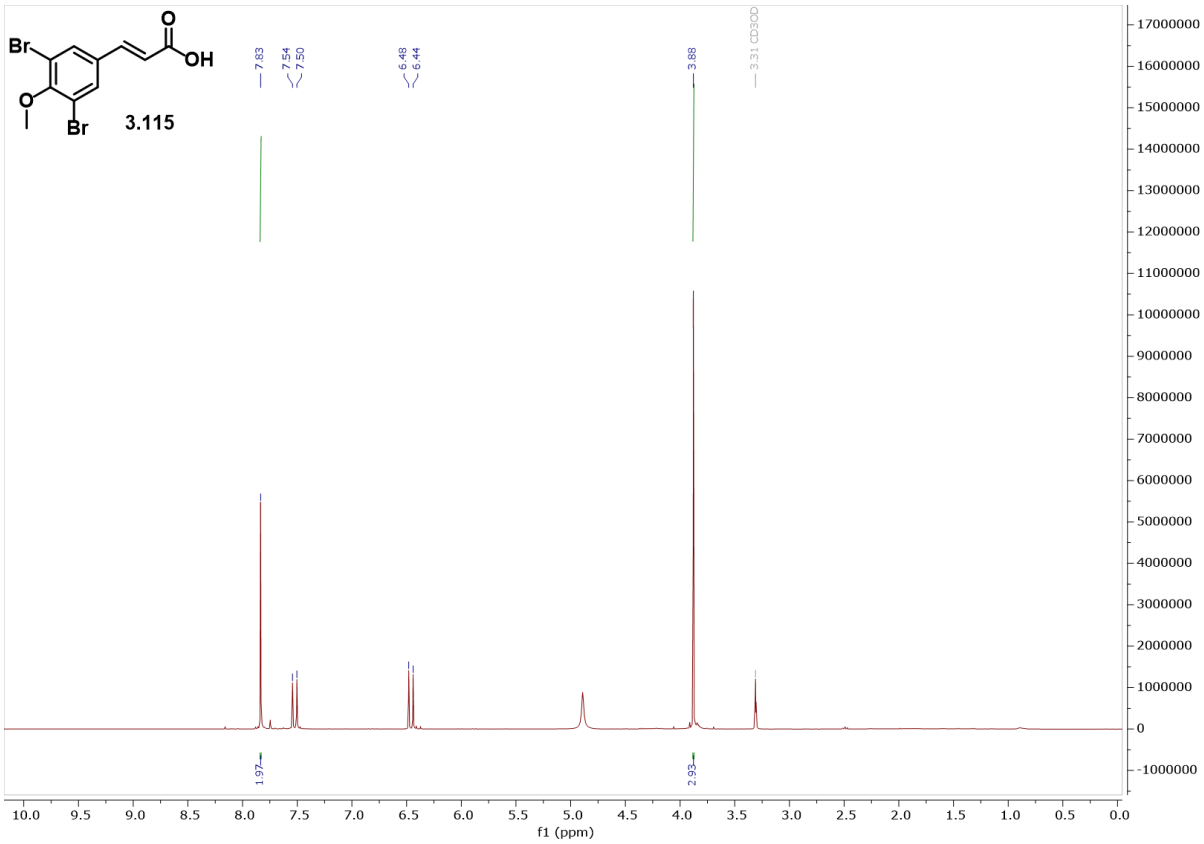
Br
O
OH
O
Br
3.115
7.83
7.54
7.50
6.48
6.44
3.88
3.31 CD3OD
1.97
2.93
f1 (ppm)

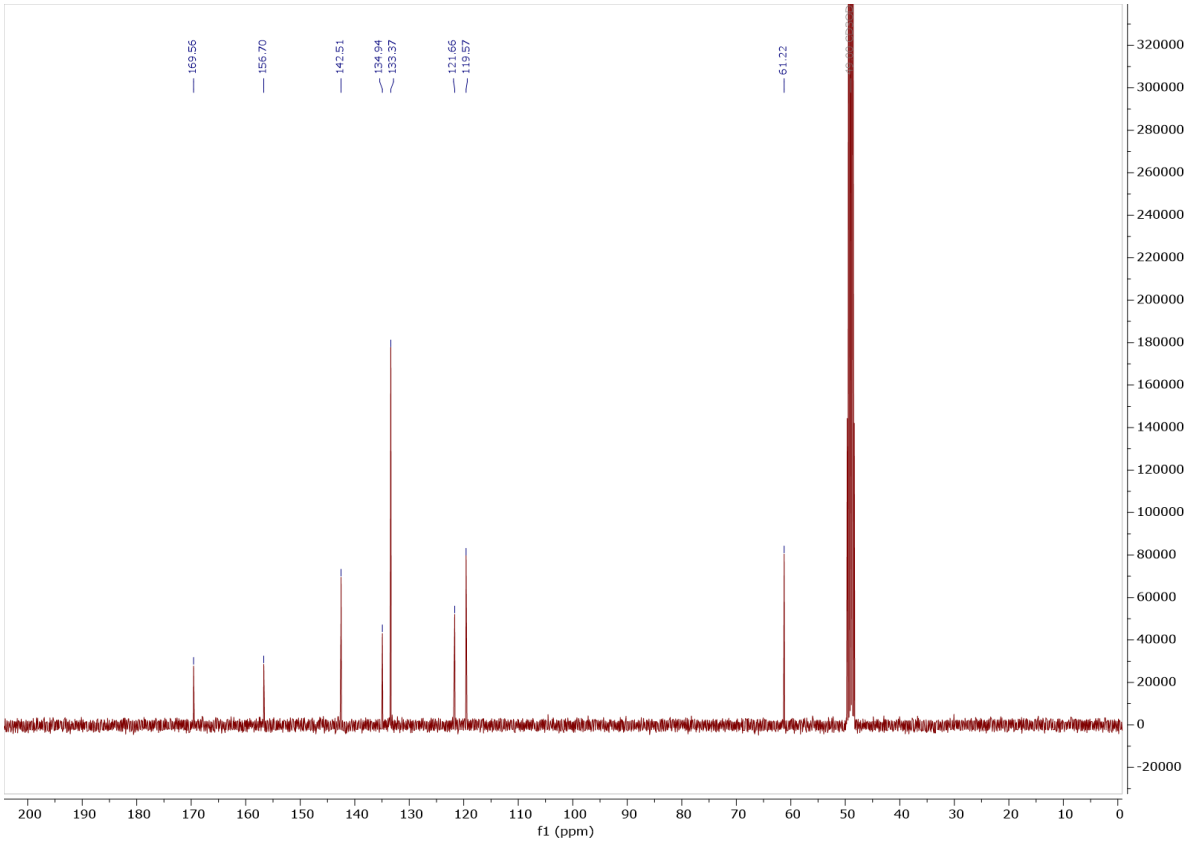
169.56
156.70
142.51
134.94
133.37
121.66
119.57
61.22
f1 (ppm)

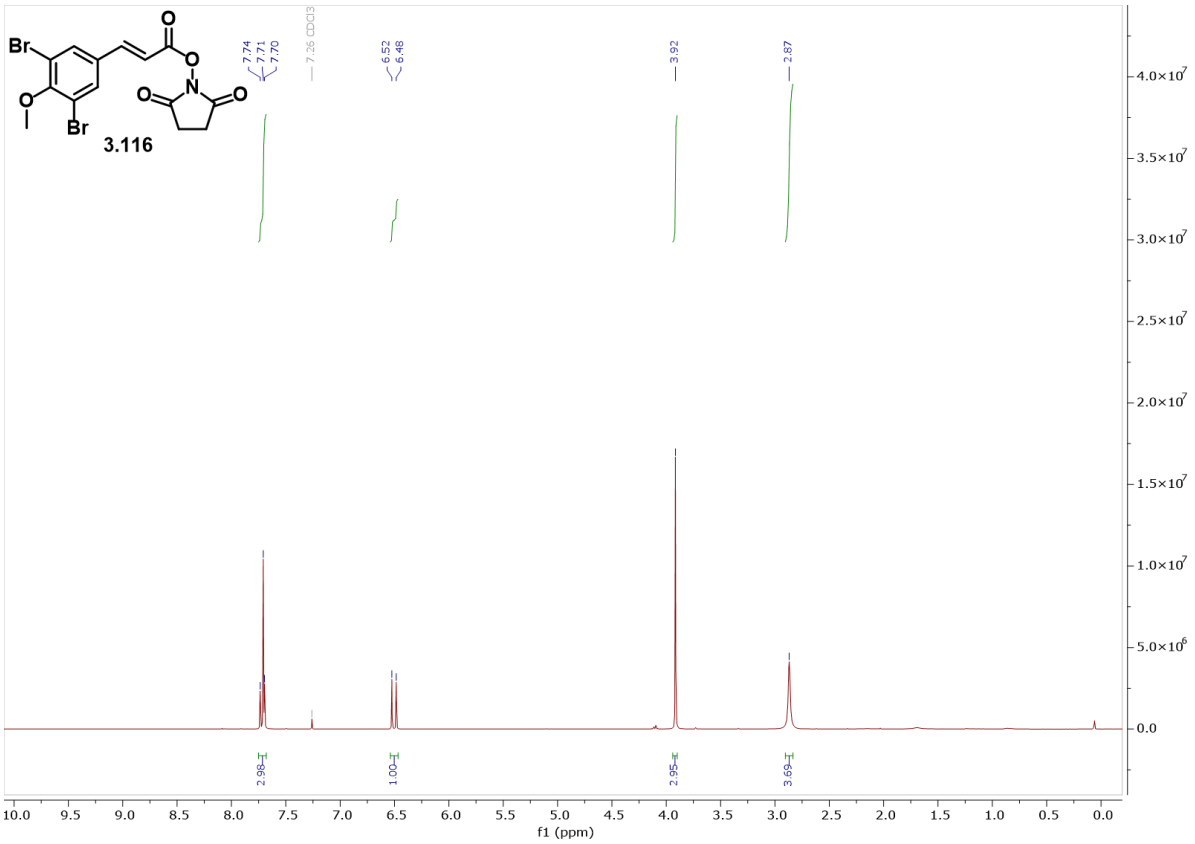
3.116
7.74
7.71
7.70
7.26 CDCl3
6.52
6.48
3.92
2.87
2.98
1.00
2.95
3.69
f1 (ppm)

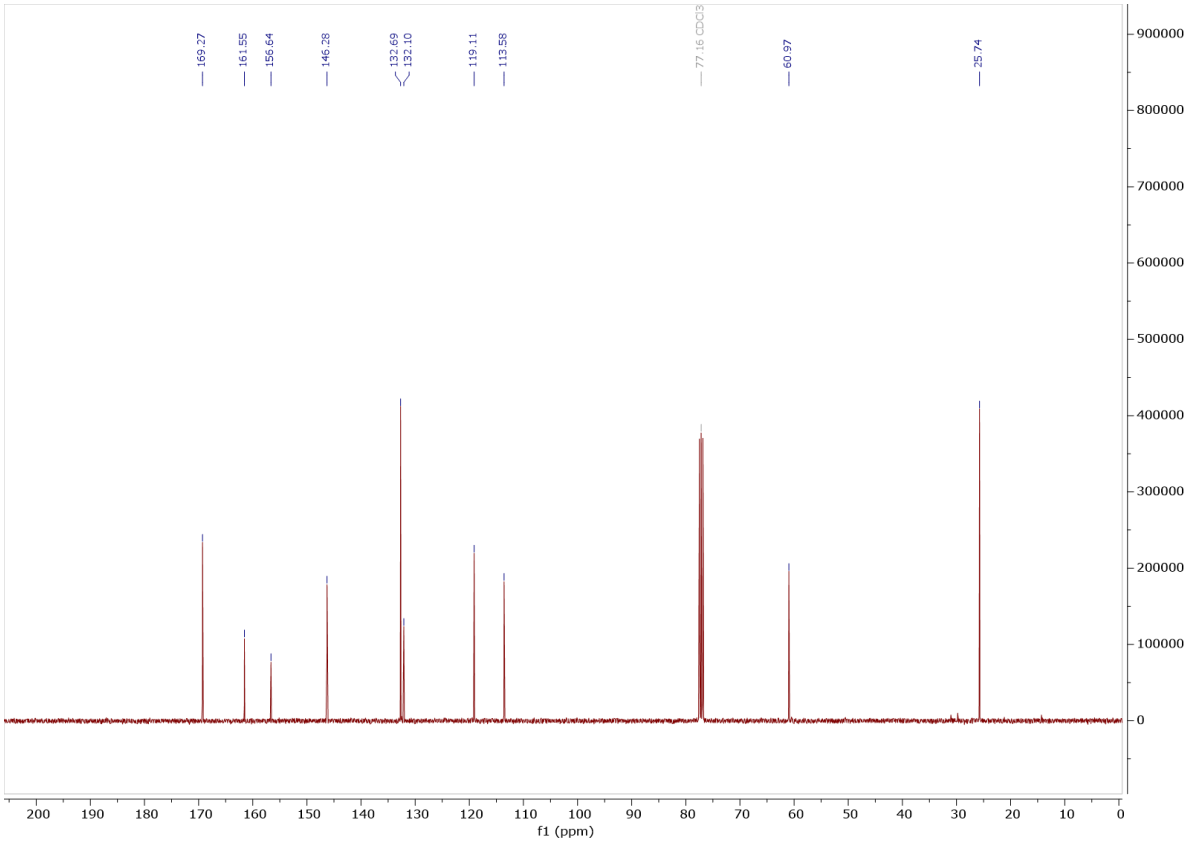
169.27
161.55
156.64
146.28
132.69
132.10
119.11
113.58
77.16 CDCl3
60.97
25.74
f1 (ppm)

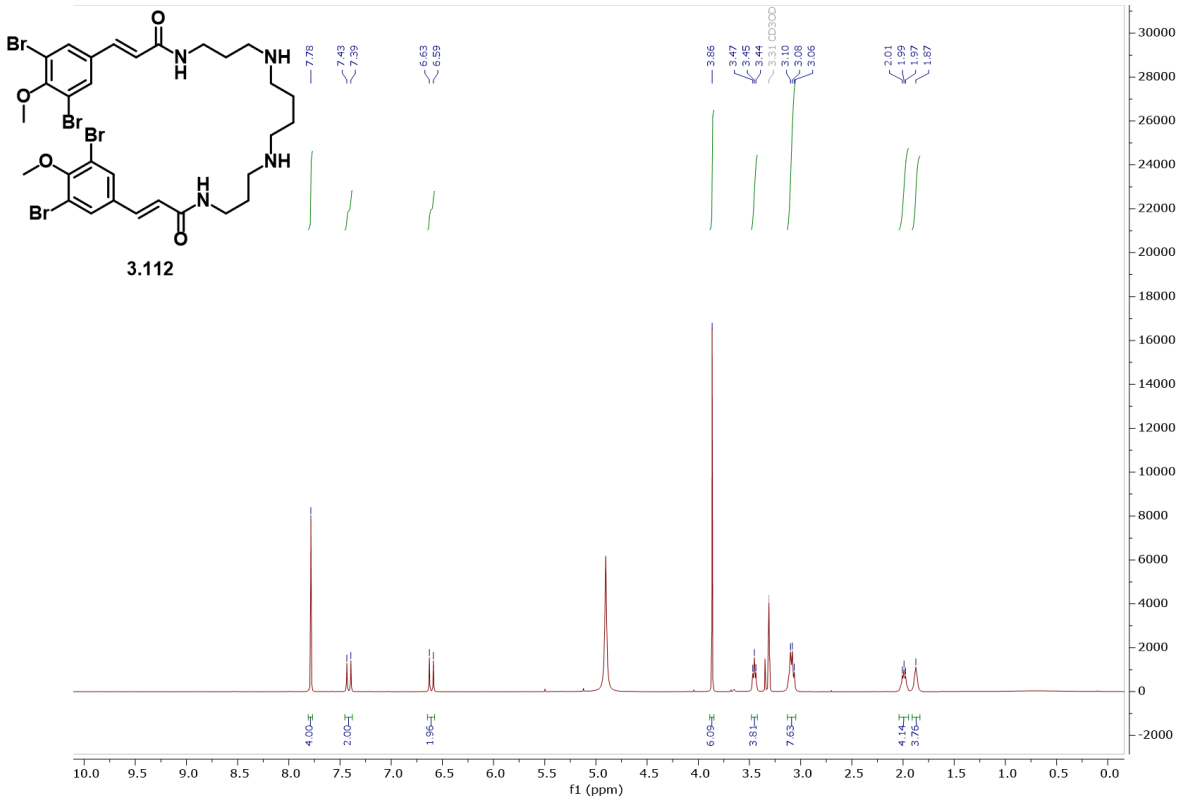
3.112
7.78
7.43
7.39
6.63
6.59
3.86
3.47
3.45
3.44
3.31 CD3OD
3.10
3.08
3.06
2.01
1.99
1.97
1.87
4.00
2.00
1.96
6.09
3.81
7.63
4.14
3.76
f1 (ppm)

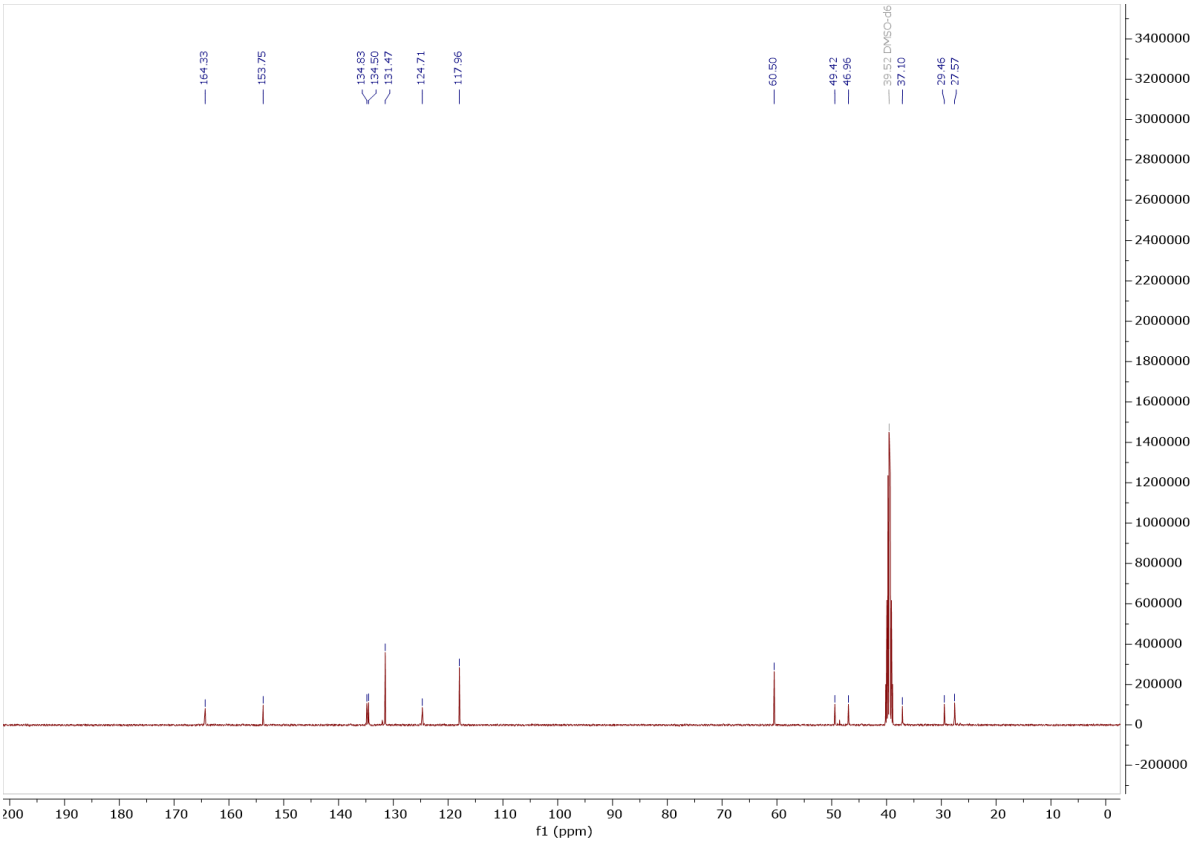
164.33
153.75
134.83
134.50
131.47
124.71
117.96
60.50
49.42
46.96
39.52 DMSO-d6
37.10
29.46
27.57
f1 (ppm)

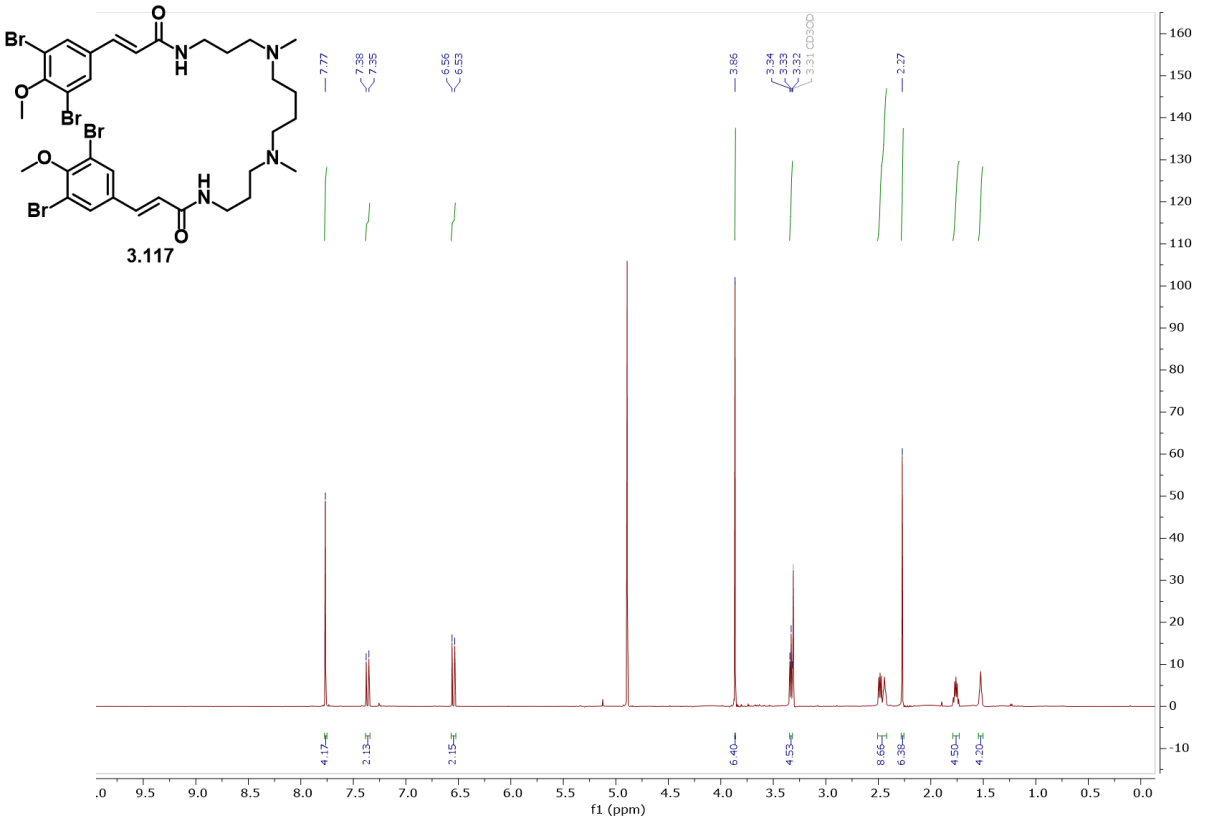
Br
O
N
H
N
Br
O
Br
Br
O
N
H
Br
N
O
3.117
7.77
7.38
7.35
6.56
6.53
3.86
3.34
3.33
3.32
3.31 CD3OD
2.27
4.17
2.13
2.15
6.40
4.53
8.66
6.38
4.50
4.20
f1 (ppm)

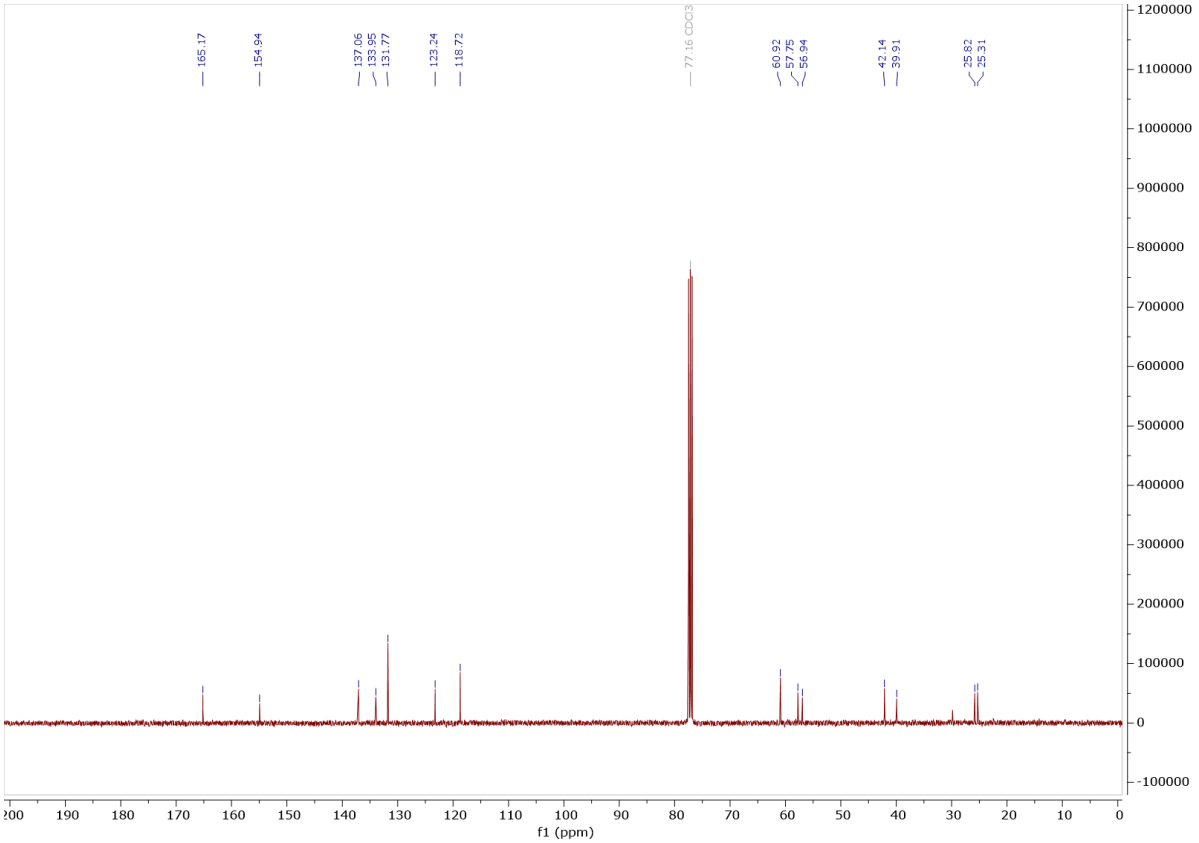
165.17
154.94
137.06
133.95
131.77
123.24
118.72
77.16 CDCl3
60.92
57.75
56.94
42.14
39.91
35.82
35.31
f1 (ppm)

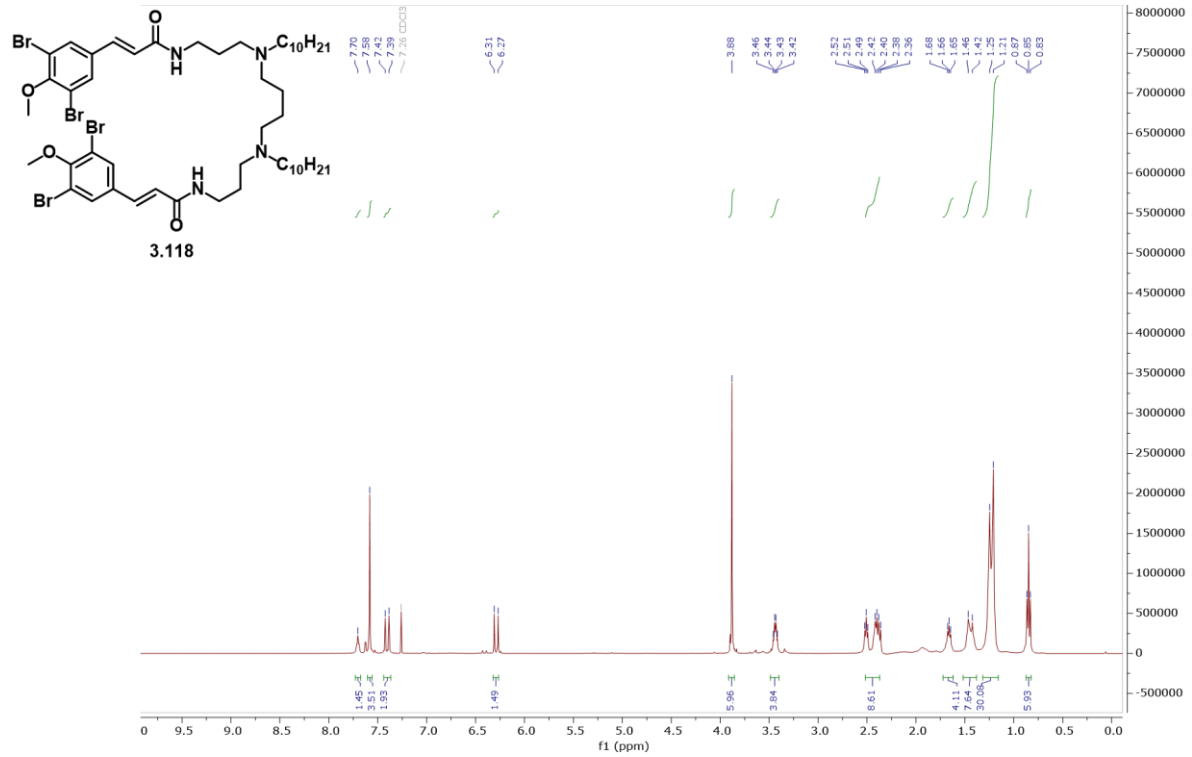
3.118
f1 (ppm)

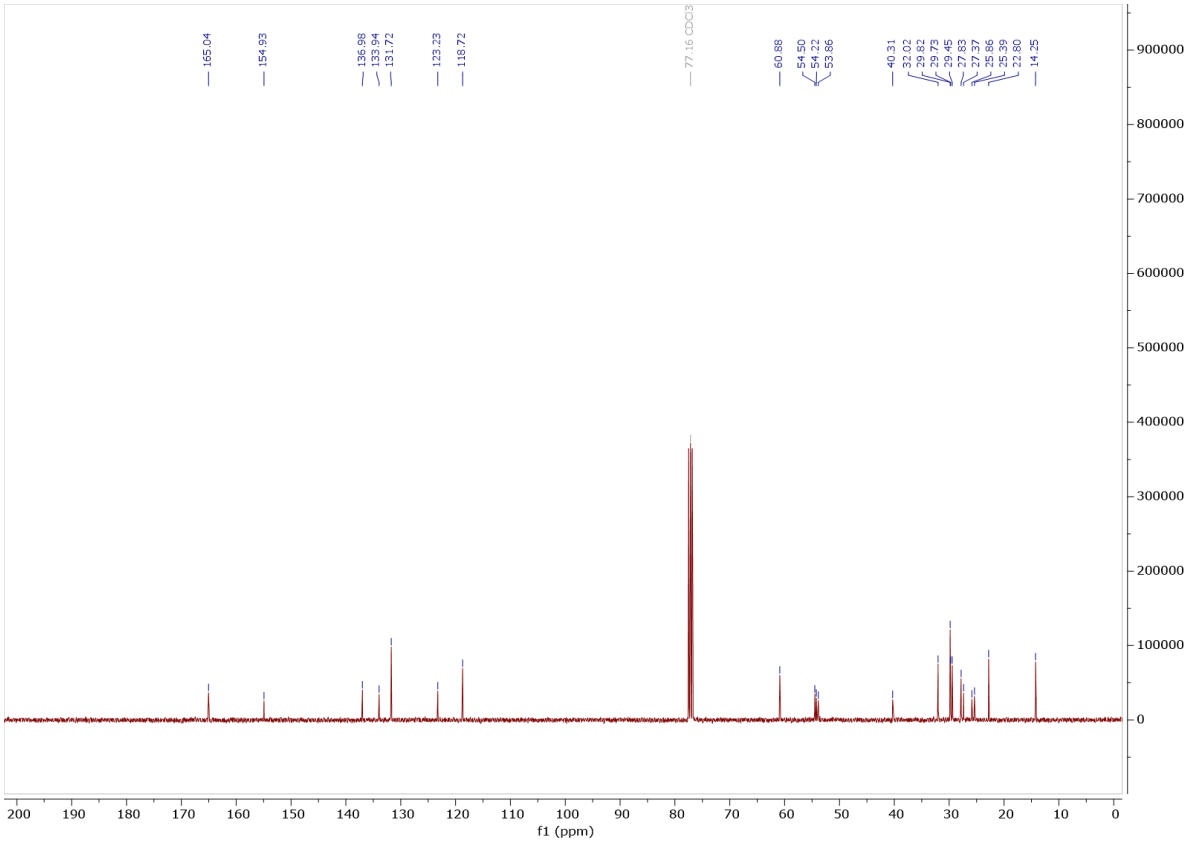
f1 (ppm)

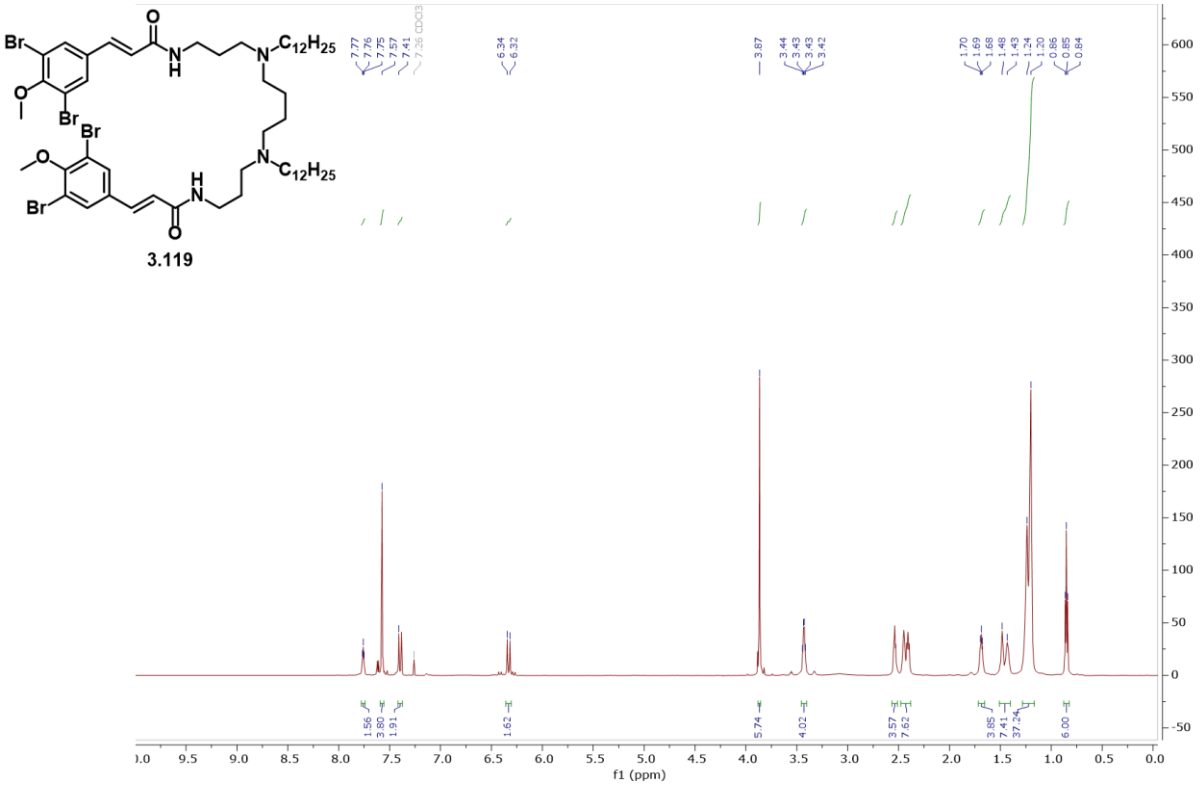
3.119
f1 (ppm)

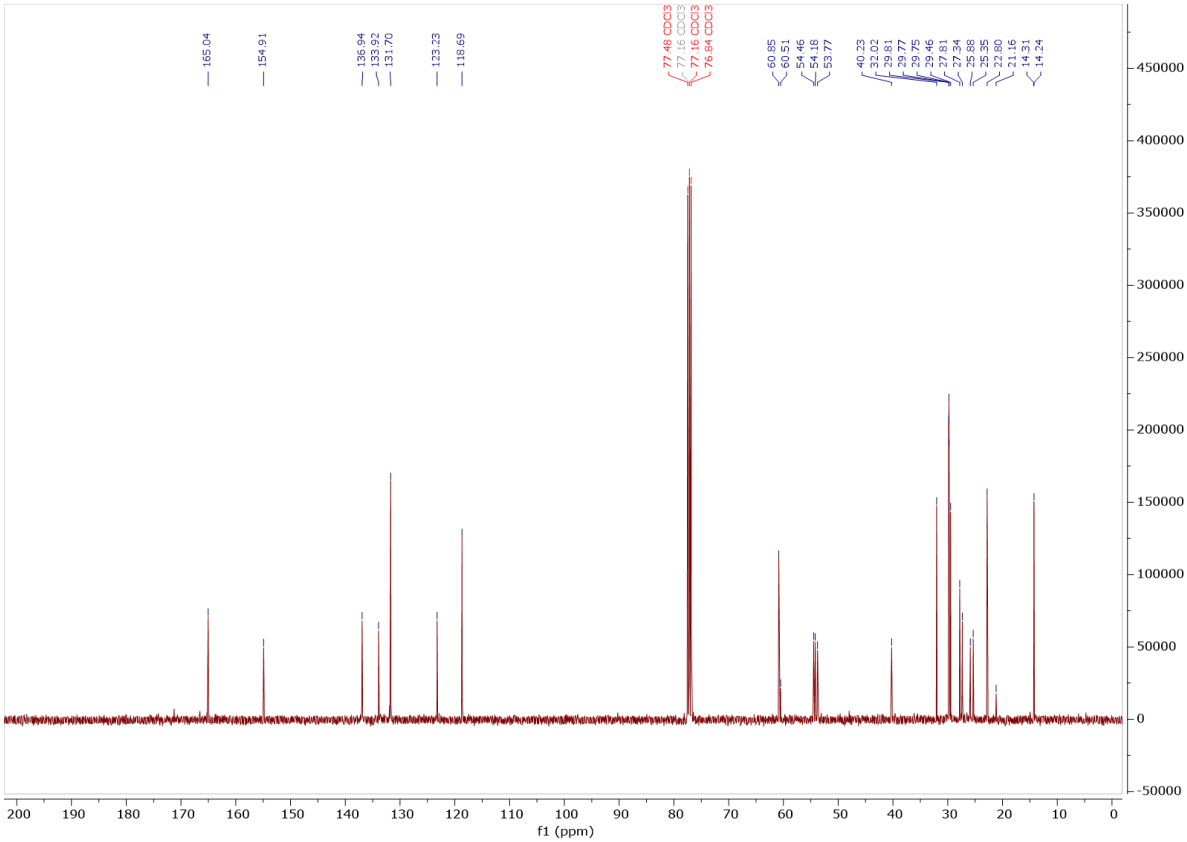
f1 (ppm)

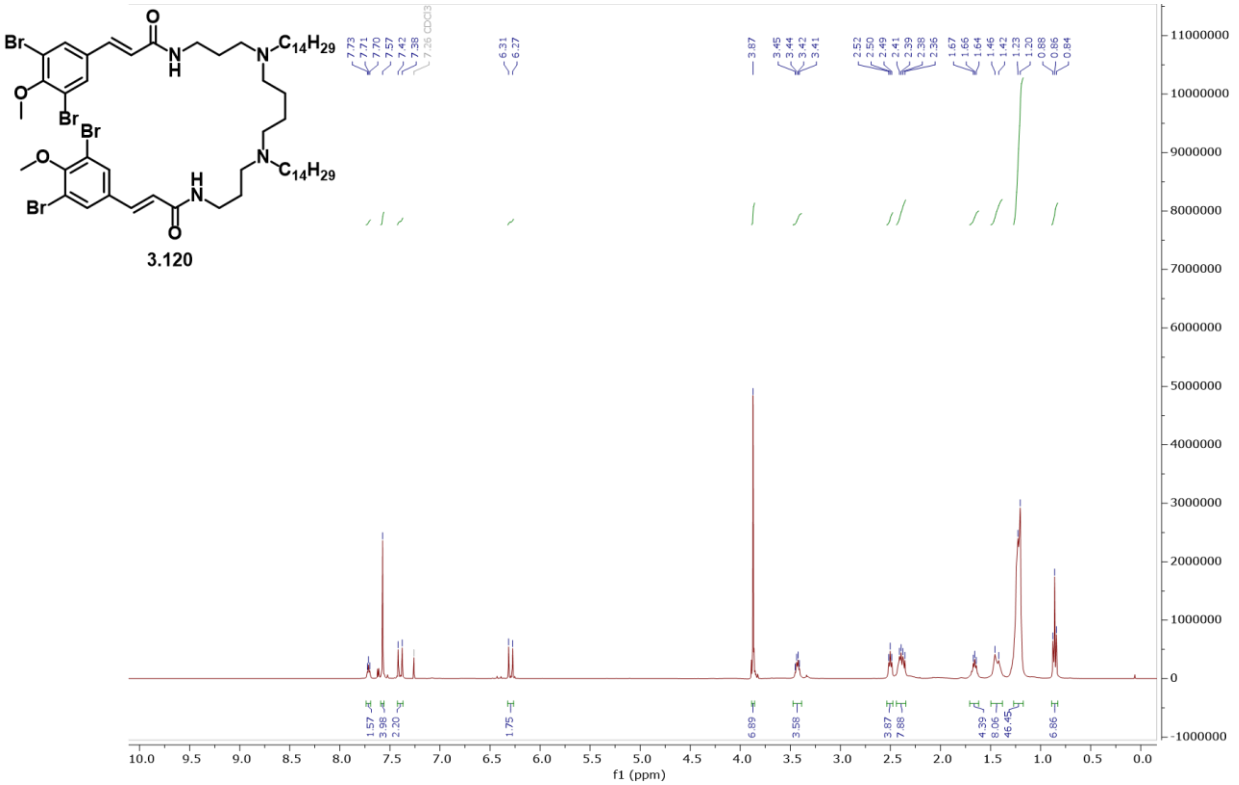
3.120
f1 (ppm)

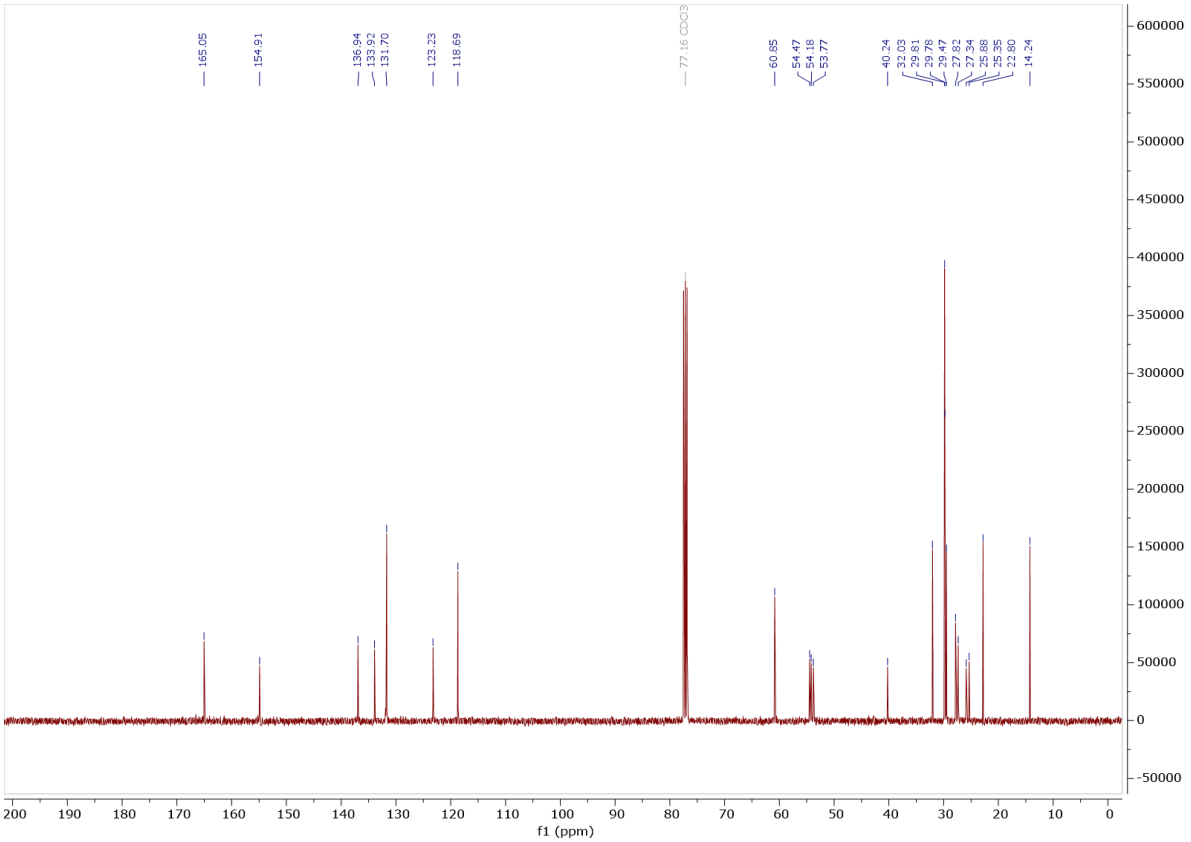
f1 (ppm)

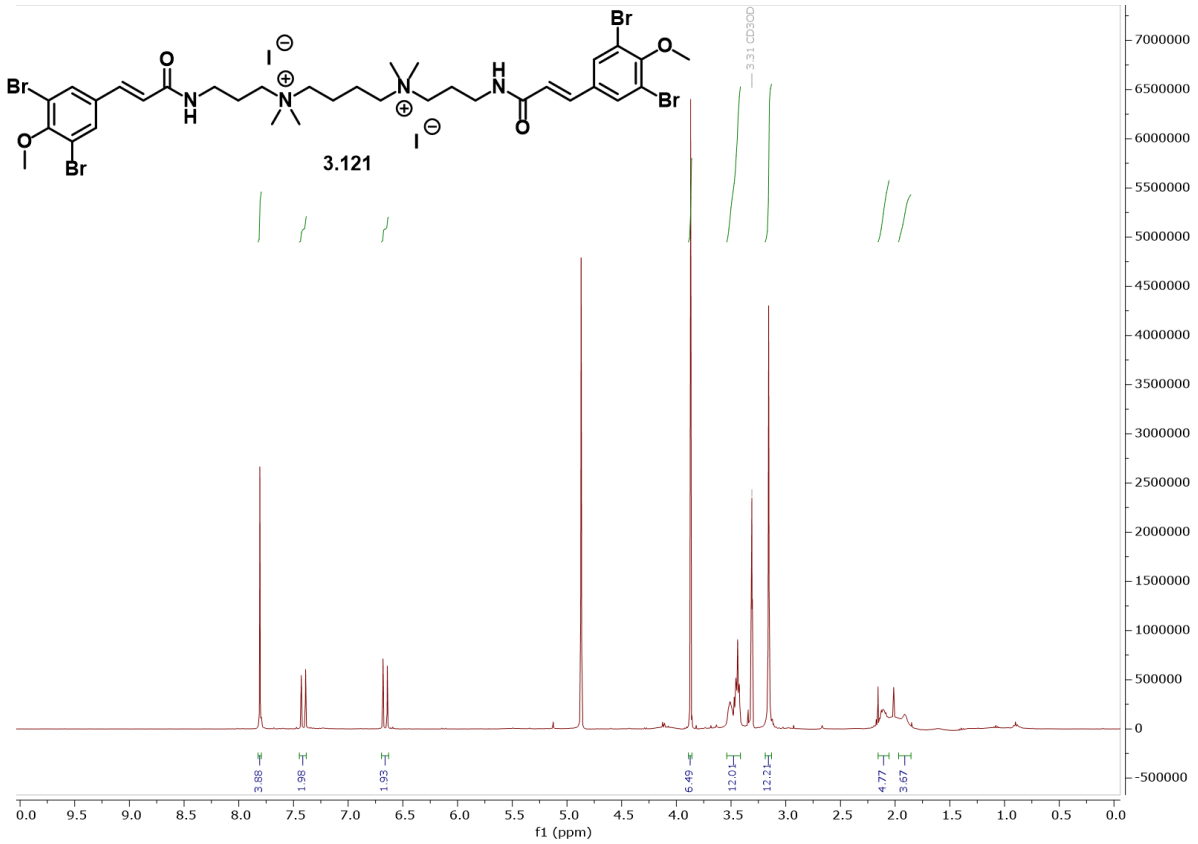
3.121
3.31 CD3OD
3.88
1.98
1.93
6.49
12.01
12.24
4.77
3.67
f1 (ppm)

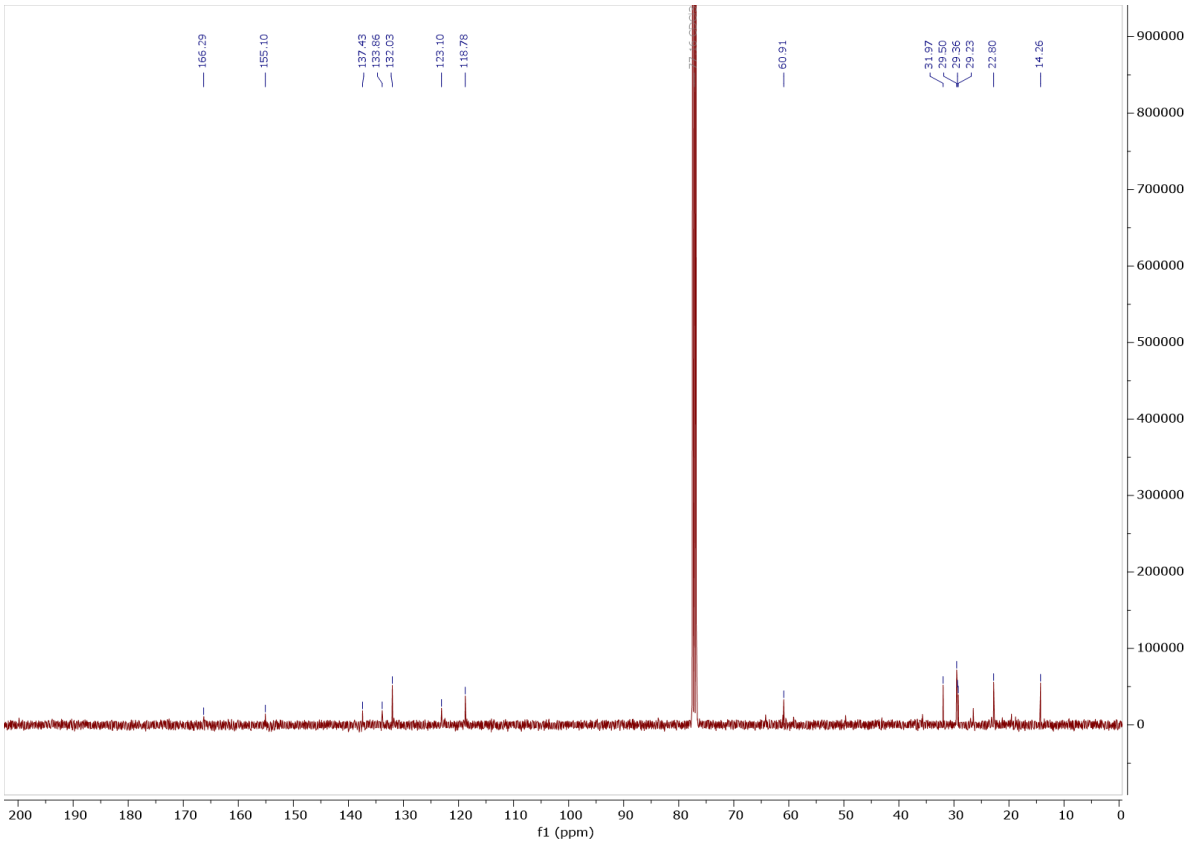
166.29
155.10
137.43
133.86
132.03
123.10
118.78
60.91
31.97
29.50
29.36
29.23
22.80
14.26
f1 (ppm)

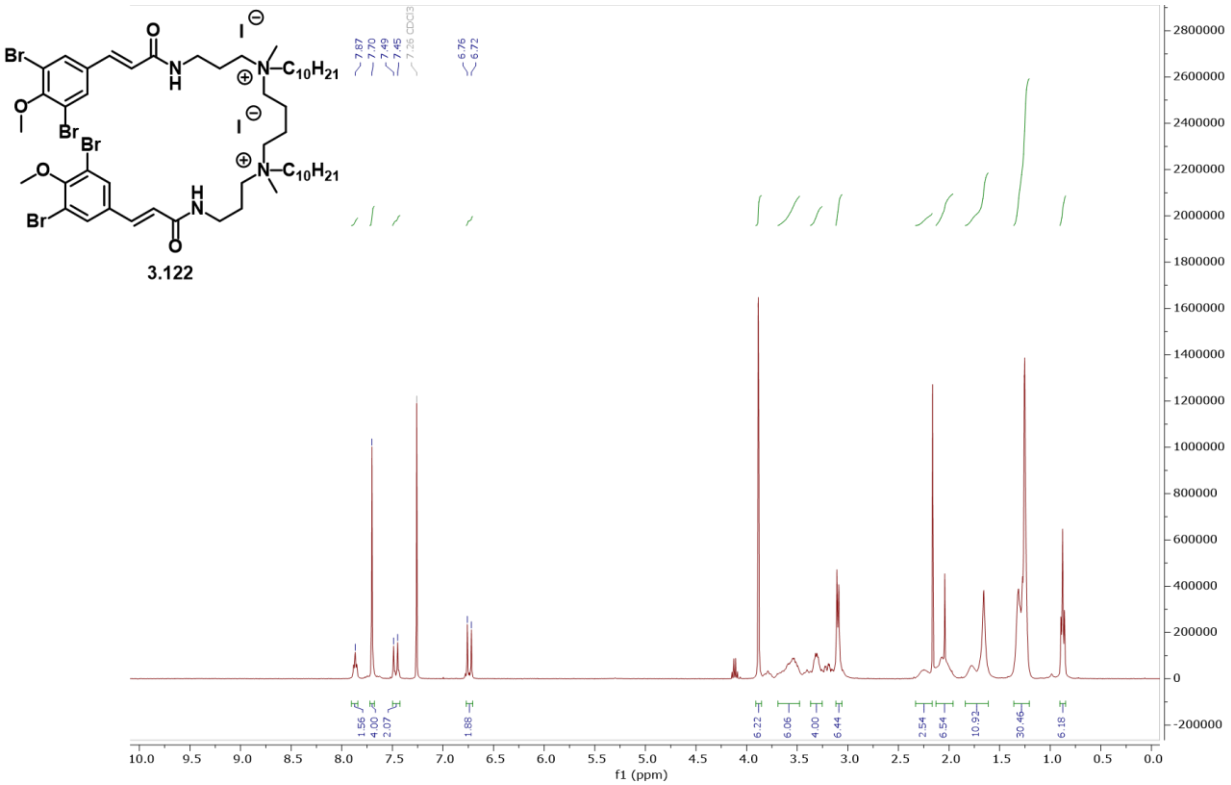
3.122
7.87
7.70
7.49
7.45
7.26 CDCl3
6.76
6.72
1.56
4.00
2.07
1.88
6.22
6.06
4.00
6.44
2.54
6.54
10.92
30.46
6.18
f1 (ppm)

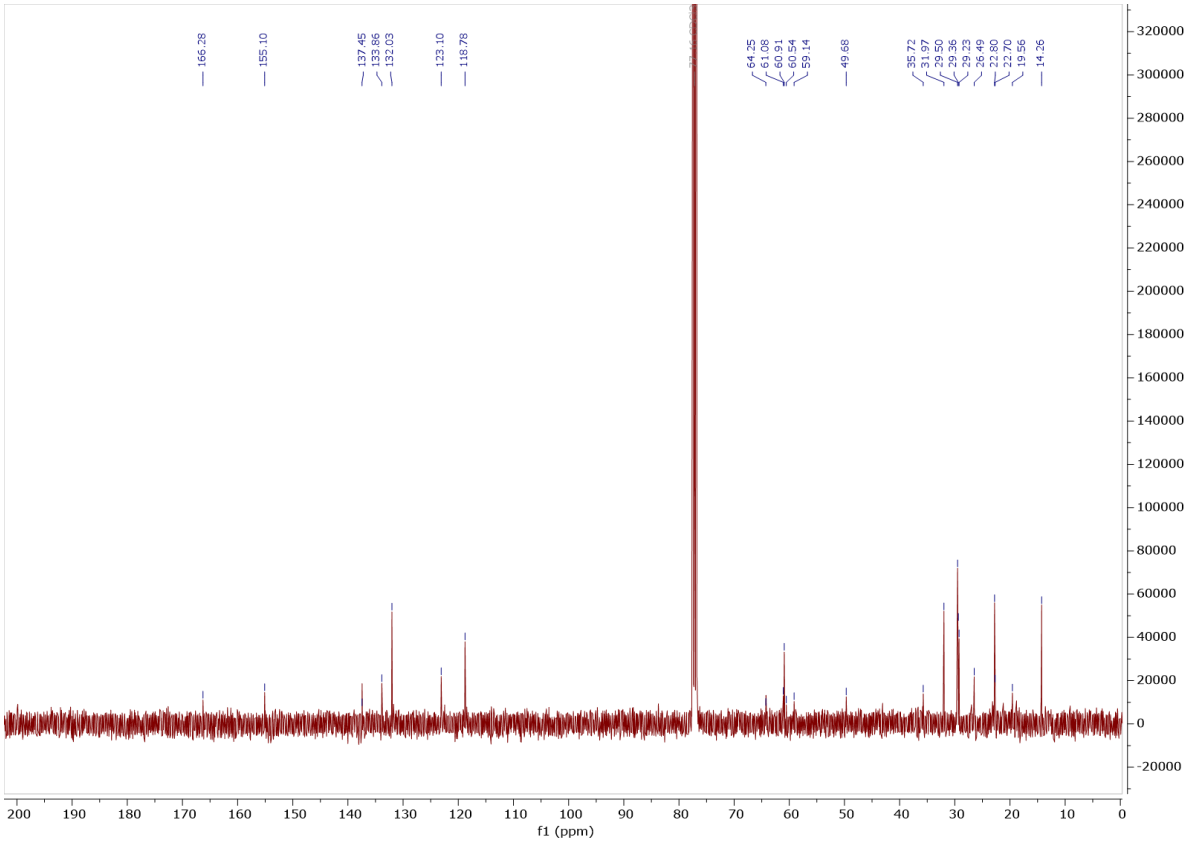
166.28
155.10
137.45
133.86
132.03
123.10
118.78
64.25
61.08
60.91
60.54
59.14
49.68
35.72
31.97
29.50
29.36
29.23
26.49
22.80
22.70
19.56
14.26
f1 (ppm)

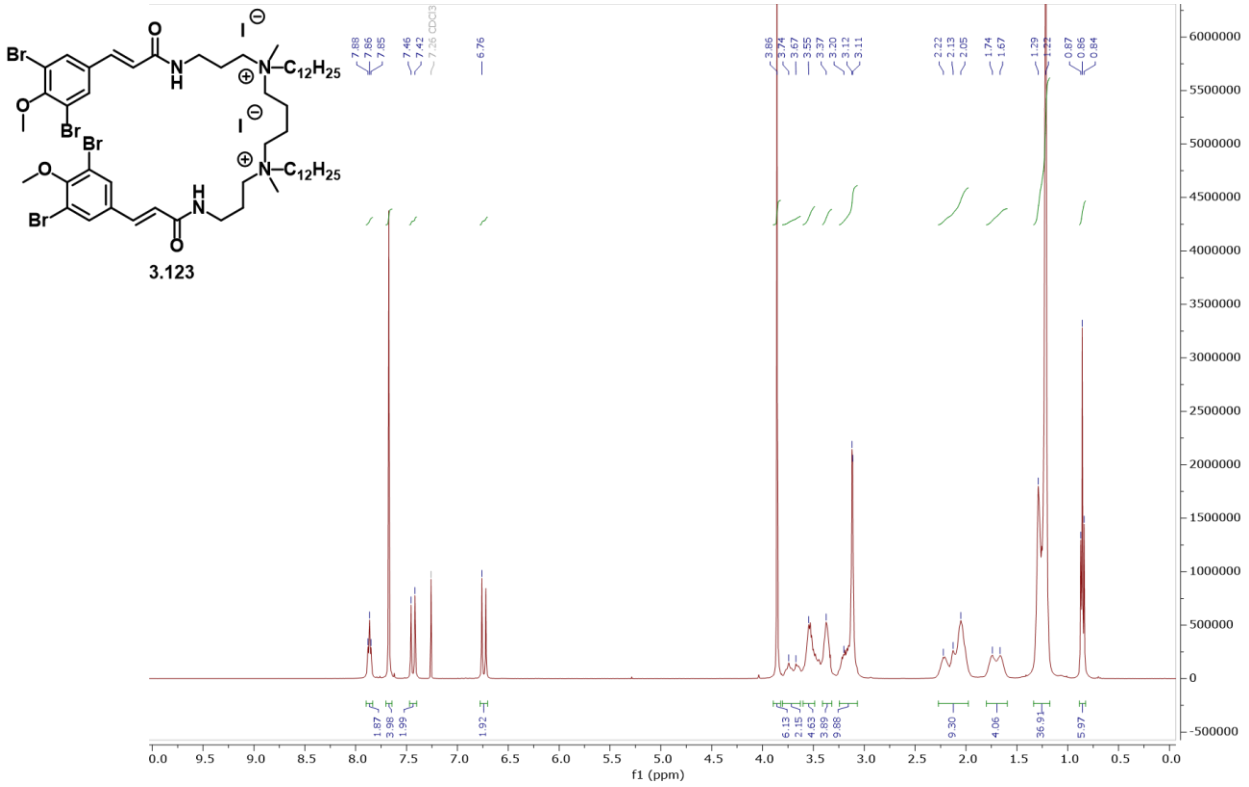
3.123
f1 (ppm)

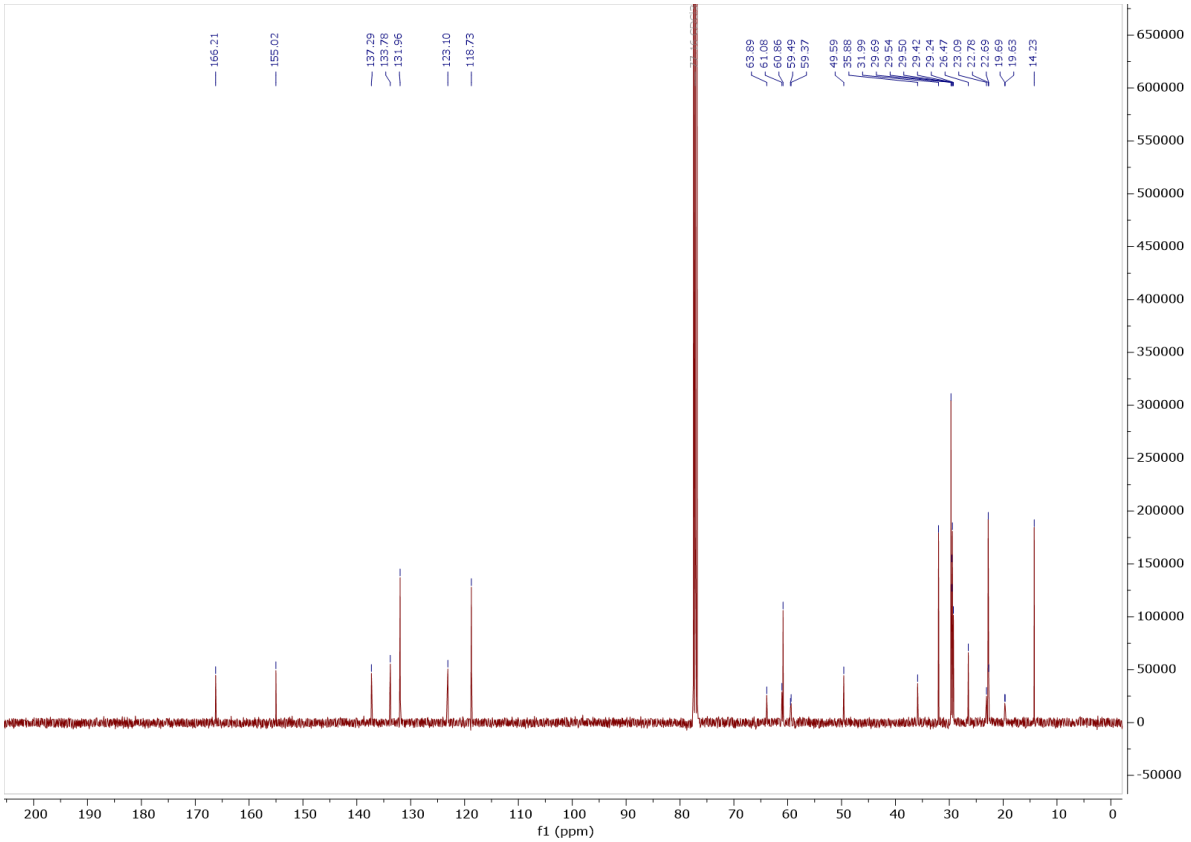
f1 (ppm)

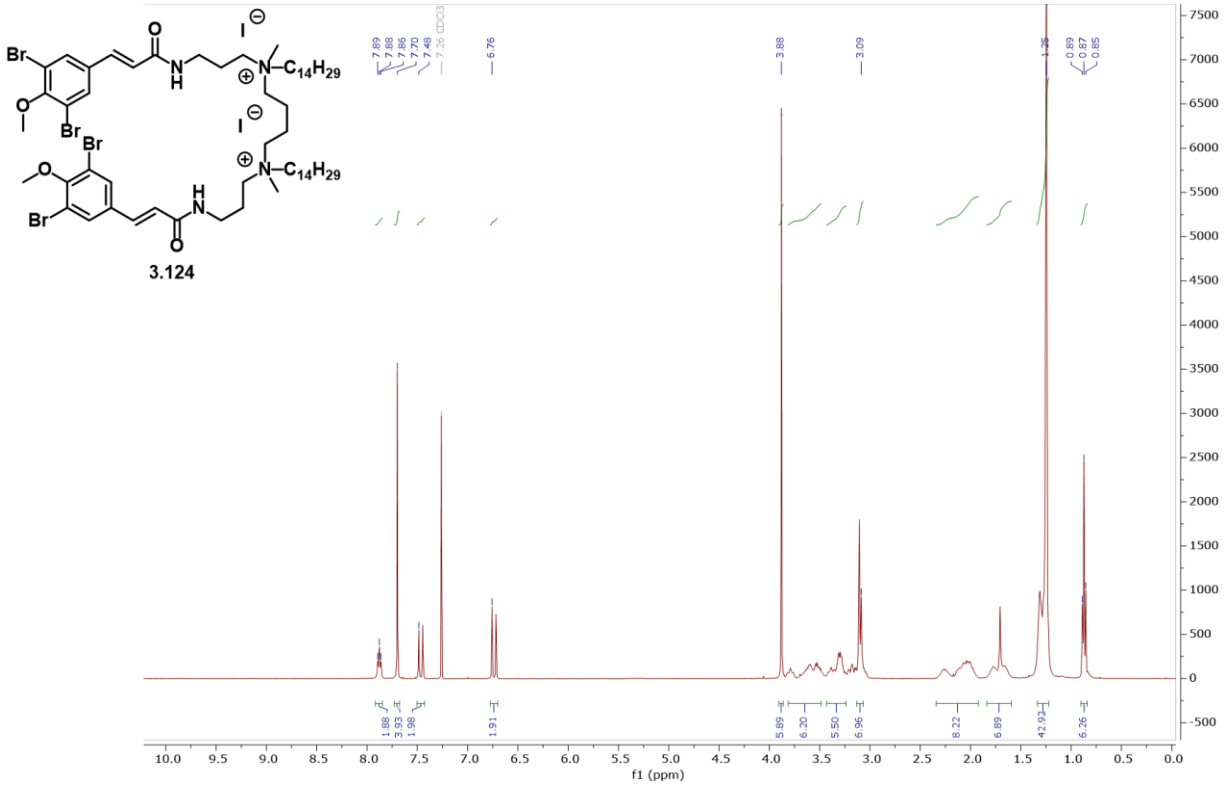
3.124
7.89
7.88
7.86
7.70
7.48
7.26 CDCl3
6.76
3.88
3.09
1.26
0.89
0.87
0.85
1.88
3.93
1.98
1.91
5.89
6.20
5.50
6.96
8.22
6.89
42.92
6.26
f1 (ppm)

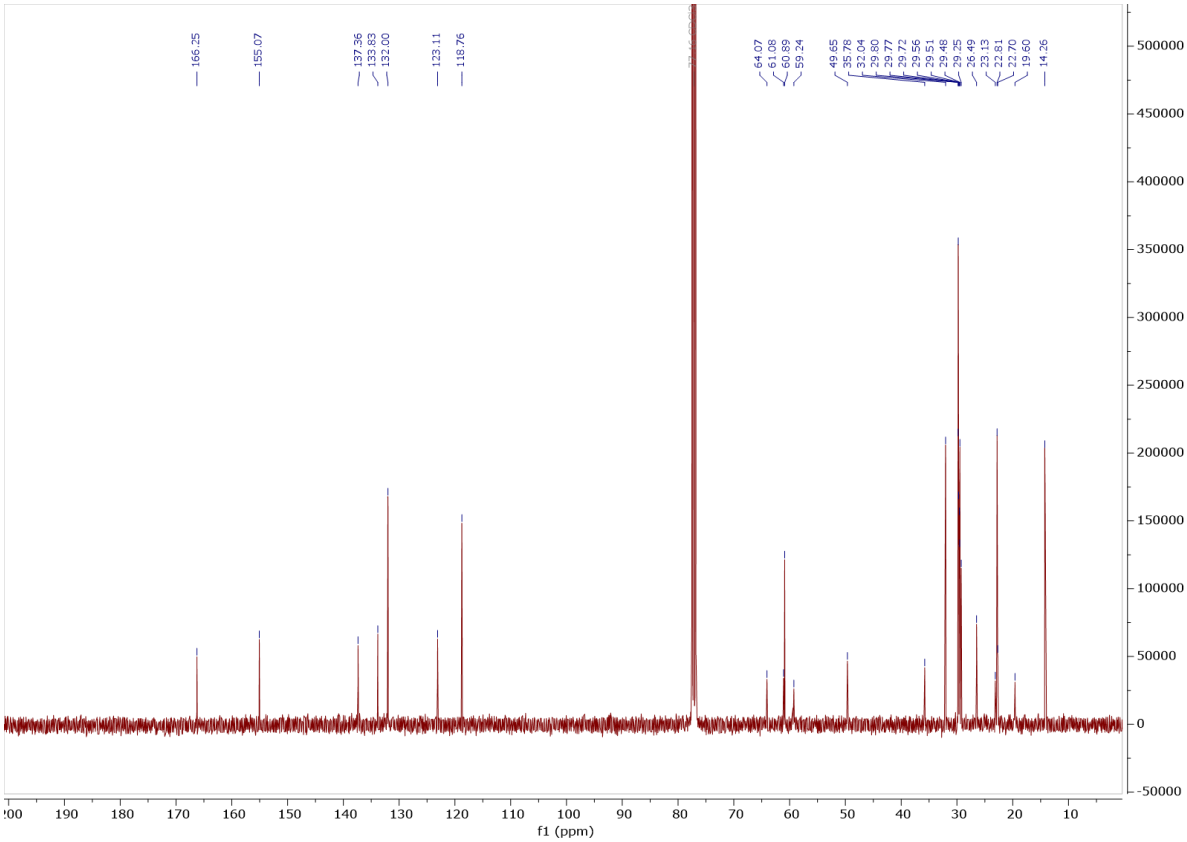
166.25
155.07
137.36
133.83
132.00
123.11
118.76
64.07
61.08
60.89
59.24
49.65
35.78
32.04
29.80
29.77
29.72
29.56
29.51
29.48
29.25
26.49
23.13
22.81
22.70
19.60
14.26
f1 (ppm)

5.4 References

(1) Cue Jr., B. W.; Dirlam, J. P.; Czuba, L. J.; Windisch, W. W. A Practical Synthesis of Pyoluteorin. *J. Heterocycl. Chem.* **1981**, *18* (1), 191–192. https://doi.org/10.1002/jhet.5570180136.

(2) Liu, Z.; Yin, S.; Zhang, R.; Zhu, W.; Fu, P. High-Efficiency Synthesis of Carbon-Bridged Dimers via Bioinspired Green Dimerization Involving Aldehydes. *ACS Sustain. Chem. Eng.* **2022**, *10* (1), 655–661. https://doi.org/10.1021/acssuschemeng.1c07635.

(3) Davies, D. G.; Hodge, P. A Synthetic Route to Pyoluteorin. *Tetrahedron Lett.* **1970**, *11* (19), 1673–1675. https://doi.org/10.1016/S0040-4039(01)98051-7.

(4) Lacerna, N. M. I.; Miller, B. W.; Lim, A. L.; Tun, J. O.; Robes, J. M. D.; Cleofas, M. J. B.; Lin, Z.; Salvador-Reyes, L. A.; Haygood, M. G.; Schmidt, E. W.; Concepcion, G. P. Mindapyrroles A–C, Pyoluteorin Analogues from a Shipworm-Associated Bacterium. *J. Nat. Prod.* **2019**, *82* (4), 1024–1028. https://doi.org/10.1021/acs.jnatprod.8b00979.

(5) Kaplan, A. R.; Musaev, D. G.; Wuest, W. M. Pyochelin Biosynthetic Metabolites Bind Iron and Promote Growth in Pseudomonads Demonstrating Siderophore-like Activity. *ACS Infect. Dis.* **2021**, *7* (3), 544–551. https://doi.org/10.1021/acsinfecdis.0c00897.

(6) Chen, Z.; Tan, M.; Shan, C.; Yuan, X.; Chen, L.; Shi, J.; Lan, Y.; Li, Y. Aryne 1,4-Disubstitution and Remote Diastereoselective 1,2,4-Trisubstitution via a Nucleophilic Annulation-[5,5]-Sigmatropic Rearrangement Process. *Angew. Chem. Int. Ed.* **2022**, *61* (47), e202212160. https://doi.org/10.1002/anie.202212160.

(7) Smolobochkin, A. V.; Gazizov, A. S.; Burilov, A. R.; Pudovik, M. A. Reaction of 4-Chloro- and 4-Bromobenzene-1,3-Diols with 1-Alkyl-3-(4,4-Diethoxybutyl)Ureas in the Presence of Trifluoroacetic Acid. *Russ. J. Org. Chem.* **2015**, *51* (9), 1261–1263. https://doi.org/10.1134/S1070428015090079.

(8) Pieri, C.; Borselli, D.; Di Giorgio, C.; De Méo, M.; Bolla, J.-M.; Vidal, N.; Combes, S.; Brunel, J. M. New Ianthelliformisamine Derivatives as Antibiotic Enhancers against Resistant Gram-Negative Bacteria. *J. Med. Chem.* **2014**, *57* (10), 4263–4272. https://doi.org/10.1021/jm500194e.